MEASUREMENTS OF WIND WAVE KINEMATICS

J.A. Battjes

J. van Heteren

Report WWKZ-G007, 1983

MEASUREMENTS OF WIND WAVE KINEMATICS

J.A. Battjes, Delft University of Technology
J. van Heteren, Rijkswaterstaat

Rijkswaterstaat
Report WWKZ-G007

July 1983

MEASUREMENTS OF WIND WAVE KINEMATICS

CONTENTS

1. INTRODUCTION

The realistic modelling of the internal kinematics of wind-generated waves, in relation to the motions of the surface, is a topic of scientific interest and practical importance. The linear Gaussian model of the wave motion provides a manageable approximation with many features which are at least qualitatively realistic. Its quantitative performance under field conditions has been checked in a number of studies, with varying and in some respects conflicting results.

In the following, some of the results published previously will be mentioned concerning spectral transfer functions between surface elevation (ζ) and horizontal ($\vec{u}$ = u,v) and vertical (w) velocity.

The theoretical gain and phase spectra between two processes x(t) and y(t) will be designated as $H_{xy}(f)$ and $\phi_{xy}(f)$, in which $H_{xy}(f)$ represents the amplitude of y per unit amplitude of x, and $\phi_{xy}(f)$ represents the phase lead of y with respect to x, both as function of frequency f. The theoretical gain function for the horizontal velocity in the propagation direction (denoted by $\tilde{u}$), for given surface elevation, is

$$H_{\zeta\tilde{u}}(f) = 2\pi f \frac{\cosh k(h+z)}{\sinh kh}$$

and for the vertical velocity it is

$$H_{\zeta w}(f) = 2\pi f \frac{\sinh k(h+z)}{\sinh kh}$$

in which h is the mean depth, z is a vertical coordinate measured positive upward from mean water level, and k is the wavenumber which varies with f according to the linear dispersion equation

$$(2\pi f)^2 = gk \tanh kh$$

The linear-theory predictions for the phases are $\phi_{\zeta u} = 0$, $\phi_{\zeta v} = 0$, $\phi_{\zeta w} = \frac{\pi}{2}$, and therefore also $\phi_{uw} = \frac{\pi}{2}$, $\phi_{vw} = \frac{\pi}{2}$.

The data by Thornton and Krapohl (1974) are by and large in agreement with the linear theory predictions as given above, except for an underestimate of the horizontal velocities for given surface elevation, to an amount of about 6% at the spectral peak frequency (f_m). However, only one series of records was analysed, in a long, low swell (rms wave height ≃ 0.27 m, in a depth of about 19 m). The results are therefore not indicative of the applicability of the linear theory in conditions of a steep, young sea.

Forristall et al. (1978) have estimated $H_{\zeta\tilde{u}}(f)$ from measurements in conditions of active wave generation, in tropical storm Delia. They also applied various nonlinear theories. They found that the internal velocities were better modelled by the linear theory, with allowance for directional and frequency spreading of the energy, than by any of the nonlinear theories for unidirectional, monochromatic waves. Although this is a very valuable result, the quantitative information about the estimated transfer functions presented by Forristall et al. is limited to one function $\hat{H}_{\zeta\tilde{u}}(f)/H_{\zeta\tilde{u}}(f)$ for each of three different elevations, in which $\hat{H}$ is the value of H estimated from the data. (No phase information is given.)
These show a trend with f, from a 10% underprediction of the velocities by the linear theory near $f = f_m$ to a roughly 20% overprediction near frequencies of about $2f_m$. The latter (overprediction) is stated to be "probably due to nonlinear phase locking effects between harmonics". If this "phase locking" refers to the occurrence of bound higher harmonics, then this hypothesis would seem to be untenable, since the wavenumber at a frequency $2f_m$ is smaller in the nonlinear approximation ($k_{nonlin} = 2k_m$, where $k_m \cong (2\pi f_m)^2/g$ in deep water) than it is in the linear approximation ($k_{lin} \cong (4\pi f_m)^2/g \simeq 4k_m$), which results in a slower decay of the velocities with depth beneath the surface in the nonlinear case. Thus, inclusion of this nonlinear effect would give an even greater overprediction of the velocities in the frequency range of about $2f_m$, from a given spectrum of surface elevation.

Cavaleri et al. (1978) and Cavaleri (1982) present gain functions which show an overprediction of the velocities ($\tilde{u}$ and w) by about 10% in the frequency range of high coherence between velocities and elevation. These results, although also taken in conditions of active wind-wave generation, contrast with those of Forristall et al. (1978) in the energetic band around the spectral peak. The differences with the linear theory exceed significantly the possible calibration errors which Cavaleri et al. estimate at a few % only. (It is noted that the under- or over-predictions referred to above appeared to occur systematically, which makes it very unlikely that they would be due to random sampling errors.)

The results with respect to the phases are more controversial than those for the gain functions. Shonting (1964), Yefimov and Khristoforov (1969), Cavaleri et al. (1978) and Cavaleri (1982) all reported significant out-of-quadrature relations between horizontal and vertical velocity, which would imply a mean vertical flux of horizontal momentrum. The magnitude of this estimated flux density is typically orders of magnitude larger than the wind-induced mean momentum transfer at the surface. Various ad hoc hypotheses have been advanced to "explain" the apparent anomaly. Shonting (1964) states somewhat vaguely that it "probably reflects an anomalous shore condition". Yefimov and Khristoforov (1969), Cavaleri et al. (1978) and Caveleri (1982) ascribe it (tentatively) to turbulence associated with the wave breaking occurring in a wind-driven sea. Cavaleri (1982) finds spport for this view in the fact that the strong phase anomaly ($\simeq 25^{o}$) was observed only in conditions of active wave generation; it virtually disappeared (to -5^{o}) when the wave breaking diminished as the sea transformed into swell. Despite this indication, the suggestion that the observed phase anomaly would be due to turbulence leaves many unanswered questions. To begin with, it is not clear how turbulence would cause such a drastic change in the phase relation between the wave-induced velocities. (The estimated coherence between surface elevation and velocities was quite high ($\gamma^2 > 0.98$) in the energetic frequency range, indicating that the observed velocities were virtually fully wave induced.)

Secondly, there is a substantial unbalanced momentum flux in the upper layers, since the flux calculated from the measured velocities (in a range which in the measurements by Cavaleri et al. goes up to 0.3 Hz) is orders of magnitude larger than the wind stress. Calling upon turbulence outside the measured range to compensate for this excess does not seem realistic since it is hard to see how such turbulence, which ultimately is due to the wind action on the surface, could result in a large upward flux of downwind momentum. In the opinion of the present authors, the anomalous phase differences and associated momentum fluxes referred to above should be held in doubt as long as no physical process has been identified (not just conjectured) which could explain the apparent imbalance.

In the context of phase estimates, reference is made to some preliminary results of the present study (Battjes and van Heteren, 1980) which also gave apparent phase differences which seemed to be unrealistic. These preliminary findings motivated a scrutinous investigation of the entire system of measurement and data handling, which brought to light numerous time delays which had previously been overlooked, and which by and large annulled the previously suspected anomalies (see below). Whereas this does not imply similar errors in the other references quoted above, it does indicate the great care needed in this type of analysis.

It appears from the preceding summary of previous results that there are unresolved questions about the applicability of linear wave theory for the prediction of velocities from surface elevations, with respect to gain as well as phase, particularly for conditions of active wind-wave interaction. The present study was undertaken to investigate this problem further. To that end, measurements were performed from a platform in the southern North Sea, and analyzed primarily with respect to spectral transfer functions. A secondary item of attention was the probability distribution of the velocity components, which in the linear theory should be Gaussian. Thirdly, the data have been analyzed to estimate directional spectrum parameters, but these results are reported elsewhere.

The contents of the present report are as follows. The platform and instrumentation are described first (chapters 2 and 3). Particular attention is thereby given to calibrations of sensors and other system components. The analysis procedures are described in chapter 4. This is followed in chapter 5 by a description of the environmental conditions during the measurements. The results are presented and discussed in chapter 6. Finally, the conclusions are stated in chapter 7.

2. OBSERVATION PLATFORM

The measurements were made from the platform Noordwijk (MNP), which is located in the southern North Sea, near Noordwijk, about 10 km off the Dutch coast (see figures 1 and 2). The bottom in the neighbourhood of the platform is rather flat. The local depth is about 17.3 m below MSL, and the local tidal range is about 1.8 m.

The platform rests on a jacket structure consisting of tubular elements. Four of the six main piles, which have a diameter of 0.8 m, are positioned in the corners of a rectangle of approximately 11.15 m x 18.30 m at Mean Sea Level (MSL) (see figure 3). They have a 6^{o} batter.
The orientation of the platform's longest axis is 85^{o} east from true North.

Sensor supports have been mounted vertically at three of the four corner piles of the jacket structure, extending from the platform deck to a point close to the sea bed. They are fairly transparent space trusses, with four .11 m diameter tubes in the corners of a 1 m x 1 m square. They can be lifted out of the water for attachment, inspection and cleaning of the sensors. For the measurements described here, sensors were used fixed to the support at the southwest corner of the platform (see figure 3).

3. INSTRUMENTATION

3.1 Introduction

The principal instruments used in this study were a velocity meter allowing measurements of three orthogonal velocity components, and a wave gauge for the measurement of the surface elevation. These are described below, together with calibration procedures. In this context, the problem of time delays introduced by the sensors and by the data logging system receives careful attention, because of the apparent phase errors in the results of preliminary data analyses (Battjes and van Heteren, 1980). This stimulated a detailed investigation of possible time delays, based on nominal properties of system components (Botma, 1981). The results were later verified with sinusoidal test signals. In the following presentation, the results of these investigations will be mentioned.

3.2 Velocity meter

The velocity meter is based on the principle of travel time of acoustic pulses. A meter of this type, designed for use in tidal rivers, has been described by Botma (1978), who also designed the meter used for the measurements reported here.

Three pairs of transducers were mounted in a frame, in three mutually orthogonal lines, at distances of 1.71 m (see figure 4). The frame consists of copper pipes (outer diameter 50.4 mm) to minimize marine fouling. For the same reason, the electric wiring was mounted inside the pipes. The joints of the pipes were glued to prevent corrosion.

The velocity meter was mounted outside the sensor support, with one of its axes aligned vertically. The orientation of the others was approximately from south-west to north-east (x-axis) and from south-east to north-west (y-axis), see figure 3. The distance from the vertical axis of the velocity meter to the centre of the sensor support was 1.75 m. In one set of measurements, the elevation of the center of the velocity meter was 4.91 m below MSL, and in a second set is was 7.83 m below MSL.

The calibration factor of the velocity meter was calculated using the nominal speed of sound in sea water. (Temperature and salinity variations are automatically corrected for.) An effective travel distance of 1.61 m was used. This is 10 cm less than the distance between the sensors, to allow for wake effects. The calculated calibration factor was checked experimentally by oscillating the frame rectilinearly in a laboratory basin. Two orientations were used. In one of these, one pair of sensors was aligned with the direction of the back-and-forth motion. In the other, they enclosed an angle of 45° with this direction. The calibration factor calculated beforehand turned out to underestimate the velocity by about 13% in the parallel alignment, which can be considered as an underestimate of the effective wakelength, and to overestimate it by about 4% in the case of the 45° angle, which corresponds to an overestimate of the effective wakelength. Deviations as large as were observed in the case of parallel alignment are not expected to occur in the actual measurements, because rectilinear flow does not occur at sea. In the analysis, the calibration factor calculated beforehand based on nominal values was used, with possible errors estimated not to exceed $\pm$ 5%.
As to the phase response of the velocity meter has it been assumed that the meter introduces no disturbance to the flow field, because it is very transparant and it is mounted outside the sensor support of the platform.

The velocity meter measures the velocity components along the survey lines connecting the three pairs of transducers, averaged over these lines. This averaging process acts like a low-pass filter on the velocities in the center. It introduces no phase shift. For the horizontal velocities its modulus is $\{\sin(\frac{1}{2}\vec{k}.\vec{r})/\frac{1}{2}\vec{k}.\vec{r})\}$, in which $\vec{k}$ is the wavenumber vector and

$\vec{r}$ the horizontal separation vector between the tranducers. The relative error introduced thereby is less than 3×10^{-3} in the frequency range carrying most of the wave energy in our measurements ($0.1\ \text{Hz} \lesssim f \lesssim 0.2\ \text{Hz}$). Even for $f = 0.3$ Hz it still is only 1.6×10^{-2} at most. For the vertical velocity component comparable numbers apply.

The output signals of the velocity meter lag behind the instantaneous mean velocities between the sensor pairs, due to a waiting time in an internal scanning cycle plus a first-order smoothing filter. The effective delay is 15 ms. The actual mean velocity between sensor pairs in turn may be slightly out of phase with the undisturbed one, due to the presence of the velocity meter. However, this effect is considered negliglible because the frame of the velocity meter is highly transparent.

3.3 Wave gauge

The wave gauge used for the measurements of the surface elevation was a 15 m long resistance step gauge ("TPD"-type) with electrodes spaced at 7.5 cm intervals. The gauge was mounted near the center of the sensor support, at a distance of 1.90 m to the vertical axis of the current meter (projected horizontally).

The calibration of the gauge itself was taken at its nominal value, determined by the distance between the electrodes.

The wave gauge output signal lags behind the instantaneous surface elevation, due to waiting times in an internal scanning cycle and a frequency smoothing. The effective delay is 52 ms. This is $\Delta t_1 = 52\ \text{ms} - 15\ \text{ms} = 37\ \text{ms}$ more than it is for the velocity signals.

Possible effects due to scattering of the incident waves by the sensor support and by the platform piles are considered in the following.

To investigate whether the fluctuations of the surface elevation inside the sensor support differed significantly from those outside, tests were carried out in a laboratory flume using a 1:5 model and periodic waves. Due to limitations of the flume and the wave generator, the model waves had a shorter wavelength, compared to the dimensions of the sensor support, than those in the field (roughly a factor 3). This is expected to give rise to an exaggerated scattering of the waves in the model. Surface elevations were measured inside and outside the model sensor support, in the same flume cross-section, for a variety of incident waves. The measurements were made with the cross-sectional diagonal of the support either parallel to the flume axis or at 45°. No significant difference could be observed due to the orientation. The measured ratios H_{in}/H_{out} were also found to be independent of wave steepness (in the range $0.016 < H/L < 0.066$); their average value is 0.98, with a standard deviation of 0.03. Phase shifts between the undisturbed surface elevations and those inside the sensor support were found to be less than 1% of the waveperiod, or less than about 4°. Considering these results, and the fact that in the model the influence of the support is expected to be exaggerated (see above), no corrections were made to the surface elevation measurements to allow for such influence.

The possible disturbances to the incident waves due to the platform support structure were estimated theoretically. To this end, the scattering of the waves by the nearest corner pile (diameter 0.80 m) was considered. This pile was taken to be vertical, at a distance of r = 3 m from the wave gauge.

The linear, potential-flow solution to the problem of the scattering of a plane, periodic wavesystem by a rigid impermeable circular cylinder, positioned vertically, has been given by Lamb (1932, art. 304). We will only need the approximation to the exact solution for the case of a slender pile, $ak \ll 1$, in which a is the pile radius and k is the wavenumber.

If the surface elevation of the incident waves is given by

$$\eta(x,y,t) = \mathrm{Re}\, e^{i(kx+\sigma t)}$$

then the elevation of the scattered wave is approximated as

$$\tilde{\eta}(r,\theta,t) = \mathrm{Re}\frac{\pi}{4}(ka)^2\{iH_0^{(2)}(kr) + 2H_1^{(2)}(kr)\cos\theta\}e^{i\sigma t} + 0(ka)^4$$

where $(x,y) = (r\cos\theta\ ,\ r\sin\theta)$, and the pile is centered at $(x = 0,\ y = 0)$. $H_n^{(2)}$ is the Hankel function of the second kind of order n. (Lamb uses the notation D_n , where $D_n(kr) = -iH_n^{(2)}(kr)$.) Using

$$H_n^{(2)}(kr) = J_0(kr) - iY_0(kr),$$

and neglecting the terms of $0(ka)^4$, the amplitude of the scattered waves relative to that of the incident waves is expressed as

$$\hat{\tilde{\eta}} = \frac{\pi}{4}(ka)^2\{J_0^2 + Y_0^2 + 4(J_1Y_0 - J_0Y_1)\cos\theta + 4(J_1^2 + Y_1^2)\cos^2\theta\}^{\frac{1}{2}}$$

where $J_0 = J_0(kr)$, etc. The maximum value of $\hat{\tilde{\eta}}$, considered as a function of θ at r = const., is

$$\hat{\tilde{\eta}}_{max} = \frac{\pi}{4}(ka)^2\{J_0^2 + Y_0^2 + 4|J_1Y_0 - J_0Y_1| + 4(J_1^2 + Y_1^2)\}^{\frac{1}{2}}$$

For $\hat{\tilde{\eta}}_{min}$, a similar expression holds, which is not shown here. Using $a = 0.4$ m , $r = 3.0$ m and $h = 17.5$ m (the latter is needed in the dispersion equation) the following values result for 3 different frequencies:

f [Hz]	ka	kr	$\hat{\tilde{\eta}}_{max}$	$\hat{\tilde{\eta}}_{min}$
0.1	.022	.163	.0038	.0005
0.2	.066	.500	.013	.002
0.3	.145	1.09	.037	.009

It appears that in the frequency range from 0.1 Hz to 0.2 Hz, which is the most energetic range in our measurements, the scattering of the waves by the nearest corner pile affects the measurements by relative amounts of the order of 10^{-3} to 10^{-2} at most, which is negligible for our purposes.

3.4 Anemometer

Measurements of wind speed and direction were made with an anemometer (type Munro, Mark 4) and a vane, both mounted on a 9.5 m high mast at an elevation of 28 m above MSL.

3.5 Data acquisition system

A 32-channel data logging and transmission system has been used to collect the data and transmit them by an FM-radio-link to a shore-based receiving station where they were recorded on magnetic tape.

Before scanning for transmission, all data had to be converted to a suitable format. For the velocity meter, which has a DC output, the delay caused hereby is only 1 ms, but the wave gauge signal requires a frequency counting, resulting in a total interface delay of 367 ms, or Δt_2 = 367 ms - 1 ms = 366 ms more than for the velocity signals.

The scanning procedure itself and the subsequent read-out for data entry in the analysis procedures cause additional lags. The velocity signals (u,v,w) and the elevation signal (ζ) were fed to adjacent channels, which were scanned at 6.25 ms intervals, in the order cited. However, in the data read-out the elevation value of one scanning cycle was combined with the velocity values of the following cycle, causing a lag of 250 ms. Thus, the procedure of scanning and read-out introduces a lag of the elevation signal behind the velocity signals given by $\Delta t_{3,w} \simeq$ 250 ms - 6 ms $\simeq$ 244 ms, $\Delta t_{3,v} \simeq$ 250 ms - 12 ms $\simeq$ 238 ms and $\Delta t_{3,u} \simeq$ 250 ms - 19 ms $\simeq$ 231 ms.

A summary of the time lags mentioned above is given in the following table, under the heading "nominal", because these values have been calculated from nominal system properties.

Lag of ζ behind	Nominal					Meas'd
	Δt_1	Δt_2	Δt_3	$\sum_{i=1}^{3} \Delta t_i$	$\sum_{i=2}^{3} \Delta t_i$	$\sum_{i=2}^{3} \Delta t_i$
u	37	366	231	634	597	589
v	37	366	238	641	604	595
w	37	366	244	647	610	601

Table A - Summary of system delay times, expressed in ms.

A partial check on the nominal values has been carried out by simulating sensor outputs with sinusoidal test signals at different frequencies, and by subjecting these to the standard procedure of interface conversion (Δt_2), scanning and read-out (Δt_3), and subsequent cross-spectral analysis. The resultant phase lags between simulated velocities and simulated elevation showed very nearly a linear variation with frequency, as expected from a constant time shift (see fig. 5 for an example). The values of the time shift calculated on this basis are given in the last column of table A given above. They serve as a check on ($\Delta t_2 + \Delta t_3$) of which the nominal value is given in the next-to-last column. There is a difference of less than 10 ms between the two sets, which is negligible in comparison to the wave periods involved.

4. DATA ANALYSIS PROCEDURE

4.1 Introduction

The data analysis to be reported in this chapter was aimed primarily at estimating spectral transfer functions between velocity components and between these and the surface elevation. A secondary objective was the estimation of probability densities of instantaneous values of the measured quantities. In addition to this, directional spectral densities were estimated, but that aspect is not discussed here. We will use only one result of the directional analysis, viz. the principal direction of propagation (θ_o) of the sea or swell as function of f.

4.2 Estimation of auto- and cross-spectra

The analyses were performed on 30-minute long records, digitized with Δt = 0.25 s. No dilution of the data was applied, so that the Nyquist frequency is at f = 2.0 Hz. This was deemed high enough to prevent significant aliasing.

Standard spectral analysis procedures as described e.g. by Bendat and Piersol (1972) and Jenkins and Watts (1968) were used. These included corrections for missing data or unaccountable values and removal of sample mean and linear trend. Singleton's (1969) FFT algorithm was applied for the spectral calculations.

The records were divided into 30 segments of 60 s each. No data or spectral window was applied, so that the resulting spectral estimates each had 60 degrees of freedom, except those at zero frequency and at the Nyquist frequency, which had 30. Using the χ^2-distribution, the lower- and upper bounds of the 90%- confidence bands of the estimates of the auto-spectra are 0.72 and 1.32 times the sample estimate in case of 60 degrees of freedom.

Each estimated spectrum is here denoted as $\hat{S}_{xy}(f)$, with subscripts indicating the processes of which it is the auto- or cross- spectrum. The auto-spectra have been made one-sided, so that their integral over all positive frequencies equals the variance of the process.

4.3 Estimation of coherence spectra

The cross-spectra have been normalized to spectra of coherence. In case of $\zeta(t)$ and $w(t)$ this is written as

$$\hat{\gamma}^2_{\zeta w}(f) = \frac{|\hat{S}_{\zeta w}(f)|^2}{\hat{S}_{\zeta\zeta}(f)\ \hat{S}_{ww}(f)}$$

90% confidence bands for the coherence were calculated using the expressions presented by Bendat and Piersol (1972, par. 6.6). These authors limit the validity of their expressions for the confidence interval of $\hat{\gamma}^2$ to the range $0.35 \leq \hat{\gamma}^2 \leq 0.95$. Outside this range no confidence bands were calculated.

In the following, coherence values are used only for the vertical velocity in relation to the surface elevation, in which case its theoretical value in absence of noise is 1 (assuming linearity). The coherences between a horizontal velocity component (u or v) and surface elevation (ζ) or vertical velocity (w) depend on the directional wave energy distribution. In fact, their values are used in estimating that distribution. Since this subject is not dealt with here no coherence values involving u or v are presented.

4.4 Estimation of phase spectra

Phase spectra were derived from cross-spectra according to

$$\hat{\psi}_{xy}(f) = \arg \hat{S}_{xy}(f)$$

Confidence bands on this estimate were calculated using the equations presented in Bendat & Piersol (1972, par. 6.7).
The spectral calculations were made without taking into account the time delays mentioned in chapter 3, which became known at a later date. The phase angles $\hat{\psi}_{\zeta w}(f)$, calculated as indicated above, therefore had to be corrected to account for a time shift, which was approximated as a constant Δt = .64 s (see table A). The corresponding phase correction is $\Delta\hat{\psi} = -2\pi f\Delta t$. (The definitions adopted imply that a positive value of ψ indicates a lag of ζ behind u, v or w.) A final phase correction was applied to account for the fact that the center of the velocity meter was 1.90 m from the wave gauge (projected horizontally; see figure 3), causing an additional phase lag of ζ behind w given by kr cos Θ, in which r = 1.90 m is the horizontal distance between the sensors, k is the wave-number and Θ is the propagation direction relative to the direction from velocity meter to wave gauge. The magnitude of this correction was calculated per frequency, using the linear dispersion equation. The principal propagation direction per frequency, $\Theta_o(f)$, as determined in the directional analysis (van Heteren and Keijser, 1981), was used as an estimate of Θ. The maximum value of this correction (assuming $\Theta = 0^o$) corresponds to a time shift of about 0.2 s in the most energetic frequency range (f between 0.1 Hz and 0.2 Hz). Altogether, the corrected estimated phase values become

$$\hat{\phi}_{\zeta w}(f) = \hat{\psi}_{\zeta w}(f) - 2\pi f\Delta t - kr \cos \Theta_o(f)$$

Cross spectra between w and either u or v were also calculated. Phase angles were calculated as arg $\hat{S}_{uw}$ or arg $\hat{S}_{vw}$. The only correction which is needed here is due to the scanning sequence, which causes a lag of 6.25 ms in case of (v,w) and 12.50 ms in case of (u,w).

In the data given below, either $\hat{\phi}_{uw}(f)$ or $\hat{\phi}_{vw}(f)$ of a record have been presented. The choice between u and v was determined by the criterion that the component should be used which most nearly coincided with the principal wave propagation direction, in order to maintain a reasonably high coherence.

4.5 Estimation of gain spectra

In order to eliminate possible influences of noise, the gain function $H_{\zeta w}(f)$ was estimated according to

$$\hat{H}_{\zeta w}(f) = \frac{|\hat{S}_{\zeta w}(f)|}{\hat{S}_{ww}(f)}$$

Confidence bands for $\hat{H}_{\zeta w}(f)$ were calculated, using the procedure described by Bendat and Piersol (1972, par. 6.7).

The horizontal velocity components require a separate treatment, because of the directional distribution of the wave energy. Gain functions were calculated for the resultant velocity in the horizontal plane ($\tilde{u}$) according to

$$\hat{H}_{\zeta\tilde{u}}(f) = \{\frac{\hat{S}_{uu}(f) + \hat{S}_{vv}(f)}{\hat{S}_{\zeta\zeta}(f)}\}^{\frac{1}{2}}$$

and

$$\hat{H}_{w\tilde{u}}(f) = \{\frac{\hat{S}_{uu}(f) + \hat{S}_{vv}(f)}{\hat{S}_{ww}(f)}\}^{\frac{1}{2}}$$

This procedure does not permit the estimation of confidence bands. Instead, these gain function values were calculated in a frequency band which was considered to be virtually free of noise, as indicated by a value of at least 0.9 of $\hat{\gamma}^2_{\zeta w}(f)$.

4.6 Estimation of probability densities

A partial check on the validity of the Gaussian model for sea waves was carried out by considering the statistical distribution of the instantaneous values of ζ , u , v and w, and by comparing it to the best fitting Gaussian distribution.

To this end, a histogram was calculated from the 7200 data points of each sample function, with a class interval of 0.10 m for ζ and of 0.02 ms^{-1} for u, v and w. No dilution of the data was applied, as would be needed to have independent samples only. Therefore, conventional quantitative tests of goodness-of-fit do not apply. A visual inspection was carried out instead.

5. OBSERVATIONS

5.1 Data sequences

In the period of the measurements, series of 30-minute records were made of the surface elevation and of the velocity components. In addition, the following parameters were calculated and printed every half hour: 10-minute averages of wind speed and direction, tidal elevation, magnitude and direction of tidal current, and significant wave height.

In order to minimize possible disturbances due to turbulence induced by tidal currents, particularly in the wake of the platform support structure, only recordings made around the times of slack water were used in the analyses reported here. The criterion adopted was that the current velocity should not exceed 0.25 ms^{-1}. An additional consequence of this selection is the virtual absence of Doppler frequency shifts in the observations (current velocity less than 0.03 times the phase speed in the energetic frequency range $f < 0.2$ Hz).

Two sets of measurements were made. In the first set, six series (number 4 through 9) were recorded, with the center of the velocity meter at 4.91 m below MSL. Of this series, 23 records were used in the analysis (record 401 through 905). Unfortunately, no surface elevation data were obtained in this entire set in or near the same vertical in which the velocities were measured, so that the data of this set could be analyzed only with respect to the velocity signals and their interrelationships.

A second set of measurements was made with the center of the velocity meter at 7.83 m below MSL. Of this set, 37 recordings were analyzed with respect to the velocities, the surface elevation, and their interrelationships (records 1501 through 2605).

5.2 Wind and sea conditions

Hourly values of the principal parameters of wind and waves on the days of the recordings are presented graphically in Appendix 1. A tabular summary of the values at the times of the recordings which were analyzed is given in Appendix 2. The following quantities pertaining to tides and wind are listed in Appendix 2: record number, date, time of record, mean water elevation above MSL, x- and y-components of mean velocity ($\bar{u}$, $\bar{v}$), 10-minute average wind velocity (V_w), and wind direction with respect to true North (Θ_w). Appendix 3 gives the principal direction of the waves with respect to North (Θ_o) at the peak frequency of the variance spectrum (f_m), significant wave height (Hm_0, calculated as $4\sqrt{m_0}$, in which m_0 is the variance of ζ), peak frequency (f_m), and finally wave age β and steepness γ, defined as

$$\beta \equiv \frac{c_m}{V_w} \quad \text{and} \quad \gamma \equiv \frac{H_s}{L_m}$$

in which

$$L_m = \frac{c_m}{f_m} = \frac{g}{2\pi f_m^2} \tanh \frac{2\pi h}{L_m}$$

The conditions ranged from a mild easterly (i.e., offshore) wind ($V_w \simeq 6$ ms^{-1}) and a low swell ($H_s \simeq 0.8$ m, wave steepness $\gamma \simeq 0.01$, wave age $\beta \simeq 2$) in the series 15, to a westerly gale (maximum $V_w \simeq 24$ ms^{-1}) with a pure sea ($H_s \simeq 4$ m, $\gamma \simeq 0.04$, $\beta \simeq 0.6$) in series 26. (Actually, the maximum wind velocity of 24 ms^{-1} occurred about 1½ hour prior to the first record in this series, nr. 2601; at the time of this recording the wind velocity had dropped to about 20 ms^{-1}.) Less severe but still pure sea conditions prevailed in the series 6, 9 (first part only), 16/17, 22/23, 24 and 25. The wave age β in these series is in almost all records less than 0.8. Series 4, 7 and 18 are cases of mixed sea and swell, with two peak frequencies, of which however only one is listed in Appendix 2, viz. the one with the highest spectral density.

6. RESULTS AND DISCUSSIONS

6.1 Introduction

In Appendix 4 through Appendix 10, a number of spectra of variance, coherence, phase and gain have been plotted as examples. In most cases, the first records of each series of the second set of measurements have been used for this purpose (records 1501, 1601, etc.). This set includes velocity and elevation data.

The spectral estimates have been plotted at a frequency interval of $\frac{1}{60}$ Hz from $\frac{1}{60}$ Hz to $\frac{20}{60}$ Hz. At higher frequencies the energy levels become quite low.

The results will be discussed in terms of spectral relationships between measured variables, as expressed in terms of coherence, phase and gain. The variance spectra of the surface elevation and their variation with wind speed etc. are not discussed since this study is not aimed at wave growth or wave forecasting. For overall measures of the sea state per record, reference is made to Appendix 3.

6.2 Coherence spectra

The coherence between elevation and vertical velocity (Appendix 4) is in all measurements close to 1 ($\hat{\gamma}^2_{\zeta w} > 0.95$) in the central, energetic frequency band. This is significant since it implies a virtually linear relation between $\zeta(t)$ and $w(t)$. It is pointed out that this conclusion holds for all the records which were analyzed, regardless of the windspeed, the wave age or the wave steepness.

A further consequence of the high observed coherence-values is that the sampling variability in the estimates of phase and gain spectra is low. The total widths of the 90% confidence intervals for these quantities in the energetic frequency band are typically less than 5^o for the phases and less than 10% of the theoretical values for the gains.

The latter value does not include an uncertainty in the calibration of the velocity meter, which however was estimated not to exceed 5% (see par. 3.2).

6.3 Phase spectra

The estimated phase lead of w with respect to ζ (Appendix 4) is in most cases in agreement with the theoretically expected value of 90°, in the sense that the latter is usually within the estimated 90%-confidence interval of the estimate. The average of $\hat{\phi}_{\zeta w}(f)$ in the energetic frequency band of each spectrum deviates generally less than 2° in absolute value from the theoretically expected value of 90°.

The majority of the estimated phase spectra $\hat{\phi}_{\zeta w}(f)$ show a weak trend with frequency, of about $6^{\circ}/(0.3$ Hz) or 20°/Hz, corresponding to a delay of ζ behind w by about 0.05 s.
Note that delays in the signal processing are already accounted for, to an estimated accuracy of 10 ms (par. 3.5). The observed delay is possibly due to the fact that the short-crestedness of the waves was not taken into account in the correction $kr \cos \Theta_o(f)$ (see par. 4.4). The use of the principal direction Θ_o only leads to an overestimation of the delay of ζ behind w which increases with increasing frequency. This is qualitatively in agreement with the observed trend. Furthermore, if this explanation is correct, no trend is expected in $\hat{\phi}_{uw}(f)$ and $\hat{\phi}_{vw}(f)$, since u, v and w have been measured in the same verticals. This agrees with the results of the measurements (see below).

The phase spectra $\hat{\phi}_{\zeta w}(f)$ of some records (1601, 2201, 2301, 2501) deviate from the general pattern in the sense that for low frequencies, where the levels of energy and coherence are low, the estimated phases deviate strongly from the expected value, to such extent that the latter is well outside the 90% confidence interval. Theoretically, the fact that the low-frequency energy level is low relative to that in the peak should not matter. Even the fact that the coherence drops to low values should not matter in the sense that this is reflected in the divergence of the upper and lower limits of the confidence band on $\hat{\phi}_{\zeta w}$.

The fact that in this low-frequency band we may still be measuring physically meaningful values is suggested by the behaviour of the estimated gain function $\hat{H}_{\zeta w}$. Yet the indicated phase relation in the low-frequency range does not seem realistic. A satisfactory explanation has not been found. However, the problem is not of much practical importance in view of the low energy levels for those frequencies where it occurs.

In the case of record 2601, the estimated phase lag of ζ behind w appears to differ significantly (about 8°) from the theoretical value in the central, energetic frequency range. In this range, the coherence is nearly 1 (as in all other records), which indicates near-linearity, so that the apparent discrepancy in the phase cannot be ascribed to nonlinear behaviour. No satisfactory explanation for this erratic result has been found.

With respect to the phase spectra $\hat{\phi}_{uw}(f)$ and $\hat{\phi}_{vw}(f)$ (Appendix 7), which are of particular interest in view of the controversy mentioned in the Introduction, similar comments apply as in the case of $\hat{\phi}_{\zeta w}(f)$. Here again the theoretically expected value of 90° is generally within the 90% confidence interval of the estimate. The average per record of the estimates in the energetic frequency band deviates generally less than 2° from 90°, record 2601° again being the exception, with an average deviation of about 8°, the same as was found for $\hat{\phi}_{\zeta w}$. The spectra $\hat{\phi}_{uw}(f)$ and $\hat{\phi}_{vw}(f)$ generally have no trend with frequency, in contrast to $\hat{\phi}_{\zeta w}(f)$. This fact, together with the absence of any visible influence of the principal wave propagation direction, is evidence that there is no significant time delay in the velocity measurements induced by the velocity sensors or their support structure. (The electronic delays have been accounted for - see par. 3.5).

The results concerning $\hat{\phi}_{uw}(f)$ and $\hat{\phi}_{vw}$ confirm the theoretically predicted quadrature relation between horizontal and vertical velocities. It is emphasized that this conclusion is based on data obtained in a wide range of wind- and sea conditions, including numerous cases of active wave generation for which some previous studies had given large deviations from quadrature, with resultant estimated momentum fluxes which could not be balanced by identified physical processes.

Cavaleri (1982) found a different phase relation between horizontal and vertical velocities for swell than for a wind-driven sea, but - - as noted above - the present data do not show such behaviour. An illustration of that is afforded by a comparison of the results of record 1501 (swell; windspeed $\simeq$ 4 ms^{-1} ; wave age $\simeq$ 2.3) to those of record 1601 (young sea; windspeed $\simeq$ 17 ms^{-1} ; wave age $\simeq$ 0.5). Their phase spectra (Appendix 7) are not essentially different.

6.4 Gain spectra

The gain spectra $\hat{H}_{\zeta w}(f)$ and $\hat{H}_{\zeta \tilde{u}}(f)$ have been compared to the linear-theoretical values in various ways. Values of $\hat{H}(f)$ and $H(f)$ have been plotted in one graph. These data have been replotted as the ratio $R(f) \equiv \hat{H}(f)/H(f)$. The same ratios, taken at $f = f_m$, have for all analyzed records been tabulated. Finally, logarithmic plots are given of variance spectra of vertical velocity and horizontal velocity, as calculated directly from the velocity measurements, compared to those calculated from the estimated surface elevation spectrum using linear theory.

Inspection of the figures in Appendix 4 and 8 shows that in most cases the theoretical values of $H_{\zeta w}(f)$ are within the 90% confidence interval of the estimate, and that $\hat{H}_{\zeta \tilde{u}}(f)$ (for which no confidence interval can be specified) is generally within $\pm$ 10% of $H_{\zeta \tilde{u}}(f)$ in the frequency interval on which $\hat{\gamma}^2_{\zeta w} > 0.9$. The records 2420 and 2501 form an exception to this, in particular record 2501.

It appears from the figures in Appendix 5 and 9 that the ratio $R_{\zeta w}(f)$ shows no trend with frequency, whereas $R_{\zeta \tilde{u}}(f)$ in general shows some increase with increasing f. It is likely that this trend is due to an increase in noise/signal ratio in the velocities with increasing frequency, because of turbulence. In this context it is important to note that $\hat{H}_{\zeta \tilde{u}}(f)$ was calculated from autospectral densities. This would explain why the trend is not present in $\hat{H}_{\zeta w}(f)$, which has been calculated by cross-spectral analysis, thereby eliminating possible noise. Further evidence for this view is available in the variance spectra, shown in Appendix 6 and 10.

Those for $\tilde{u}$ (strictly speaking, $S_{uu} + S_{vv}$) behave quite similarly to those for w, viz. in the energetic frequency band there is by and large agreement between directly measured velocity spectra and those calculated from the surface elevation, and an increasing underestimation of the measured velocities with increasing frequency. Moreover, this underestimation is similar between $\tilde{u}$ and w, as would be expected if the difference would be due to turbulence.

The trend in $R_{\zeta\tilde{u}}(f)$ in the present data is opposite to the one found by Forristall et al. (1978). It is pointed out that the trend in their data cannot be ascribed to high-frequency turbulence (nor to nonlinear bound higher harmonics - see the comments about this in the Introduction).

Since the ratio $R_{\zeta w}(f)$ shows no trend with f, and $R_{\zeta\tilde{u}}(f)$ only a weak one, the values of these rations at the peak frequency ($f = f_m$) are more or less representative for each record, apart from sampling variability within each record. Their values are listed in Appendix 11 for all the records. Plots of these values against wave steepness (not shown here) showed that these variables were not correlated, although on theoretical grounds a correlation could be expected. The average and standard deviation of $R_{\zeta w}(f_m)$, $R_{\zeta\tilde{u}}(f_m)$ and $R_{w\tilde{u}}(f_m)$, as determined from all analyzed records (a total number indicated by n), are listed in Table B.

	n	Av.	St.dev.
$R_{\zeta w}(f_m)$	37	1.00	0.08
$R_{\zeta\tilde{u}}(f_m)$	37	0.95	0.05
$R_{w\tilde{u}}(f_m)$	60	0.96	0.05

Table B.

These values suggest excellent agreement with the linear theory for the vertical velocities and a systematic overprediction of the horizontal velocities by an estimated 5%. However, it should be remembered that the

calibration may be systematically $\pm$ 5% off, so that it would be better to say that on the average the data are consistent with the theory to within a margin of $\pm$ 5%.

6.5 Probability densities of instantaneous values

Sample histograms of u, v, w and ζ of records 1501 and 1601 are presented in Appendix 12. These records are of a low swell in a very light wind (wave age $\beta \simeq 2.26$, steepness $\gamma \simeq 0.017$, $V_w \simeq 4$ ms^{-1}, see Appendix 3) and of a young sea in a strong wind ($\beta \simeq 0.54$, $\gamma \simeq 0.037$, $V_w \simeq 17$ ms^{-1}) respectively. The corresponding least-squares best-fitted Gaussian probability density functions have been plotted for comparison.

It has been noted above (par. 4.6) that all sampled values of each record at intervals of 0.25 s have been included in the histograms, so that the samples are highly dependent. For such cases, no meaningful, quantitative test of goodness-of-fit seems to have been developed. Only a visual inspection has been carried out. This indicates an acceptable fit in all cases. It is noteworthy that there is no obvious difference in this respect between the swell records (1501) and those taken in conditions of active wave generation (1601).

7. SUMMARY AND CONCLUSIONS

Measurements have been performed of surface elevation and internal velocities in the frequency range of wind-generated waves at a location in the southern North Sea, 10 km off the Dutch coast, where the depth is about 17 m. Velocities were measured at two different elevations, viz. approximately 9 m and 12 m above the sea bed. The data cover a wide range of conditions of wind and sea, from young sea to old swell, including mixed cases. Significant wave heights reached values up to 3.7 m, whereas the most energetic frequency band typically extended from 0.1 Hz to 0.2 Hz.

The data have been analyzed mainly with respect to spectral transfer functions, in an effort to verify linear theory predictions.

The preceding chapter has dealt with results for various aspects separately, and in some cases with results of individual records if they were seen to deviate from the general pattern. This procedure gives perhaps undue weight to exceptional cases. A more global presentation is given here, which focusses on the overall picture emerging from the results.

In the summary of the results, a distinction is made between relations of the vertical velocity to surface elevation, those of the horizontal velocity to surface elevation, and those between the horizontal velocity and the vertical velocity. These cases are affected differently by directional spreading, noise and calibration errors.

Relation between vertical velocity and surface elevation

The results in this category can be affected by calibration errors in the wave gauge and in the velocity meters, with a possible systematic error in the estimated transfer function which is estimated to be less than 4^{o} in phase and 5% in gain. There is theoretically no bias due to directional spreading of wave energy or noise. Estimation of sampling variability is possible by standard methods.

Results

(1) The estimated squared coherence exceeds 0.95 in the energetic frequency band.

(2) The theoretical phase difference of 90° is generally within the 90% confidence band of the estimate (based on sampling variability).

(3) The estimated phase difference shows a weak trend with frequency, corresponding to a time shift of a few tens of ms.

(4) The average of the estimated phase difference in the energetic, coherent frequency band (per record) is generally within $\pm 2^{\circ}$ of the theoretical value of 90°.

(5) The theoretical value of the gain function is generally within the 90% confidence band of the estimate (based on sampling variability).

(6) The ratio of the estimated gain function value to the theoretical one shows no trend with frequency.

(7) Said ratio deviates generally less than 5% from unity in the energetic, coherent frequency range.

(8) The set of values of said ratio at the peak frequency, for all analyzed records (Table B), has an average of 1.00 and a standard deviation of 0.08.

(9) The value of said ratio at the peak frequency is not correlated with wave steepness or wave age.

The high coherence (item 1) implies an approximately linear relation between vertical velocity and surface elevation; the validity of this conclusion is independent of phase- or gain errors in calibration.

The estimated phases are as close to the linear theory prediction as can be expected in view of sampling variability and calibration errors. The observed trend (item 3) is possibly due to the fact that short-crestedness was not accounted for in the phase correction for the horizontal separation between the two sensors.

As far as the gain function is concerned, item (6) is a confirmation of its frequency-dependence as predicted by linear theory, regardless of possible calibration errors. Items (5), (7) and (8) confirm the theoretical prediction in absolute value to within the experimental error.

Relation between horizontal velocity and surface elevation

Because of directional energy spreading, the gain function is estimated from autospectra, rather than cross-spectra, so that the results can be contaminated (biassed) with noise. The results listed below pertain to the most energetic frequency interval, in which noise is expected to be of minor influence, as determined by the condition that the estimated squared coherence between vertical velocity and surface elevation should exceed 0.9.

Results

(10) The estimated gain function is generally within $\pm$ 10% from the theoretical value.

(11) The ratio of estimated gain function value to the theretical one shows a slight trend from overprediction to underprediction of the velocities with increasing frequency.

(12) The set of values of said ratio at the peak frequency, for all analyzed records, has an average of 0.95 and a standard deviation of 0.05.

(13) Said ratio, evaluated at the peak frequency, is not correlated with wave steepness.

These results are consistent with linear theory to within the experimental error. The trend mentioned in item (11) can be ascribed to relatively higher noise (turbulence) levels with increasing frequency. (This is not inconsistent with item (6) because in that case the noise has been eliminated from the estimate.)

Relation between horizontal and vertical velocities

The results with respect to the gain function for this category are not repeated here because they are of less practical importance than the ones discussed above, and the information would largely be redundant anyway. Instead, we focus on the phase relationship, in view of its importance for the momentum fluxes in the upper layers, and the controversy associated with it.

The estimated phase relationships for this case are not biassed by directional energy spreading, nor by a possible systematic error in the estimated phase-reponse of the surface wave gauge. "Noise" in the form of turbulence can introduce a bias in the estimated phase relation between the wave-induced (coherent) velocities if there is non-zero correlation between horizontal and vertical turbulent velocity fluctuation, and if there is significant turbulence kinetic energy in the wave-frequency band. The latter is believed not to be the case in the present data because of the high coherence between vertical velocity and surface elevation.

Results

(14) The theoretical phase difference of 90° is generally within the 90% confidence band of the estimate (based on sampling variability).

(15) The estimated phase difference shows no trend with frequency.

(16) The estimated phase difference in the energetic, coherent frequency band is generally within $\pm 5^{\circ}$ from the theoretical value of 90°.

These results essentially confirm the theoretical prediction of a quadrature relation between horizontal and vertical velocity, in contrast to some previous studies. The data do not show a marked difference between sea or swell in this regard.

Statistical distributions

Statistical distributions of instantaneous values were compared to the linear-theoretically expected Gaussian probability density function. A visual inspection indicates a reasonably good fit for all records tested, both in sea and in swell. Quantitative tests of goodness of fit were not made because the samples are dependent.

Overall evaluation

The overall picture which emerges from the data is one of agreement with the linear theory - within the margin of experimental error as indicated above - concerning gain and phase between surface elevation and either horizontal or vertical velocity at some depth below the surface, as well as those between these velocity components. This conclusion rests on analysis of an extensive data set obtained in a wide range of conditions of wind and sea, including conditions of swell and active wind-wave generation.

In order to place this result in a proper perspective, it is emphasized that this study deals mainly with spectral transfer functions, and that in the most energetic frequency range only (from $0.5f_m$ to $2f_m$, say). It is pointed out specifically that it does not deal with the gradual processes of growth, propagation and decay of wind waves, nor with their microstructure at high frequencies. It is known that for these aspects nonlinearities cannot be ignored. What the present study does indicate is that given a wavefield as specified by the variance spectrum of the surface elevation, the bulk of the internal kinematics can be estimated reliably by the linear theory.

ACKNOWLEDGEMENTS

This study was carried out as part of the Coastal Research Programma (TOW) of the Department of Public Works (Rijkswaterstaat) in The Netherlands. The cooperation of the North-Sea Directorate (Rijkswaterstaat) during the measurements at MNP is gratefully acknowledged. We are particularly grateful to G. Visser, Delta department (Rijkswaterstaat), who performed a magnificent job in carrying out the computer computations. A special word of thanks is due to H.C. Botma, of the Institute of Applied Physics (TPD), who designed and built the velocity meter, and who carried out a detailed investigation of the phase response of the entire system of sensors, data transmission, storage and treatment.

The Shipbuilding Department of the Delft University of Technology supported this study by providing the Laboratory basins for the calibration of the velocity meter and for the investigation of the influence of the sensor support on the wave measurements.

REFERENCES

Battjes, J.A. and J. van Heteren, 1980.
Field measurements of wind wave kinematics.
Proc. 17th Coastal Eng. Conf., Sydney, I, 347-361.

Botma, H.C., 1978.
Acoustic flow meter for use with hydraulic models, in:
Flow measurements of fluids, North-Holland Publishing Company, 285-390.

Botma, H.C., 1981.
Some considerations about time delays in wave measurements on platform Noordwijk, Report of the Institute of Applied Physics (T.P.D.) nr. 110.288.

Bendat, J.S. and A.G. Piersol, 1971.
Random data: analysis and measurement procedures, Wiley-Interscience, N.Y.

Cavaleri, L., J.A. Ewing and N.D. Smith, 1977.
Measurement of the pressure and velocity field below surface waves.
In: Turbulent fluxes through the sea surface, wave dynamics, and prediction, Eds. A. Favre and K. Hasselmann. Plenum Press, N.Y., 257-270.

Cavaleri, L., 1982.
Directional spectra in shallow water./Proc. Conf. Wave and wind directionality, Editions Technip, Paris, 215-238.

Forristall, G.Z., E.G. Ward, V.J. Cardone and L.E. Borgman, 1978.
The directional spectra and kinematics of surface gravity waves in tropical storm Delia./J. Phys. Oc. 8, 888-909.

Heteren, J. van and H. Keyser, 1981.
Comparison of three methods to obtain directional wave spectra,
Proc. Symp. Directional Wave Spectra Applications '81, Berkeley, 116-128.

Jenkins, G.M. and D.G. Watts, 1968.
Spectral Analysis and its applications, Holden-day, San Francisco.

Lamb, H., 1932.
Hydrodynamics, Dover.

Shonting, D.H., 1964.
A preliminary investigation of momentum flux in ocean waves. Pure and Applied Geoph., 57, 149-152.

Singleton, R.C., 1969.
An algorithm for computing the mixed radix fast Fourier transform.
IEEE Trans. Audio Electro-Acoustic, AU-17, 2, 93-103.

Thornton, E.B. and Krapohl, R.F. 1974.
Wave particle velocities measured under ocean waves, J. of Geoph. Res., 79, 847-852.

Yefimov, V.V. and G.N. Khristoforov, 1969.
Some features of the velocity field in the layer of wind-driven swell,
Izv. Atm. and Ocean Phys., 5, 597-602.

List of Appendices

FIGURES

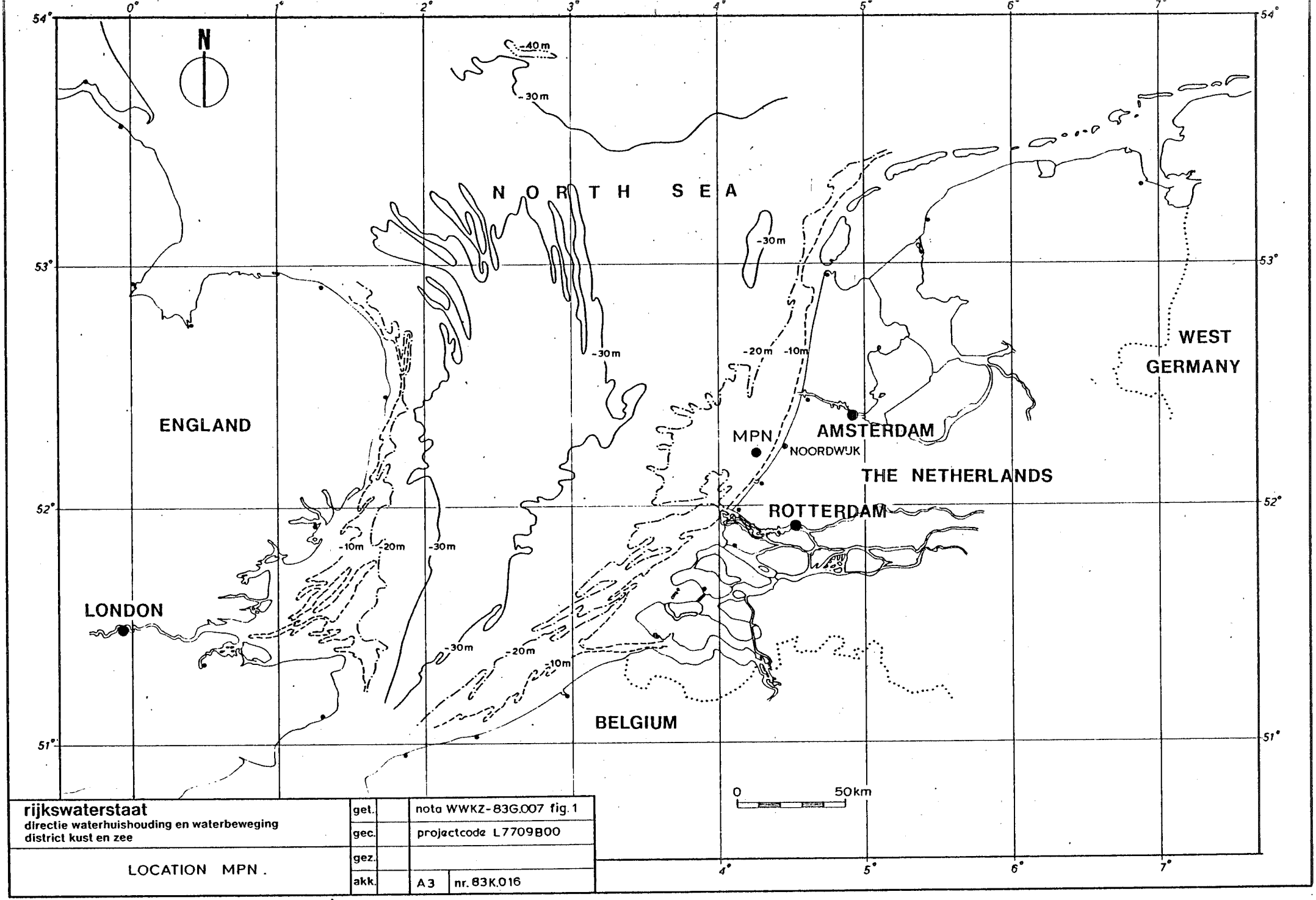

rijkswaterstaat directie waterhuishouding en waterbeweging district kust en zee	get.		nota WWKZ-83G.007 fig. 1	
	gec.		projectcode L7709B00	
LOCATION MPN.	gez.			
	akk.		A3	nr. 83K.016

rijkswaterstaat directie waterhuishouding en waterbeweging district kust en zee	get.		nota WWKZ-83G.007 fig. 2	
	gec.		projectcode L7709B00	
SIDE VIEW PLATFORM NOORDWIJK (M.P.N.)	gez.		schaal	
	akk.		A 4	nr. 83K113

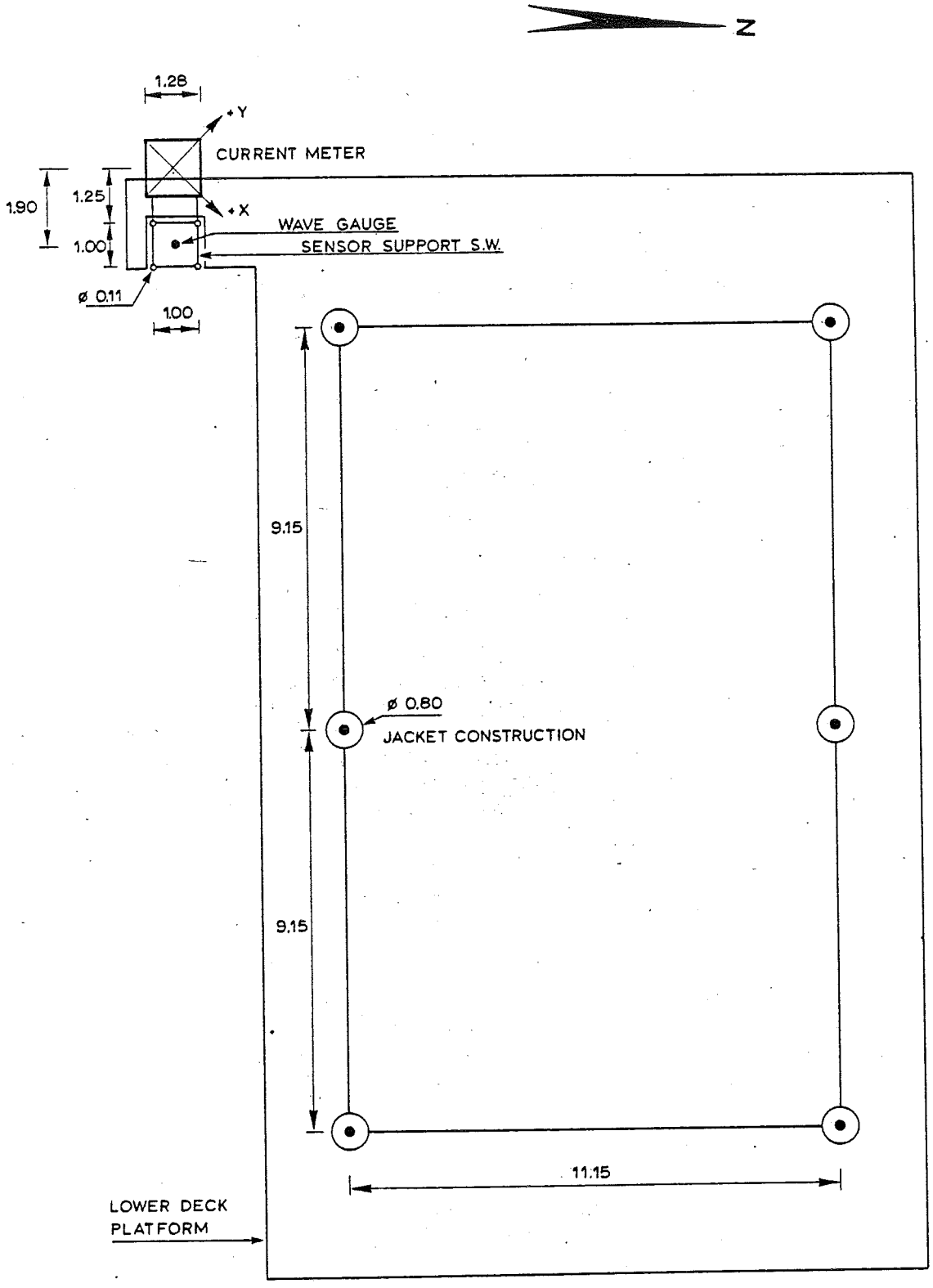

rijkswaterstaat directie waterhuishouding en waterbeweging district kust en zee	get.		nota WWKZ-83G.007 fig. 3	
	gec.		projectcode L7709B00	
SITUATION SENSORS	gez.		measures in meters.	
	akk.		A 3	nr. 83K017

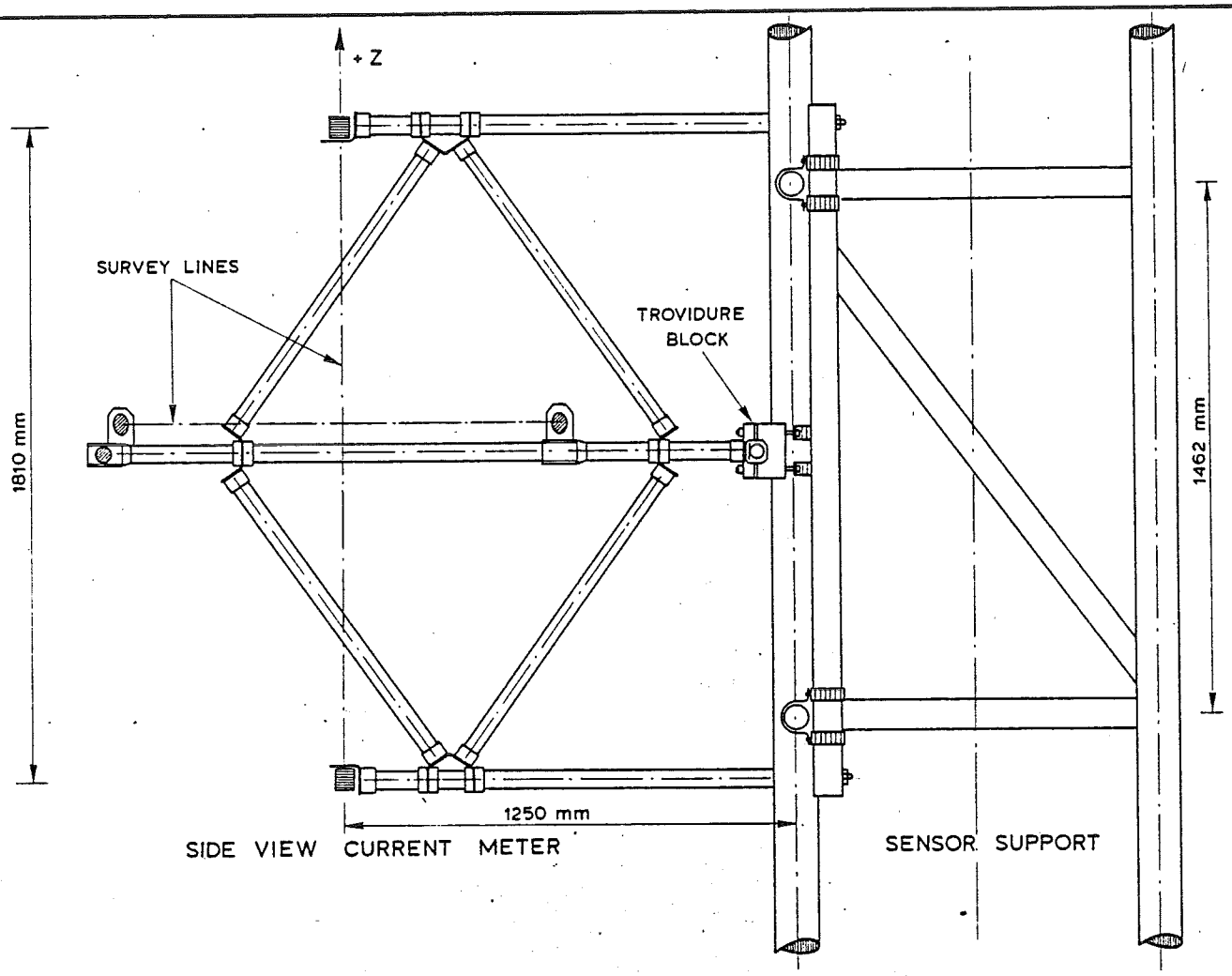

SIDE VIEW CURRENT METER

SENSOR SUPPORT

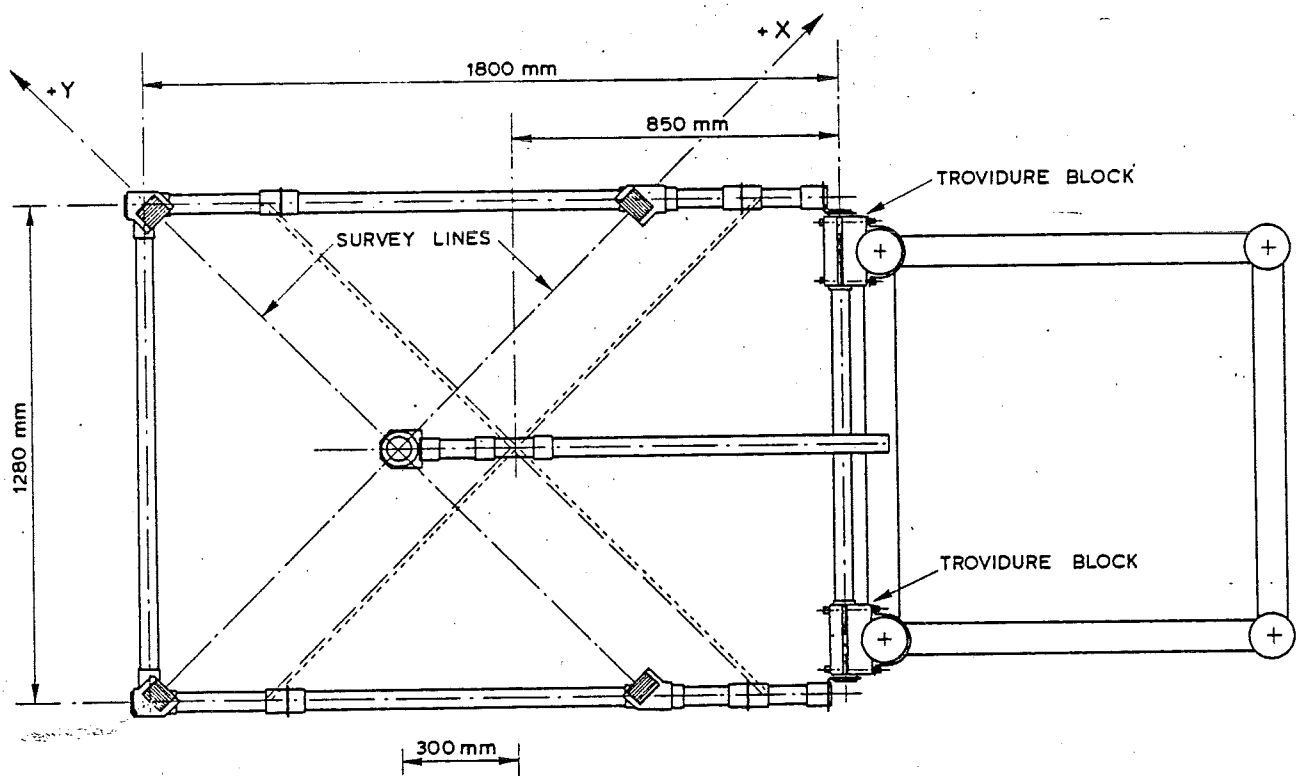

PLAN VIEW CURRENT METER

SENSOR SUPPORT

TRANSDUCER

rijkswaterstaat directie waterhuishouding en waterbeweging district kust en zee	get.		nota WWKZ-83G.007 fig. 4
	gec.		projectcode L7709B00
SIDE AND PLAN VIEW CURRENT METER WITH SENSOR SUPPORT	gez.		schaal
	akk.		A 3 nr. 83K.018

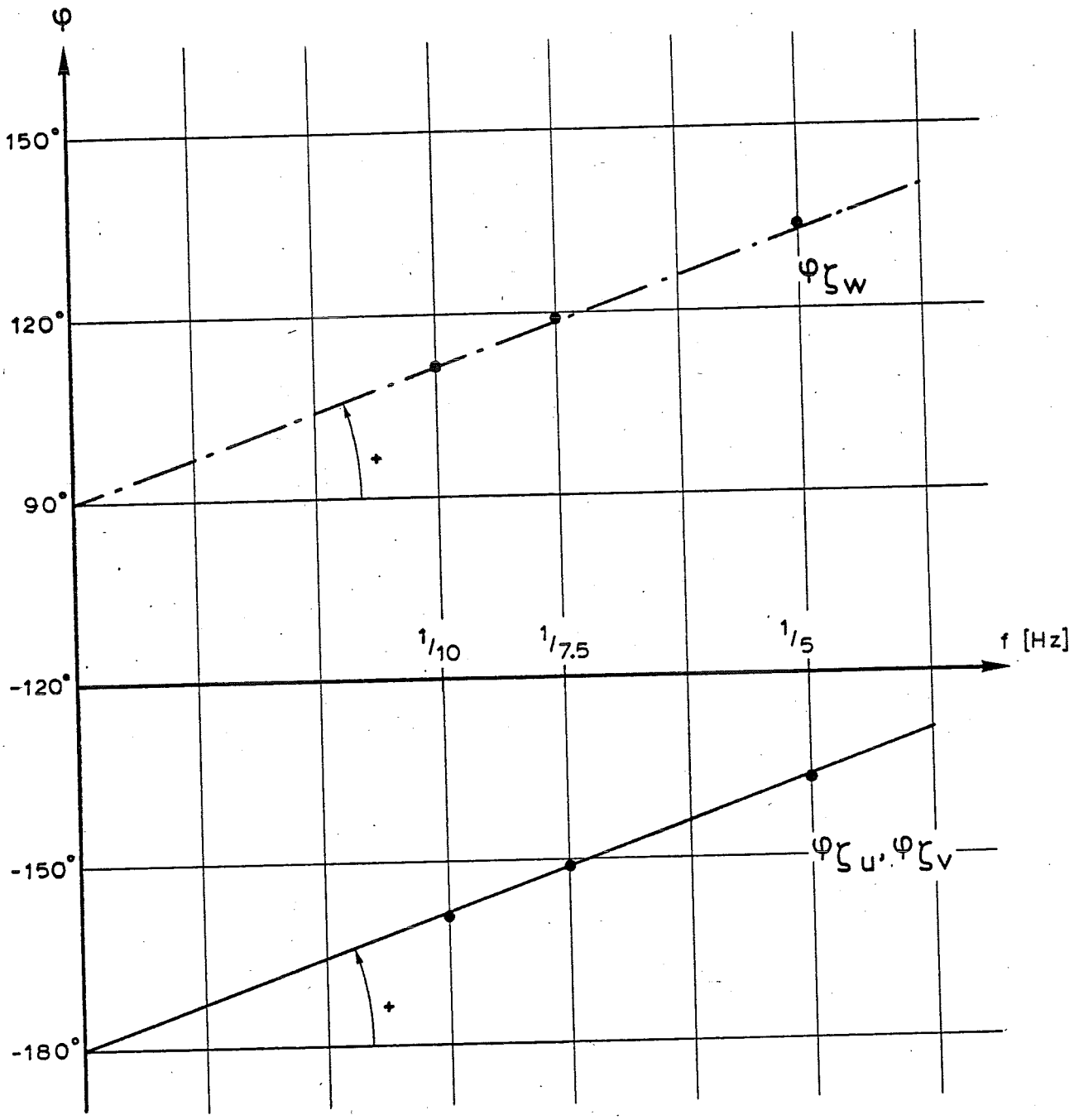

ζ - w : Δt = 0.601 s

ζ - u : Δt = 0.589 s

ζ - v : Δt = 0.595 s

rijkswaterstaat directie waterhuishouding en waterbeweging district kust en zee	get.		nota WWKZ-83G.007 fig. 5
	gec.		projectcode L7709B00
RESULTS OF INVESTIGATION TIME SHIFT DUE TO SYSTEM OF INSTRUMENTATION	gez.		schaal
	akk.		A4 nr. 83 K019

APPENDIX 1.

WIND AND WAVE PARAMETERS.

TAPE 4

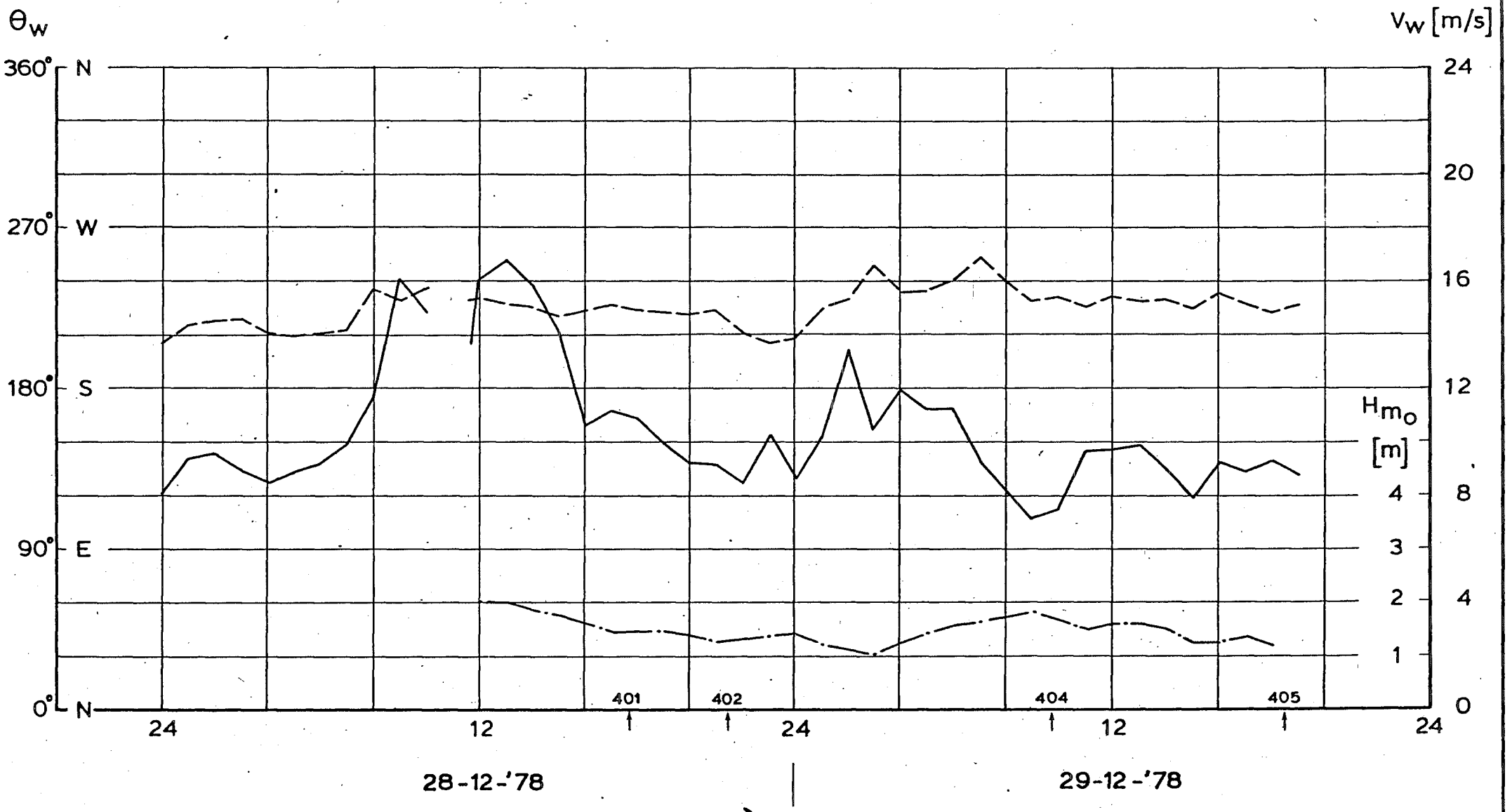

rijkswaterstaat directie waterhuishouding en waterbeweging district kust en zee	get.		appendix 1. fig. 1
	gec.		projectcode L7709B00
WIND AND WAVE PARAMETERS SERIES: 4. DATE: 28/29-12-'78	gez.		nota WWKZ-83G.007
	akk.		A4 nr. 83K.020

TAPE 5

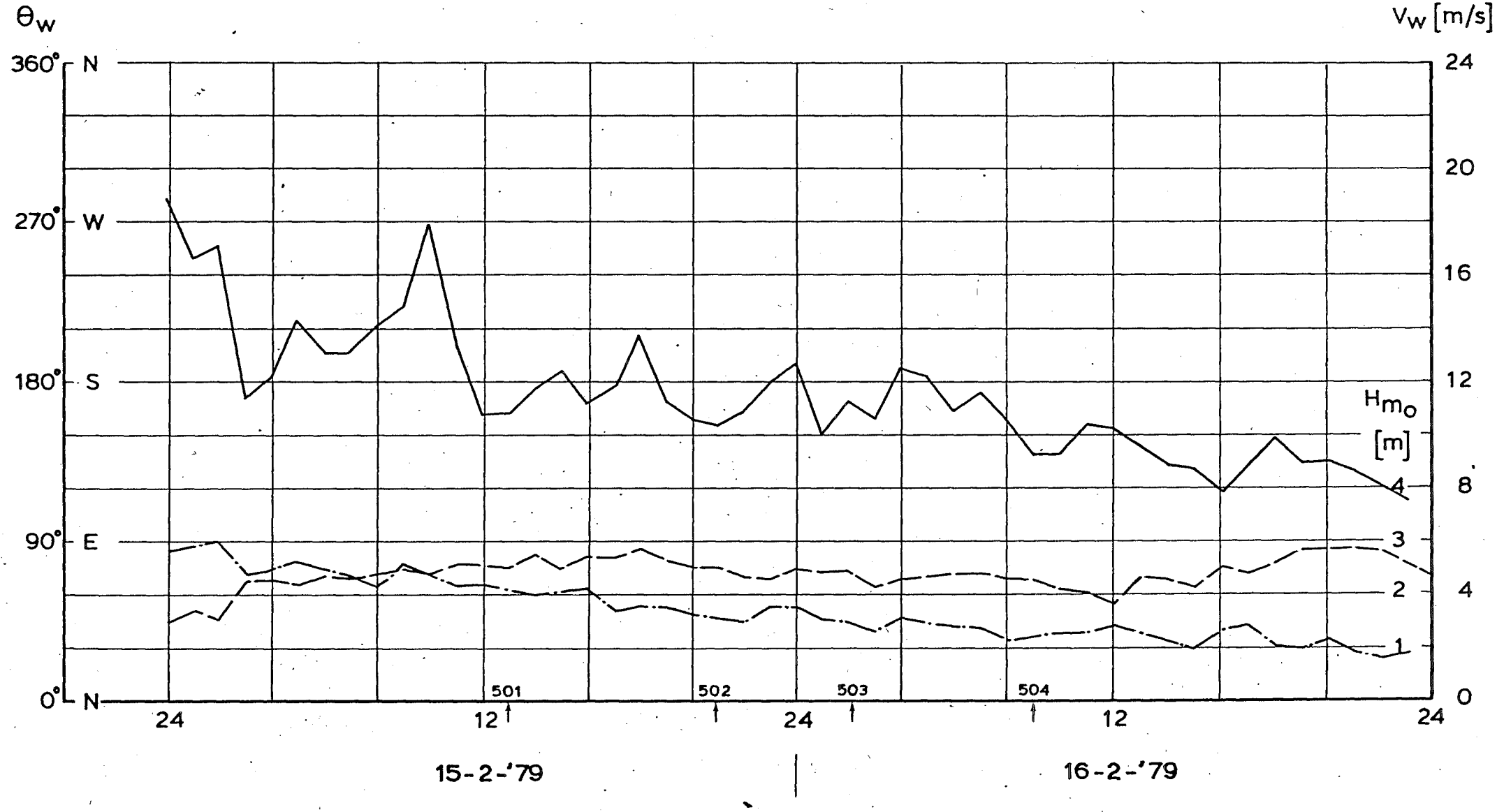

rijkswaterstaat directie waterhuishouding en waterbeweging district kust en zee	get.	appendix 1. fig. 2	
	gec.	projectcode L7709B00	
WIND AND WAVE PARAMETERS SERIES: 5. DATE: 15/16-3-'79	gez.	nota WWKZ-83G.007	
	akk.	A4	nr. 83K.021

V_w ——— WIND-SPEED

θ_w — — — WIND-DIRECTION

H_{mo} —·—·— SIGNIFICANT WAVEHEIGHT

TAPE 6

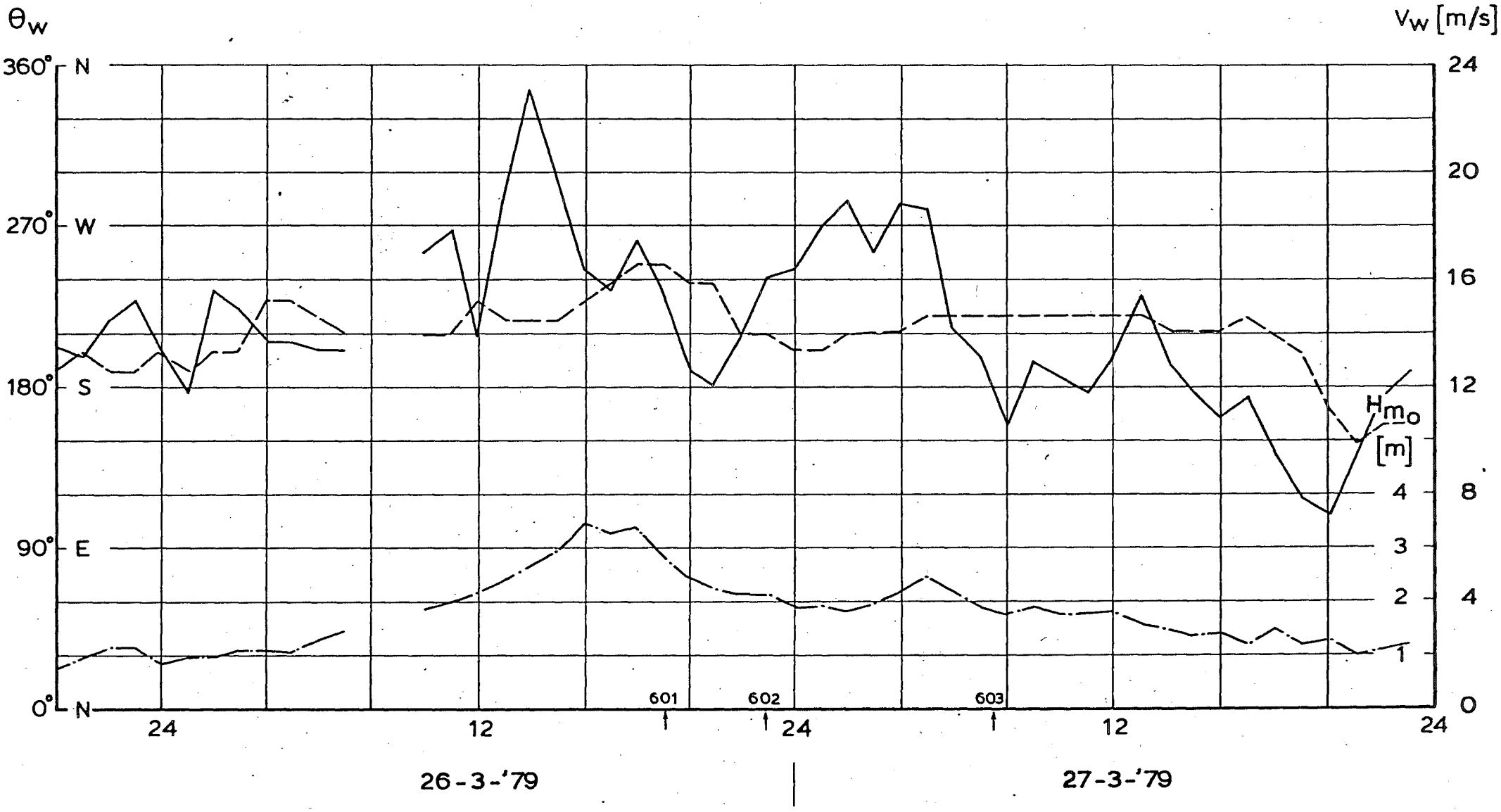

Vw ——— WIND-SPEED

θw — — — WIND-DIRECTION

Hmo —·—·— SIGNIFICANT WAVEHEIGHT

rijkswaterstaat directie waterhuishouding en waterbeweging district kust en zee	get.	appendix 1. fig. 3	
	gec.	projectcode L7709B00	
WIND AND WAVE PARAMETERS SERIES: 6 DATE: 26/27-3-'79	gez.	nota WWKZ-83G.007	
	akk.	A4	nr. 83 K.022

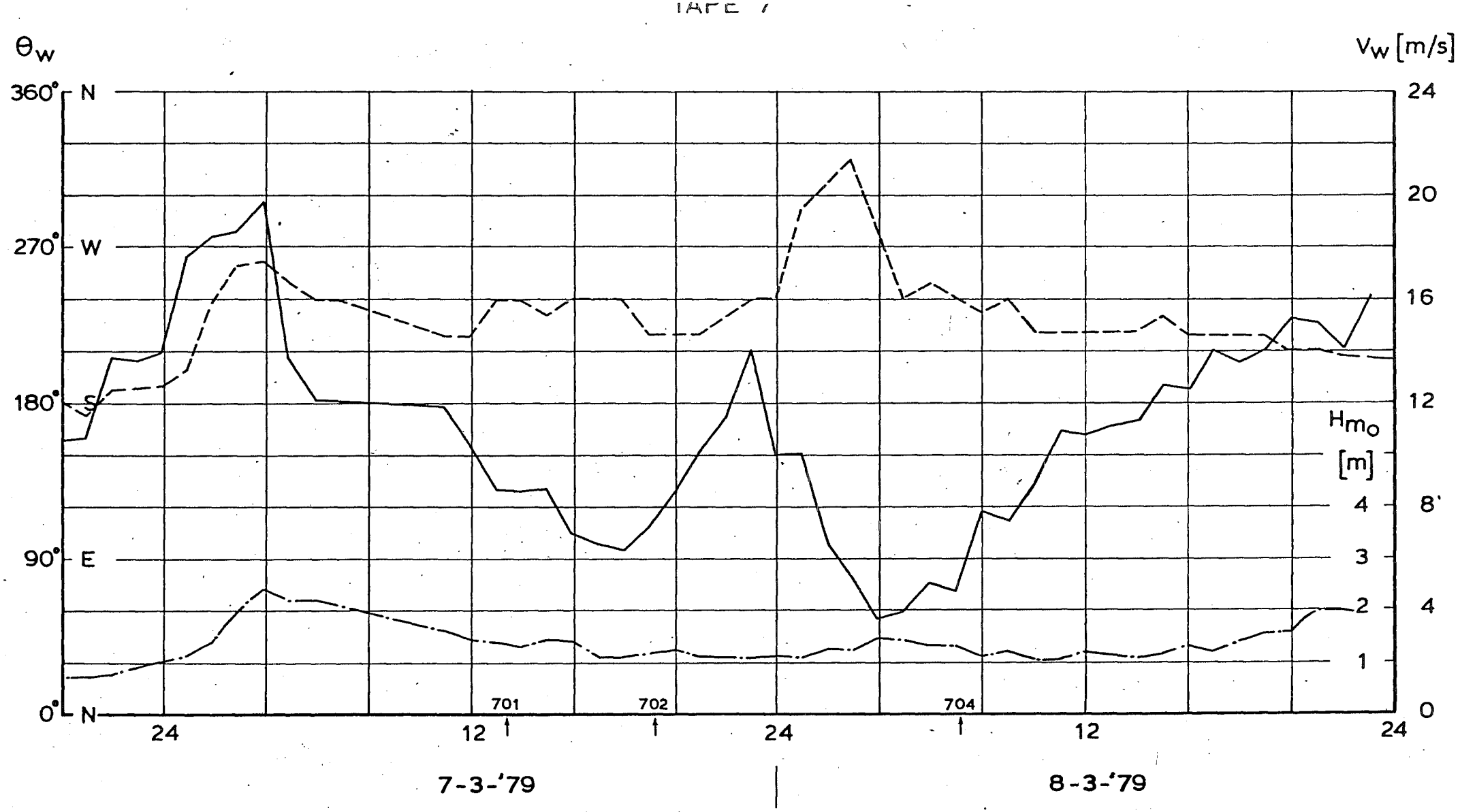

rijkswaterstaat directie waterhuishouding en waterbeweging district kust en zee	get.		appendix 1. fig.4
	gec.		projectcode L7709B00
WIND AND WAVE PARAMETERS SERIES: 7 DATE: 7/8-3-'79	gez.		nota WWKZ-83G.007
	akk.		A4 nr. 83K.023

TAPE 8

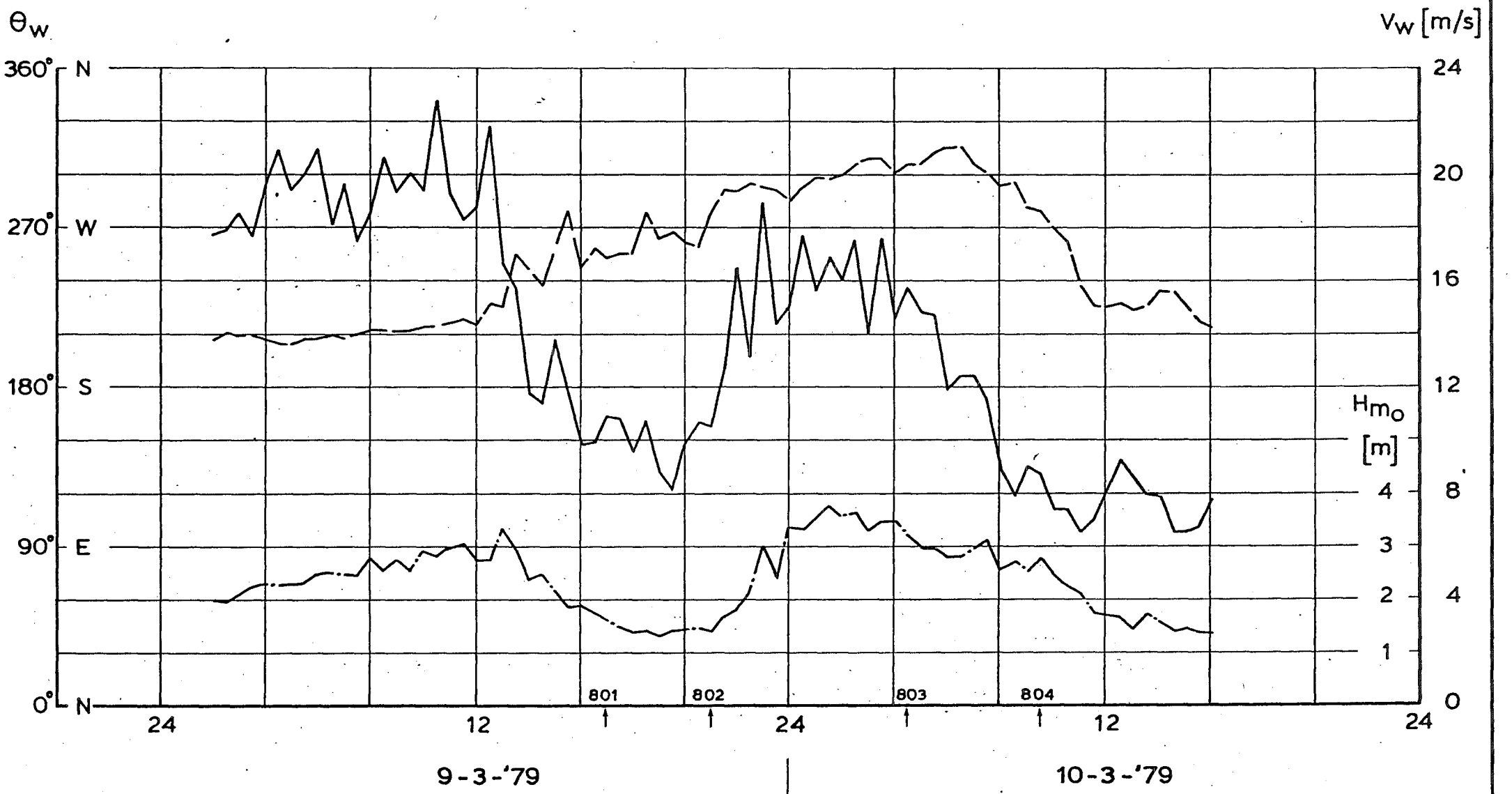

rijkswaterstaat directie waterhuishouding en waterbeweging district kust en zee	get.	appendix 1. fig. 5	
	gec.	projectcode L7709B00	
WIND AND WAVE PARAMETERS SERIES: 8. DATE: 9/10-3-'79	gez.	nota WWKZ-83G.007	
	akk.	A4	nr. 83K.024

TAPE 9

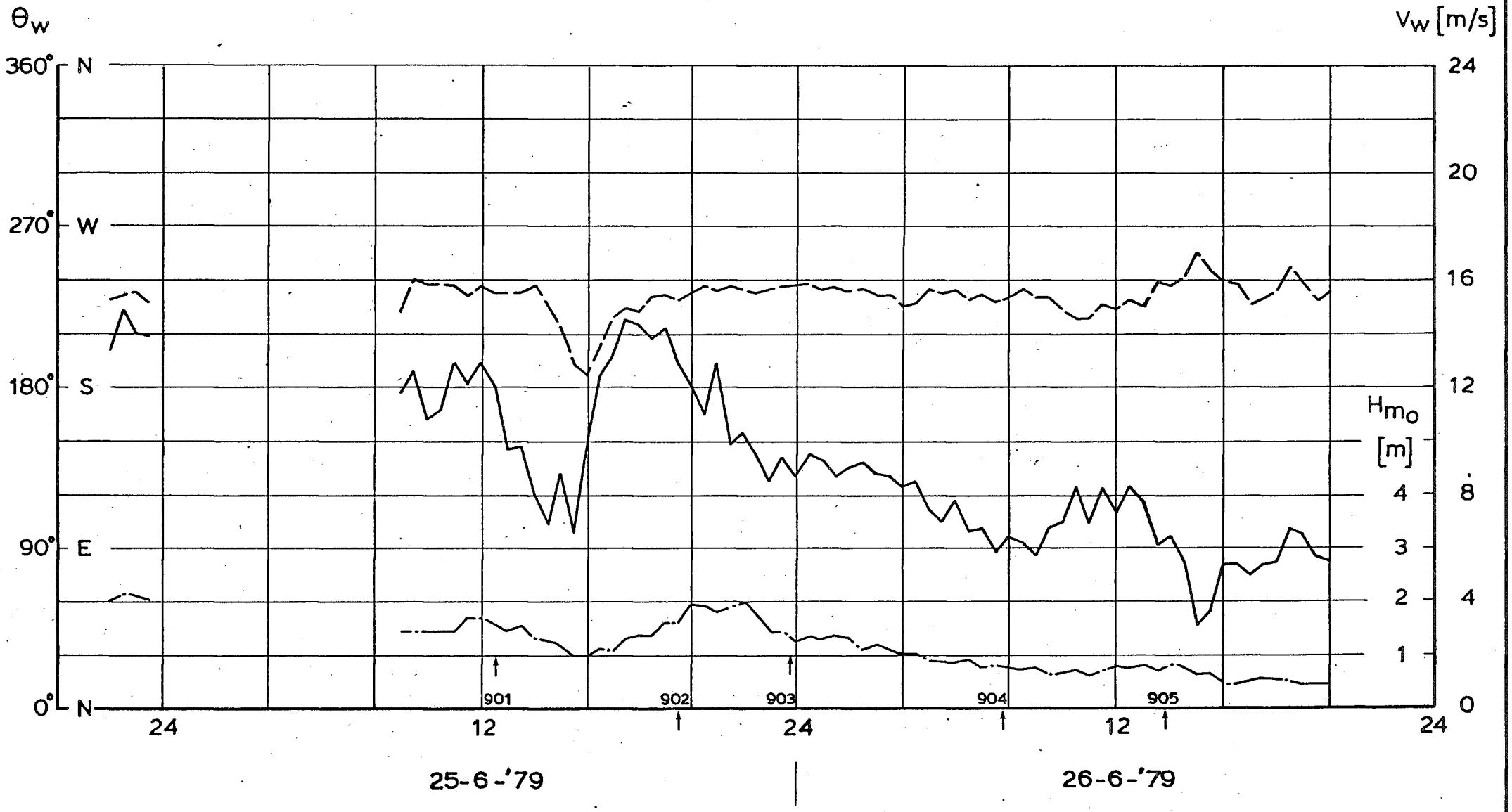

rijkswaterstaat directie waterhuishouding en waterbeweging district kust en zee	get.		appendix 1. fig 6
	gec.		projectcode L7709800
WIND AND WAVE PARAMETERS SERIES: 9 DATE: 25/26-6-'79	gez.		nota WWKZ-83G.007
	akk.		A4 nr. 83K.025

V_w ——— WIND-SPEED

θ_w — — — WIND-DIRECTION

H_{mo} —·—·— SIGNIFICANT WAVEHEIGHT

TAPE 15

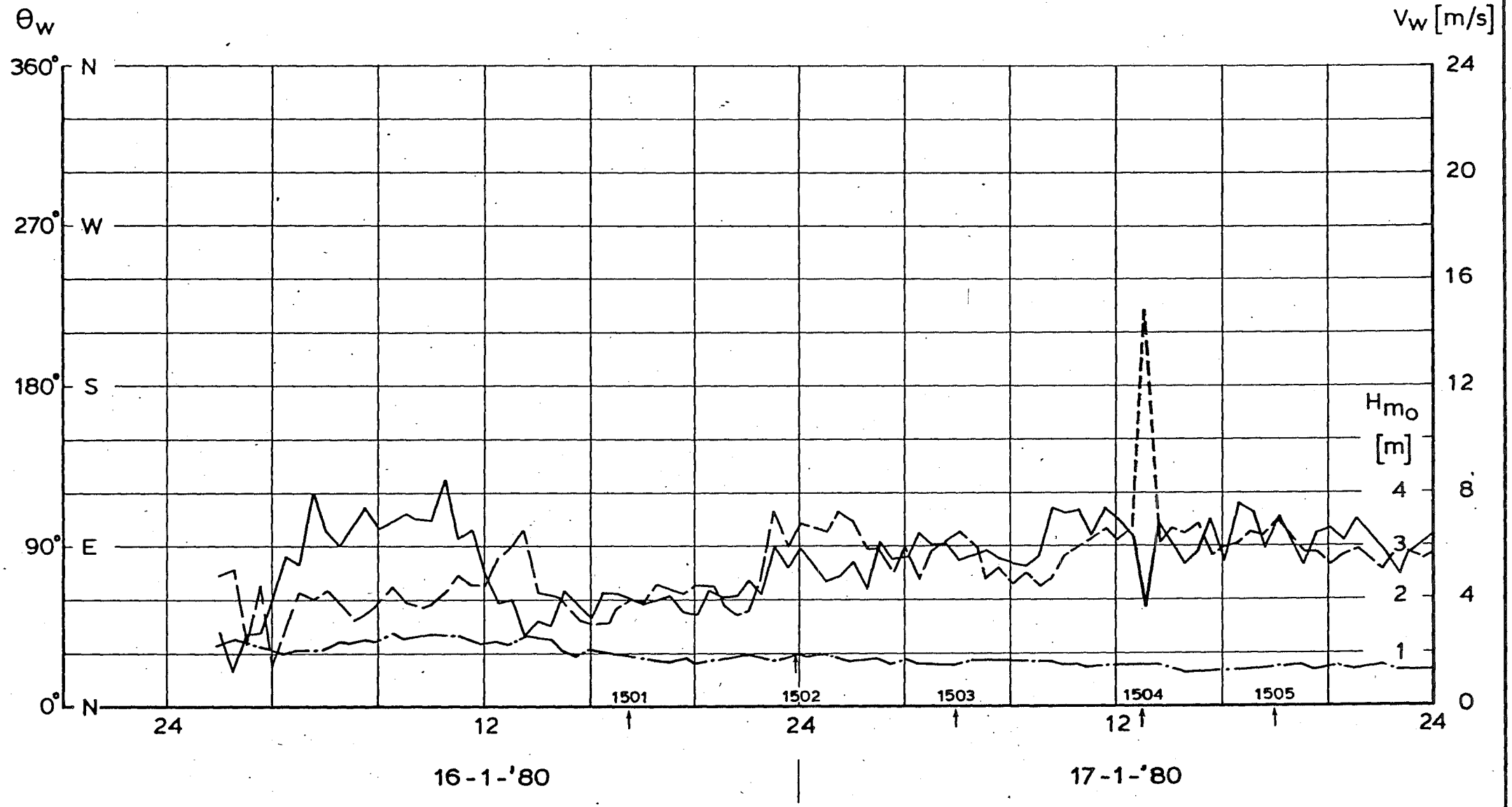

rijkswaterstaat directie waterhuishouding en waterbeweging district kust en zee	get.		appendix 1. fig.7
	gec.		projectcode L7709B00
WIND AND WAVE PARAMETERS SERIES: 15 DATE: 16/17-1-'80	gez.		nota WWKZ-83G.007
	akk.		A4 nr. 83 K.026

V_w ——— WIND-SPEED

θ_w — — — WIND-DIRECTION

H_{mo} —·—·— SIGNIFICANT WAVEHEIGHT

TAPE 16/17

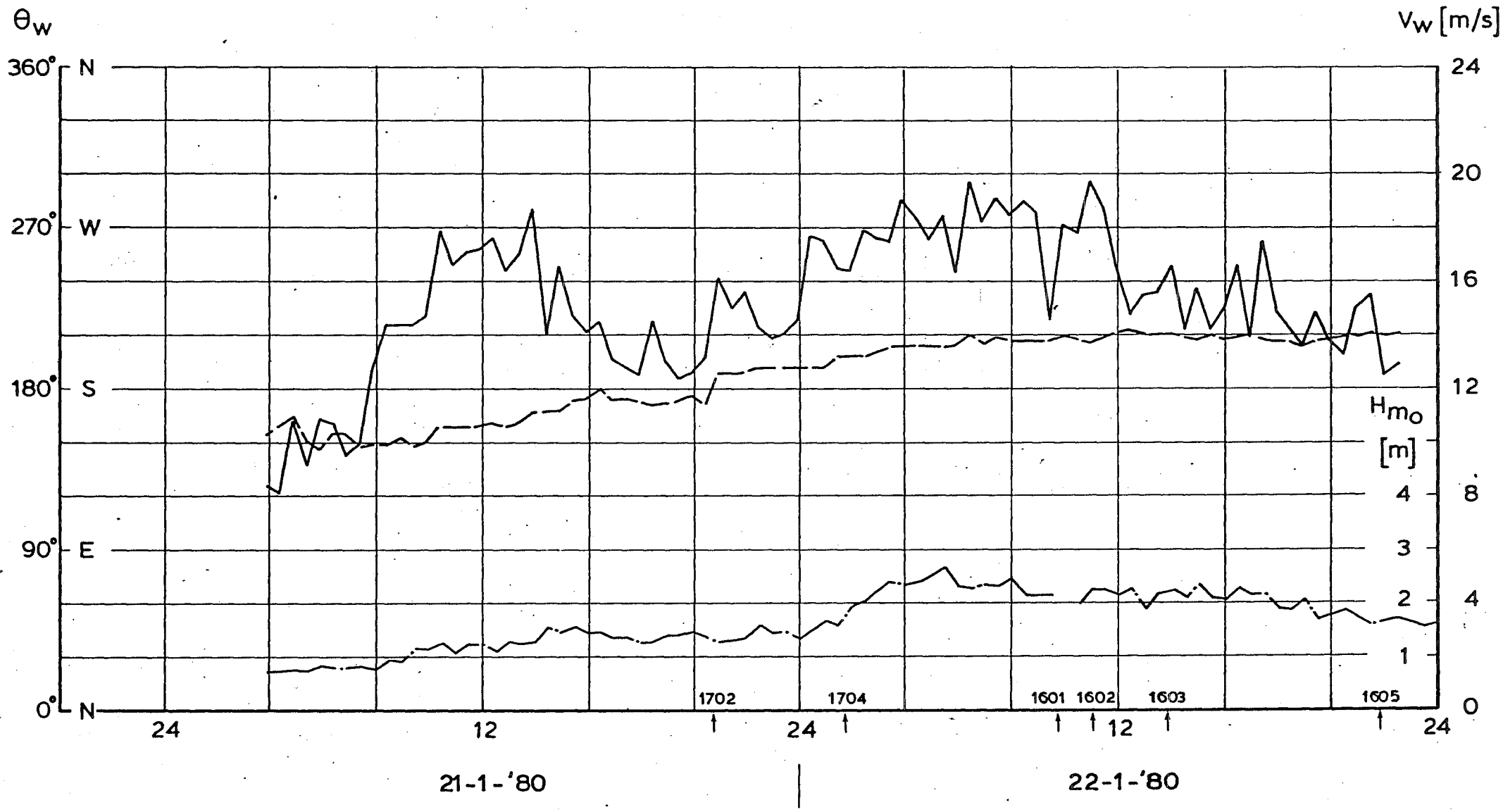

rijkswaterstaat directie waterhuishouding en waterbeweging district kust en zee	get.		appendix 1. fig. 8	
	gec.		projectcode L7709B00	
WIND AND WAVE PARAMETERS SERIES: 16/17 DATE: 21/22-1-'80	gez.		nota WWKZ-83G.007	
	akk.		A 4	nr. 83K.027

V_w ——— WIND-SPEED

θ_w — — — WIND-DIRECTION

H_{mo} —·—·— SIGNIFICANT WAVEHEIGHT

TAPE 18

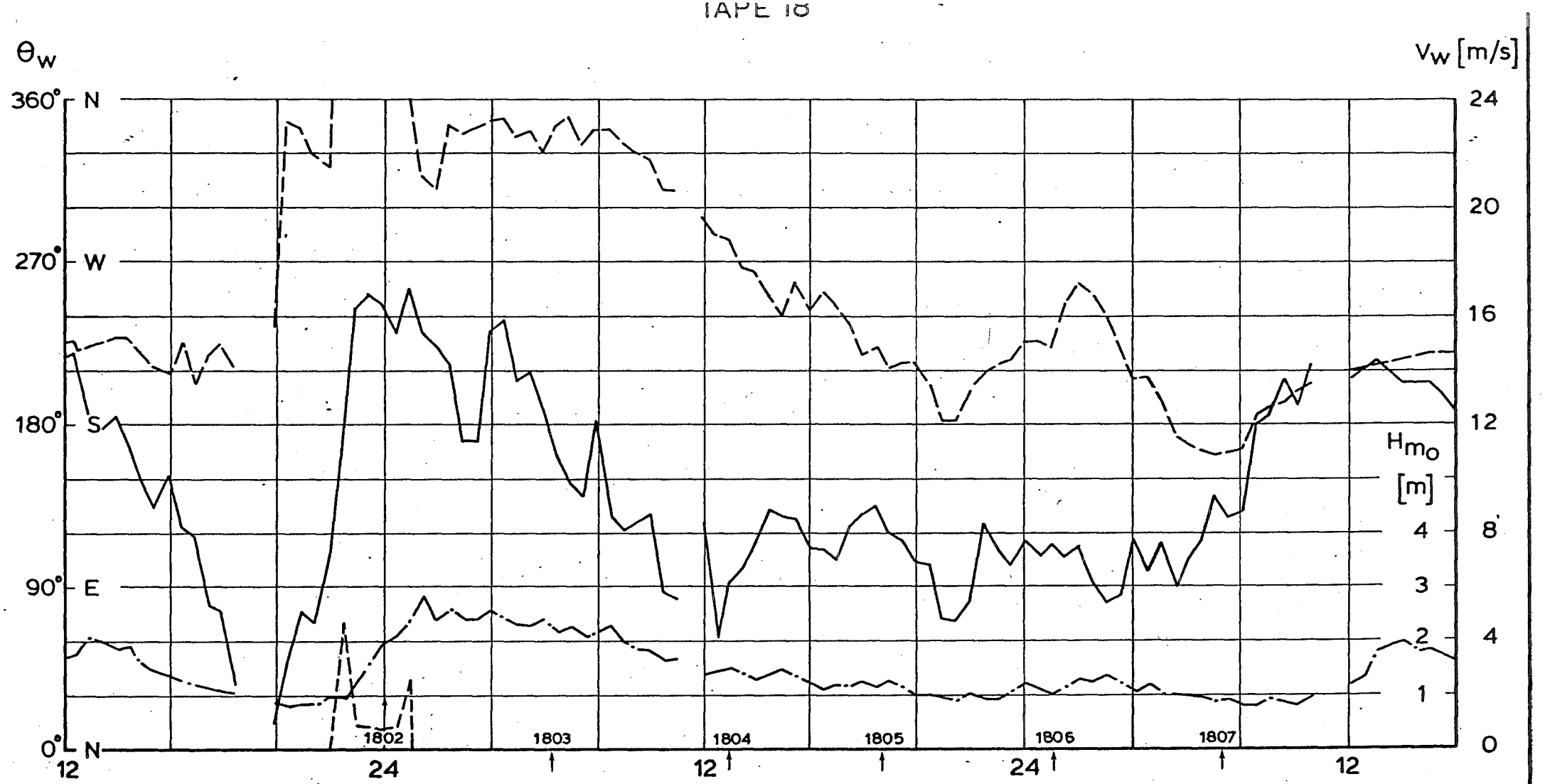

rijkswaterstaat directie waterhuishouding en waterbeweging district kust en zee	get.	appendix 1. fig. 9	
	gec.	projectcode L7709B00	
WIND AND WAVE PARAMETERS SERIES: 18 DATE: 31-1, 1/2-2-'80	gez.	nota WWKZ-83G.007	
	akk.	A4	nr. 83K.028

TAPE 22/23

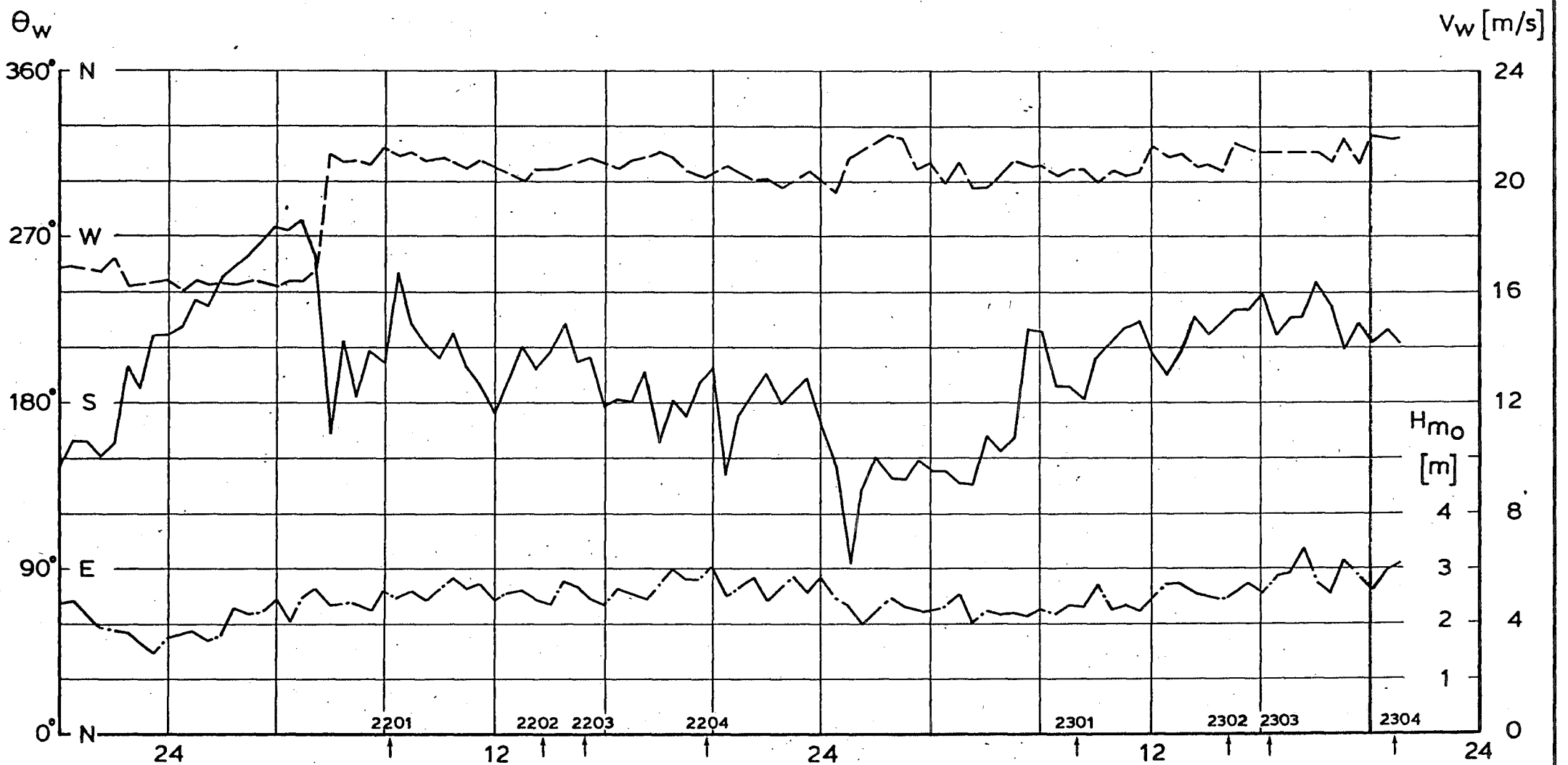

rijkswaterstaat directie waterhuishouding en waterbeweging district kust en zee	get.		appendix 1. fig. 10
	gec.		projectcode L7709B00
WIND AND WAVE PARAMETERS SERIES: 22/23 DATE: 21/22-8-'80	gez.		nota WWKZ-83G.007
	akk.		A4 nr. 83K.029

V_w ——— WIND-SPEED

θ_w — — — WIND-DIRECTION

H_{mo} ——·——· SIGNIFICANT WAVEHEIGHT

TAPE 24

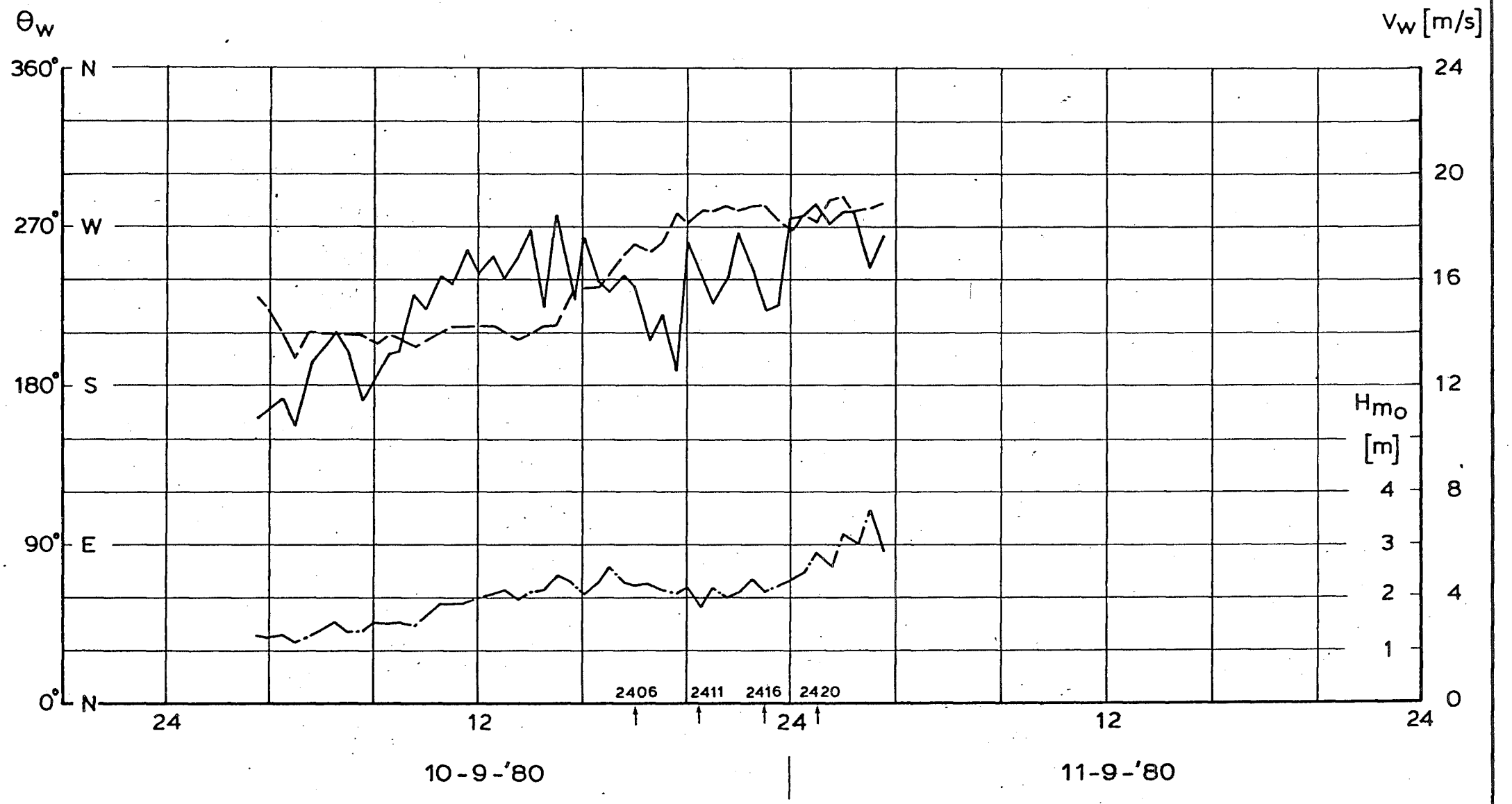

rijkswaterstaat directie waterhuishouding en waterbeweging district kust en zee	get.	appendix 1. fig. 11	
	gec.	projectcode L7709800	
WIND AND WAVE PARAMETERS SERIES: 24 DATE: 10/11-9-'80	gez.	nota WWKZ-83G.007	
	akk.	A4	nr. 83K.030

V_w ——— WIND-SPEED

θ_w — — — WIND-DIRECTION

H_{mo} —·—·— SIGNIFICANT WAVEHEIGHT

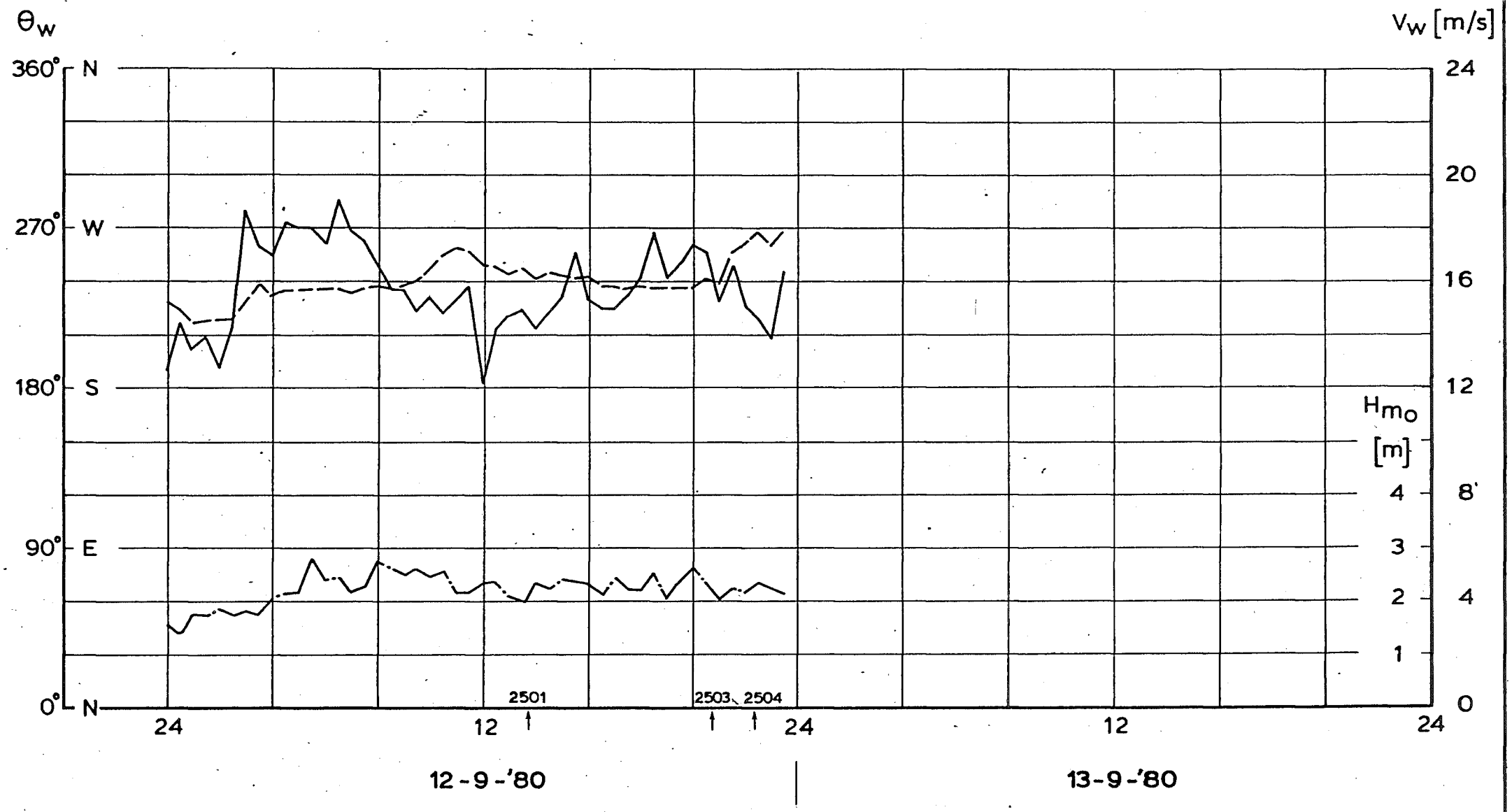

rijkswaterstaat directie waterhuishouding en waterbeweging district kust en zee	get.		appendix 1. fig. 12	
	gec.		projectcode L7709B00	
WIND AND WAVE PARAMETERS SERIES: 25 DATE: 12/13-9-'80	gez.		nota WWKZ-83G.007	
	akk.		A 4	nr. 83 K.031

V_w ——— WIND-SPEED

θ_w — — — WIND-DIRECTION

H_{mo} ——·—— SIGNIFICANT WAVEHEIGHT

TAPE 26

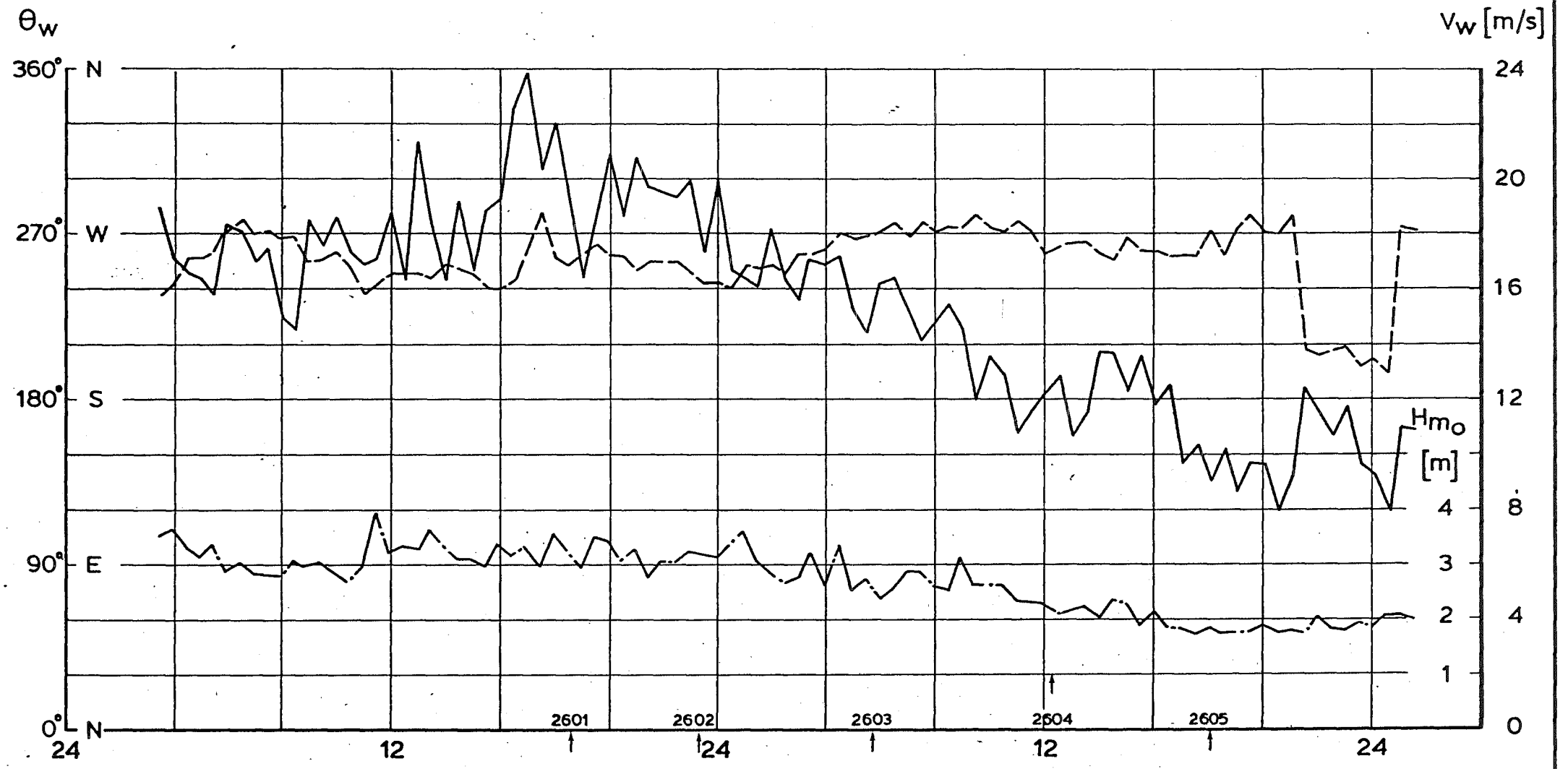

rijkswaterstaat directie waterhuishouding en waterbeweging district kust en zee	get.		appendix 1. fig. 13
	gec.		projectcode L7709B00
WIND AND WAVE PARAMETERS SERIES: 26 DATE: 7/8-10-'80	gez.		nota WWKZ-83G.007
	akk.		A4 nr. 83K.032

APPENDIX 2.

ENVIRONMENTAL PARAMETERS - TIDE AND WIND.

Appendix 2 - Environmental parameters (tide and wind)

Series	Record number	Date	Time[1]	Tide[2]			Wind	
				$\bar{\zeta}$ [m]	$\bar{u}$ [cm/s]	$\bar{V}$ [cm/s]	V_w [m/s]	θ_w
4	401	28-12-78	17.45	-0.2	- 2	0	11	230
	402		21.25	-0.7	-14	- 1	9	220
	404	29-12-78	09.45	-0.3	-10	+ 2	9	220
	405		18.25	-0.2	0	0	9	220
5	501	15-02-79	12.55	-0.8	- 6	- 1	11	80
	502		20.40	-0.3	+ 5	0	10	70
	503	16-02-79	02.10	-0.8	- 2	- 1	11	70
	504		09.00	-0.9	- 1	- 1	11	70
6	601	26-03-79	19.05	+0.2	- 6	- 6	15	250
	602		22.55	-0.4	- 3	+ 6	15	210
	603	27-03-79	07.30	-0.1	-12	- 1	12	220
7	701	07-03-79	13.25	+0.3	+14	+ 8	9	240
	702		19.10	-0.1	- 4	+ 3	7	220
	704	08-03-79	07.10	-0.4	- 5	+ 8	5	240
8	801	09-03-79	17.00	+0.6	- 3	+ 5	10	260
	802		21.00	+0.5	- 1	- 1	11	270
	803	10-03-79	04.30	+0.7	+ 0	+ 4	15	300
	804		09.30	+0.1	- 5	+ 4	9	280
9	901	25-06-79	12.30	-0.5	- 1	- 1	13	240
	902		19.30	-0.3	- 1	+ 1	14	230
	903		23.45	-0.9	- 5	+ 1	9	240
	904	26-06-79	07.45	-0.2	- 4	0	6	230
	905		13.45	-0.4	+ 2	+18	6	240
15	1501	16-01-80	17.25	-0.4	+ 3	- 2	4	60
	1502		23.55	-0.5	- 8	- 2	5	100
	1503	17-01-80	05.55	-0.5	- 1	- 2	6	100
	1504		12.55	-0.1	- 1	- 2	6	120
	1505		17.55	-0.3	+ 8	+ 3	6	100
16	1601	22-01-80	09.45	-0.6	- 1	+ 4	17	210
	1602		11.00	-0.6	- 6	- 1	19	210
	1603		13.45	-1.2	- 8	0	16	210
	1605		21.45	0.0	- 2	- 3	13	210

1) starttime record, reference time: G.M.T.

2) at mean time of record.

series	Record number	Date	Time[1]	Tide[2]			Wind	
				$\bar{\zeta}$ [m]	$\bar{u}$ [cm/s]	$\bar{V}$ [cm/s]	V_w [m/s]	θ_w
17	1702	21-01-80	20.45	-0.3	+ 8	0	15	190
	1704	22-01-80	01.45	-0.9	- 5	0	17	200
18	1802	31-01-80	00.00	0.2	- 2	- 7	16	12
	1803	01-02-80	06.15	0.1	0	0	11	344
	1804		13.00	-0.2	- 7	-13	6	283
	1805		18.45	0.0	- 4	- 4	9	223
	1806	02-20-80	01.00	-0.4	- 4	- 6	8	222
	1807		07.15	-0.4	- 4	+ 1	9	162
22	2201	21-08-80	08.15	0.8	+19	+ 5	14	317
	2202		13.45	0.4	- 2	+ 1	14	306
	2203		15.15	0.2	- 8	+ 2	14	312
	2204		19.45	0.3	0	+ 2	13	302
23	2301	22-08-80	09.15	0.1	+ 1	+ 2	13	305
	2302		14.45	0.3	0	+ 1	15	305
	2303		16.15	0.0	-17	- 1	14	316
	2304		20.45	0.1	-14	- 4	15	323
24	2406	10-09-80	18.03	0.1	+21	+10	16	260
	2415		20.33	0.0	-12	- 2	16	280
	2416		23.03	-0.5	-15	+ 2	15	283
	2420		01.03	0.1	0	2	19	272
25	2501	12-09-80	13.45	-0.5	- 2	- 2	15	248
	2503		20.45	-0.1	- 4	- 1	17	241
	2504		22.15	-0.1	-10	0	15	261
26	2601	07-10-80	18.35	0.6	- 3	- 4	20	253
	2602		23.15	0.3	+ 2	+ 1	20	249
	2603	08-10-80	05.45	0.8	- 3	+ 2	14	269
	2604		12.15	0.3	+ 4	+ 3	12	259
	2605		18.00	0.2	- 2	0	10	258

1) starttime record, reference time: G.M.T.

2) at mean time of record.

APPENDIX 3.

ENVIRONMENTAL PARAMETERS - WAVES.

Appendix 3 - Environmental parameters (waves)

series	Record number	Waves				
		θ_o (f_m)[1)]	$H_{1/3}$ [m]	f_m [$\frac{1}{60}$ Hz]	β	γ [
4	401	262	1.4	7	1.02	1.4
	402	258	1.2	9	1.11	1.8
	404	277	1.2	7	1.25	1.3
	405	313	1.3	10	1.02	2.
5	501	353	2.1	8	.97	2.
	502	354	1.6	7	1.12	1.
	503	353	1.5	9	.90	2.
	504	342	1.2	6	1.07	1.
6	601	253	2.8	7	.75	2
	602	256	2.1	9	.67	4
	603	252	1.8	7	.93	1
7	701	267	1.4	10	1.02	1
	702	303	1.2	10	1.31	2
	704	307	1.2	10	1.83	2
8	801	246	1.7	7	1.11	
	802	256	1.4	10	.83	
	803	296	3.2	6	1.31	
	804	293	2.6	7	1.25	
9	901	244	1.6	10	.70	
	902	252	1.6	10	.65	
	903	248	1.4	10	1.02	
	904	256	0.8	10	1.53	
	905	308	0.7	12	1.31	
15	1501	329	0.9	10	2.26	
	1502	333	0.9	8	2.13	
	1503	337	0.7	9	1.66	
	1504	337	0.7	9	1.66	
	1505	338	0.7	8	1.77	
16	1601	248	2.1	10	.54	
	1602	251	2.2	9	.53	
	1603	245	2.2	8	.67	
	1605	253	1.7	8	.66	

series	Record number	Waves				
		θ_o (f_m)[1]	$H_{1/3}$ [m]	f_m [$\frac{1}{60}$ Hz]	β	γ [%]
17	1702	256	1.3	8	.71	1.64
	1704	250	1.9	9	.58	2.85
18	1802	340	2.1	13	.46	6.20
	1803	344	2.4	10	.84	4.44
	1804	329	1.4	7	1.30	1.46
	1805	336	1.1	11	.94	2.37
	1806	329	1.1	11	1.06	2.37
	1807	328	0.9	9	1.11	1.35
22	2201	260	2.2	9	.71	3.30
	2202	310	3.0	8	.76	3.78
	2203	306	2.7	8	.76	3.40
	2204	312	3.0	6	.90	2.54
23	2301	321	2.2	10	.70	4.01
	2302	314	2.5	7	.75	2.61
	2303	318	2.8	8	.76	3.53
	2304	328	2.9	6	.78	2.46
24	2406	252	2.2	8	.67	2.76
	2411	249	1.8	8	.67	2.26
	2416	263	2.1	8	.71	2.64
	2420	271	2.8	8	.56	3.53
25	2501	257	2.3	8	.71	2.90
	2503	253	2.2	8	.62	2.76
	2504	247	2.3	8	.71	2.90
26	2601	253	3.7	7	.56	3.85
	2602	247	3.0	7	.56	3.24
	2603	269	2.7	8	.76	3.40
	2604	284	2.0	8	.89	2.52
	2605	280	1.7	9	1.00	2.55

1) direction from which the waves approache, in a right handed coordinate system.

APPENDIX 4.

VARIANCE DENSITY FUNCTIONS, SQUARED COHERENCE- GAIN- AND PHASE FUNCTIONS OF SURFACE ELEVATION AND VERTICAL VELOCITY COMPONENT.

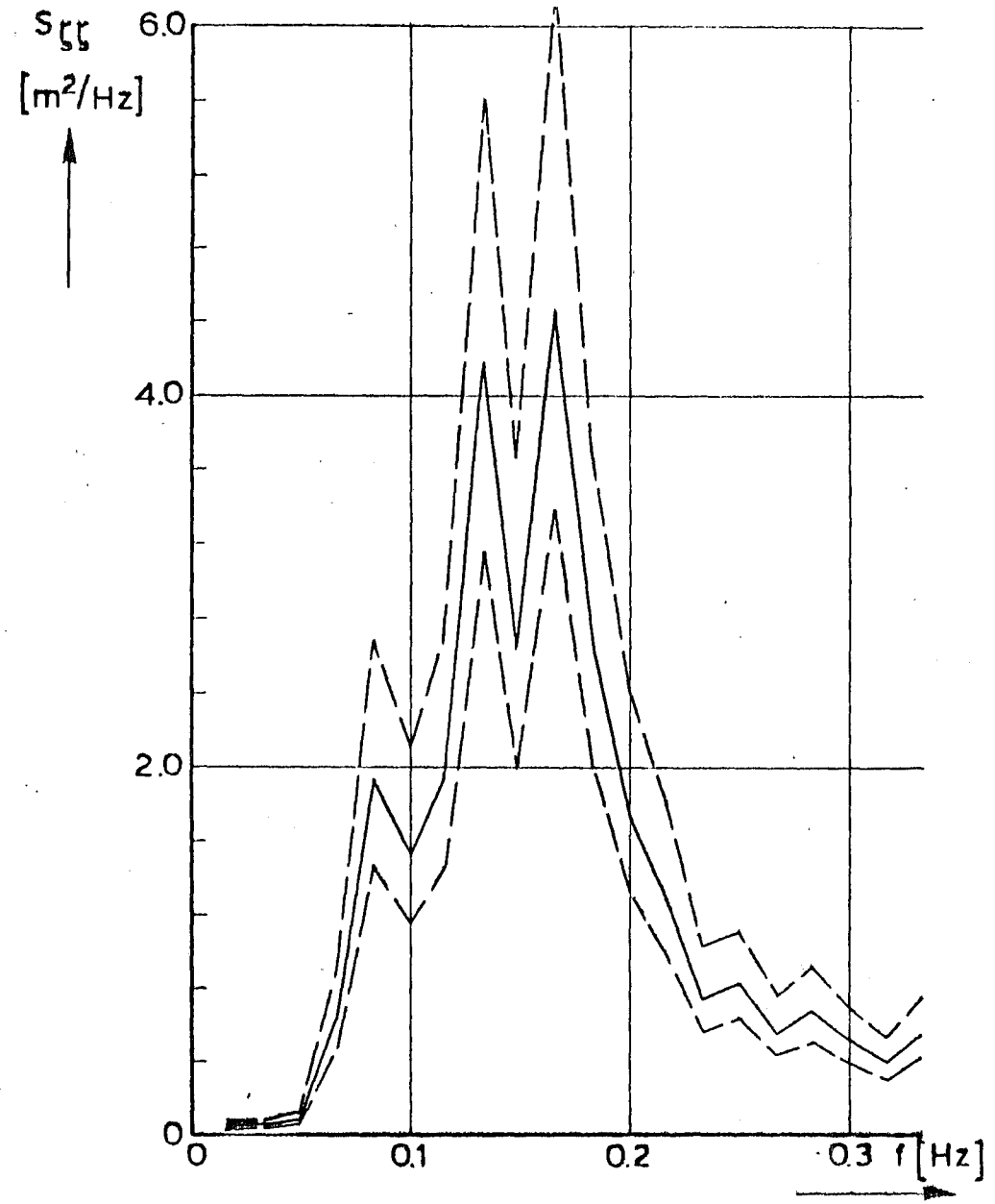

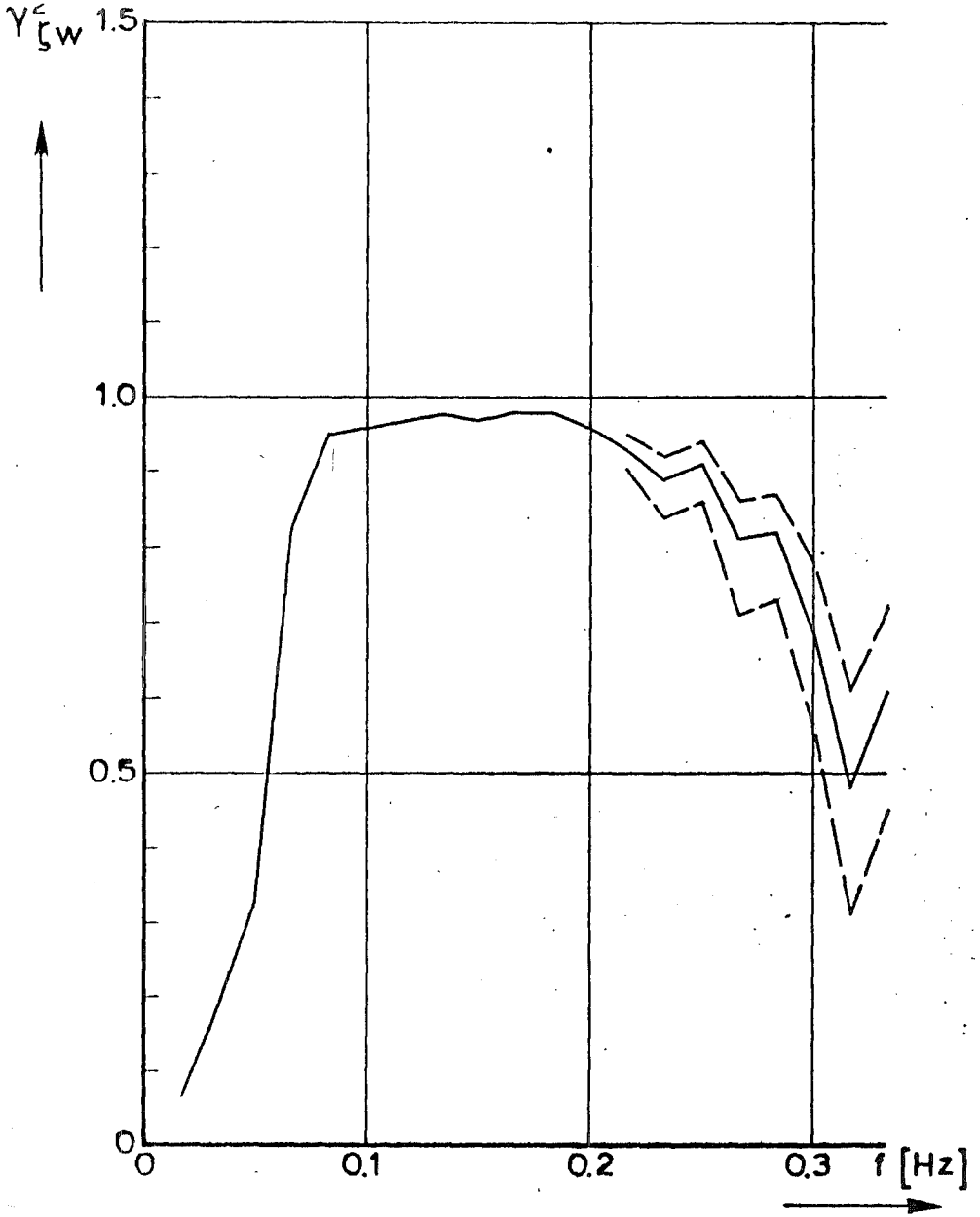

rijkswaterstaat **directie waterhuishouding en waterbeweging** **district kust en zee**	get.		appendix 4. fig 1a
	gec.		projectcode L7709B00
VARIANCE DENSITY FUNCTION OF ζ ($S_{\zeta\zeta}$) AND SQUARED COHERENCE FUNCTION w AND ζ ($\gamma^2_{\zeta w}$) WITH 90% CONFIDENCE INTERVALS (— — —) 1501	gez.		nota WWKZ-83G.007
	akk		A 4 nr. 83K.033

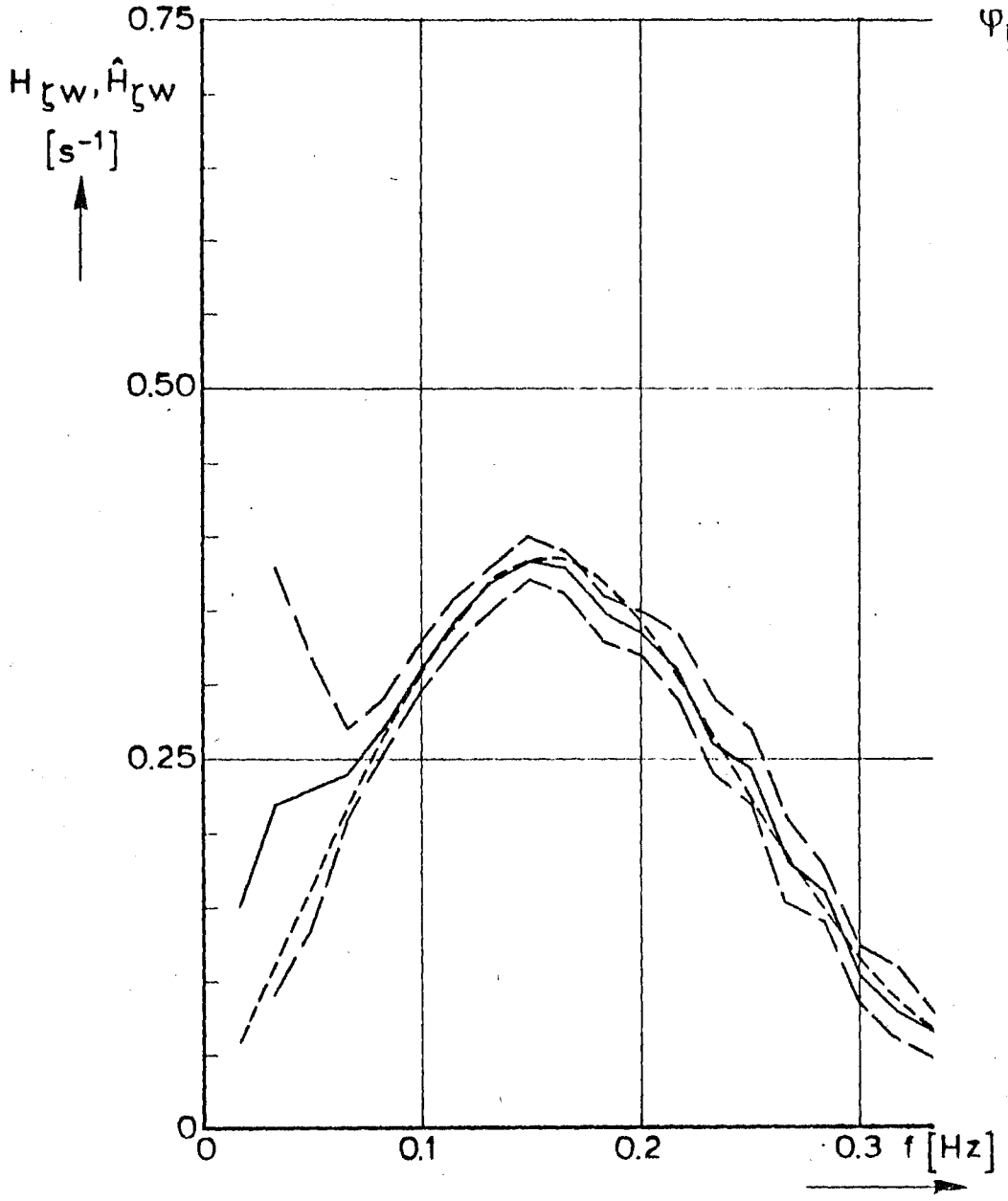

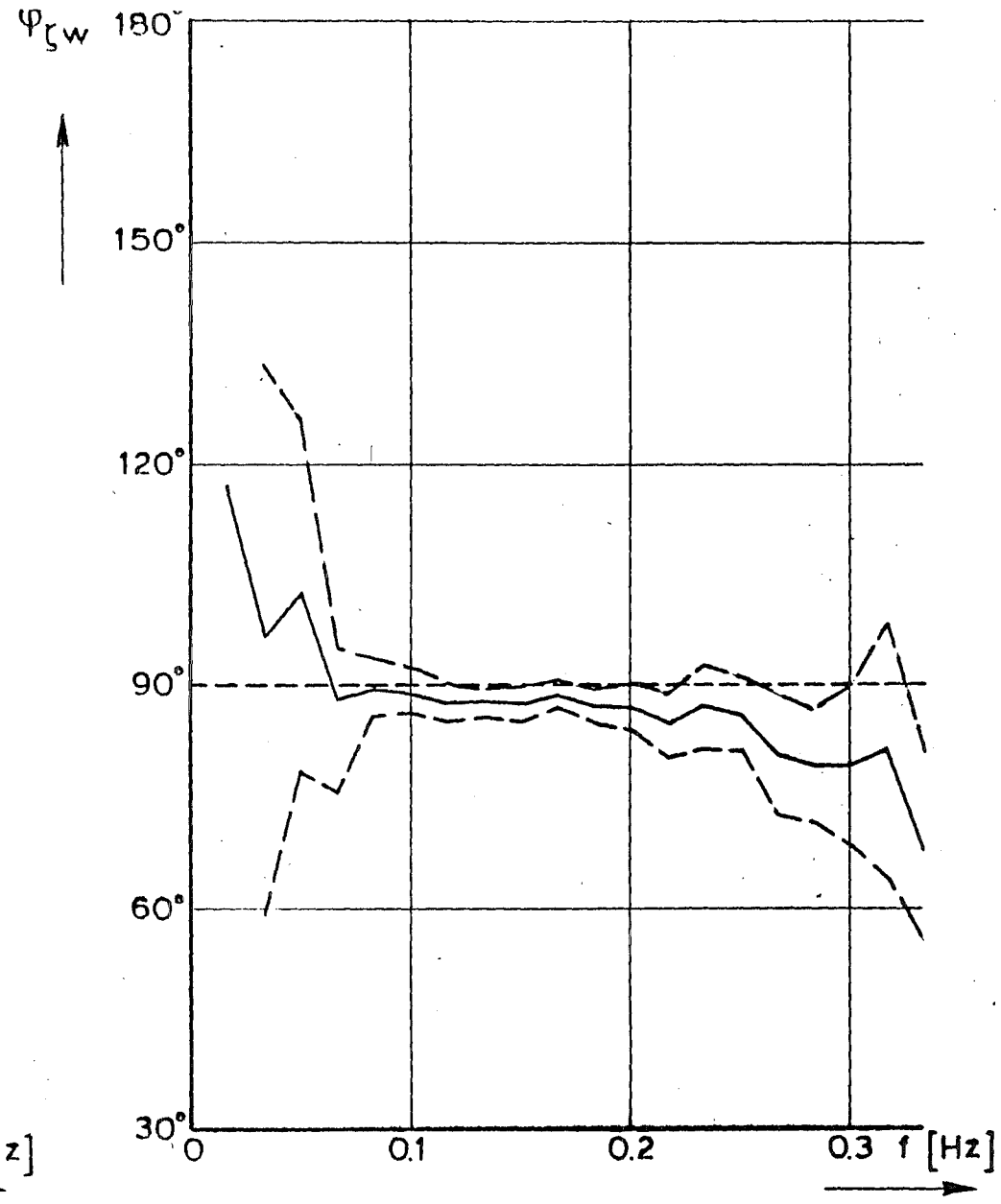

rijkswaterstaat directie waterhuishouding en waterbeweging district kust en zee	get.		appendix 4. fig. 1b
	gec.		projectcode L7709B00
MEASURED GAINFUNCTION $H_{\zeta w}$ AND PHASEFUNCTION $\varphi_{\zeta w}$ (———) WITH 90% CONFIDENCE INTERVALS (— —) AND THEORETICAL GAIN AND PHASEFUNCTION (- - - -) 1501	gez.		nota WWKZ-83G.007
	akk		A 4 nr 83K.034

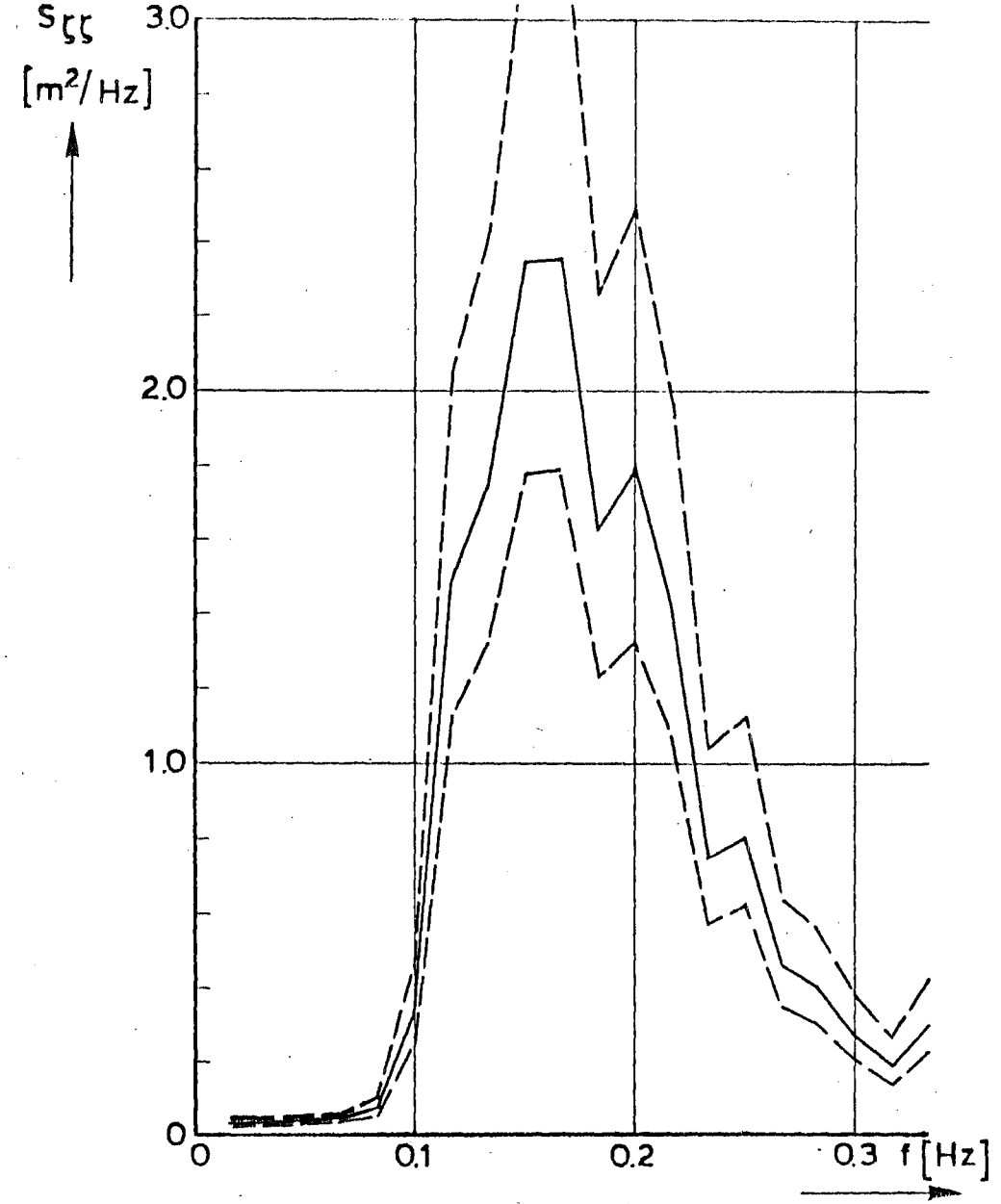

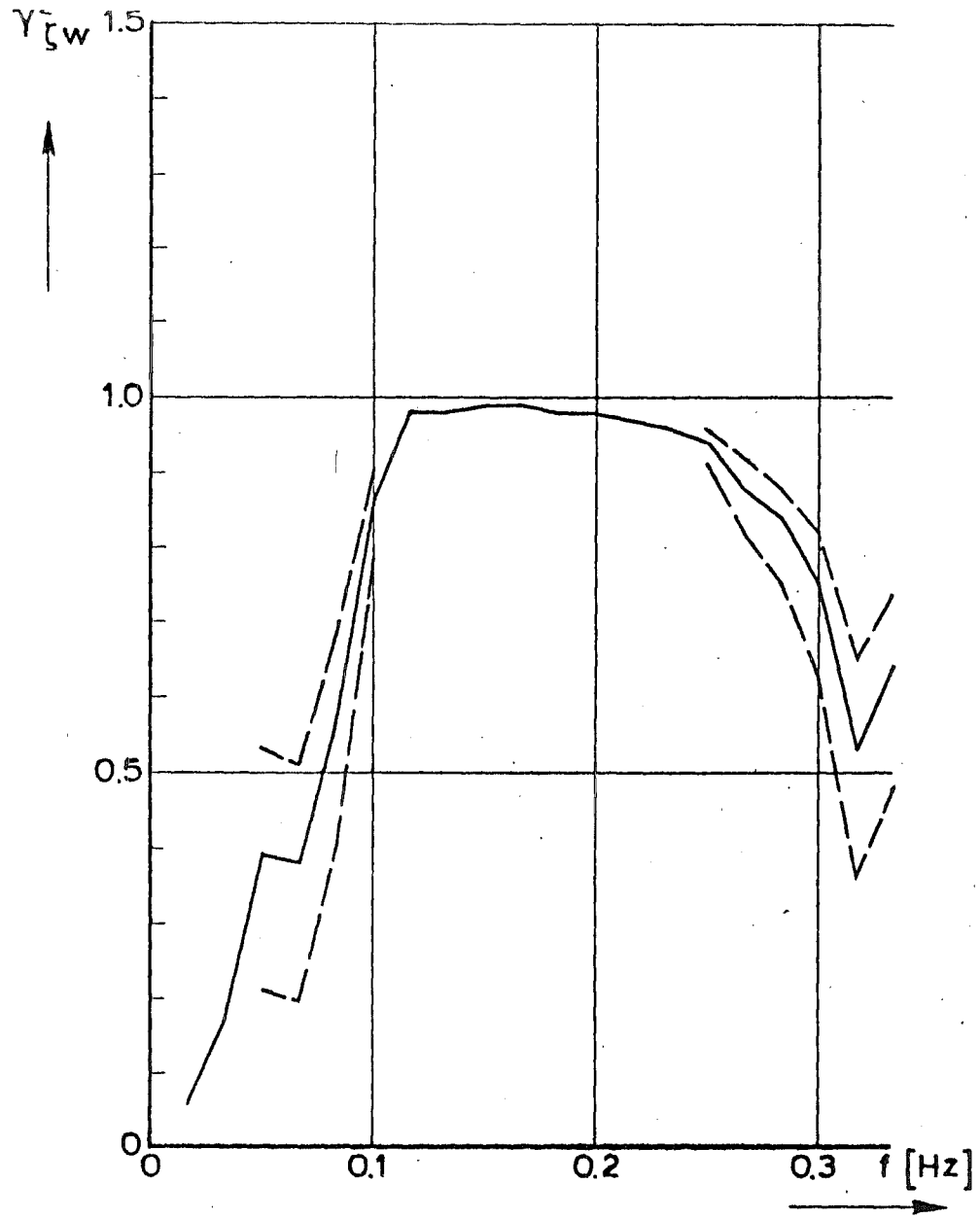

rijkswaterstaat directie waterhuishouding en waterbeweging district kust en zee	get.		appendix 4. fig. 2a	
	gec.		projectcode L7709B00	
VARIANCE DENSITY FUNCTION OF ζ ($S_{\zeta\zeta}$) AND SQUARED COHERENCE FUNCTION w AND ζ ($\gamma^2_{\zeta w}$) WITH 90% CONFIDENCE INTERVALS (— —) 1601.	gez.		nota WWKZ-83G.007	
	akk.		A 4	nr. 83K.035

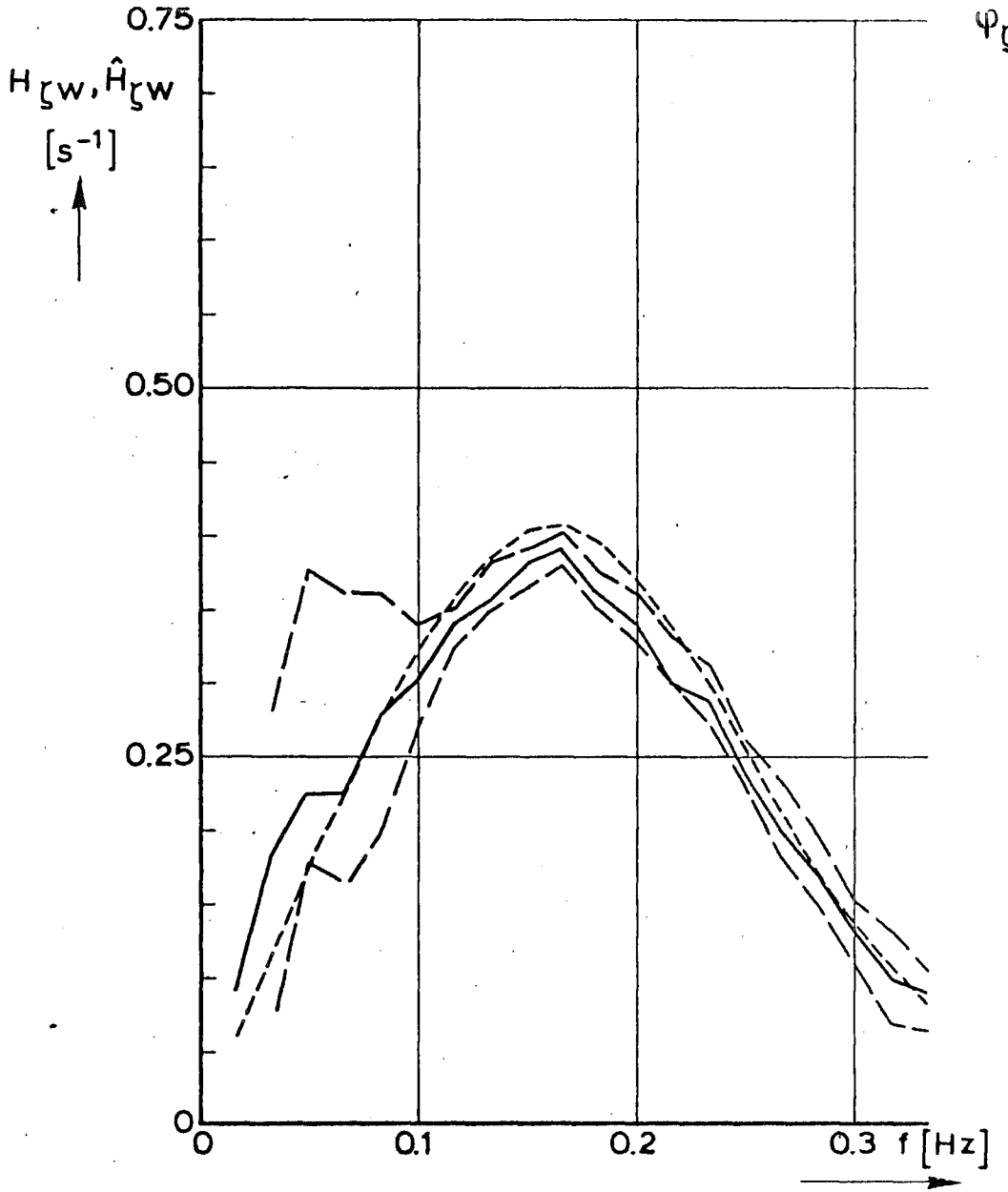

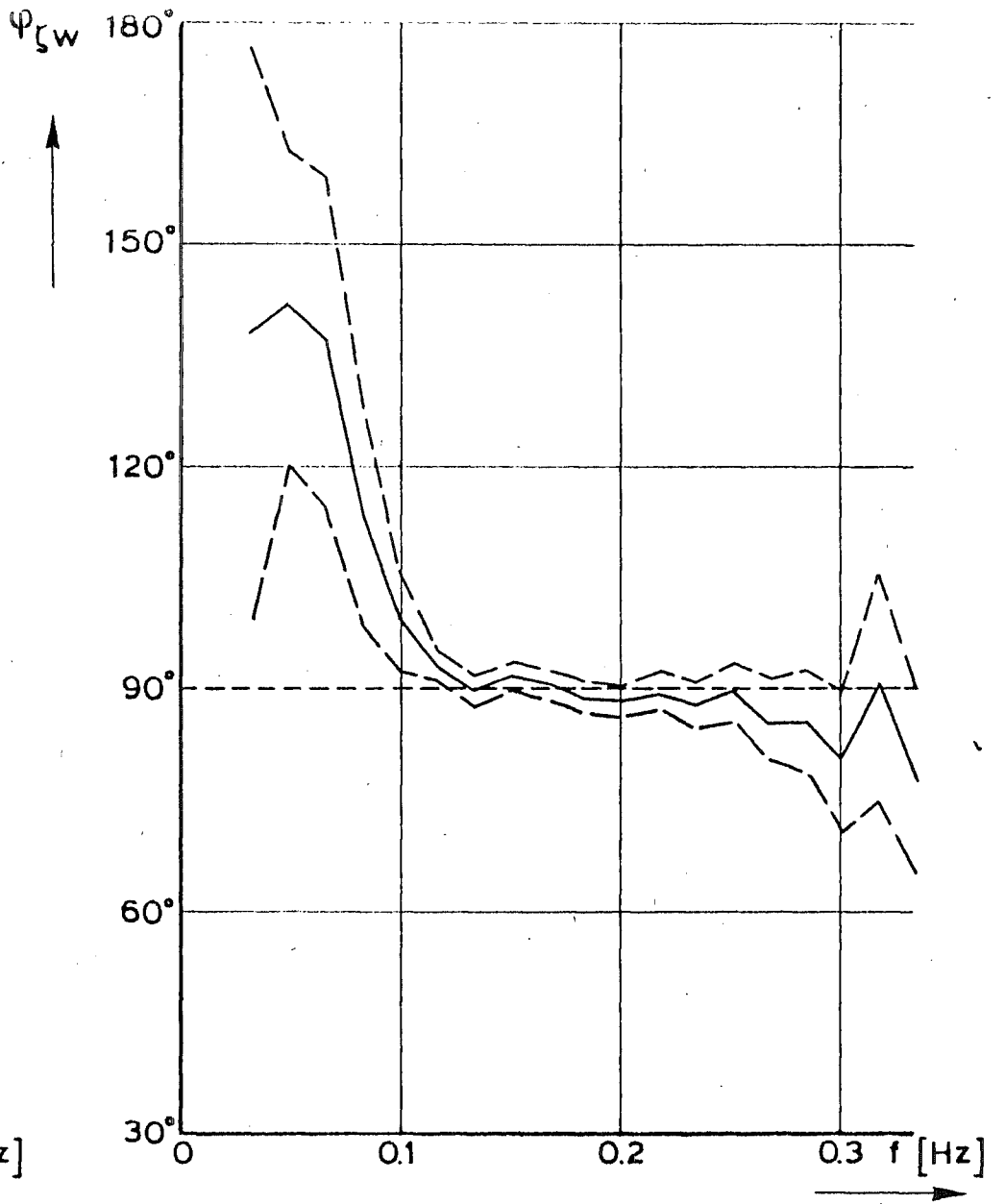

rijkswaterstaat
directie waterhuishouding en waterbeweging
district kust en zee

MEASURED GAINFUNCTION $H_{\zeta w}$ AND PHASEFUNCTION $\varphi_{\zeta w}$ (———) WITH 90% CONFIDENCE INTERVALS (— —) AND THEORETICAL GAIN AND PHASEFUNCTION (- - - - -), 1601.

get.		appendix 4. fig. 2b	
gec.		projectcode L7709B00	
gez.		nota WWKZ-83G.007	
akk.		A 4	nr. 83 K.036

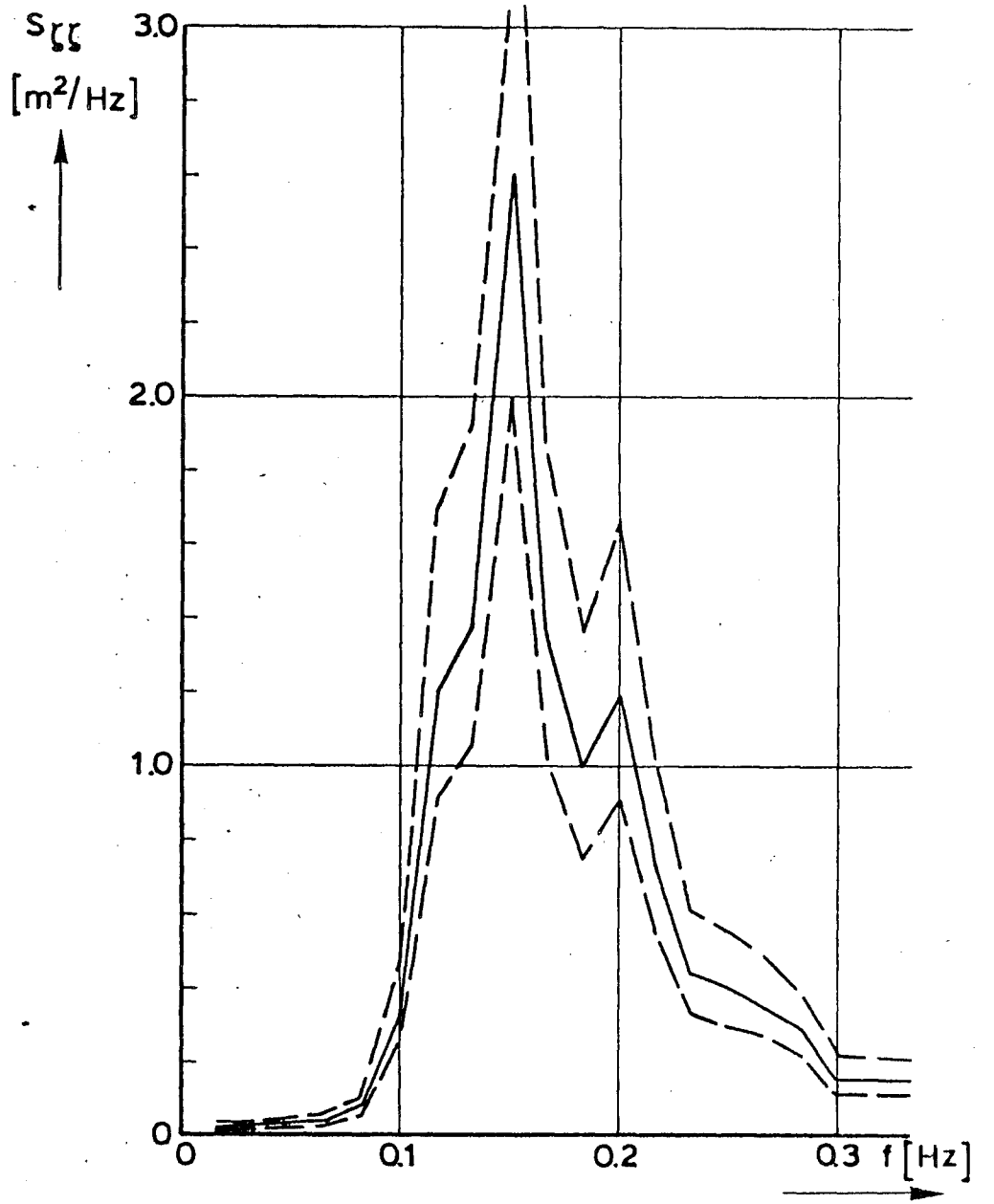

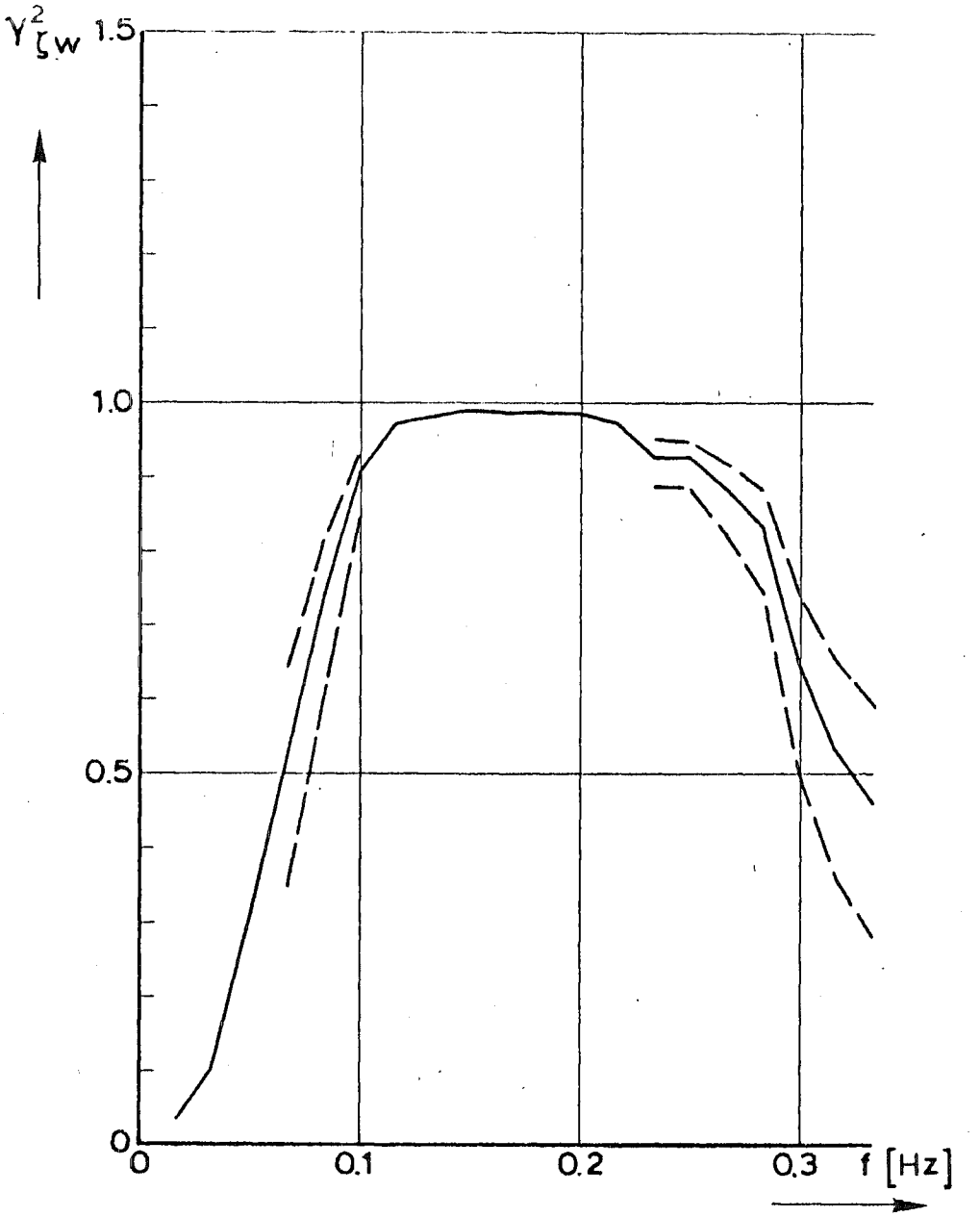

rijkswaterstaat
directie waterhuishouding en waterbeweging
district kust en zee

VARIANCE DENSITY FUNCTION OF ζ ($S_{\zeta\zeta}$) AND SQUARED COHERENCE FUNCTION w AND ζ ($\gamma^2_{\zeta w}$) WITH 90% CONFIDENCE INTERVALS (— —) 1704.

get.		appendix 4. fig 3a	
gec.		projectcode L7709B00	
gez.		nota WWKZ-83G.007	
akk.		A 4	nr. 83 K.037

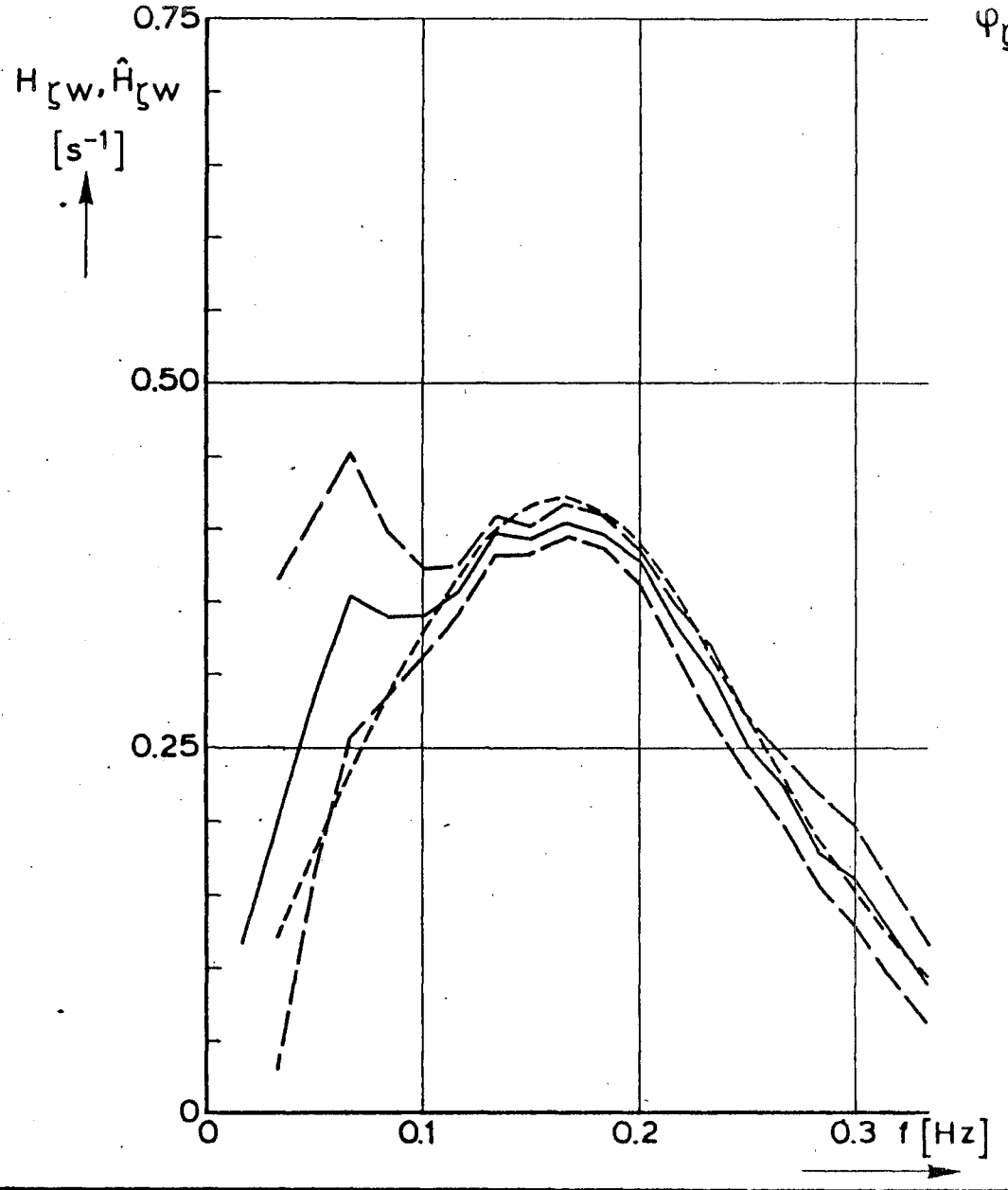

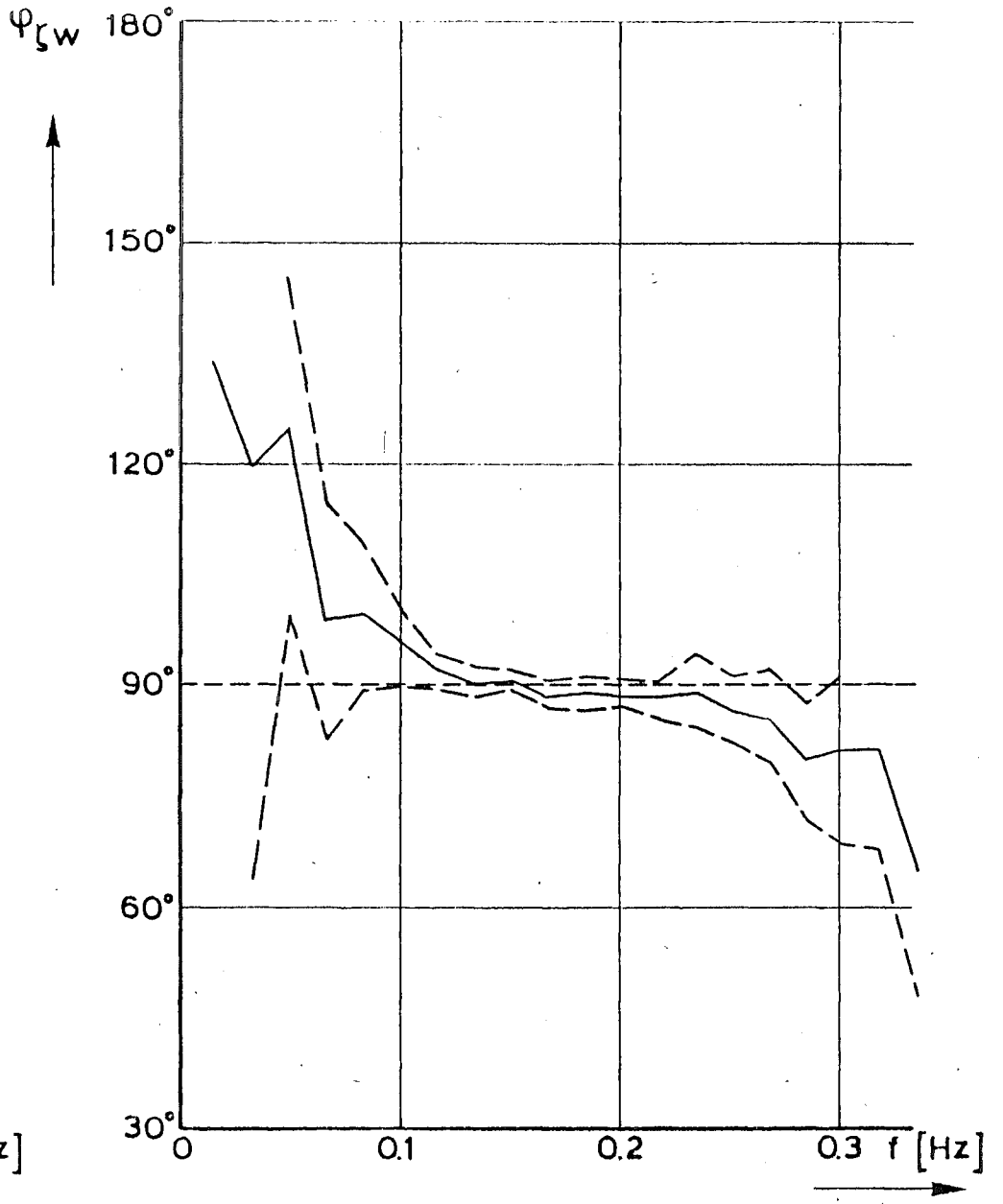

rijkswaterstaat **directie waterhuishouding en waterbeweging** **district kust en zee**	get.	appendix 4. fig. 3b
	gec.	projectcode L7709.B00
MEASURED GAINFUNCTION $H_{\zeta w}$ AND PHASEFUNCTION $\varphi_{\zeta w}$ (———) WITH 90% CONFIDENCE INTERVALS (— —) AND THEORETICAL GAIN AND PHASEFUNCTION (- - - - -). 1704	gez.	nota WWKZ-83G.007
	akk.	A 4 nr 83 K.038

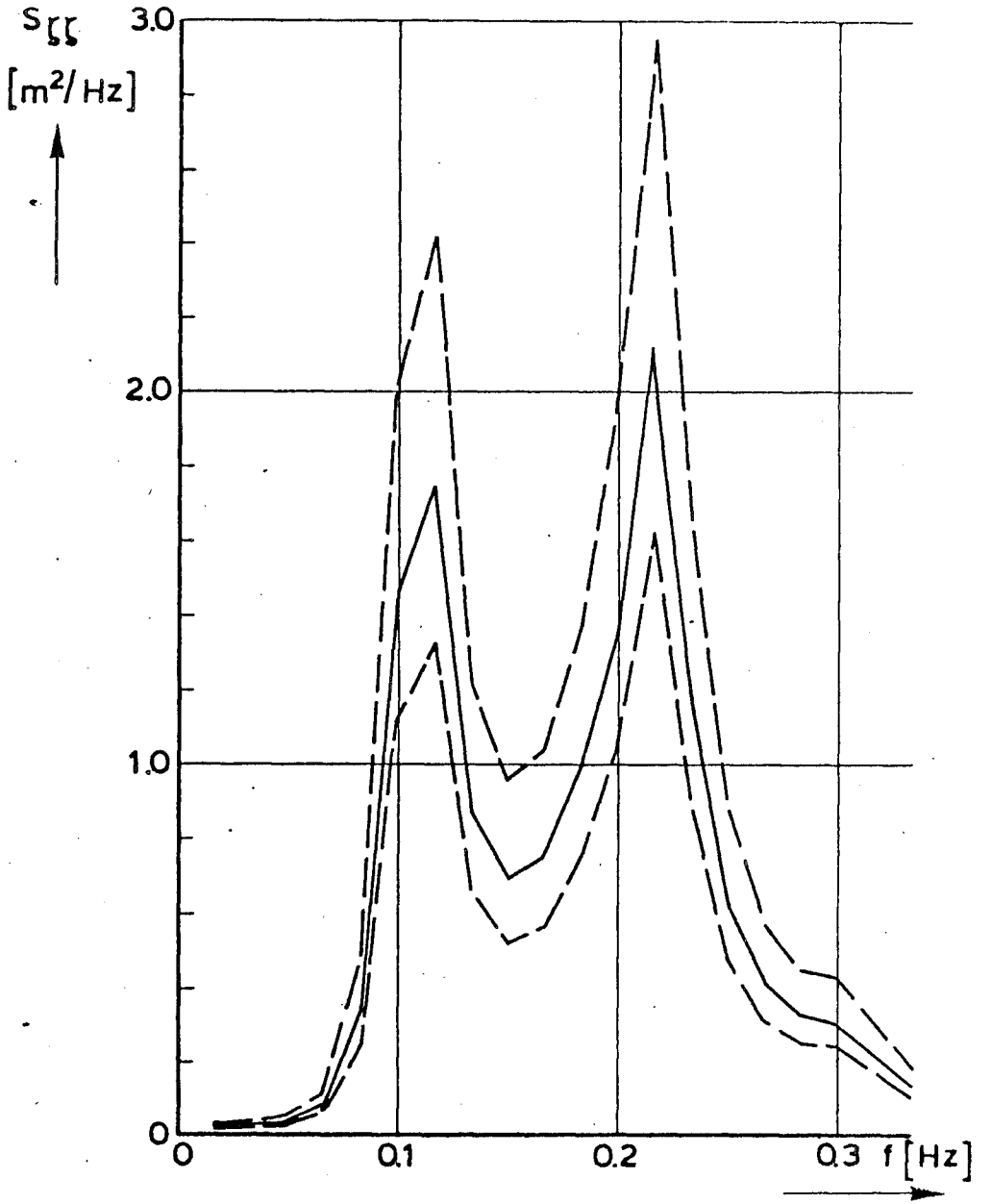

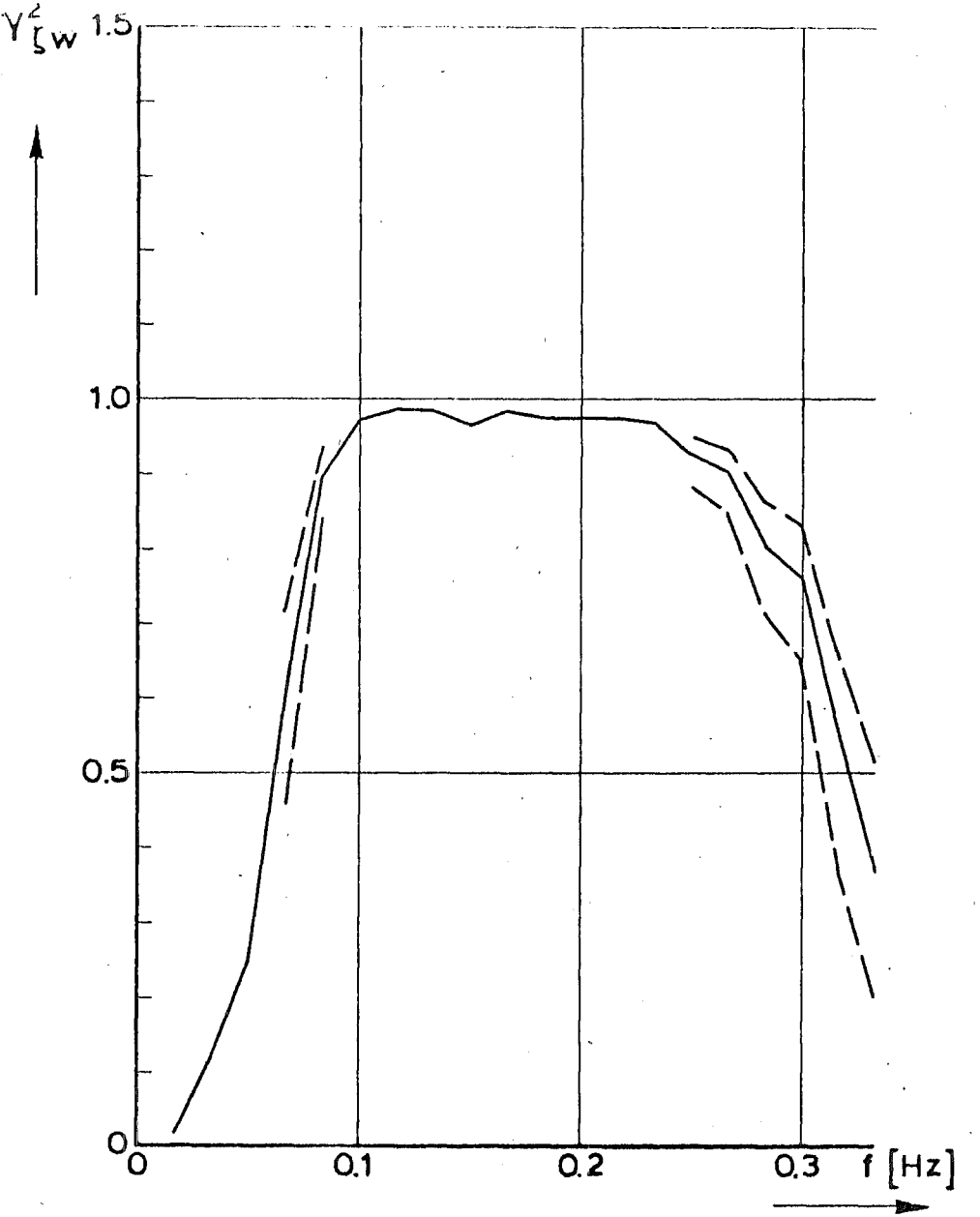

rijkswaterstaat
directie waterhuishouding en waterbeweging
district kust en zee

VARIANCE DENSITY FUNCTION OF ζ ($S_{\zeta\zeta}$) AND SQUARED COHERENCE FUNCTION w AND ζ ($\gamma^2_{\zeta w}$) WITH 90% CONFIDENCE INTERVALS (— —) 1802.

get.		appendix 4. fig. 4a	
gec.		projectcode L7709B00	
gez.		nota WWKZ-83G.007	
akk.		A 4	nr. 83K.039

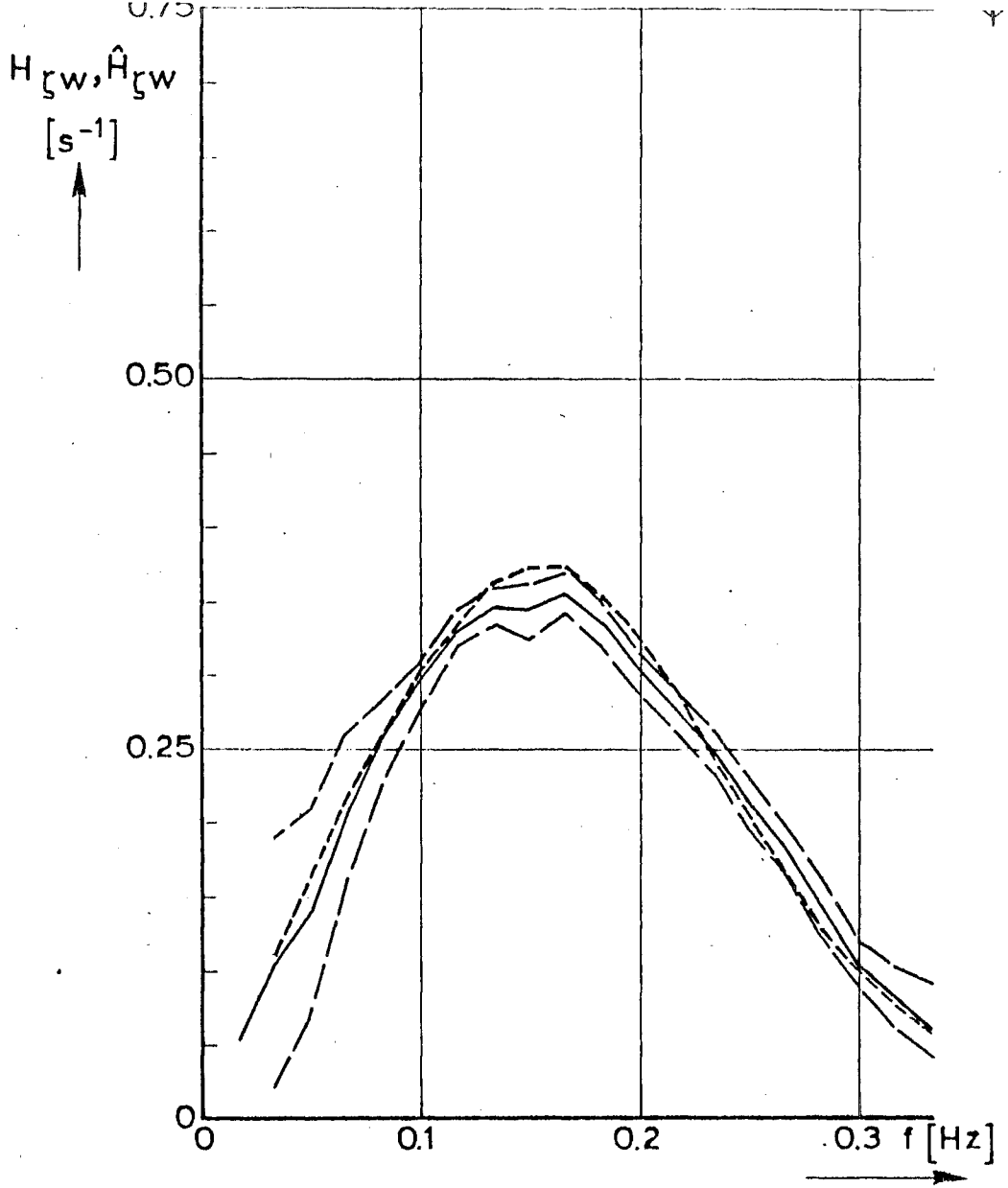

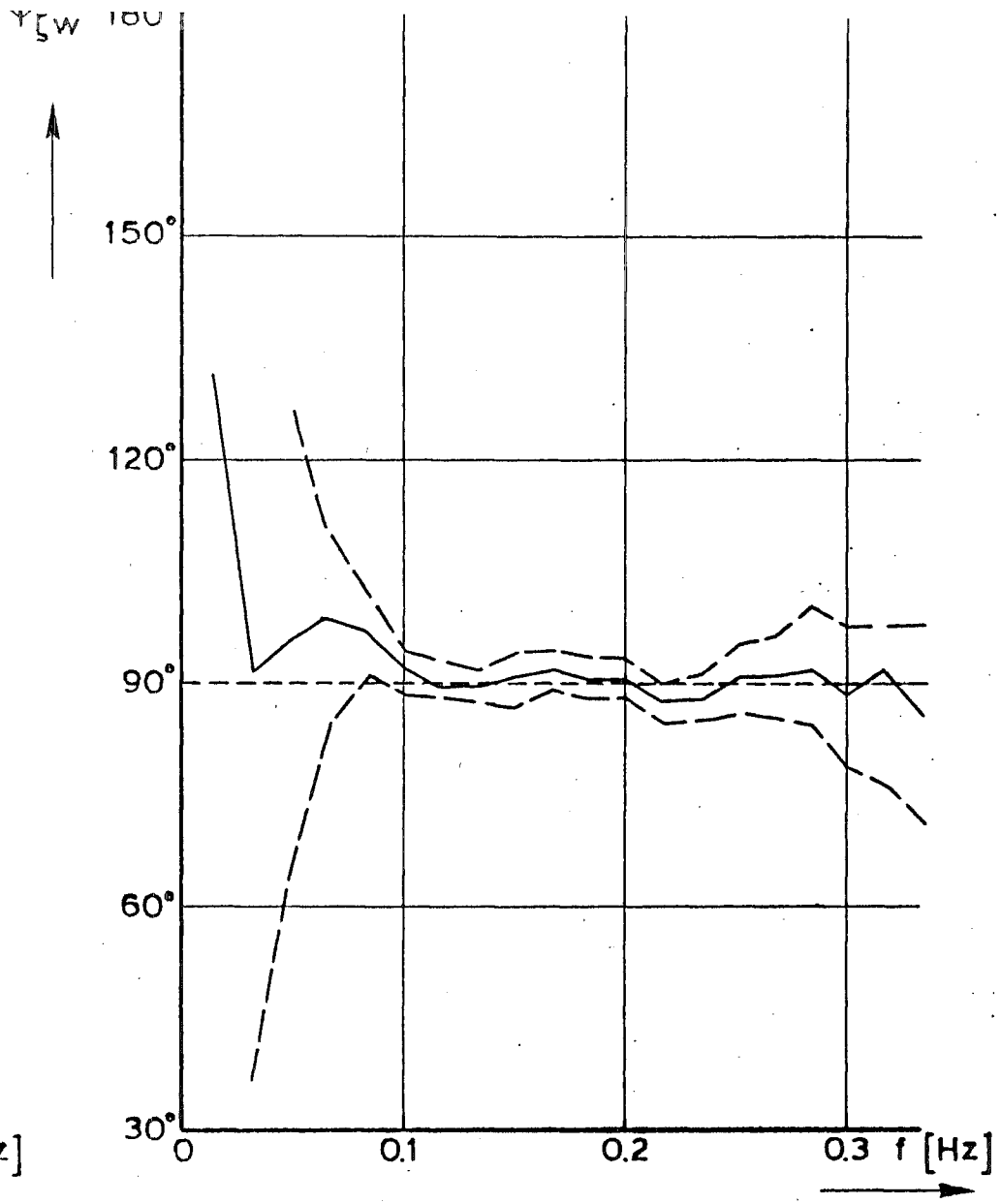

rijkswaterstaat **directie waterhuishouding en waterbeweging** **district kust en zee**	get.		appendix 4. fig. 4b
	gec.		projectcode L7709B00
MEASURED GAINFUNCTION $H_{\zeta w}$ AND PHASEFUNCTION $\varphi_{\zeta w}$ (———) WITH 90% CONFIDENCE INTERVALS (— —) AND THEORETICAL GAIN AND PHASEFUNCTION (- - - - -). 1802	gez.		nota WWKZ-83G.007
	akk.		A 4 nr 83 K.040

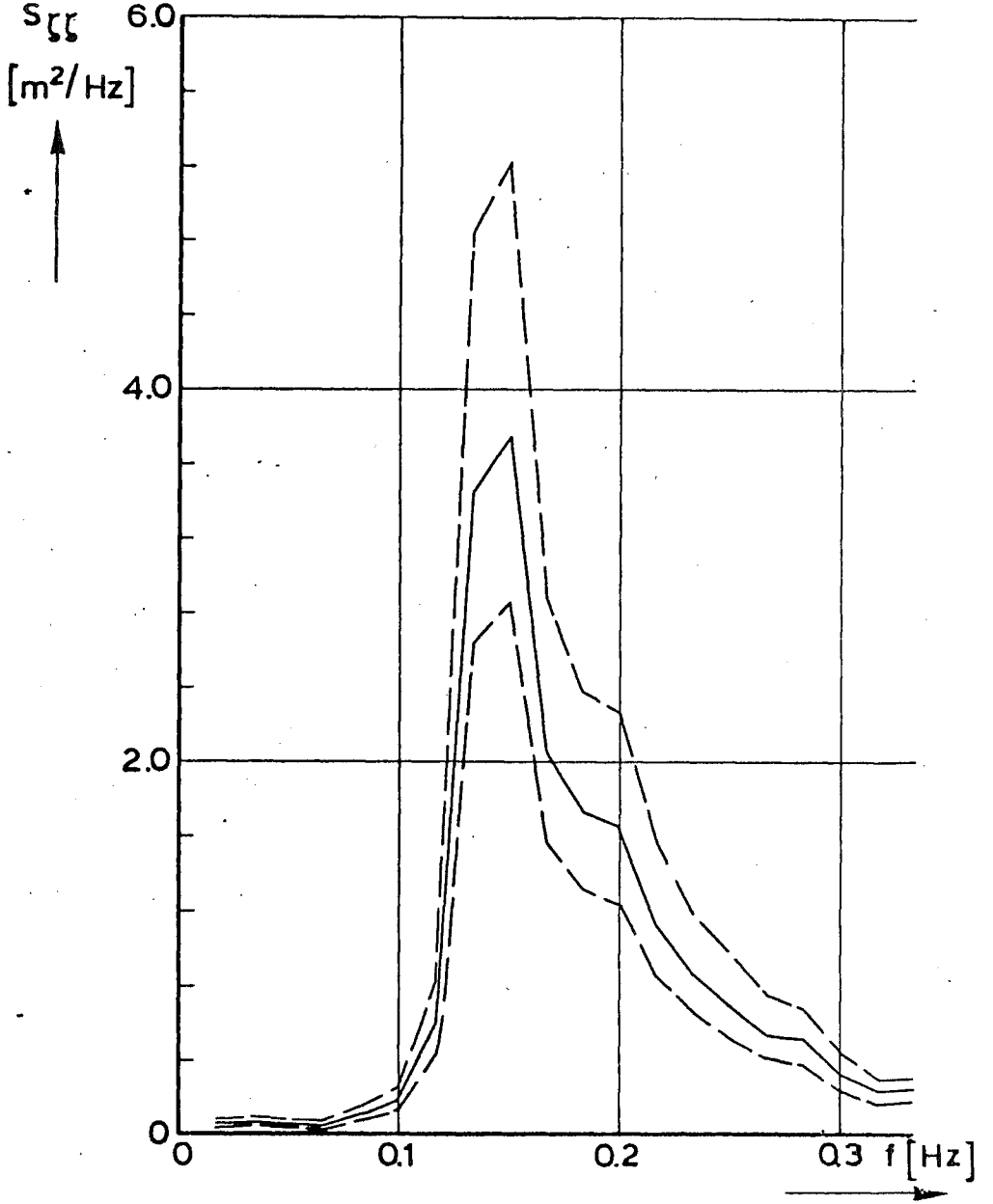

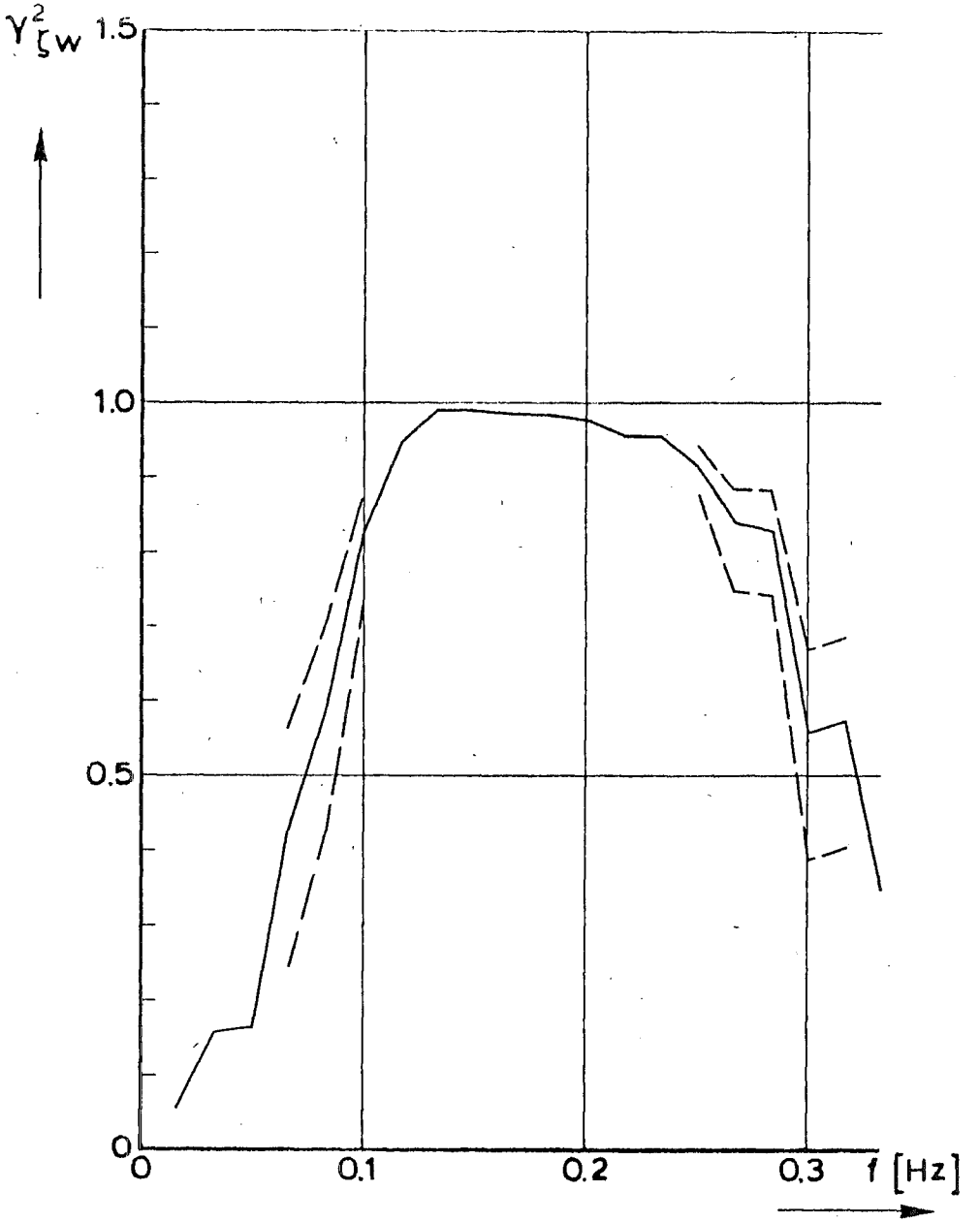

rijkswaterstaat
directie waterhuishouding en waterbeweging
district kust en zee

VARIANCE DENSITY FUNCTION OF ζ ($S_{\zeta\zeta}$) AND SQUARED COHERENCE FUNCTION w AND ζ ($\gamma^2_{\zeta w}$) WITH 90% CONFIDENCE INTERVALS (— —) 2201

get.		appendix 4. fig. 5a	
gec.		projectcode L7709B00	
gez.		nota WWKZ-83G.007	
akk.		A 4	nr. 83K.041

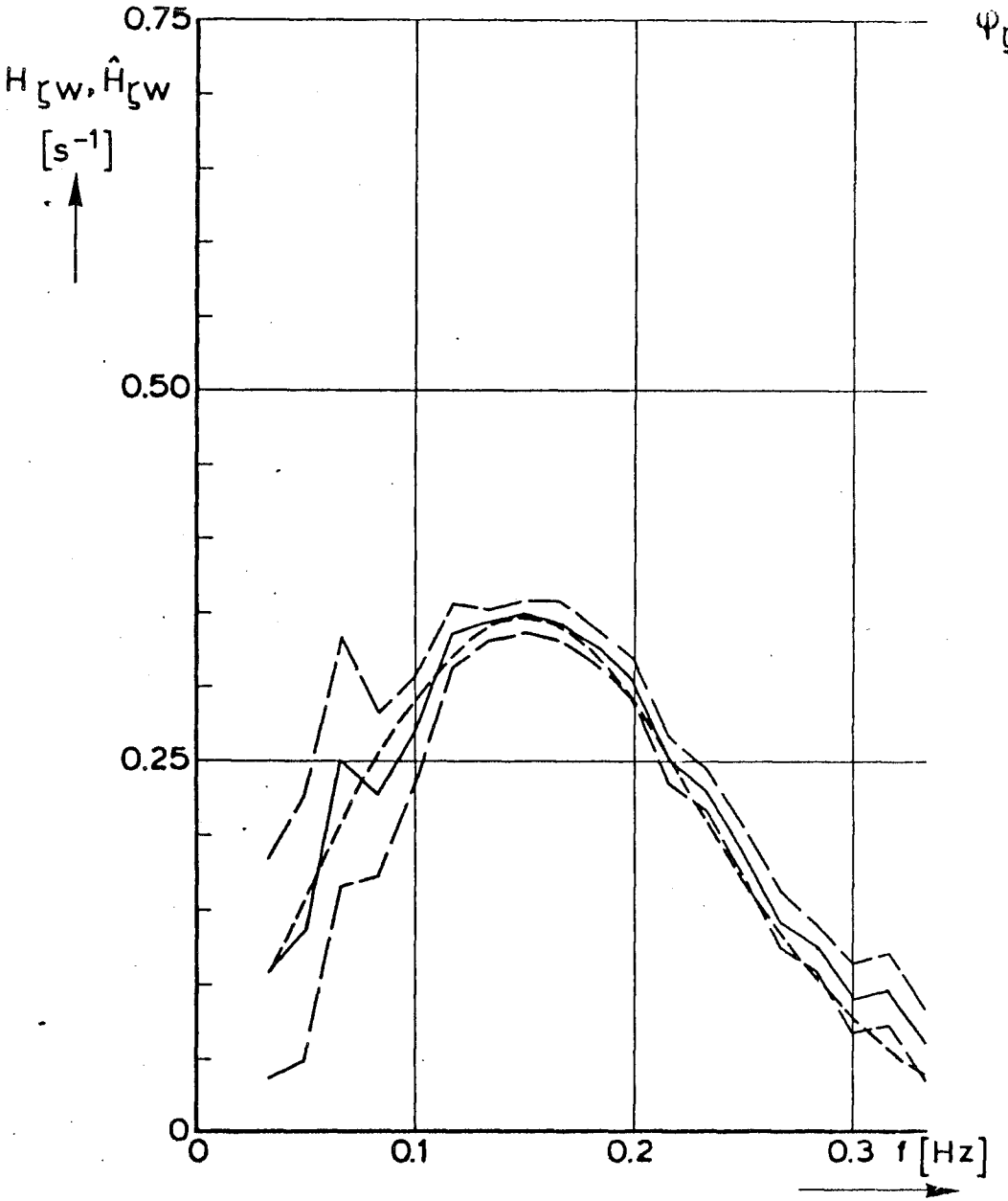

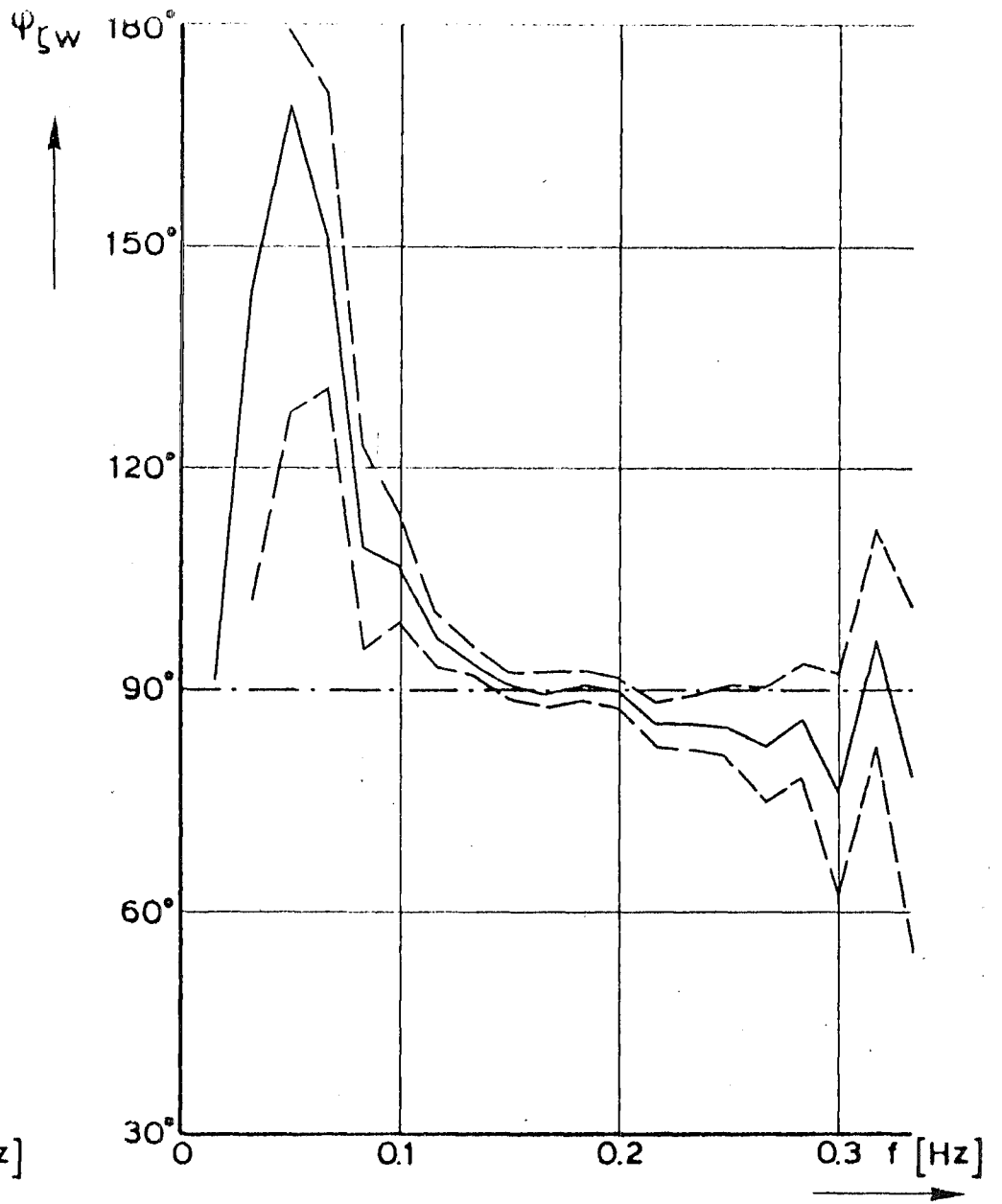

rijkswaterstaat **directie waterhuishouding en waterbeweging** **district kust en zee**	get.		appendix 4. fig. 5b
	gec.		projectcode L7709B00
MEASURED GAINFUNCTION $H_{\zeta w}$ AND PHASEFUNCTION $\Psi_{\zeta w}$ (———) WITH 90% CONFIDENCE INTERVALS (— —) AND THEORETICAL GAIN AND PHASEFUNCTION (- - - - -). 2201	gez.		nota WWKZ-83G.007
	akk.		A 4 nr. 83 K.042

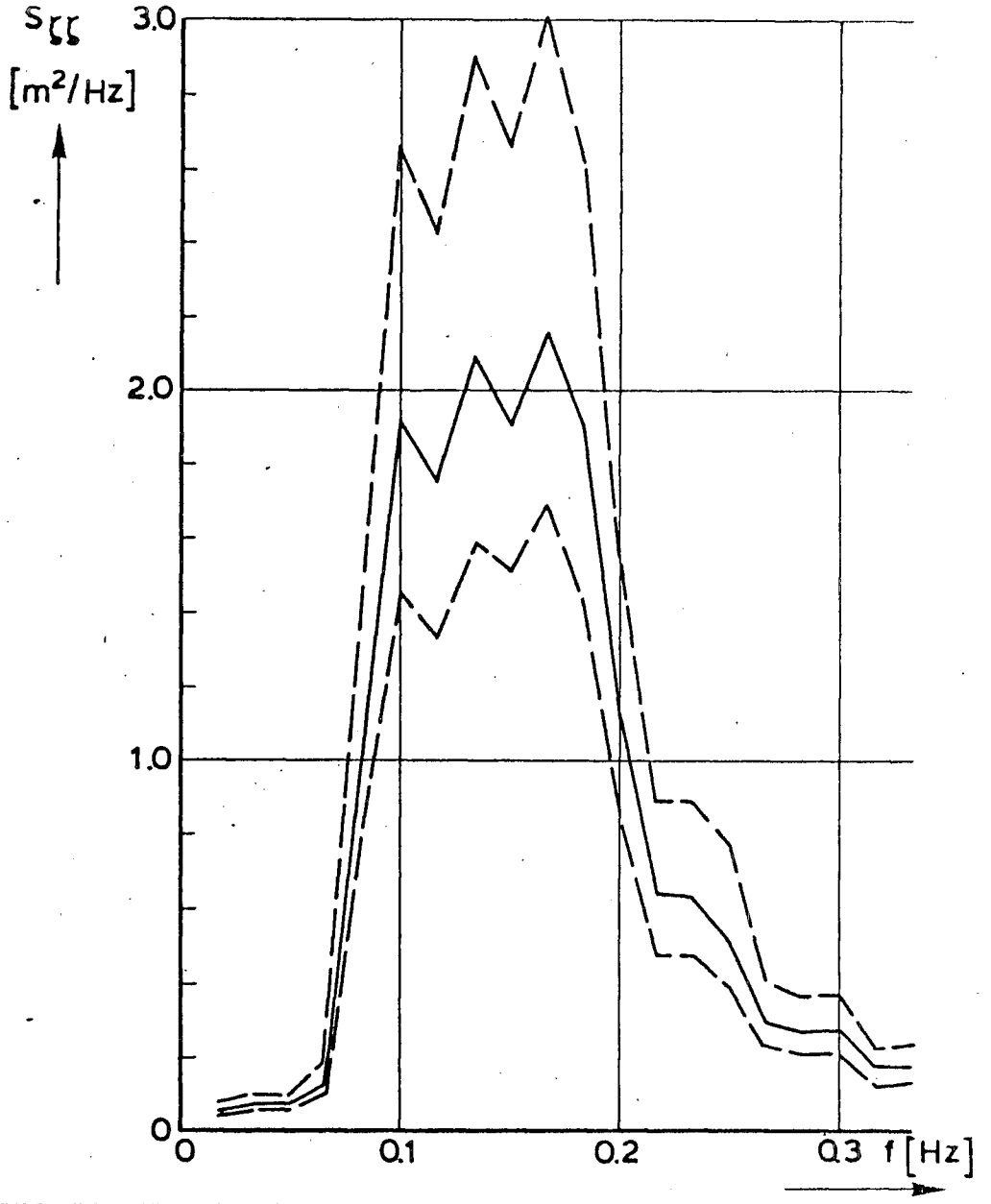

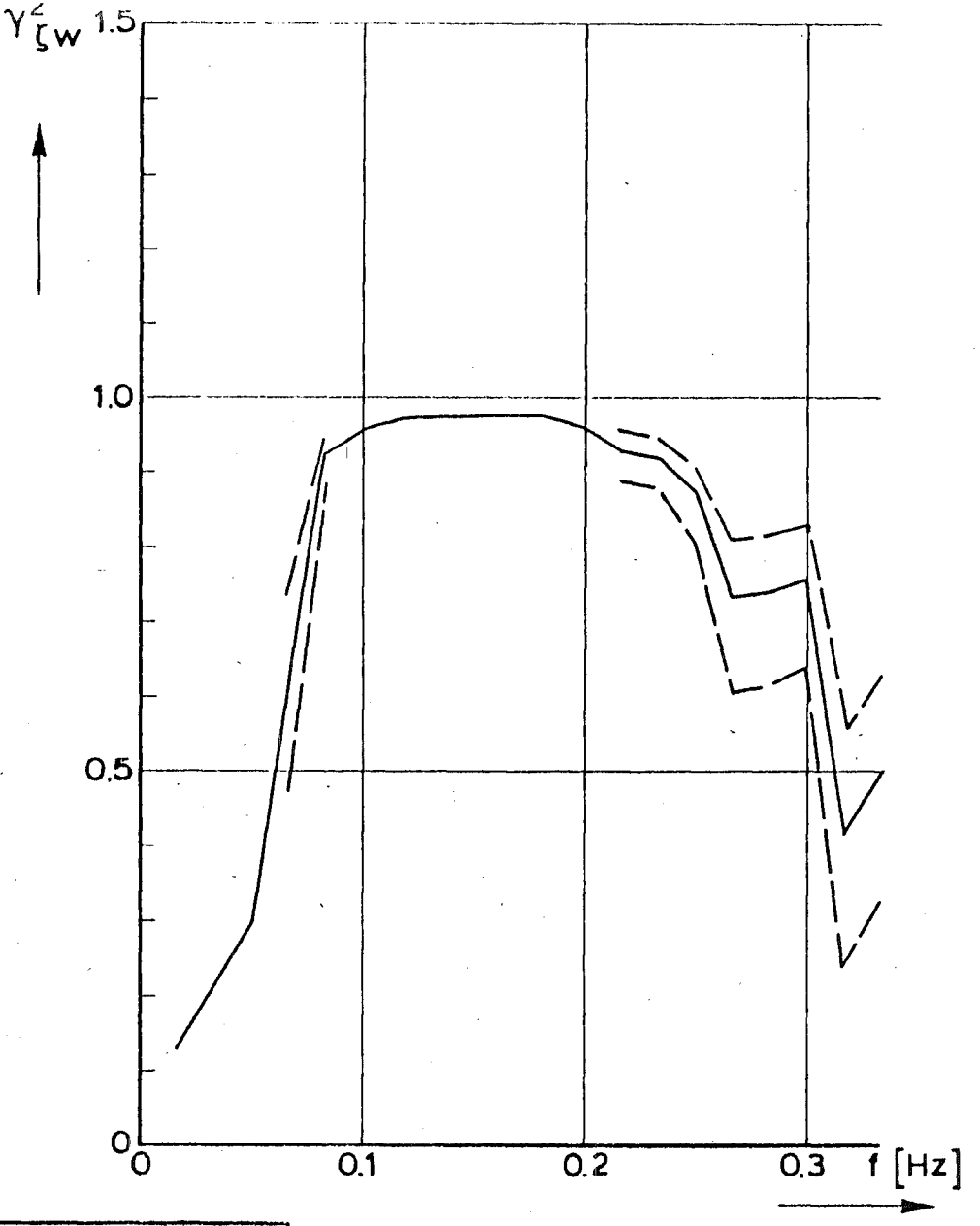

rijkswaterstaat
directie waterhuishouding en waterbeweging
district kust en zee

VARIANCE DENSITY FUNCTION OF ζ ($S_{\zeta\zeta}$) AND SQUARED COHERENCE FUNCTION w AND ζ ($\gamma^2_{\zeta w}$) WITH 90% CONFIDENCE INTERVALS (— —) 2301.

get.		appendix 4. fig. 6a	
gec.		projectcode L7709B00	
gez.		nota WWKZ-83G.007	
akk.		A 4	nr. 83K.043

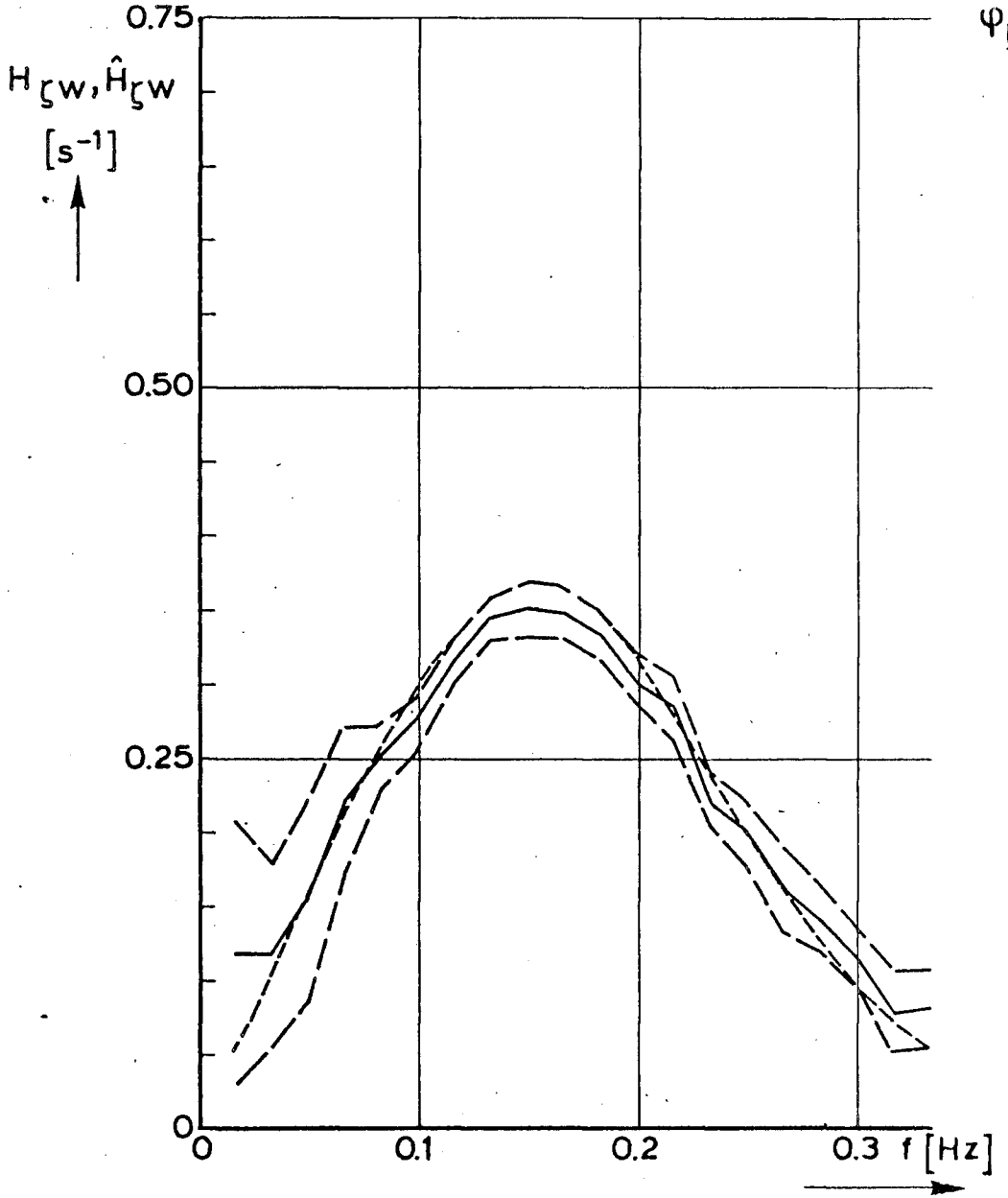

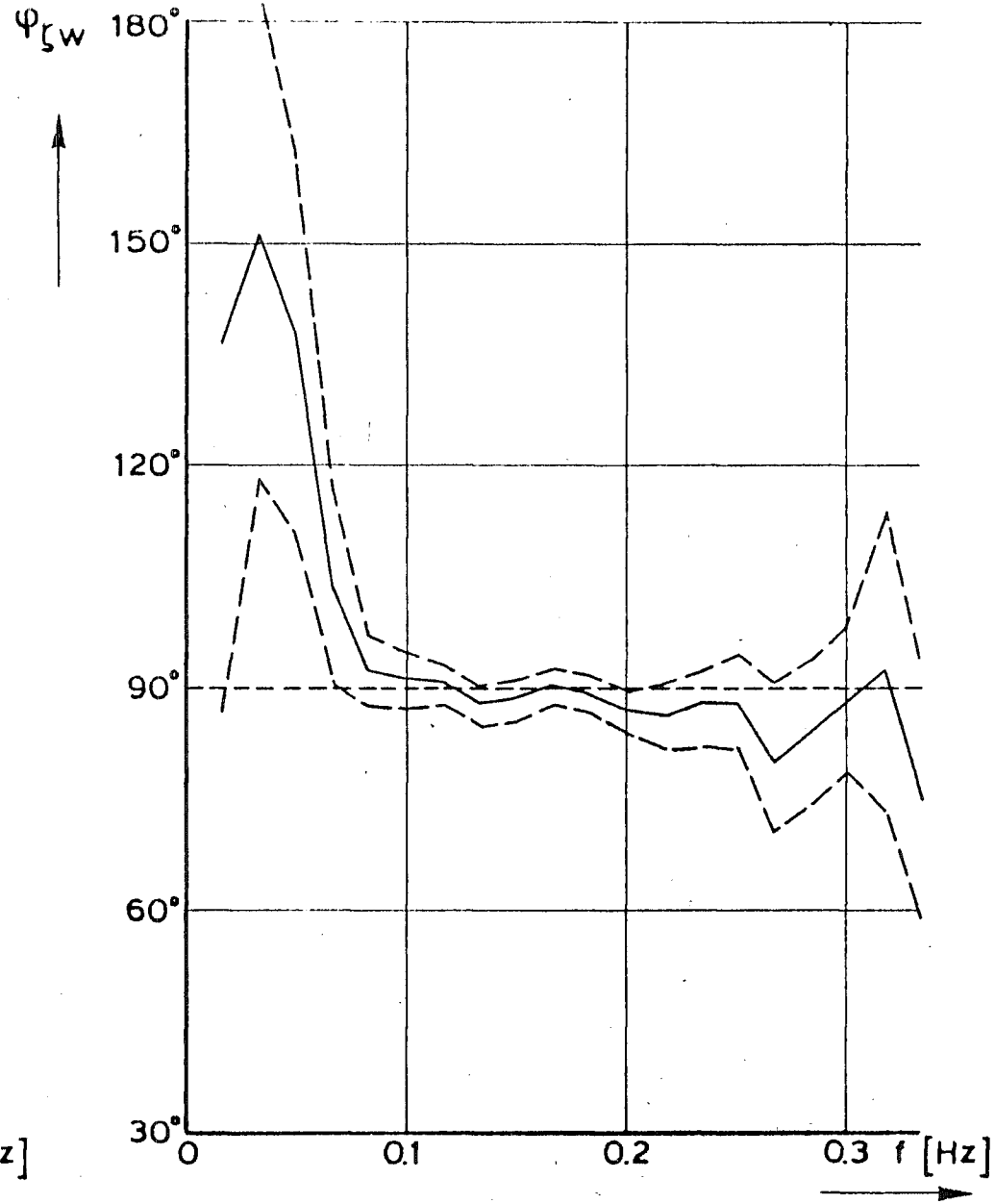

rijkswaterstaat **directie waterhuishouding en waterbeweging** **district kust en zee**	get.		appendix 4. fig. 6b
	gec.		projectcode L7709B00
MEASURED GAINFUNCTION $H_{\zeta w}$ AND PHASEFUNCTION $\varphi_{\zeta w}$ (———) WITH 90% CONFIDENCE INTERVALS (— —) AND THEORETICAL GAIN AND PHASEFUNCTION (- - - - -). 2301	gez.		nota WWKZ-83G.007
	akk.		A 4 nr. 83 K.044

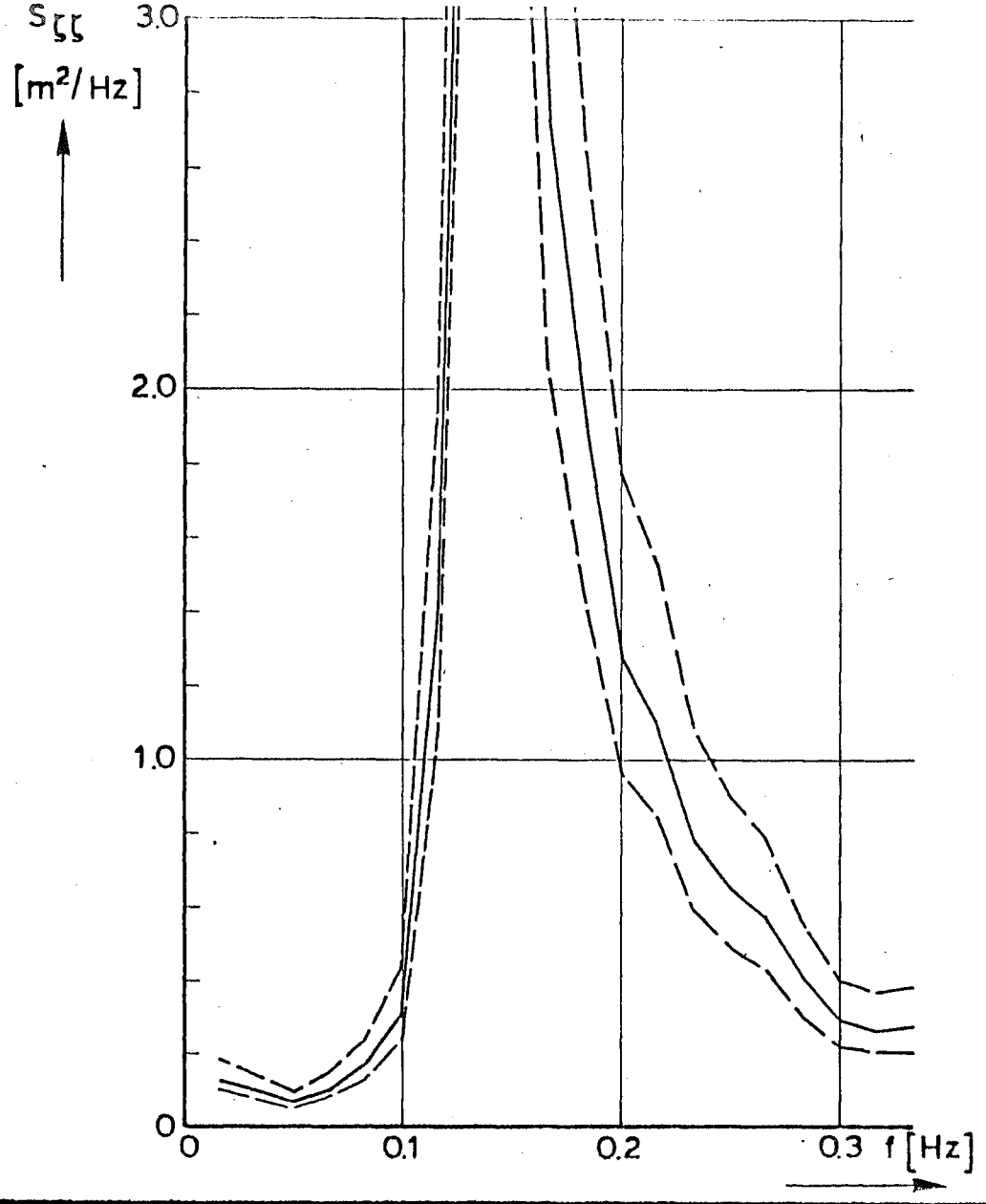

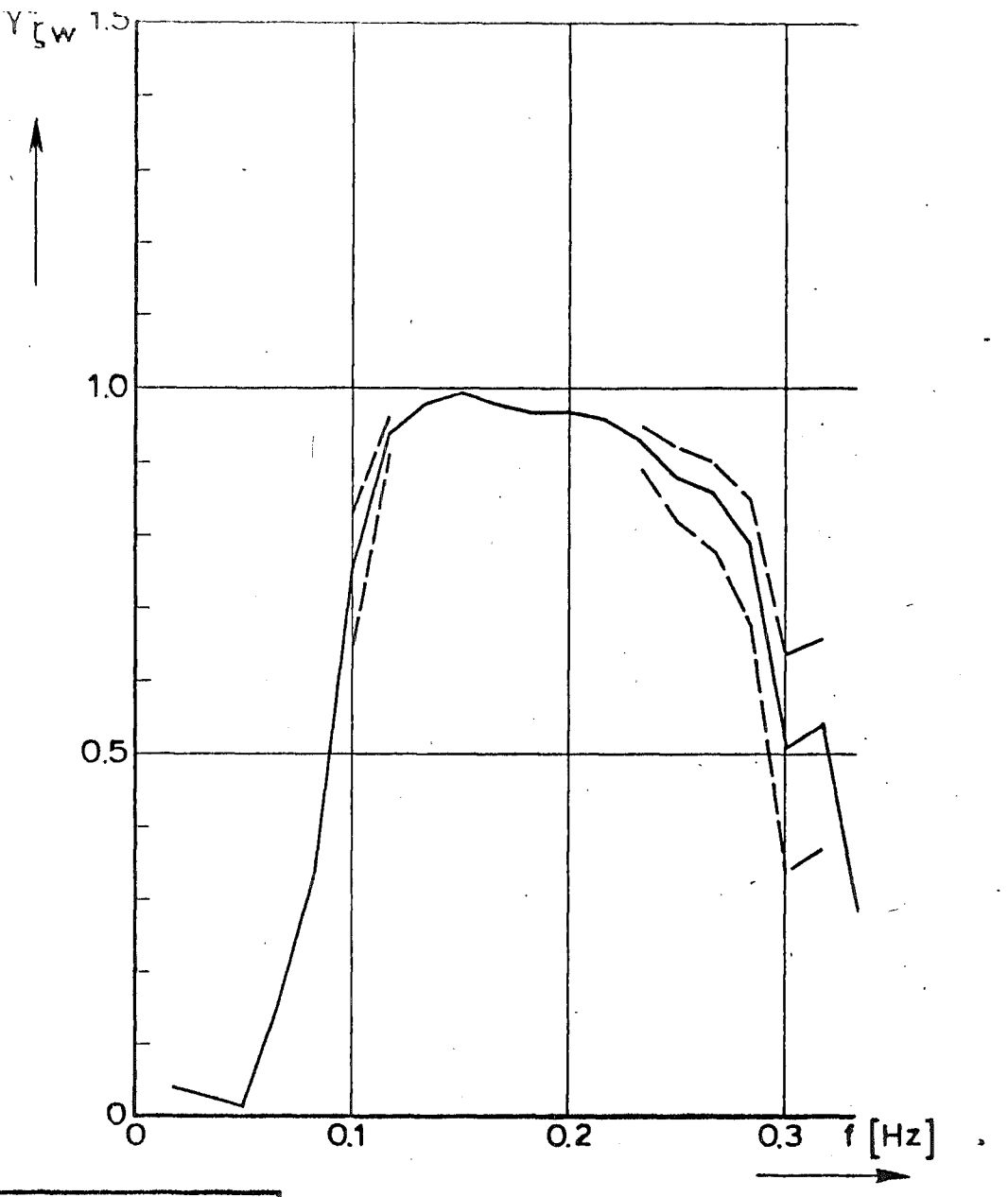

rijkswaterstaat **directie waterhuishouding en waterbeweging** **district kust en zee**	get.		appendix 4. fig. 7a
	gec.		projectcode L7709B00
VARIANCE DENSITY FUNCTION OF ζ ($S_{\zeta\zeta}$) AND SQUARED COHERENCE FUNCTION w AND ζ ($\gamma^2_{\zeta w}$) WITH 90% CONFIDENCE INTERVALS (— —) 2420.	gez.		nota WWKZ-83G.007
	akk.		A 4 nr. 83K.045

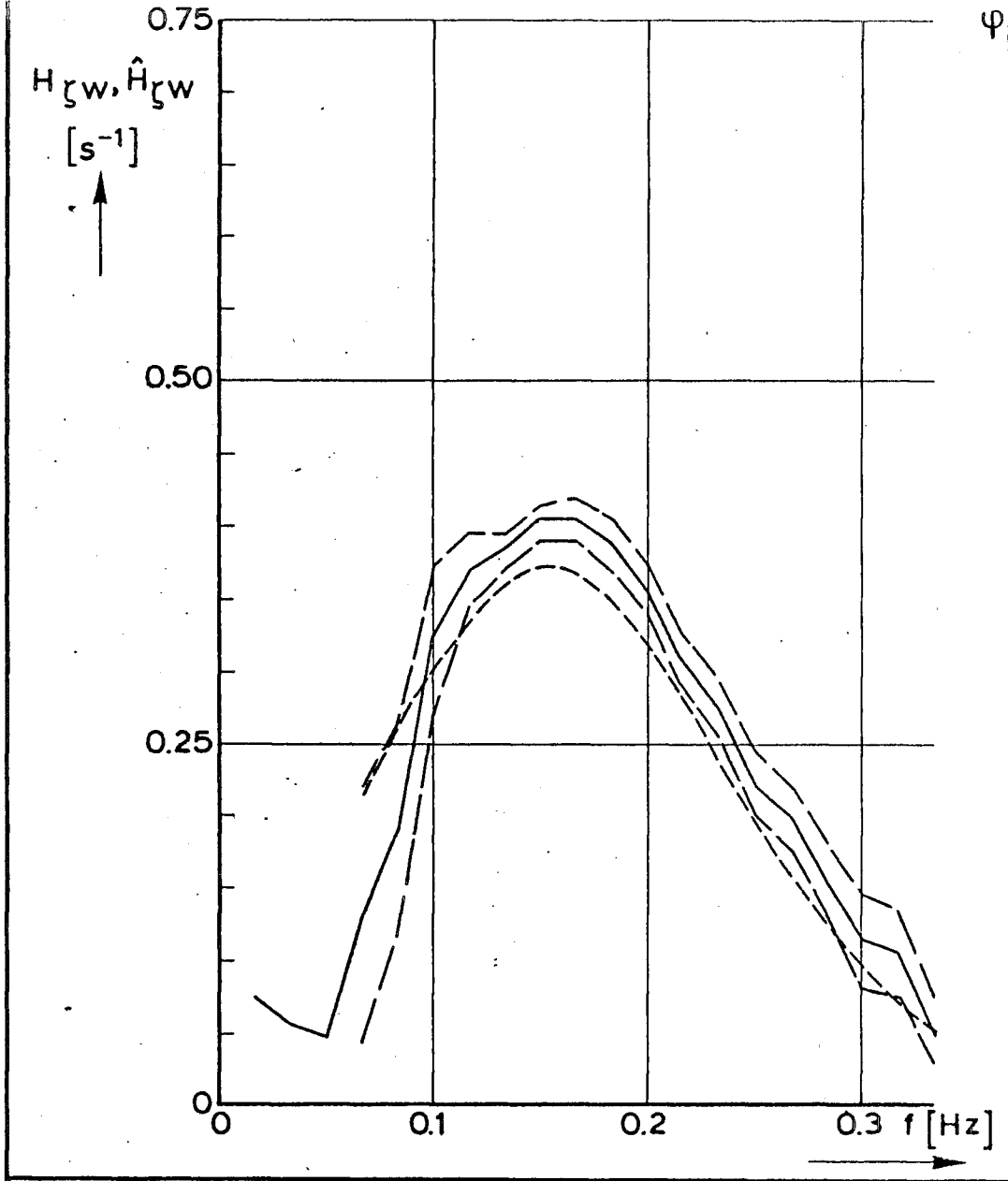

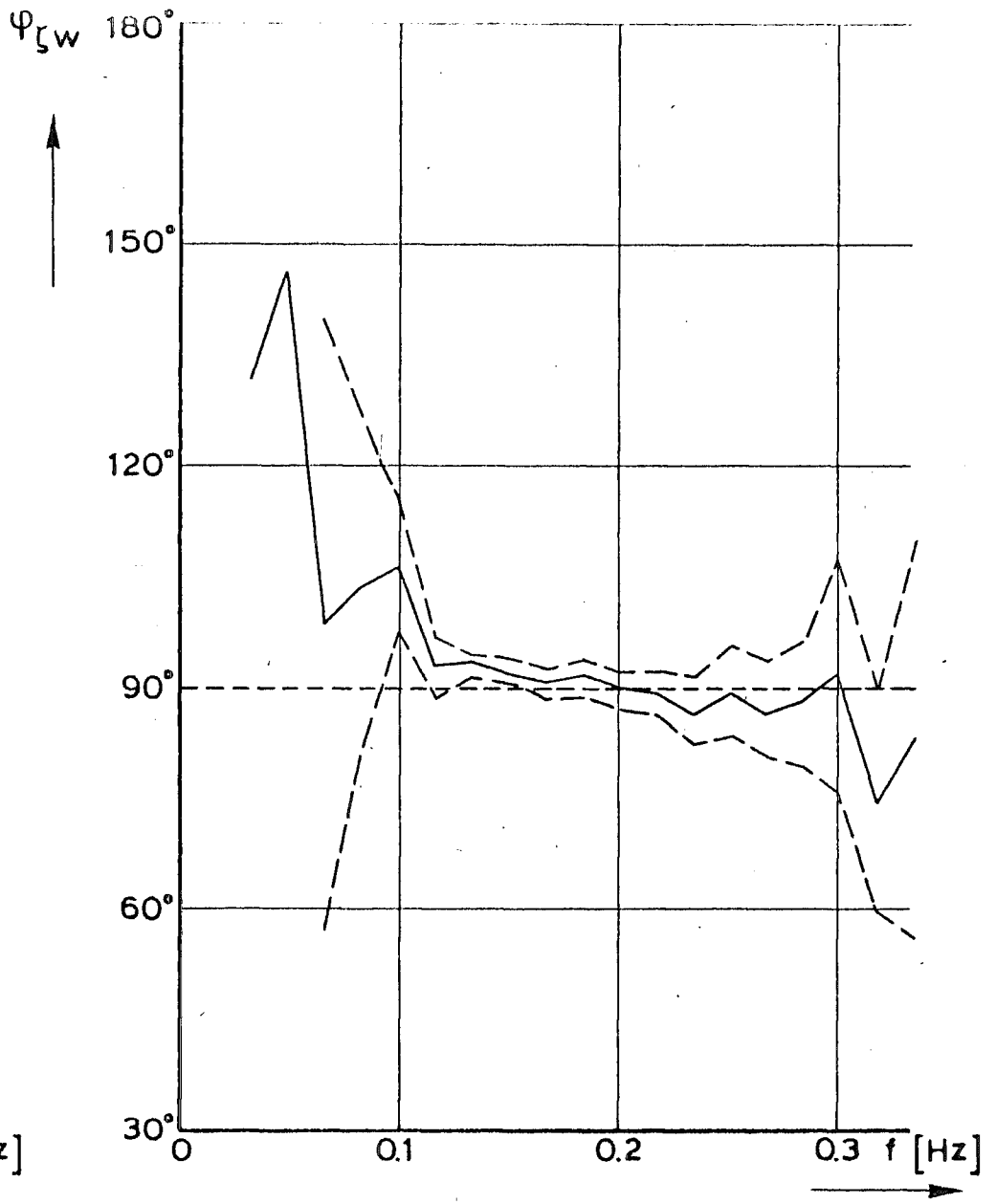

rijkswaterstaat **directie waterhuishouding en waterbeweging** **district kust en zee**	get.		appendix 4. fig. 7b
	gec.		projectcode L7709B00
MEASURED GAINFUNCTION $H_{\zeta w}$ AND PHASEFUNCTION $\varphi_{\zeta w}$ (———) WITH 90% CONFIDENCE INTERVALS (— —) AND THEORETICAL GAIN AND PHASEFUNCTION (- - - - -). 2420	gez.		nota WWKZ-83G.007
	akk.		A 4 nr. 83 K.046

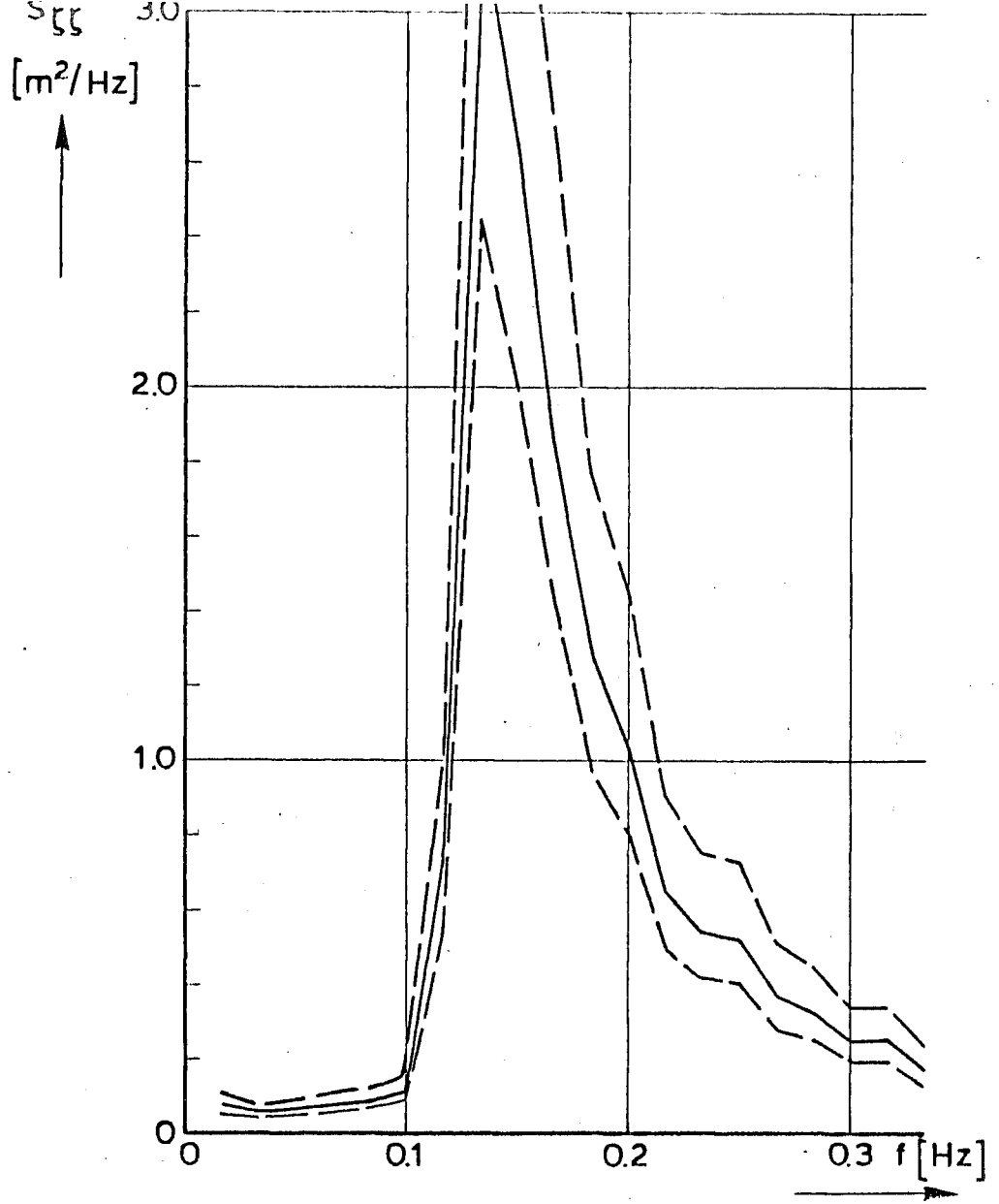

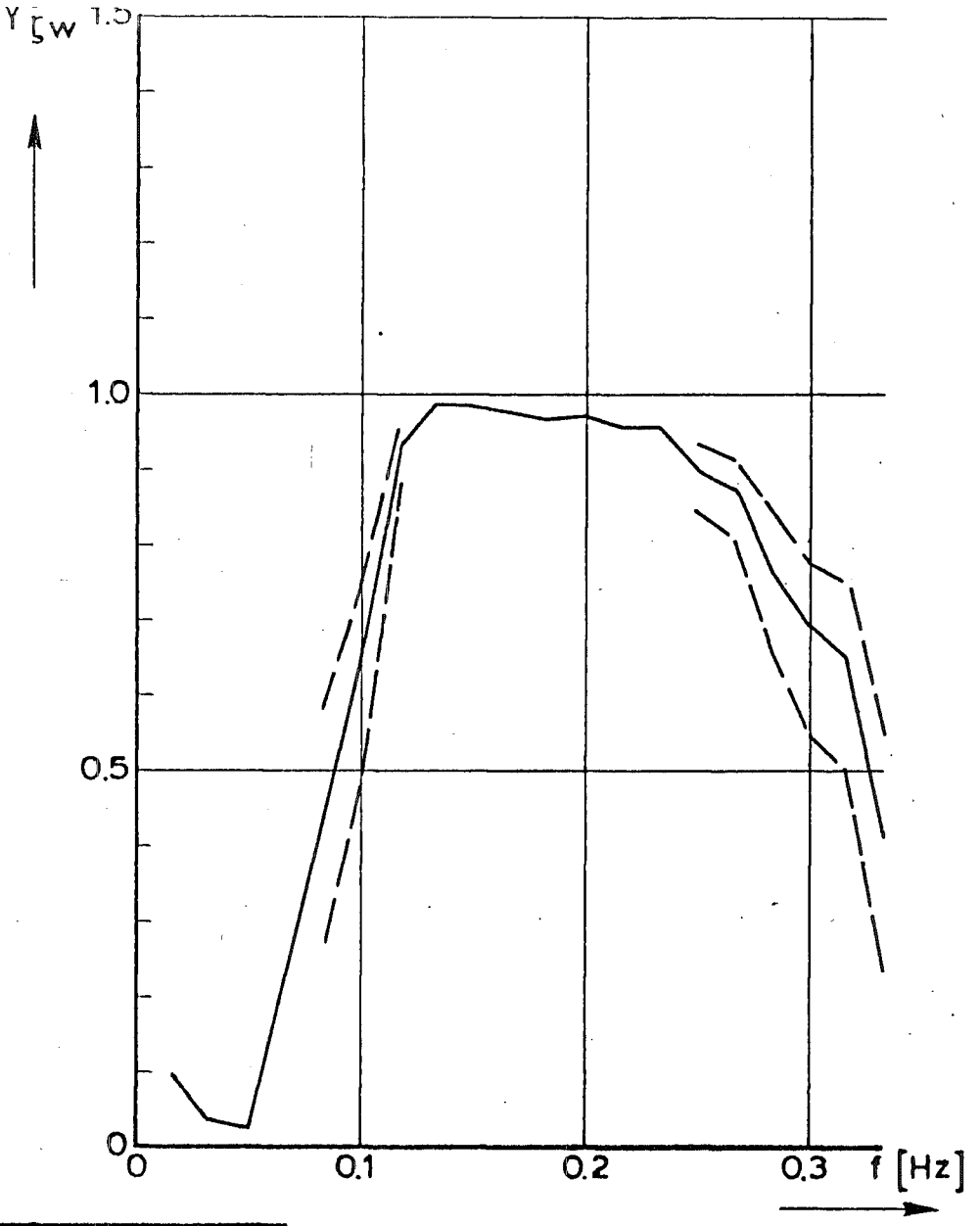

rijkswaterstaat **directie waterhuishouding en waterbeweging** **district kust en zee**	get.		appendix 4. fig. 8a
	gec.		projectcode L7709B00
VARIANCE DENSITY FUNCTION OF ζ ($S_{\zeta\zeta}$) AND SQUARED COHERENCE FUNCTION w AND ζ ($\gamma^2_{\zeta w}$) WITH 90% CONFIDENCE INTERVALS (— —) 2501.	gez.		nota WWKZ-83G.007
	akk.		A 4 nr. 83K.047

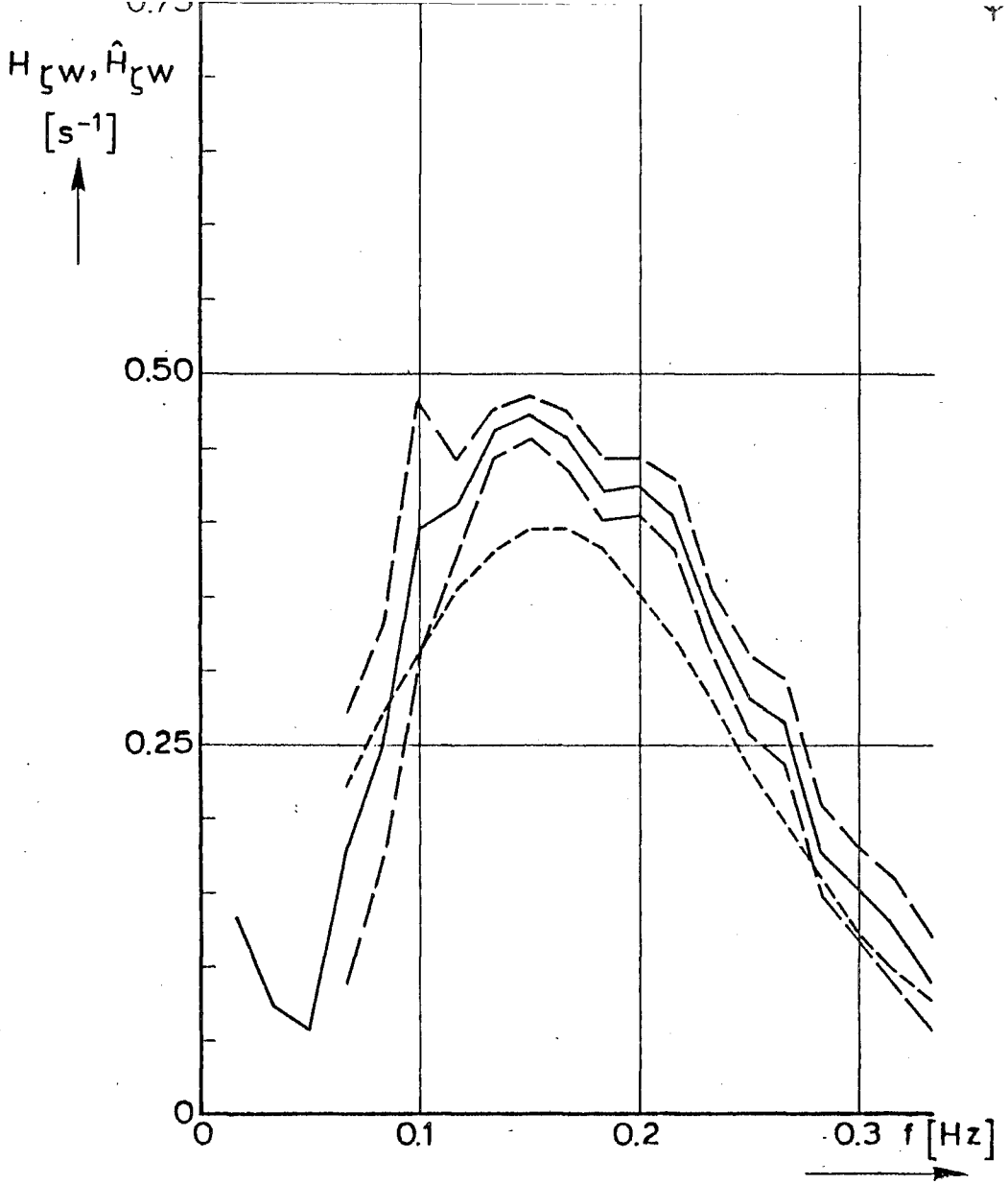

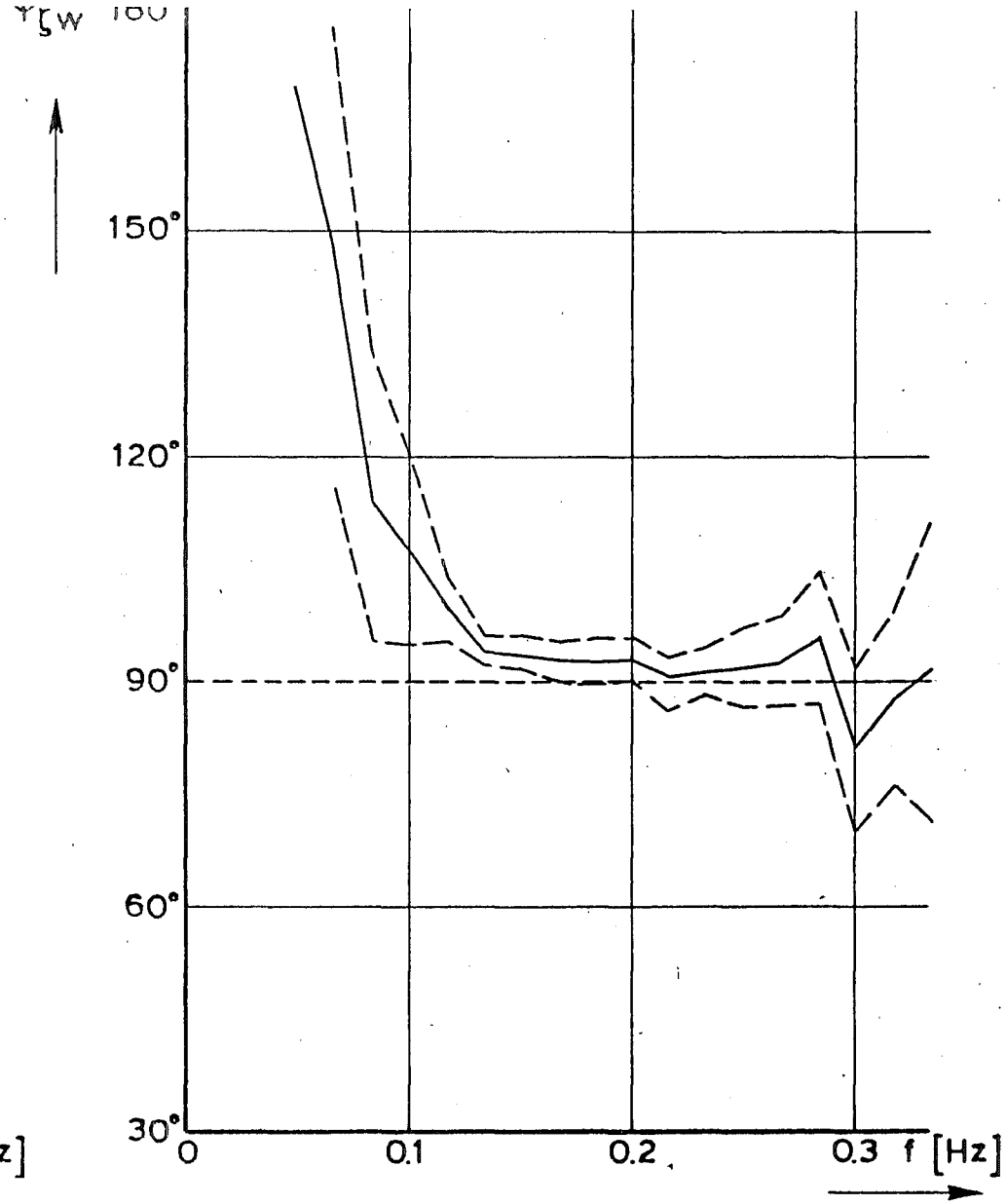

rijkswaterstaat **directie waterhuishouding en waterbeweging** **district kust en zee**	get.		appendix 4. fig. 8b
	gec.		projectcode L7709B00
MEASURED GAINFUNCTION $H_{\zeta w}$ AND PHASEFUNCTION $\varphi_{\zeta w}$ (———) WITH 90% CONFIDENCE INTERVALS (— —) AND THEORETICAL GAIN AND PHASEFUNCTION (- - - - -), 2501	gez.		nota WWKZ-83G.007
	skk.		A 4 nr. 83 K.048

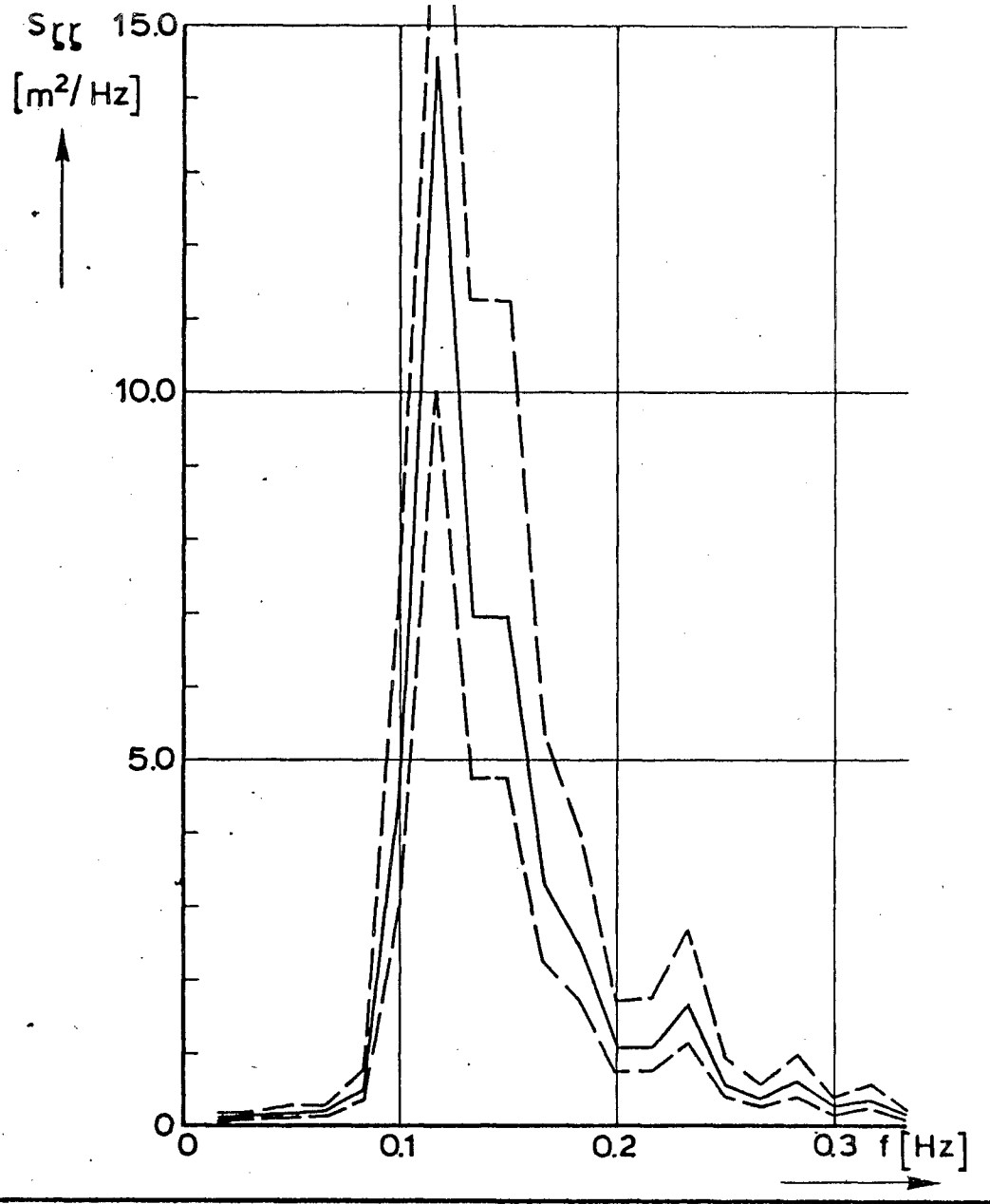

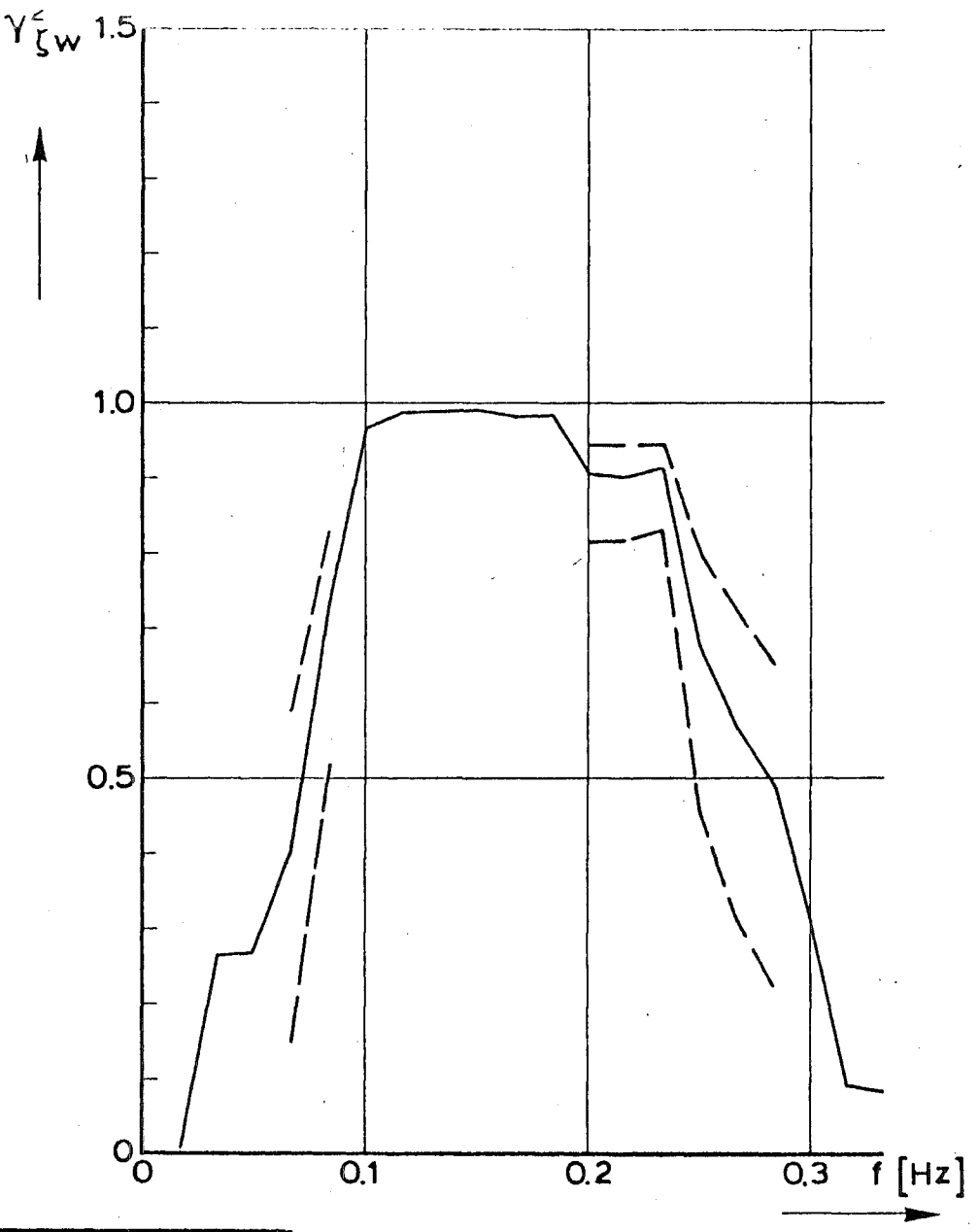

rijkswaterstaat
directie waterhuishouding en waterbeweging
district kust en zee

VARIANCE DENSITY FUNCTION OF ζ ($S_{\zeta\zeta}$) AND SQUARED COHERENCE FUNCTION w AND ζ ($\gamma^2_{\zeta w}$) WITH 90% CONFIDENCE INTERVALS (— —) 2601.

get.		appendix 4. fig. 9a	
gec.		projectcode L7709B00	
gez.		nota WWKZ-83G.007	
akk.		A 4	nr. 83K.049

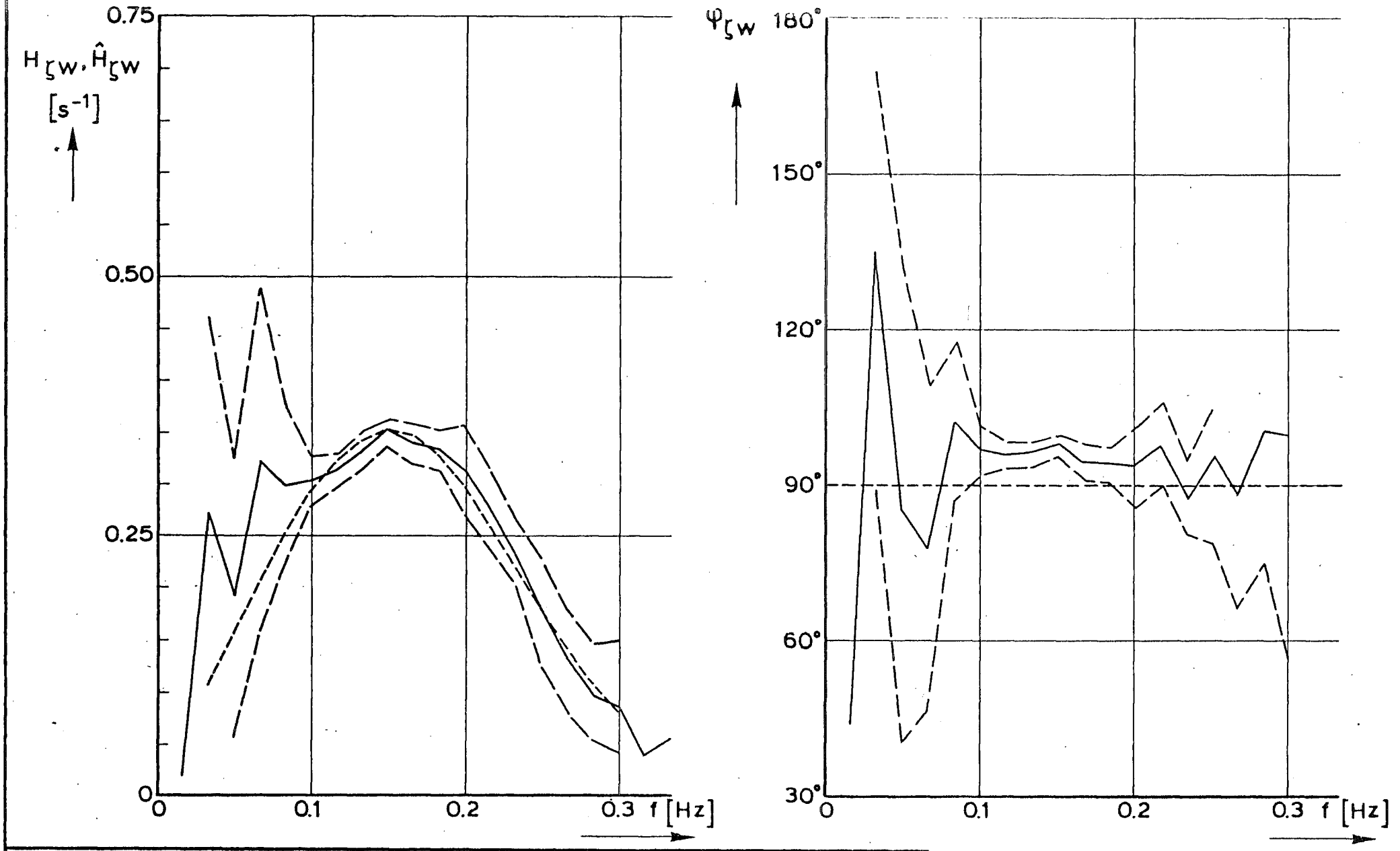

rijkswaterstaat **directie waterhuishouding en waterbeweging** **district kust en zee**	get.		appendix 4. fig. 9b
	gec.		projectcode L7709B00
MEASURED GAINFUNCTION. $H_{\zeta w}$ AND PHASEFUNCTION $\Psi_{\zeta w}$ (———) WITH 90% CONFIDENCE INTERVALS (— —) AND THEORETICAL GAIN AND PHASEFUNCTION (- - - - -). 2601	gez.		nota WWKZ-83G.007
	akk.		A 4 nr. 83 K.050

APPENDIX 5.

COMPARISON MEASURED GAIN FUNCTIONS OF SURFACE ELEVATION AND VERTICAL VELOCITY COMPONENT WITH LINEAR THEORY.

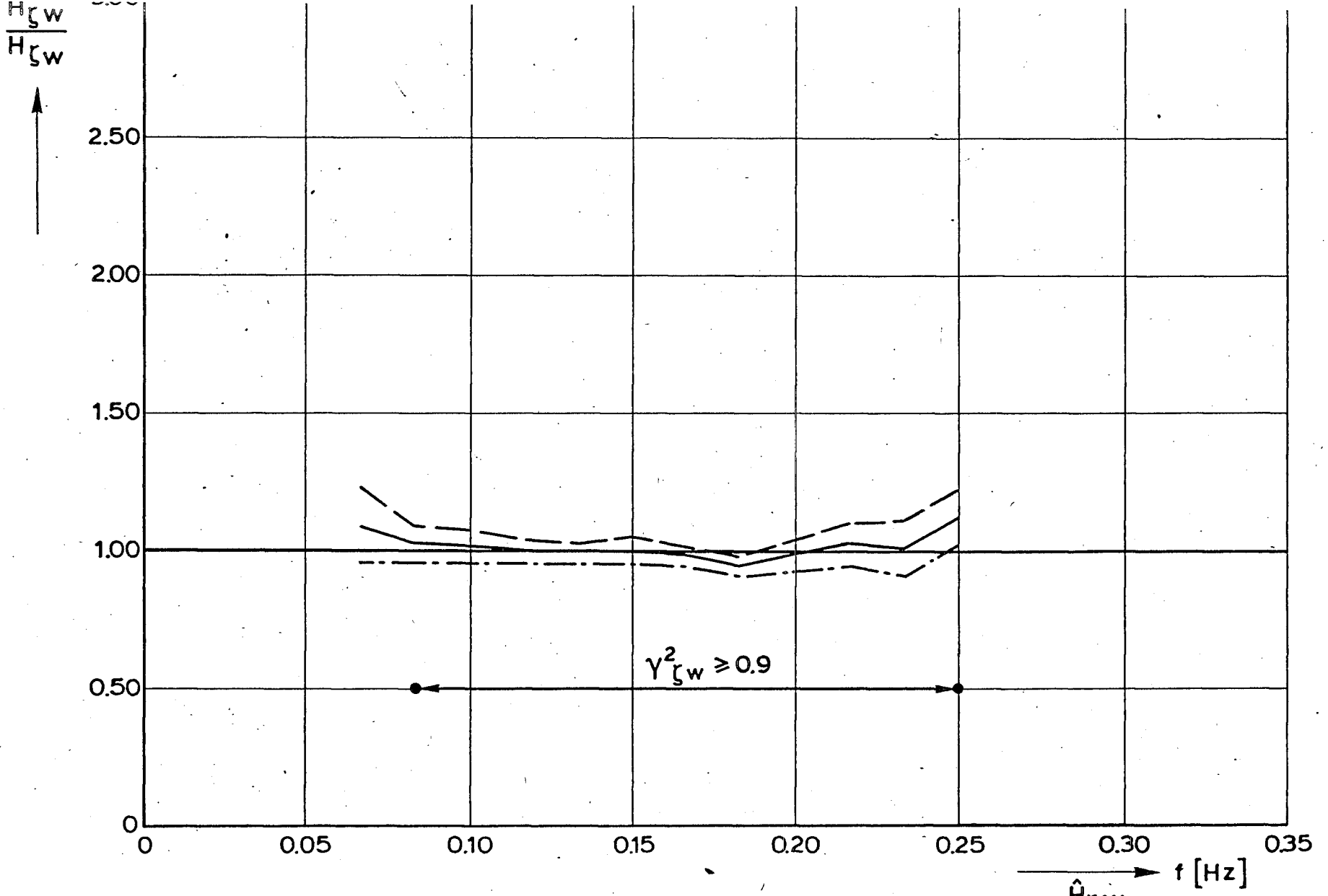

rijkswaterstaat directie waterhuishouding en waterbeweging district kust en zee	get.		appendix 5. fig 1
	gec.		projectcode L7709B00
COMPARISON MEASURED GAINFUNCTION OF ζ AND w WITH LINEAR THEORY (1501)	gez.		nota WWKZ-83G.007
	akk.		A 4 nr. 83K.051

——— $\frac{\hat{H}_{\zeta w}}{H_{\zeta w}}$ WITH

– – – } 90 % CONFIDENCE INTERVAL.

– · – · –

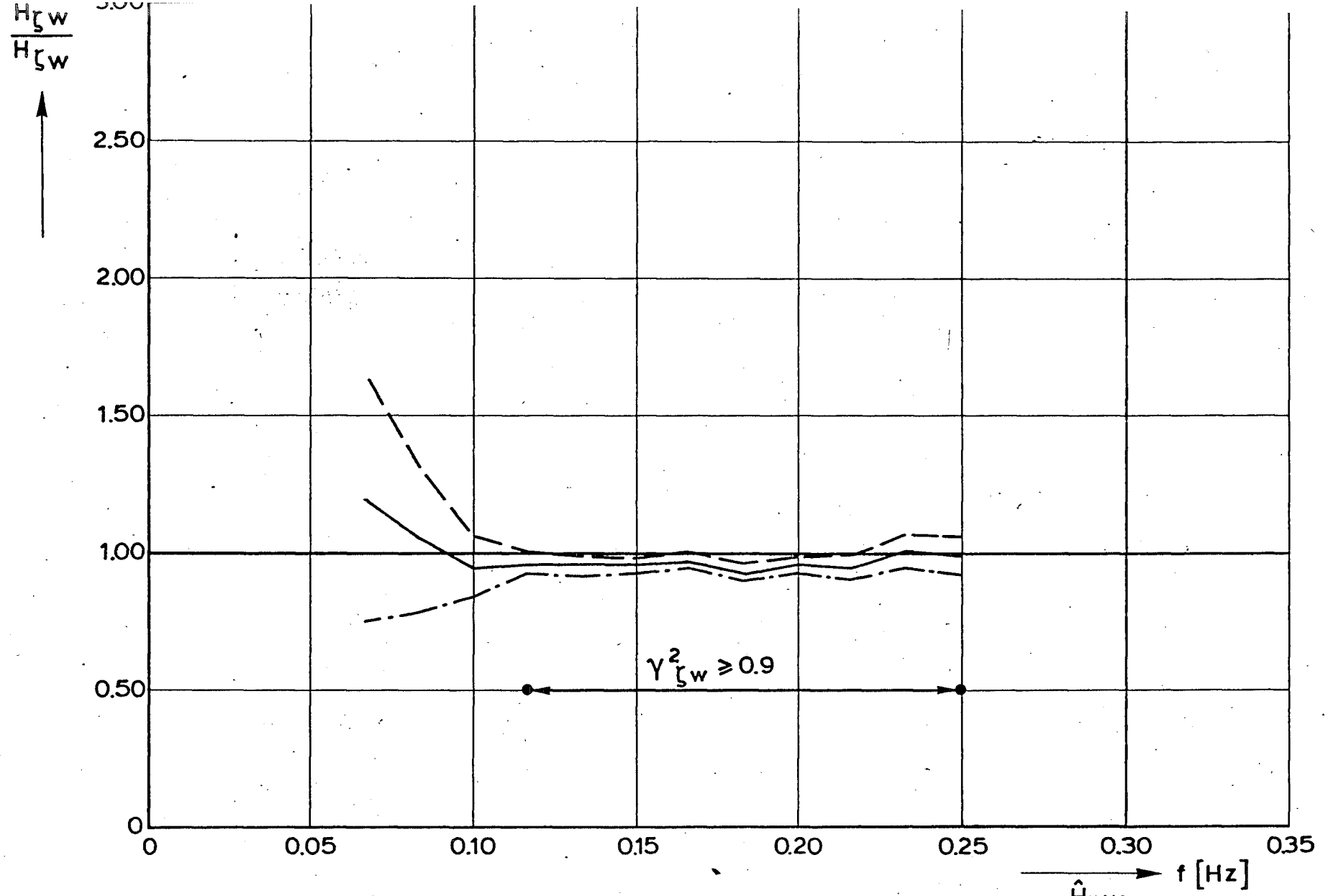

rijkswaterstaat directie waterhuishouding en waterbeweging district kust en zee	get.	appendix 5. fig. 2	
	gec.	projectcode L7709B00	
COMPARISON MEASURED GAINFUNCTION OF ζ AND w WITH LINEAR THEORY (1601)	gez.	nota WWKZ-83G.007	
	akk.	A 4	nr. 83K.052

——— $\frac{\hat{H}_{\zeta w}}{H_{\zeta w}}$ WITH

– – – } 90 % CONFIDENCE INTERVAL.

–·–·– }

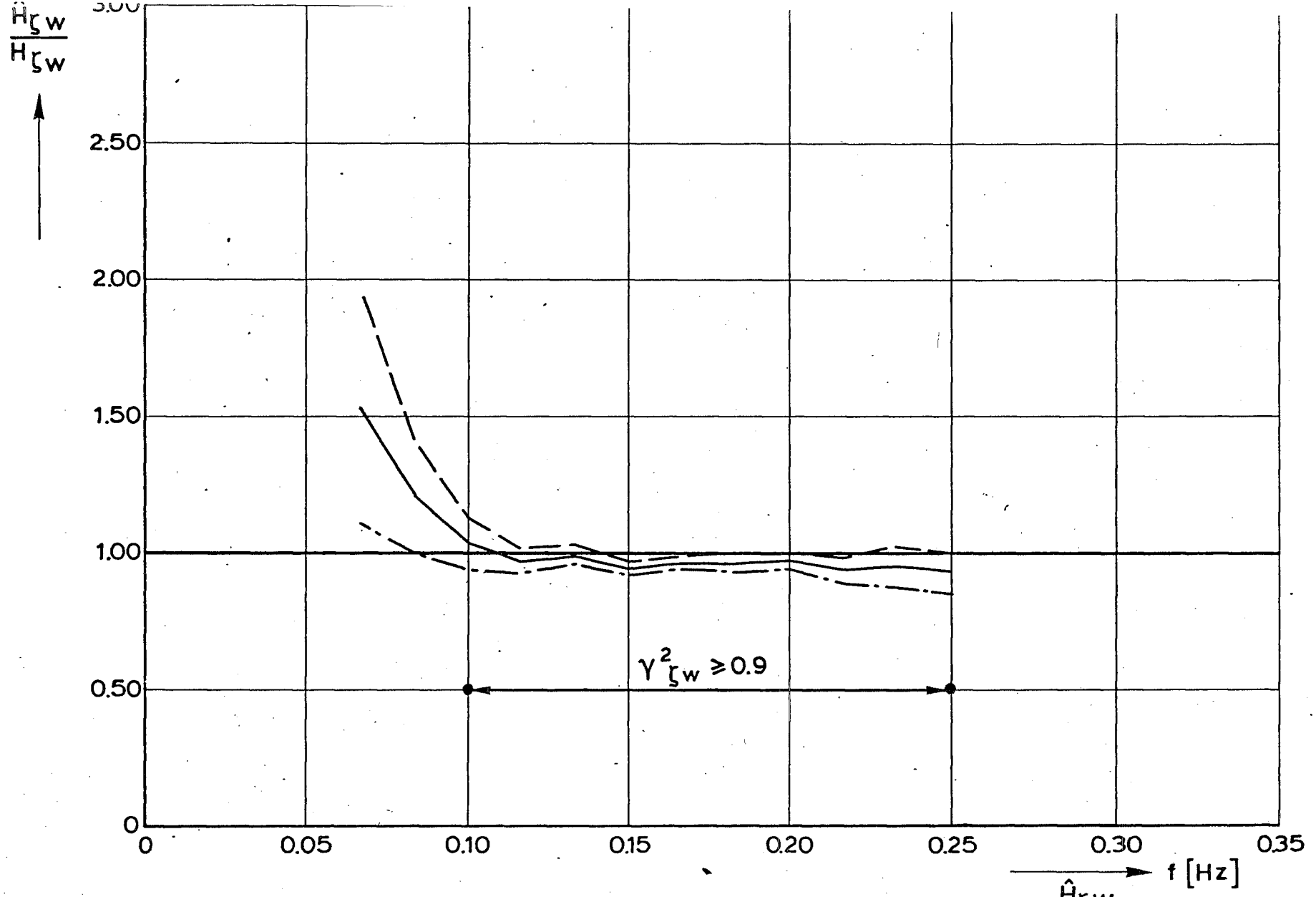

rijkswaterstaat directie waterhuishouding en waterbeweging district kust en zee	get.		appendix 5. fig. 3
	gec.		projectcode L7709B00
COMPARISON MEASURED GAINFUNCTION	gez.		nota WWKZ-83G.007
OF ζ AND w WITH LINEAR THEORY (1704)	akk.		A 4 nr. 83K.053

——— $\frac{\hat{H}_{\zeta w}}{H_{\zeta w}}$ WITH

— — — } 90 % CONFIDENCE INTERVAL.

— · — ·

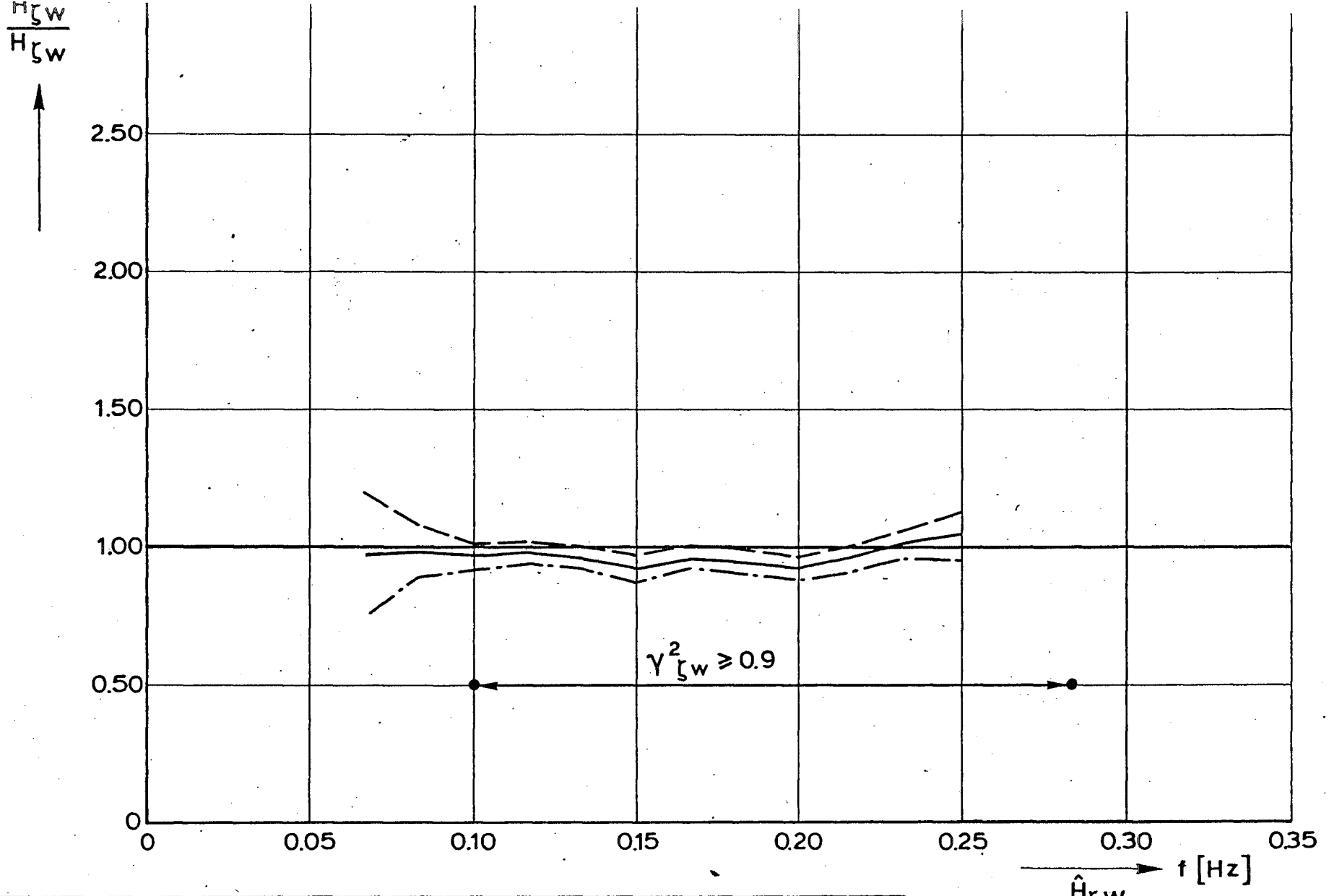

rijkswaterstaat
directie waterhuishouding en waterbeweging
district kust en zee

COMPARISON MEASURED GAINFUNCTION
OF ζ AND w WITH LINEAR THEORY (1802)

get.		appendix 5. fig. 4	
gec.		projectcode L7709B00	
gez.		nota WWKZ-83G.007	
akk.		A 4	nr. 83K.054

——— $\frac{\hat{H}_{\zeta w}}{H_{\zeta w}}$ WITH

— — — } 90% CONFIDENCE INTERVAL.

— · — ·

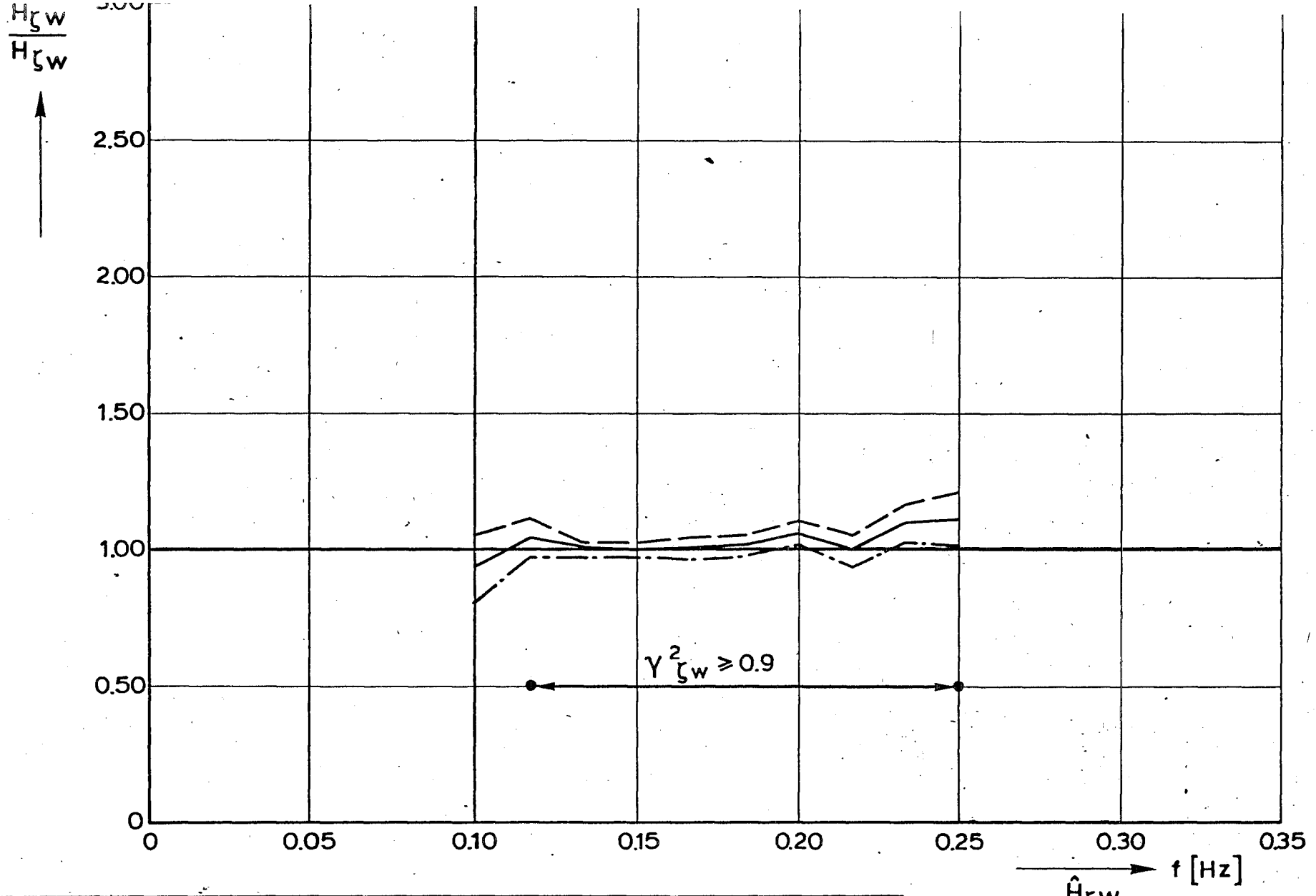

rijkswaterstaat directie waterhuishouding en waterbeweging district kust en zee	get.		appendix 5 fig. 5	
	gec.		projectcode L7709B00	
COMPARISON MEASURED GAINFUNCTION OF ζ AND w WITH LINEAR THEORY (2201)	gez.		nota WWKZ-83G.007	
	akk.		A 4	nr. 83K.055

$\frac{\hat{H}_{\zeta w}}{H_{\zeta w}}$ WITH

} 90 % CONFIDENCE INTERVAL.

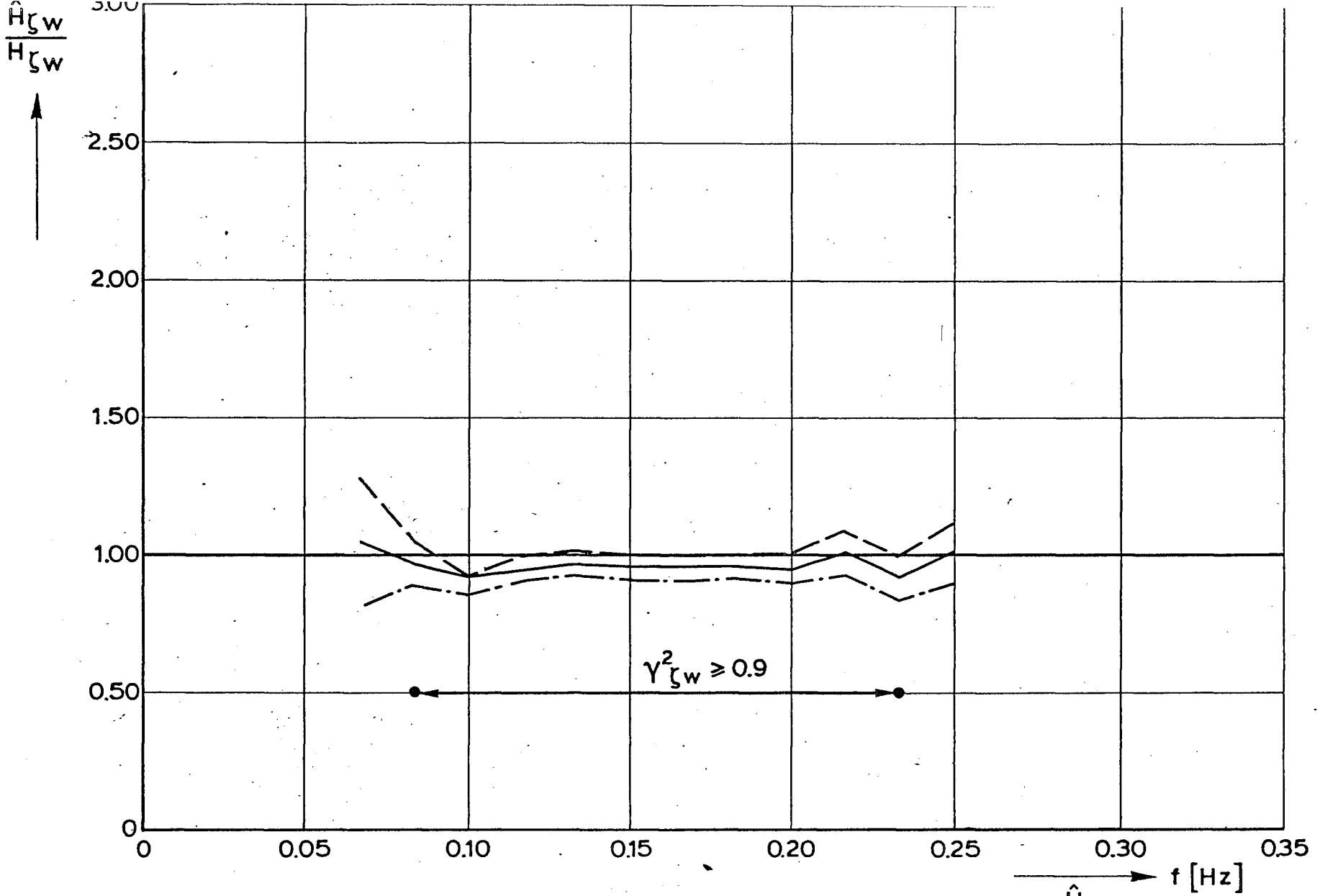

rijkswaterstaat directie waterhuishouding en waterbeweging district kust en zee	get.		appendix 5. fig. 6
	gec.		projectcode L7709B00
COMPARISON MEASURED GAINFUNCTION OF ζ AND w WITH LINEAR THEORY (2301)	gez.		nota WWKZ-83G.007
	akk.		A 4 nr. 83K.056

——— $\frac{\hat{H}_{\zeta w}}{H_{\zeta w}}$ WITH

— — — } 90 % CONFIDENCE INTERVAL.

— · — ·

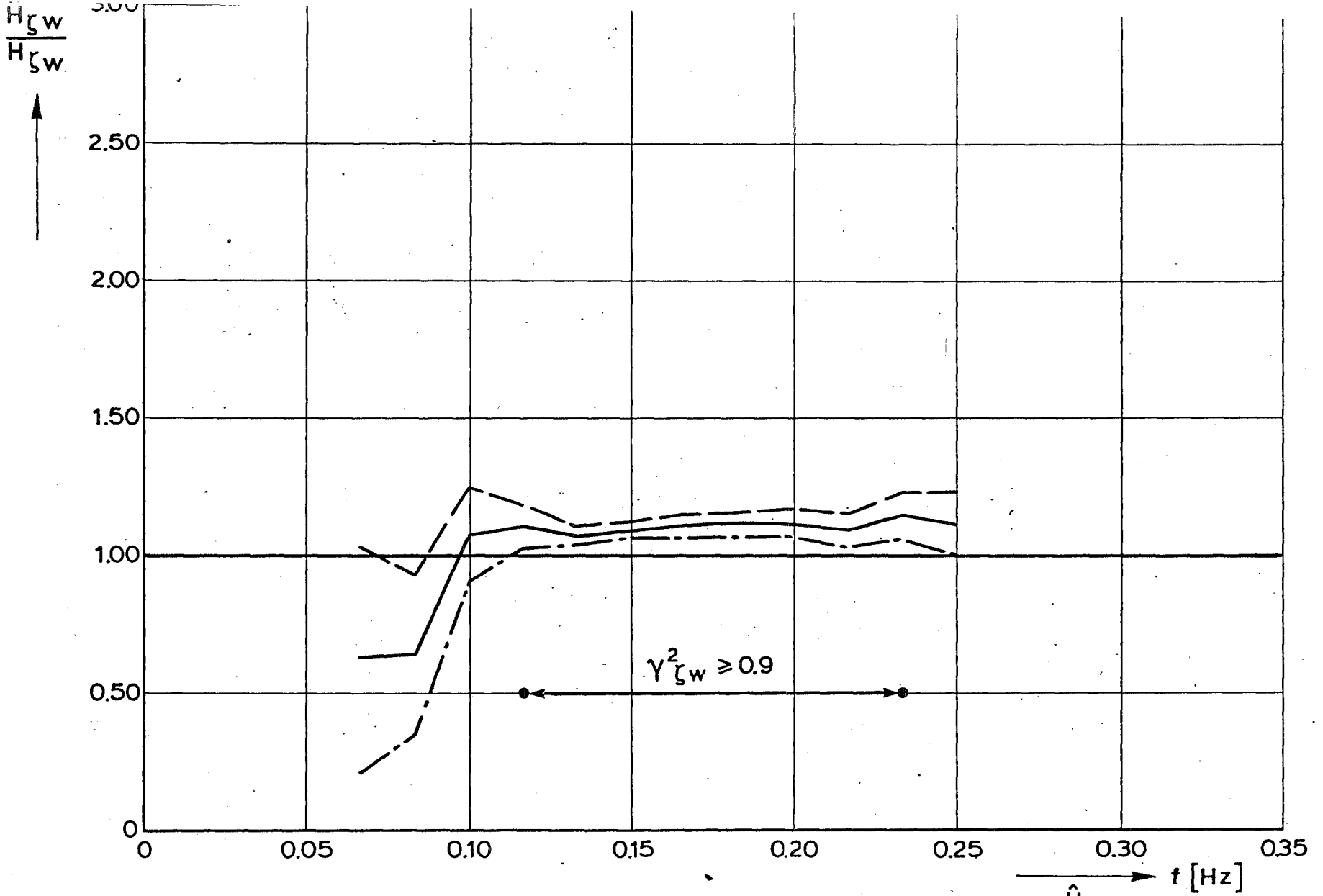

rijkswaterstaat directie waterhuishouding en waterbeweging district kust en zee	get.		appendix 5. fig.7	
	gec.		projectcode L7709B00	
COMPARISON MEASURED GAINFUNCTION	gez.		nota WWKZ-83G.007	
OF ζ AND w WITH LINEAR THEORY (2420)	akk.		A 4	nr. 83K.057

——— $\frac{\hat{H}_{\zeta w}}{H_{\zeta w}}$ WITH

– – – } 90 % CONFIDENCE INTERVAL.

–·–·– }

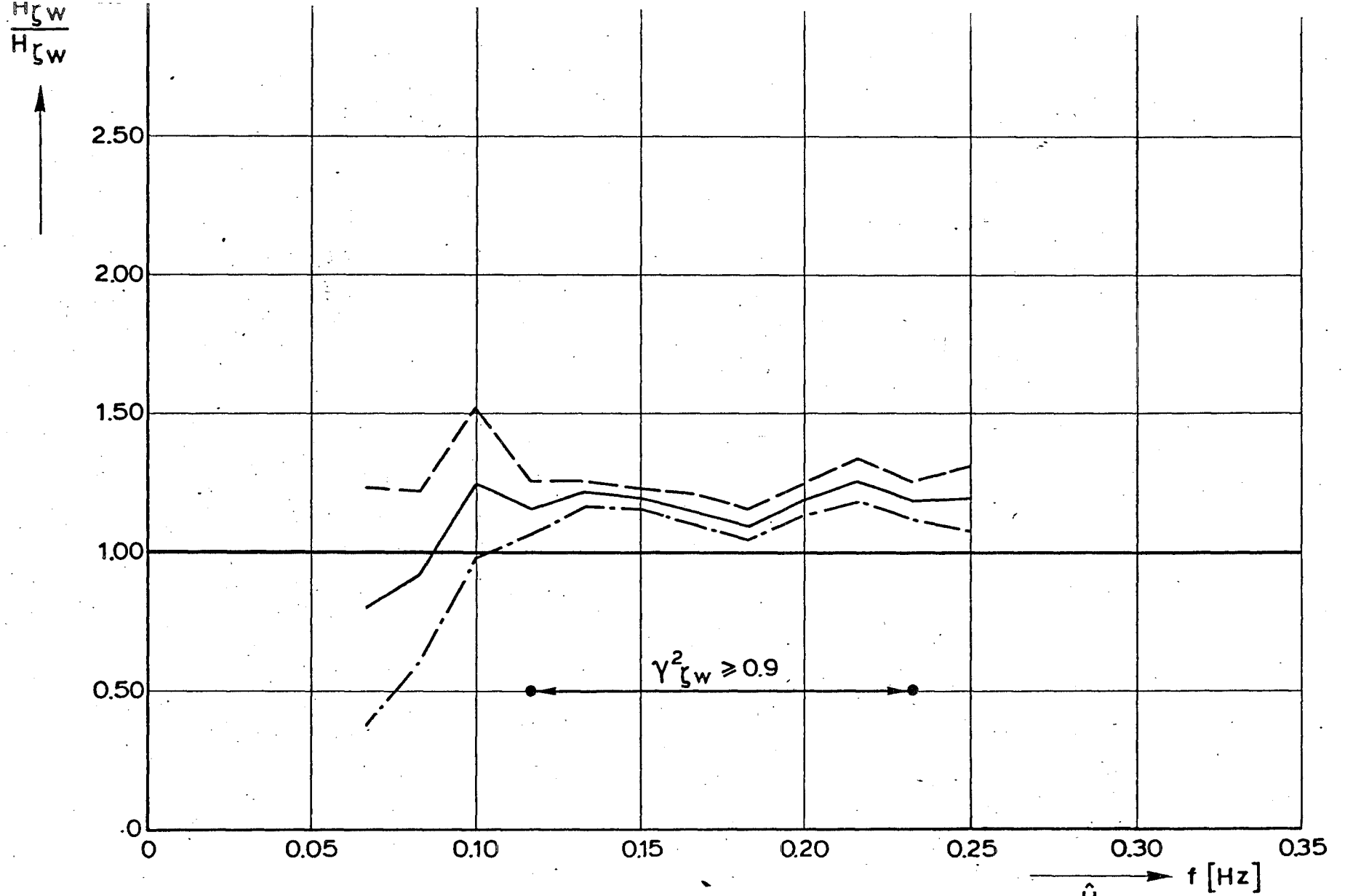

rijkswaterstaat directie waterhuishouding en waterbeweging district kust en zee	get.		appendix 5. fig. 8
	gec.		projectcode L7709B00
COMPARISON MEASURED GAINFUNCTION OF ζ AND w WITH LINEAR THEORY (2501)	gez.		nota WWKZ-83G.007
	akk.		A4 nr. 83K.058

——— $\frac{\hat{H}_{\zeta w}}{H_{\zeta w}}$ WITH

– – – } 90 % CONFIDENCE INTERVAL.

– · – · –

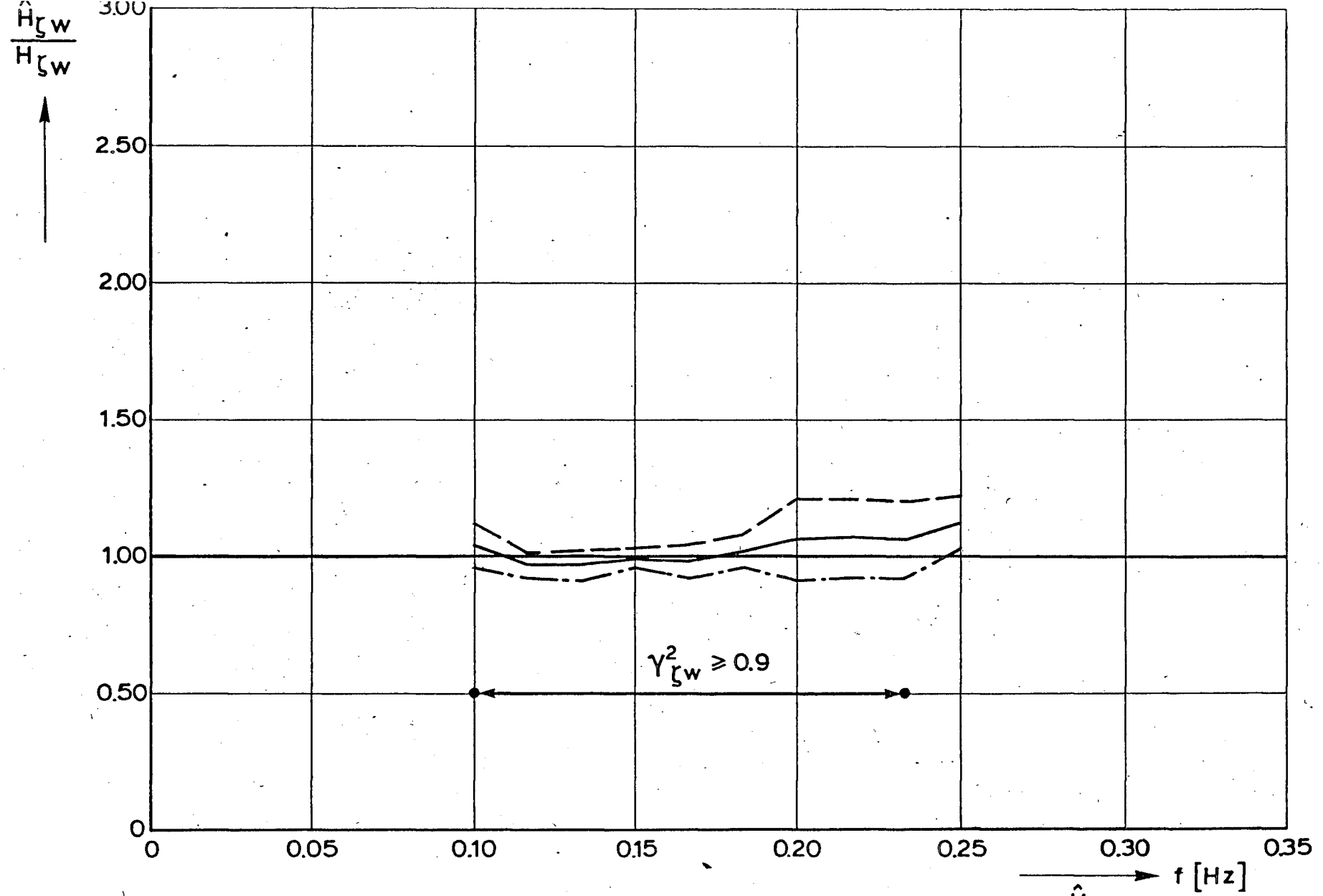

rijkswaterstaat directie waterhuishouding en waterbeweging district kust en zee	get.		appendix 5. fig. 9
	gec.		projectcode L7709B00
COMPARISON MEASURED GAINFUNCTION OF ζ AND w WITH LINEAR THEORY (2601)	gez.		nota WWKZ-83G.007
	akk.		A 4 nr. 83K.059

$\frac{\hat{H}_{\zeta w}}{H_{\zeta w}}$ WITH

} 90 % CONFIDENCE INTERVAL.

APPENDIX 6.

COMPARISON OF MEASURED AND CALCULATED SPECTRA OF VERTICAL VELOCITY COMPONENT.

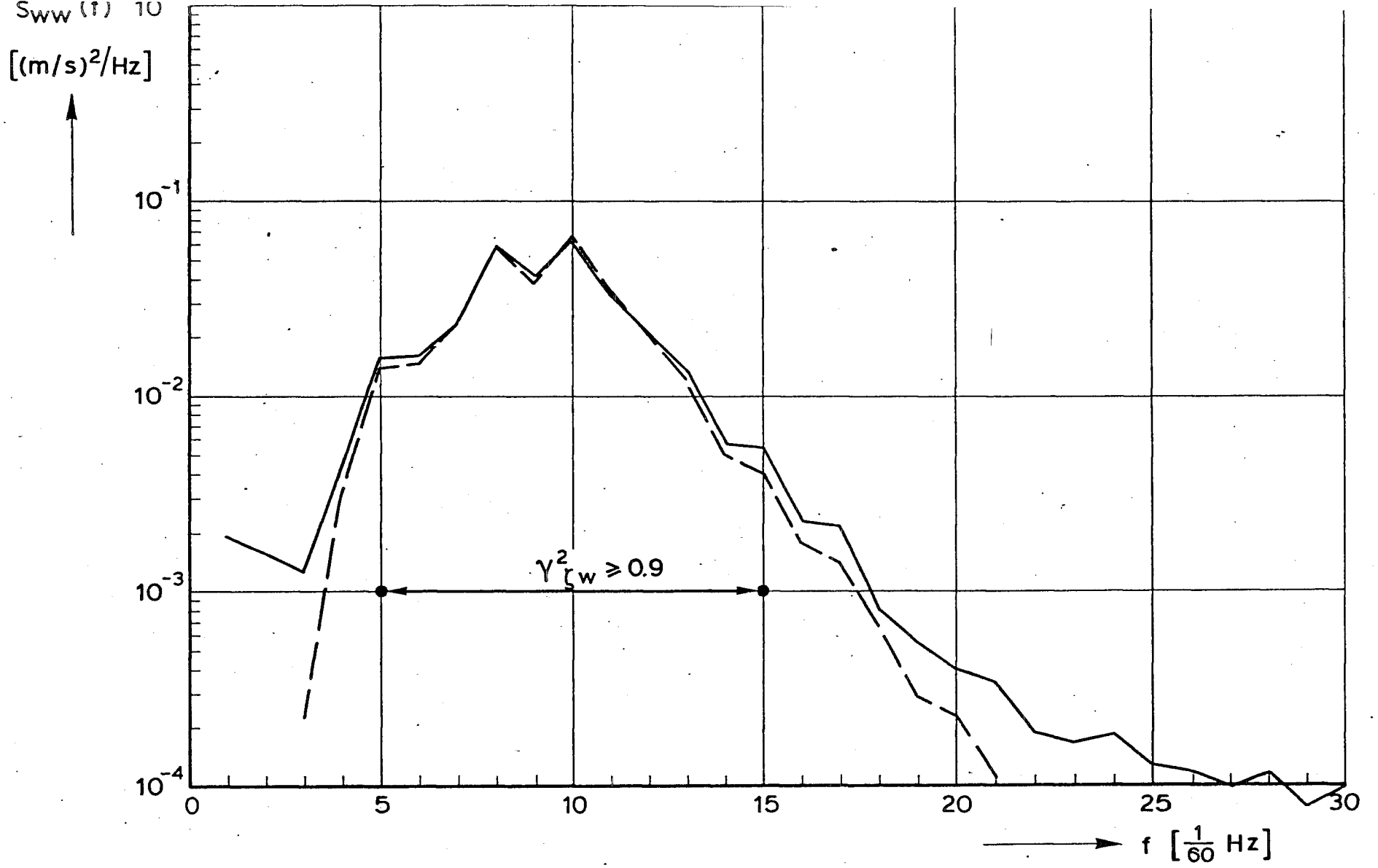

rijkswaterstaat directie waterhuishouding en waterbeweging district kust en zee	get.		appendix 6. fig.1	
	gec.		projectcode L7709B00	
COMPARISON OF MEASURED AND CALCULATED SPECTRUM OF w USING THE LINEAR THEORY (1501)	gez.		nota WWKZ-83G.007	
	akk.		A 4	nr. 83K.060

——— $S_{ww}(f)$

— — — $H^2_{\zeta w}$ theor. $(f) \times S_{\zeta\zeta}(f)$

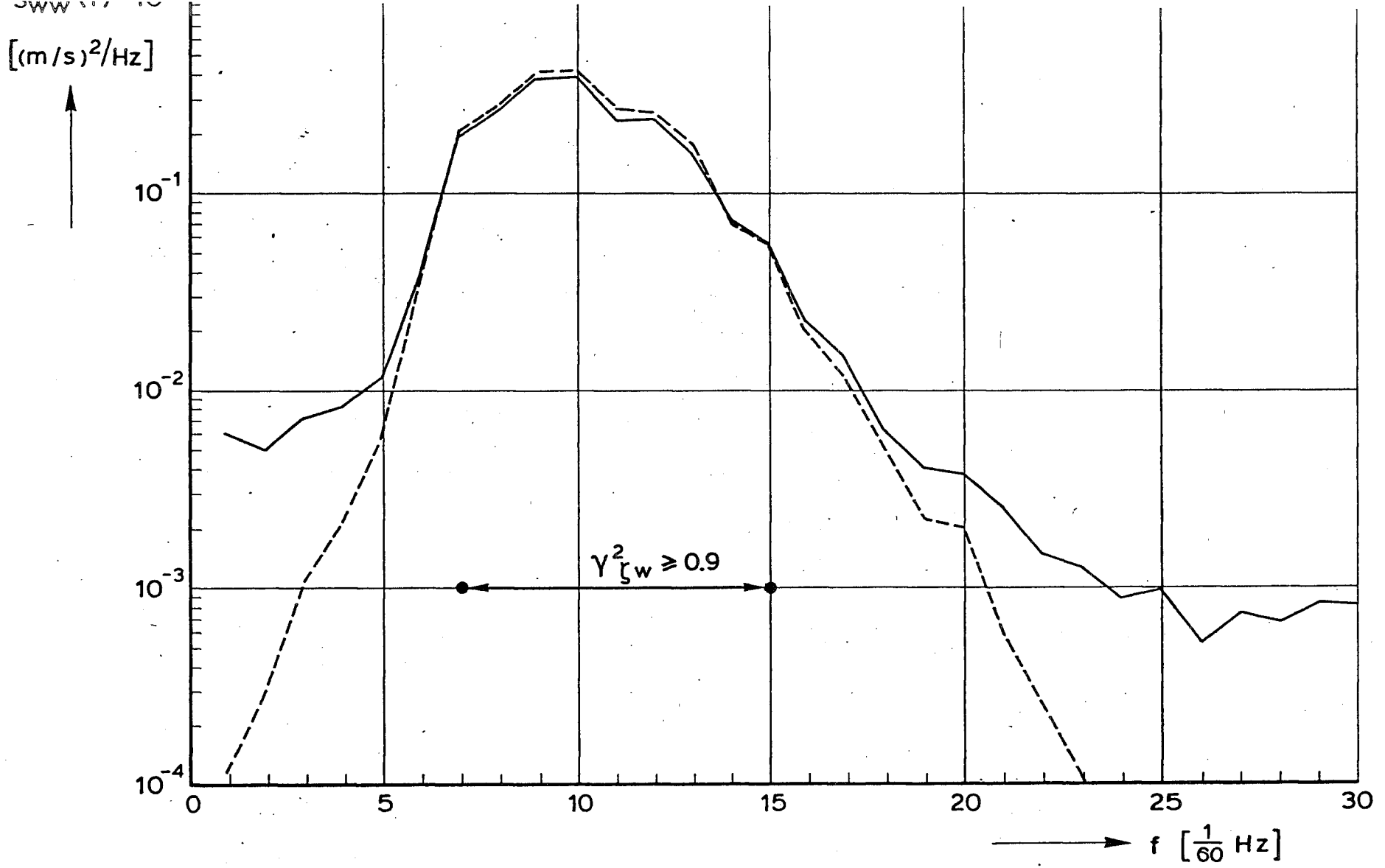

rijkswaterstaat directie waterhuishouding en waterbeweging district kust en zee	get.		appendix 6. fig. 2	
	gec.		projectcode L7709B00	
COMPARISON OF MEASURED AND CALCULATED SPECTRUM OF w USING THE LINEAR THEORY (1601)	gez.		nota WWKZ-83G.007	
	akk.		A 4	nr. 83K.061

——— $S_{ww}(f)$

— — — $H^2_{\zeta w}$ theor. $(f) \times S_{\zeta\zeta}(f)$

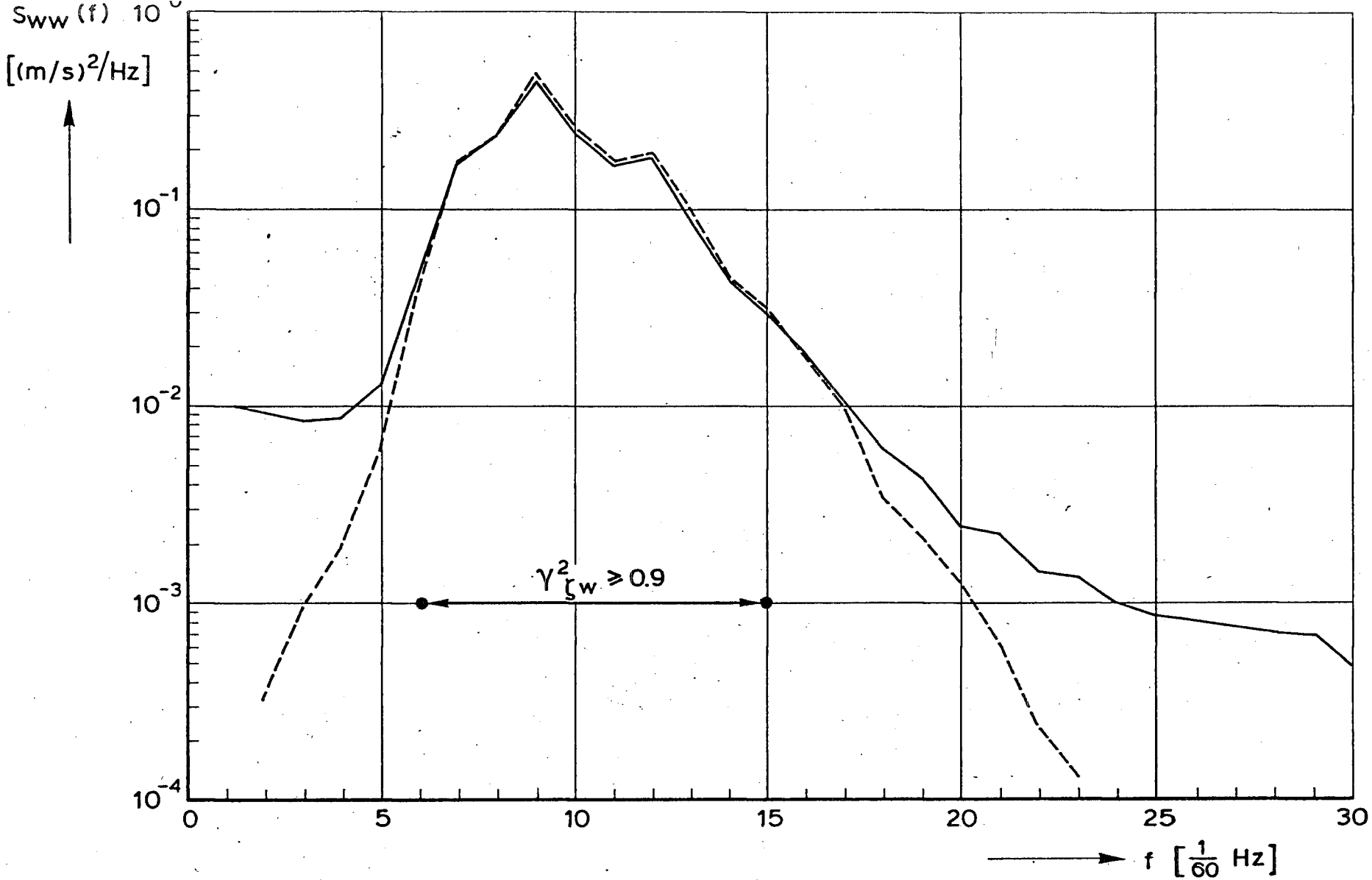

rijkswaterstaat directie waterhuishouding en waterbeweging district kust en zee	get.		appendix 6. fig. 3
	gec.		projectcode L7709B00
COMPARISON OF MEASURED AND CALCULATED SPECTRUM OF w USING THE LINEAR THEORY (1704)	gez.		nota WWKZ-83G.007
	akk.		A 4 nr. 83K.062

——— $S_{ww}(f)$

— — — $H^2_{\zeta w}$ theor. $(f) \times S_{\zeta\zeta}(f)$

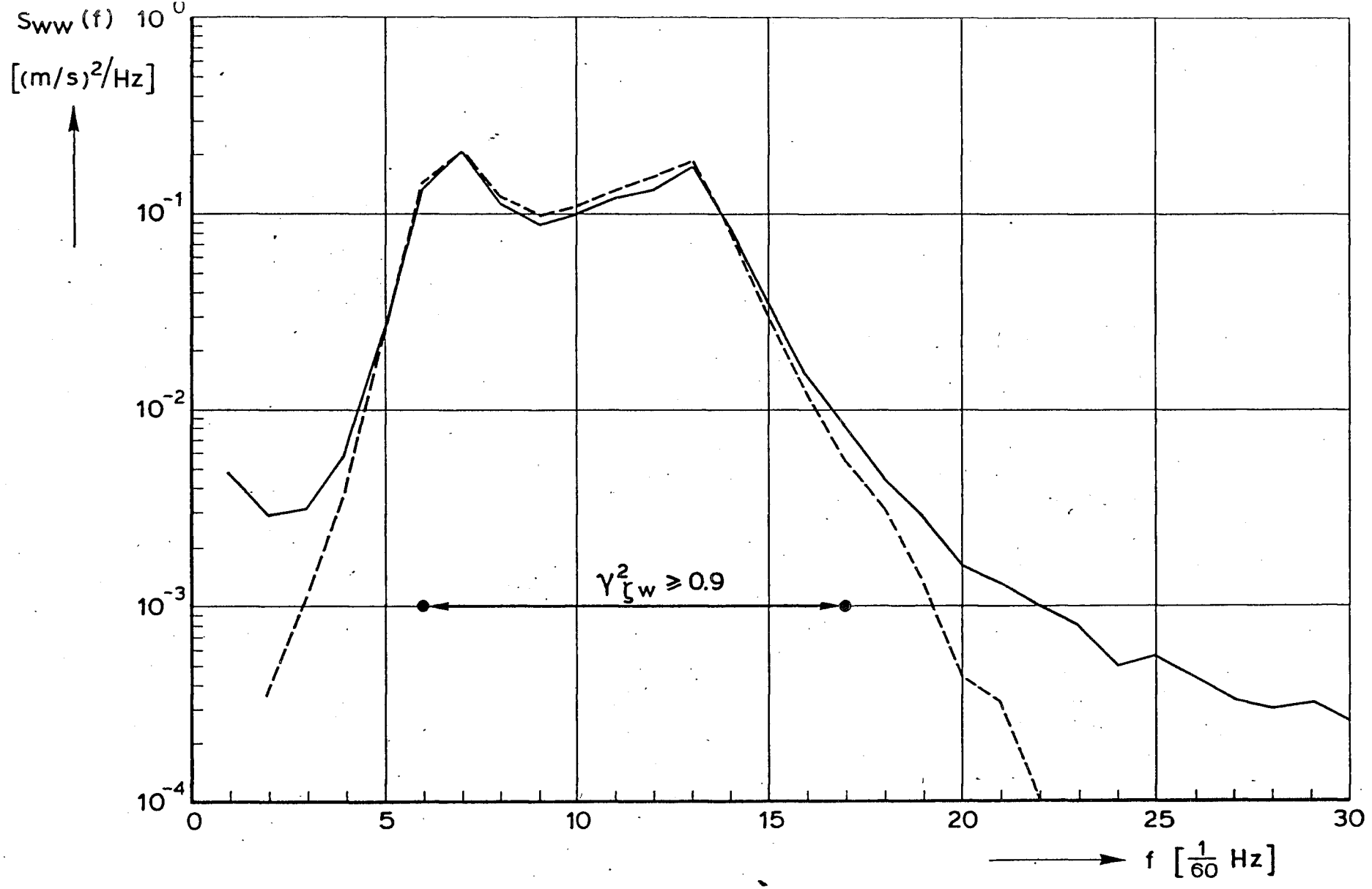

rijkswaterstaat directie waterhuishouding en waterbeweging district kust en zee	get.		appendix 6. fig. 4	
	gec.		projectcode L7709B00	
COMPARISON OF MEASURED AND CALCULATED SPECTRUM OF w USING THE LINEAR THEORY (1802)	gez.		nota WWKZ-83G.007	
	akk.		A 4	nr. 83K.063

——— $S_{ww}(f)$

— — — $H^2_{\zeta w}$ theor. $(f) \times S_{\zeta\zeta}(f)$

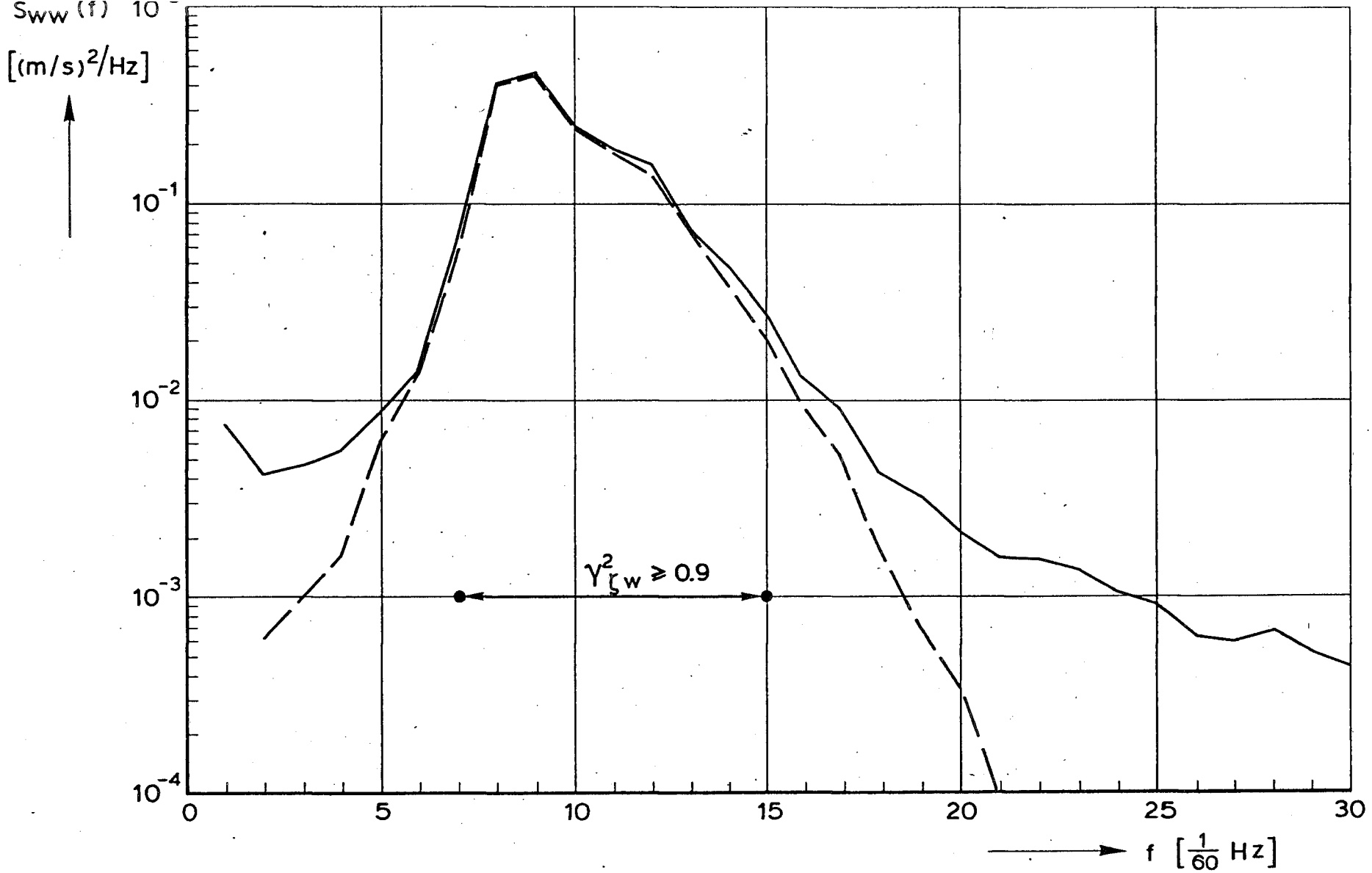

rijkswaterstaat directie waterhuishouding en waterbeweging district kust en zee	get.		appendix 6. fig. 5	
	gec.		projectcode L7709B00	
COMPARISON OF MEASURED AND CALCULATED SPECTRUM OF w USING THE LINEAR THEORY (2201)	gez.		nota WWKZ-83G.007	
	akk.		A 4	nr. 83K.064

——— $S_{ww}(f)$

— — — $H^2_{\zeta w}$ theor. $(f) \times S_{\zeta\zeta}(f)$

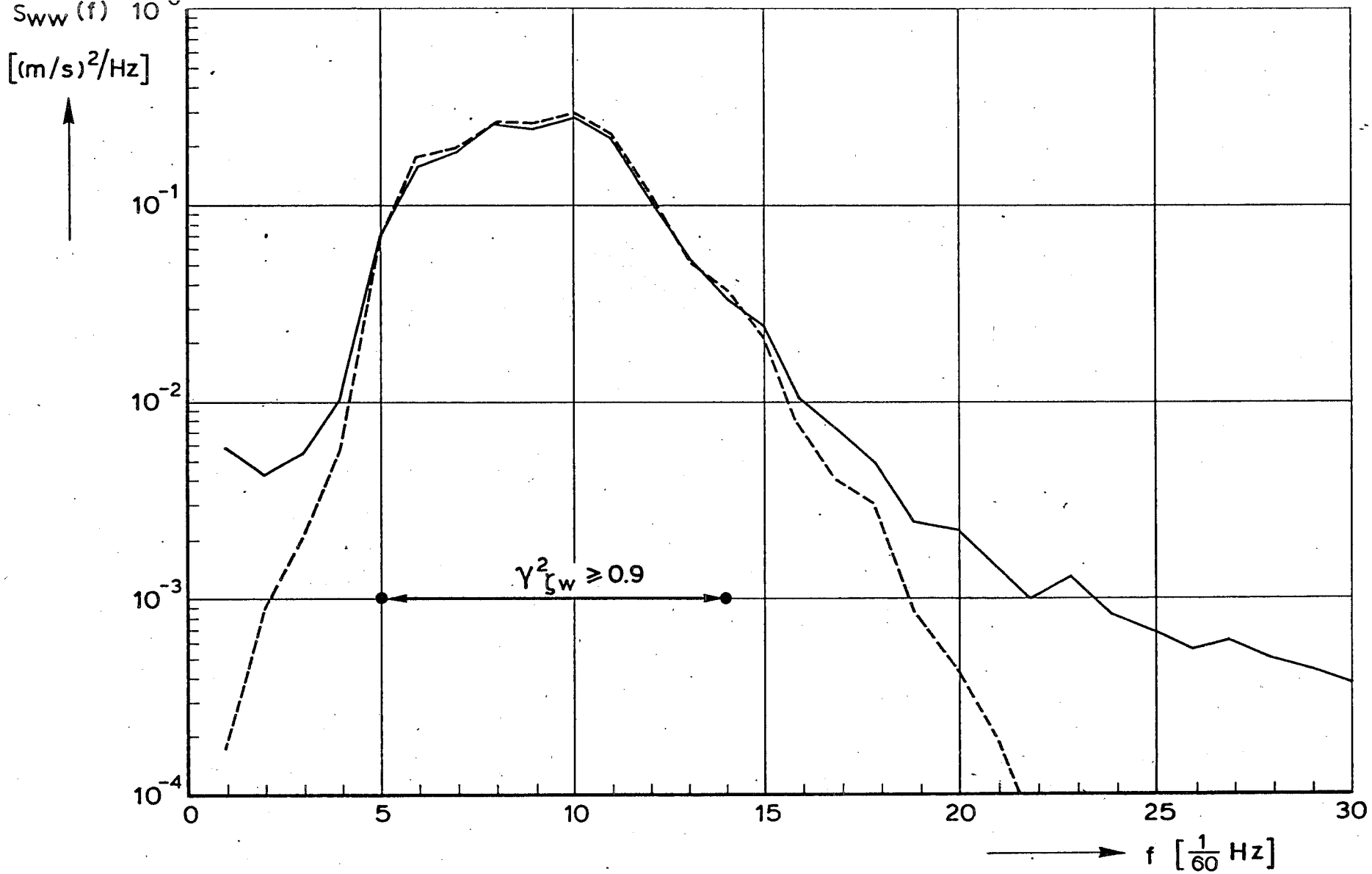

rijkswaterstaat directie waterhuishouding en waterbeweging district kust en zee	get.		appendix 6. fig. 6	
	gec.		projectcode L7709B00	
COMPARISON OF MEASURED AND CALCULATED SPECTRUM OF w USING THE LINEAR THEORY (2301)	gez.		nota WWKZ-83G.007	
	akk.		A 4	nr. 83K.065

——— $S_{ww}(f)$

— — — $H^2_{\zeta w}$ theor. $(f) \times S_{\zeta\zeta}(f)$

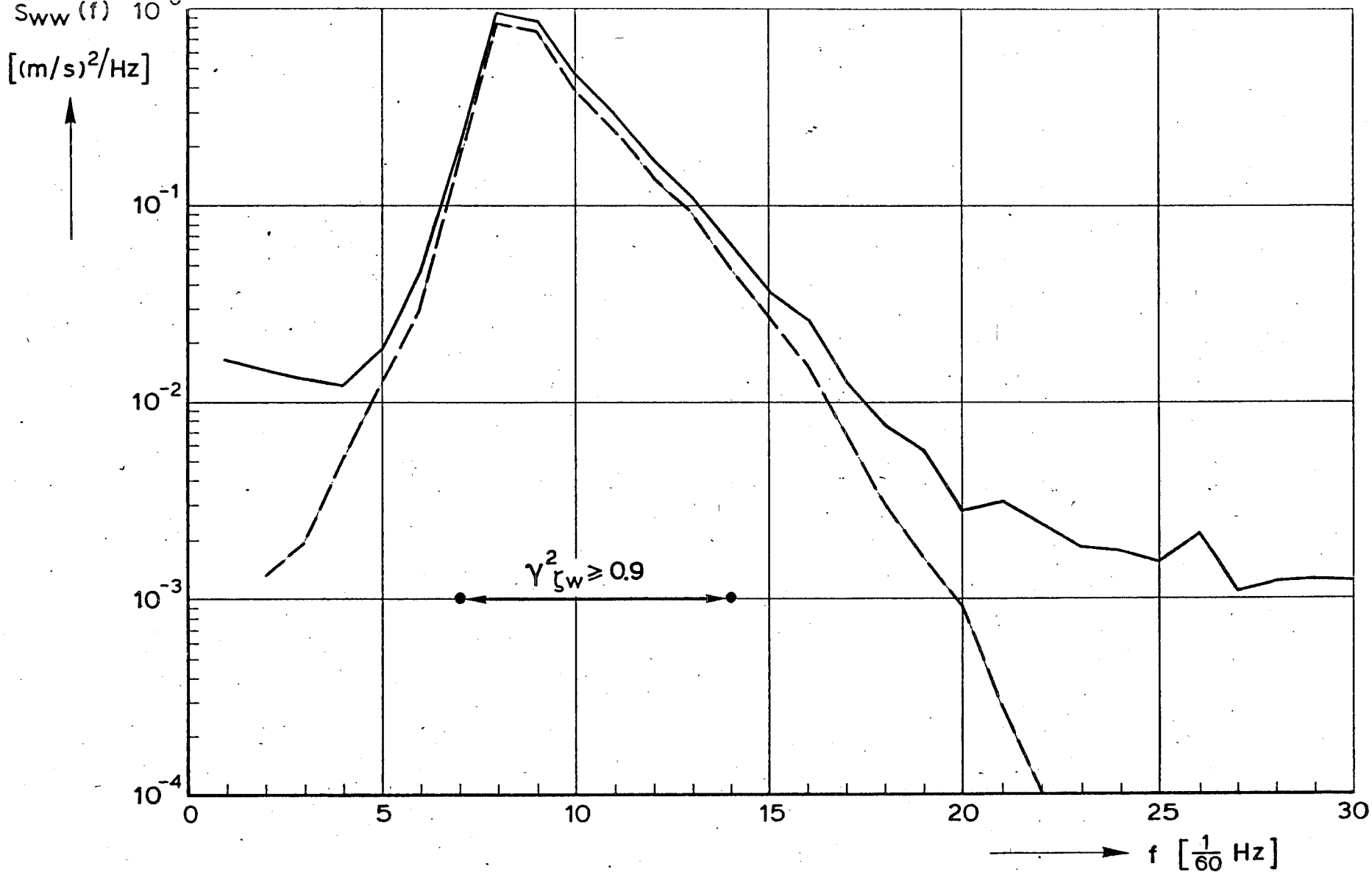

rijkswaterstaat directie waterhuishouding en waterbeweging district kust en zee	get.		appendix 6. fig. 7
	gec.		projectcode L7709B00
COMPARISON OF MEASURED AND CALCULATED SPECTRUM OF w USING THE LINEAR THEORY (2420)	gez.		nota WWKZ-83G.007
	akk.		A 4 nr. 83K.066

——— $S_{ww}(f)$

— — — $H^2_{\zeta w}$ theor. $(f) \times S_{\zeta\zeta}(f)$

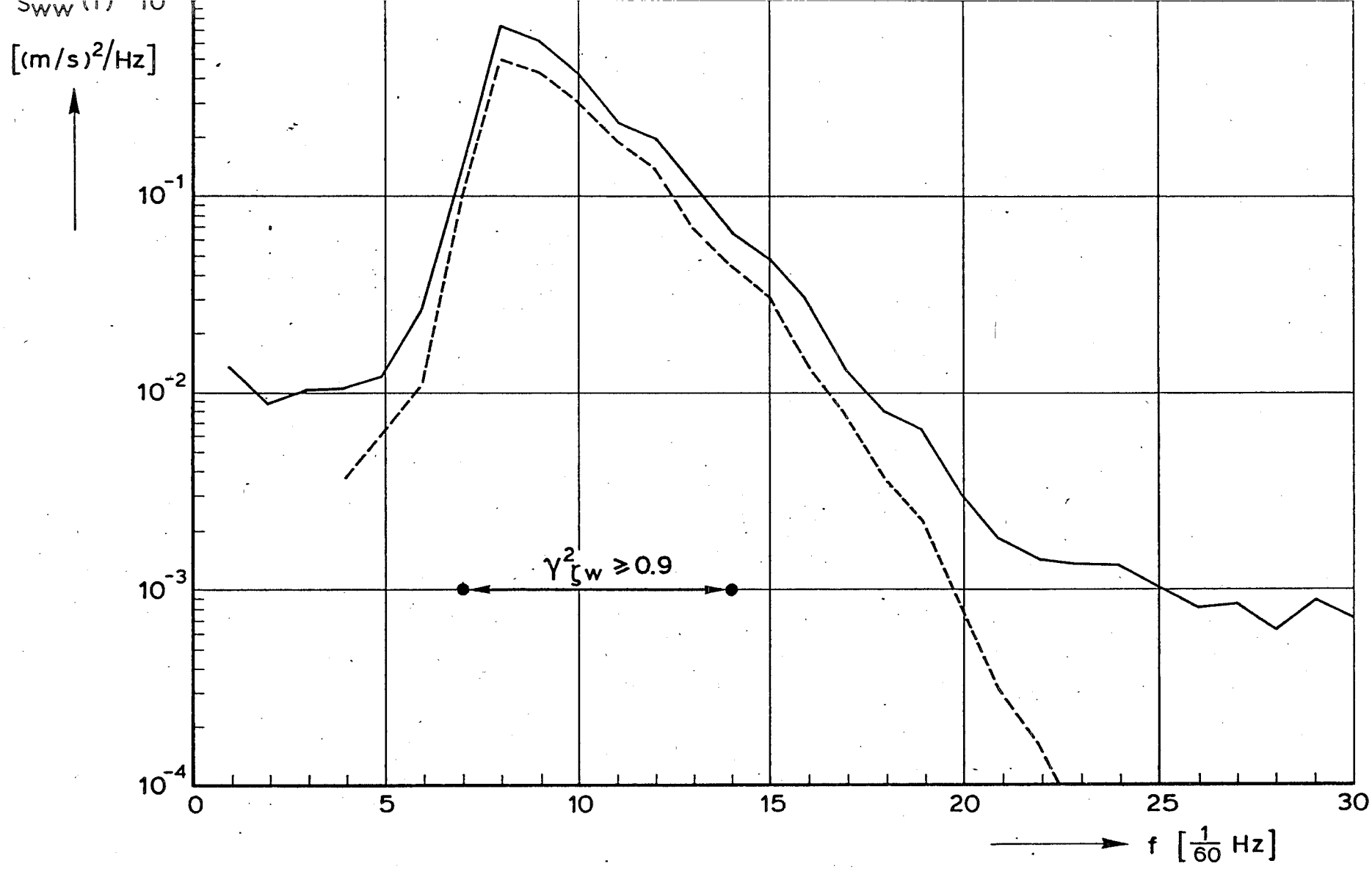

rijkswaterstaat directie waterhuishouding en waterbeweging district kust en zee	get.		appendix 6. fig 8	
	gec.		projectcode L7709B00	
COMPARISON OF MEASURED AND CALCULATED SPECTRUM OF w USING THE LINEAR THEORY (2501)	gez.		nota WWKZ-83G.007	
	akk.		A 4	nr. 83K.067

——— $S_{ww}(f)$

— — — $H^2_{\zeta w}$ theor. $(f) \times S_{\zeta\zeta}(f)$

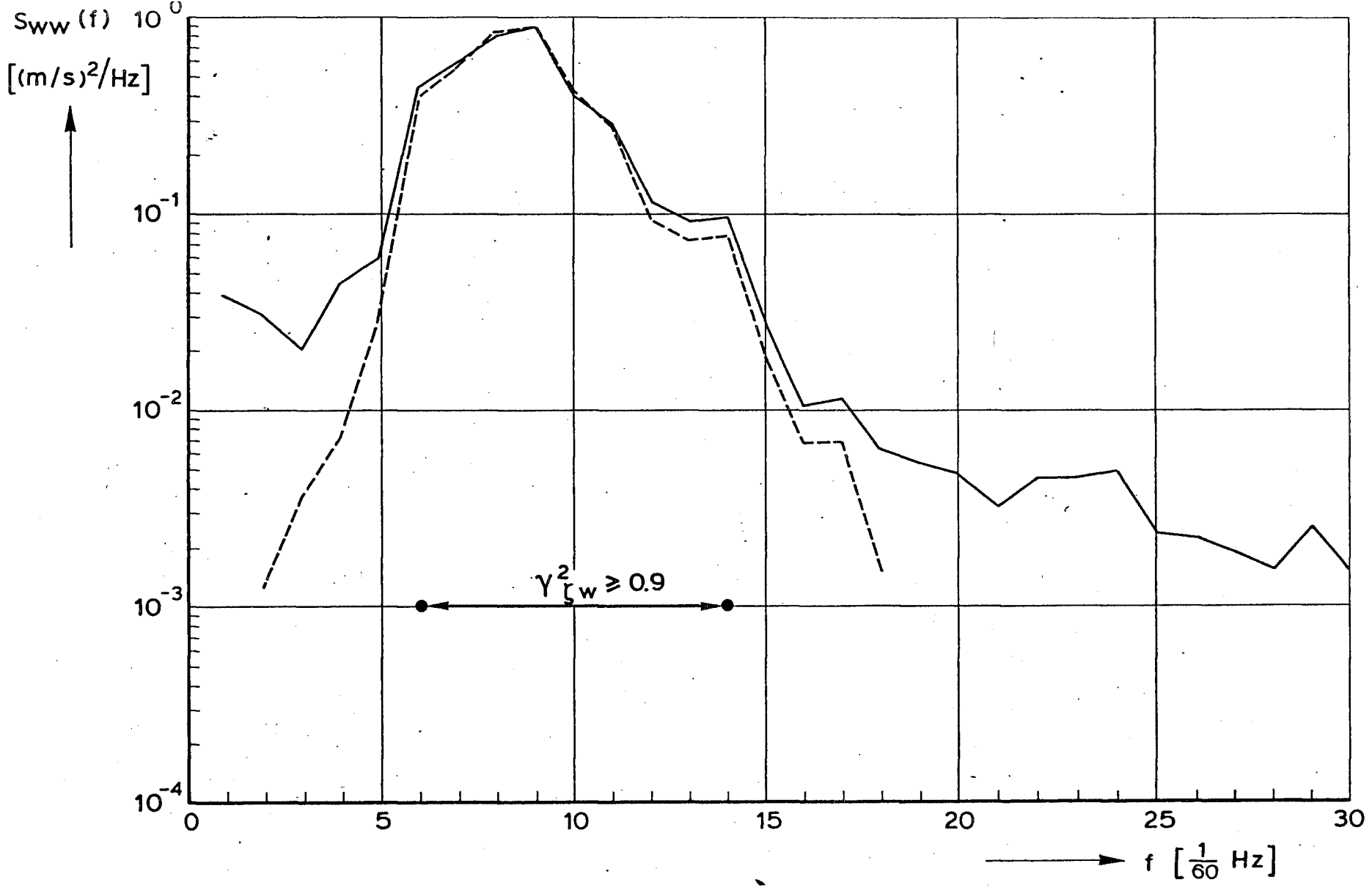

rijkswaterstaat
directie waterhuishouding en waterbeweging
district kust en zee

COMPARISON OF MEASURED AND CALCULATED SPECTRUM OF w USING THE LINEAR THEORY (2601)

get.		appendix 6. fig. 9	
gec.		projectcode L7709B00	
gez.		nota WWKZ-83G.007	
akk.		A 4	nr. 83K.068

——— $S_{ww}(f)$

— — — $H^2_{\zeta w}$ theor. $(f) \times S_{\zeta\zeta}(f)$

APPENDIX 7.

PHASE FUNCTIONS OF HORIZONTAL AND VERTICAL VELOCITY COMPONENT

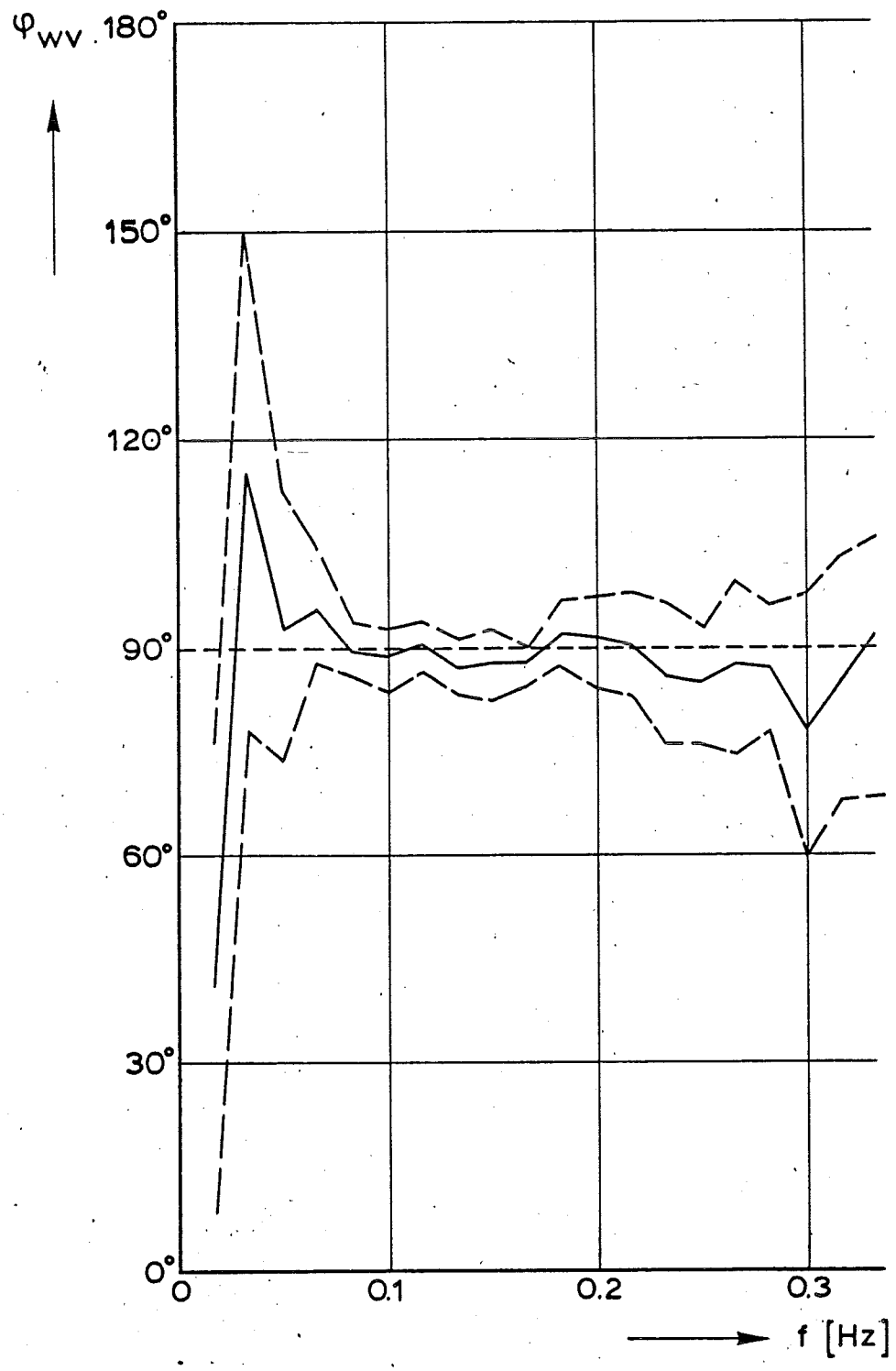

ijkswaterstaat irectie waterhuishouding en waterbeweging istrict kust en zee	get.		appendix 7. fig. 1
	gec.		projectcode L7709B00
MEASURED PHASEFUNCTION φ_{wv} (———) WITH 0% CONFIDENCE INTERVALS (— —) AND HEORETICAL PHASEFUNCTION (– – – –) . 1501	gez.		nota WWKZ-83G.007
	akk.		A 4 nr. 83 K.069

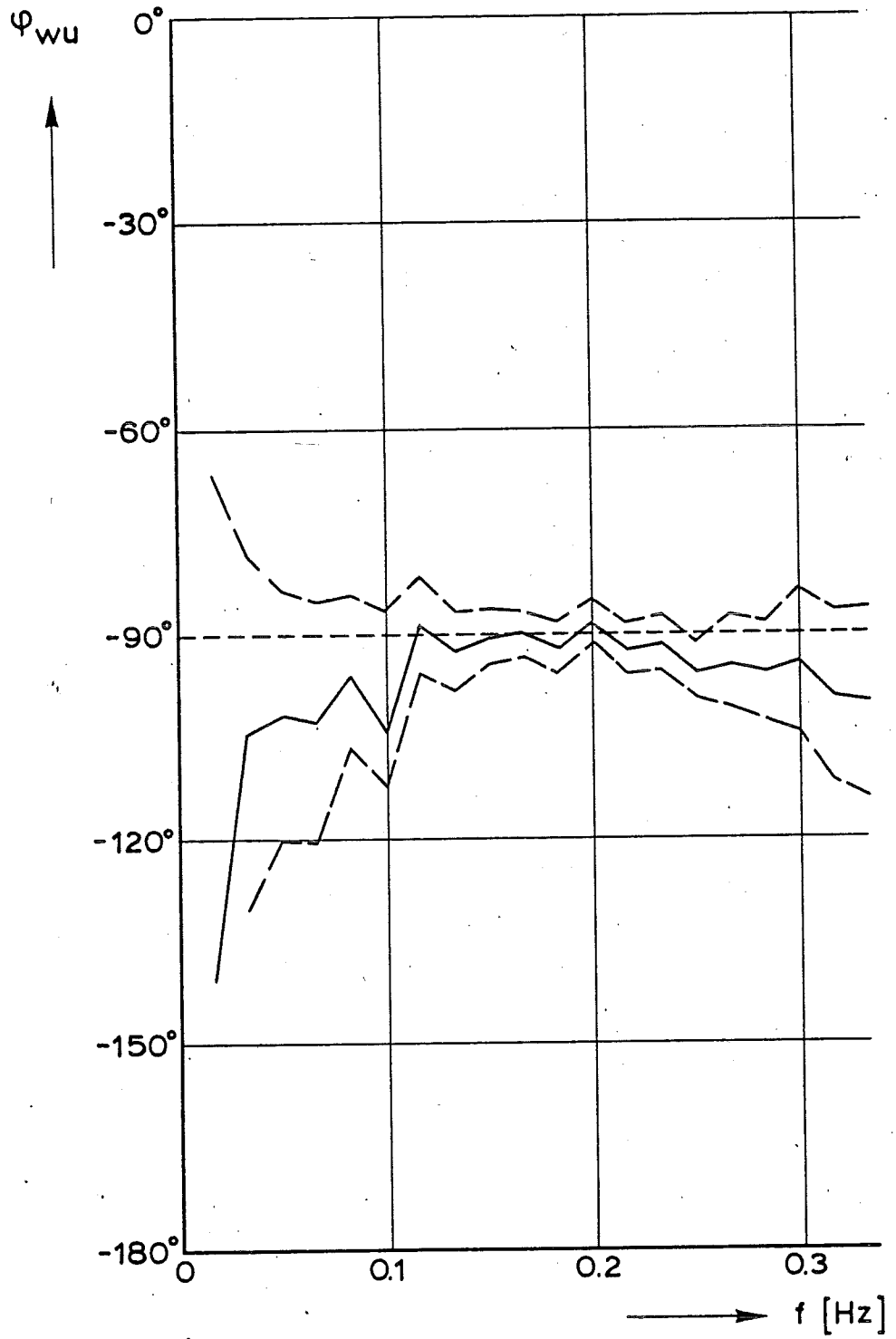

ijkswaterstaat rectie waterhuishouding en waterbeweging istrict kust en zee	get.		appendix 7. fig. 2
	gec.		projectcode L7709B00
IEASURED PHASEFUNCTION φ_{wu} (———) WITH 0% CONFIDENCE INTERVALS (— —) AND HEORETICAL PHASEFUNCTION (– – – –) . 1601	gez.		nota WWKZ-83G.007
	akk.		A 4 nr. 83 K.070

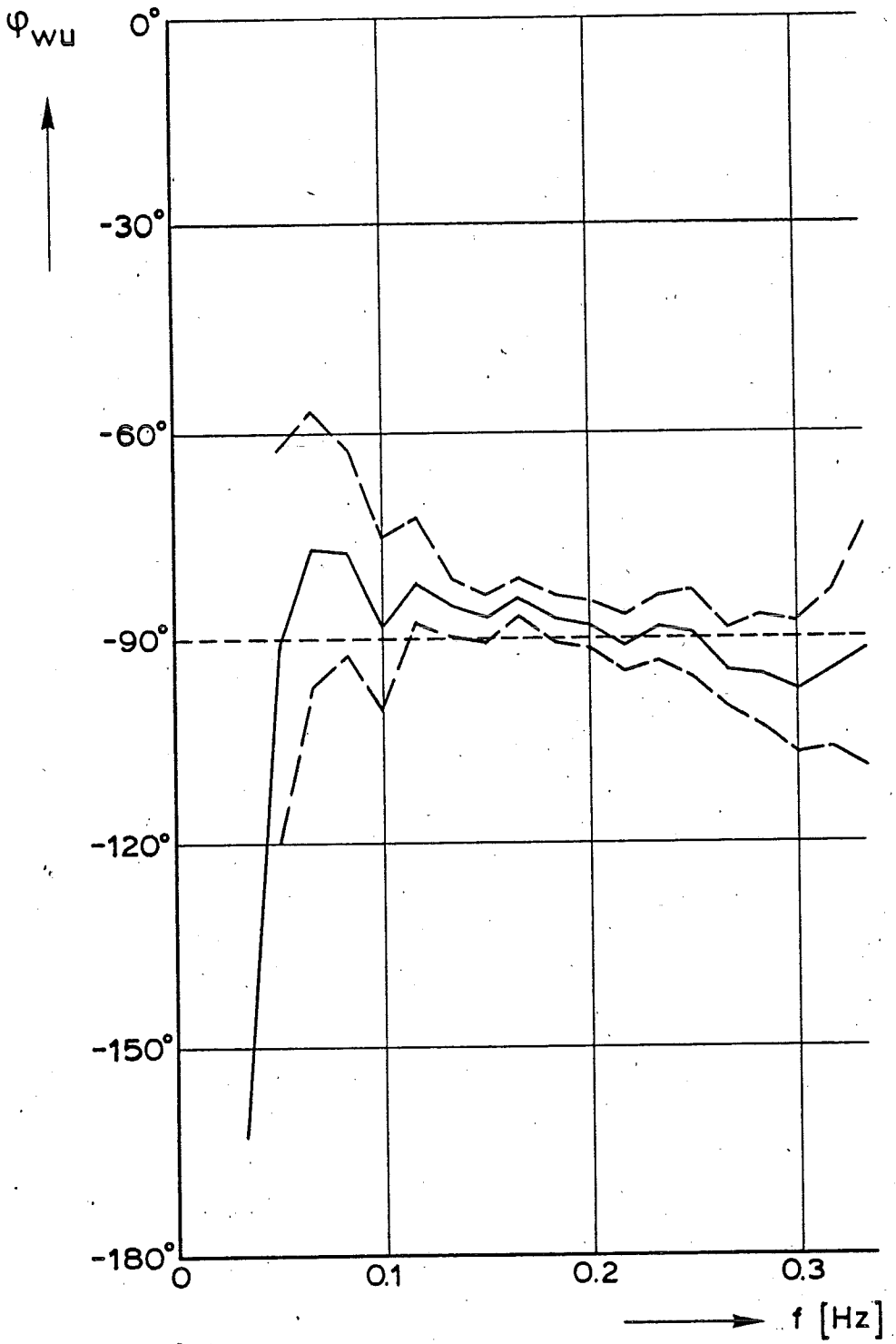

ijkswaterstaat irectie waterhuishouding en waterbeweging istrict kust en zee	get.		appendix 7. fig. 3
	gec.		projectcode L7709B00
IEASURED PHASEFUNCTION φ_{wu} (———) WITH 0% CONFIDENCE INTERVALS (— —) AND HEORETICAL PHASEFUNCTION (– – –) . 1704	gez.		nota WWKZ-83G.007
	akk.		A 4 nr. 83 K.071

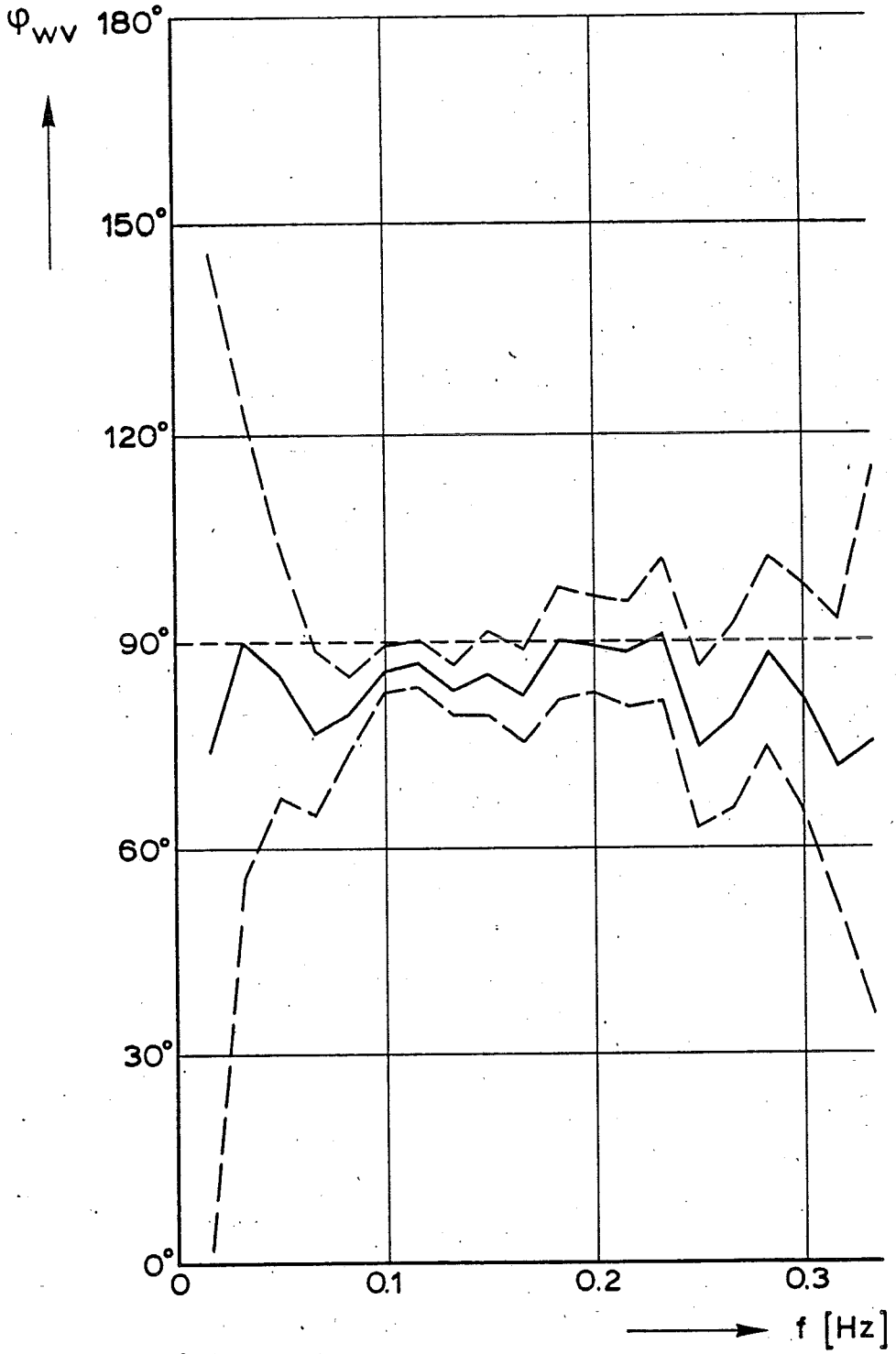

jkswaterstaat rectie waterhuishouding en waterbeweging istrict kust en zee	get.		appendix 7. fig. 4	
	gec.		projectcode L7709B00	
EASURED PHASEFUNCTION φ_{wv} (———) WITH 0% CONFIDENCE INTERVALS (— —) AND HEORETICAL PHASEFUNCTION (– – – –) . 1802	gez.		nota WWKZ-83G.007	
	akk.		A 4	nr. 83 K.072

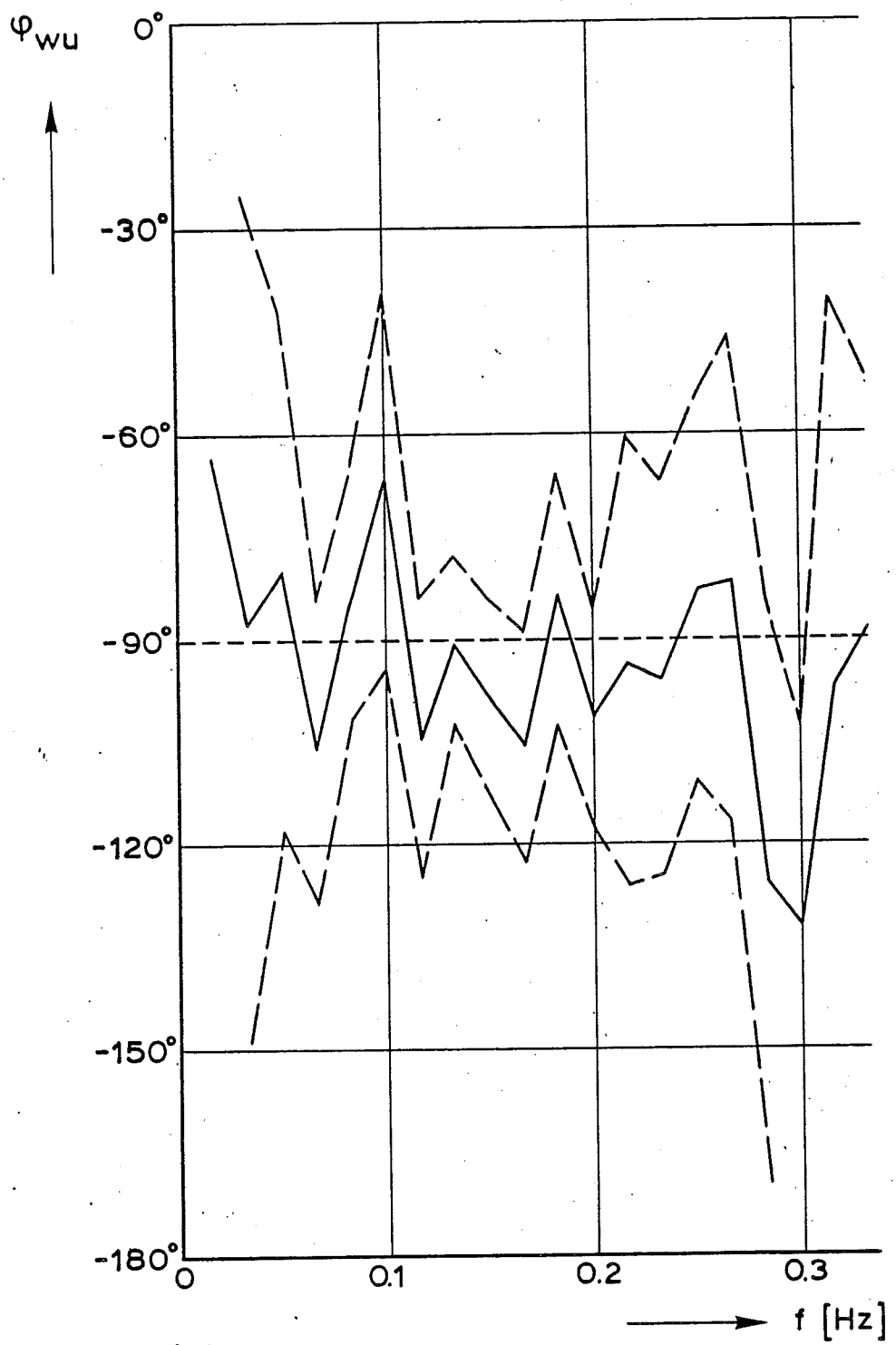

ijkswaterstaat irectie waterhuishouding en waterbeweging listrict kust en zee	get.		appendix 7. fig. 5
	gec.		projectcode L7709B00
MEASURED PHASEFUNCTION φ_{wu} (———) WITH)0% CONFIDENCE INTERVALS (— —) AND HEORETICAL PHASEFUNCTION (– – –) . 2201	gez.		nota WWKZ-83G.007
	akk.		A 4 nr. 83 K.073

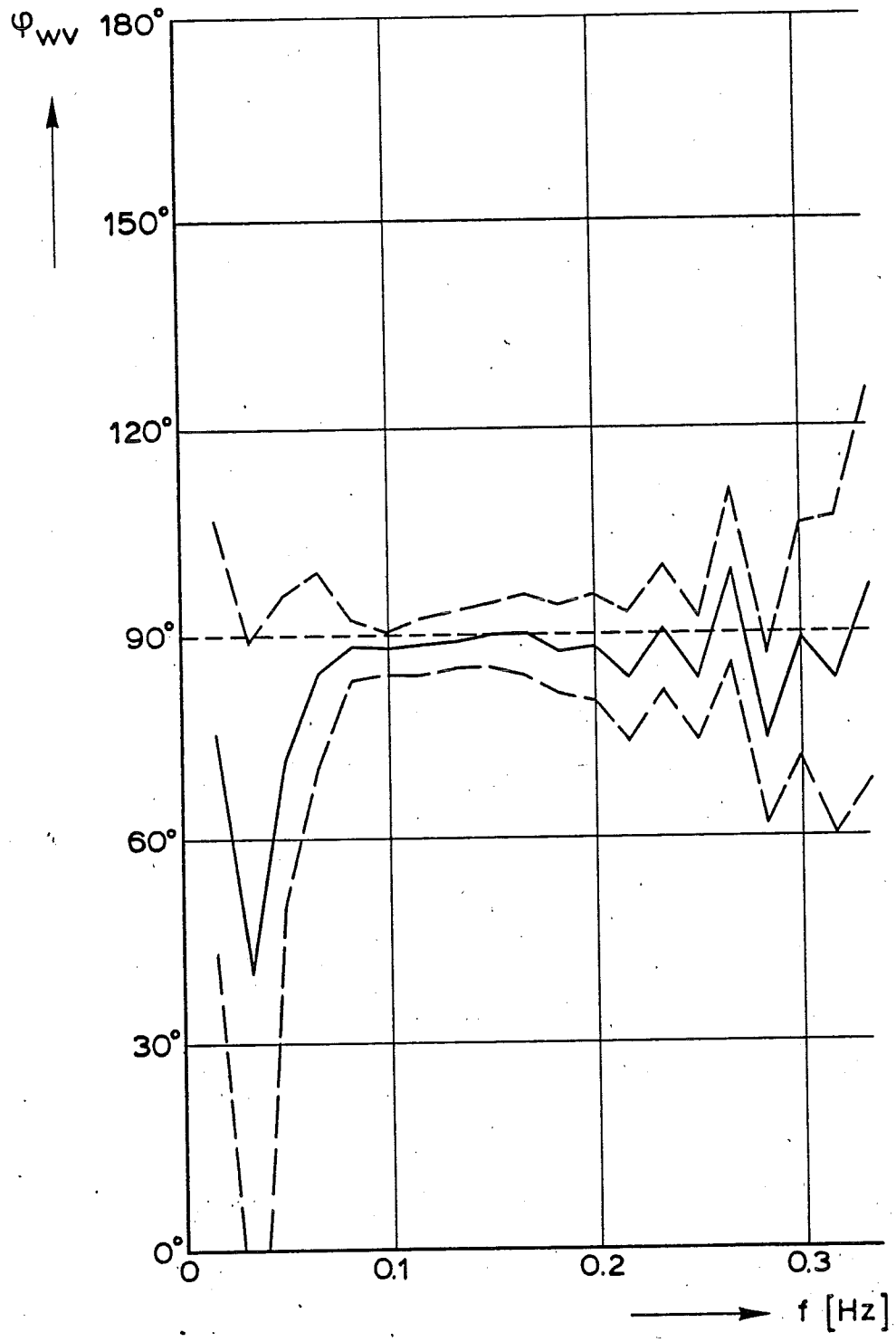

ijkswaterstaat lirectie waterhuishouding en waterbeweging listrict kust en zee	get.		appendix 7 fig. 6
	gec.		projectcode L7709B00
MEASURED PHASEFUNCTION φ_{wv} (———) WITH 90% CONFIDENCE INTERVALS (— —) AND THEORETICAL PHASEFUNCTION (– – – –) . 2301	gez.		nota WWKZ-83G.007
	akk.		A 4 nr. 83 K.074

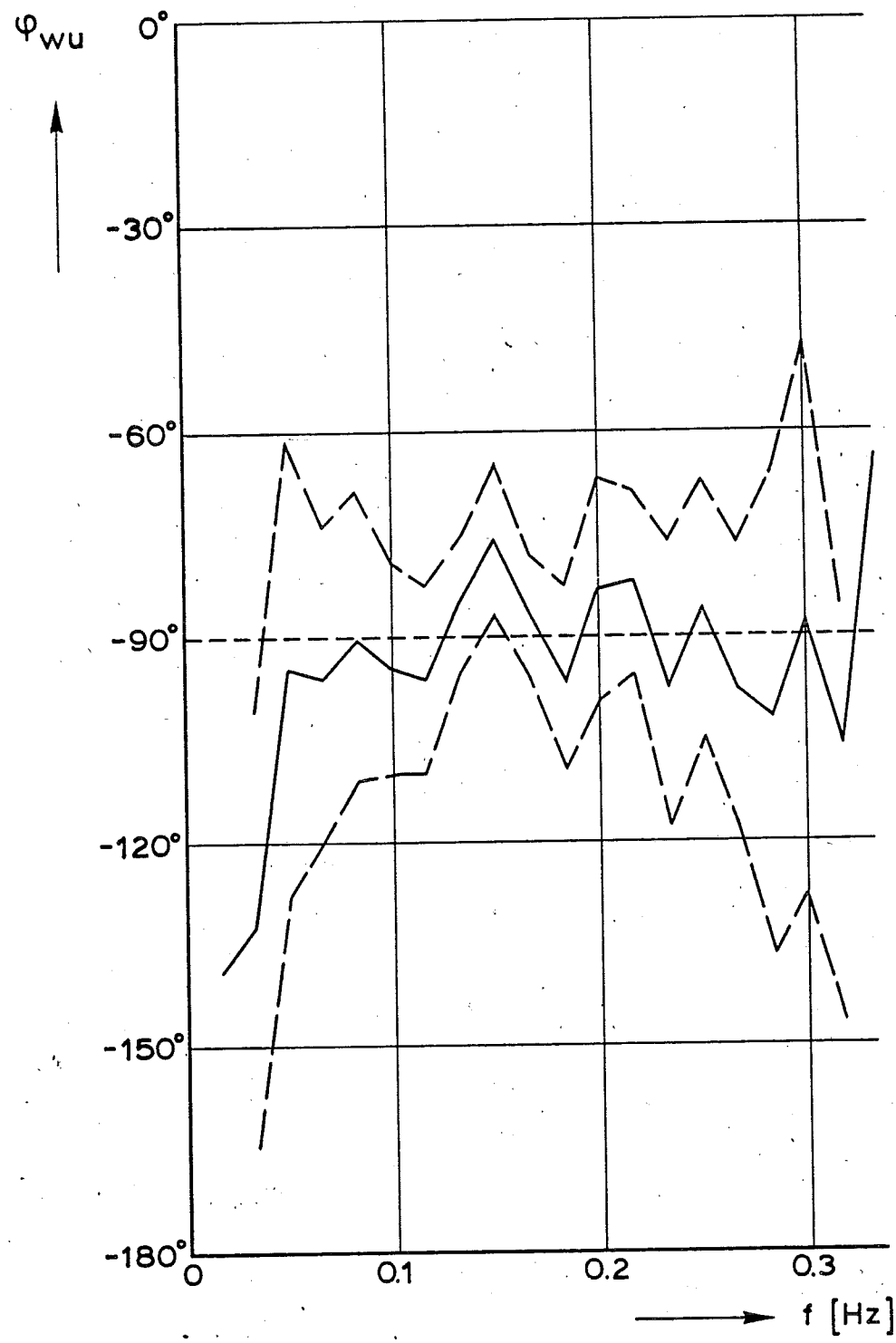

ijkswaterstaat lirectie waterhuishouding en waterbeweging listrict kust en zee	get.		appendix 7. fig 7
	gec.		projectcode L7709B00
MEASURED PHASEFUNCTION φ_{wu} (———) WITH 90% CONFIDENCE INTERVALS (— —) AND THEORETICAL PHASEFUNCTION (– – –) . 2420	gez.		nota WWKZ-83G.007
	akk.		A4 nr. 83 K.075

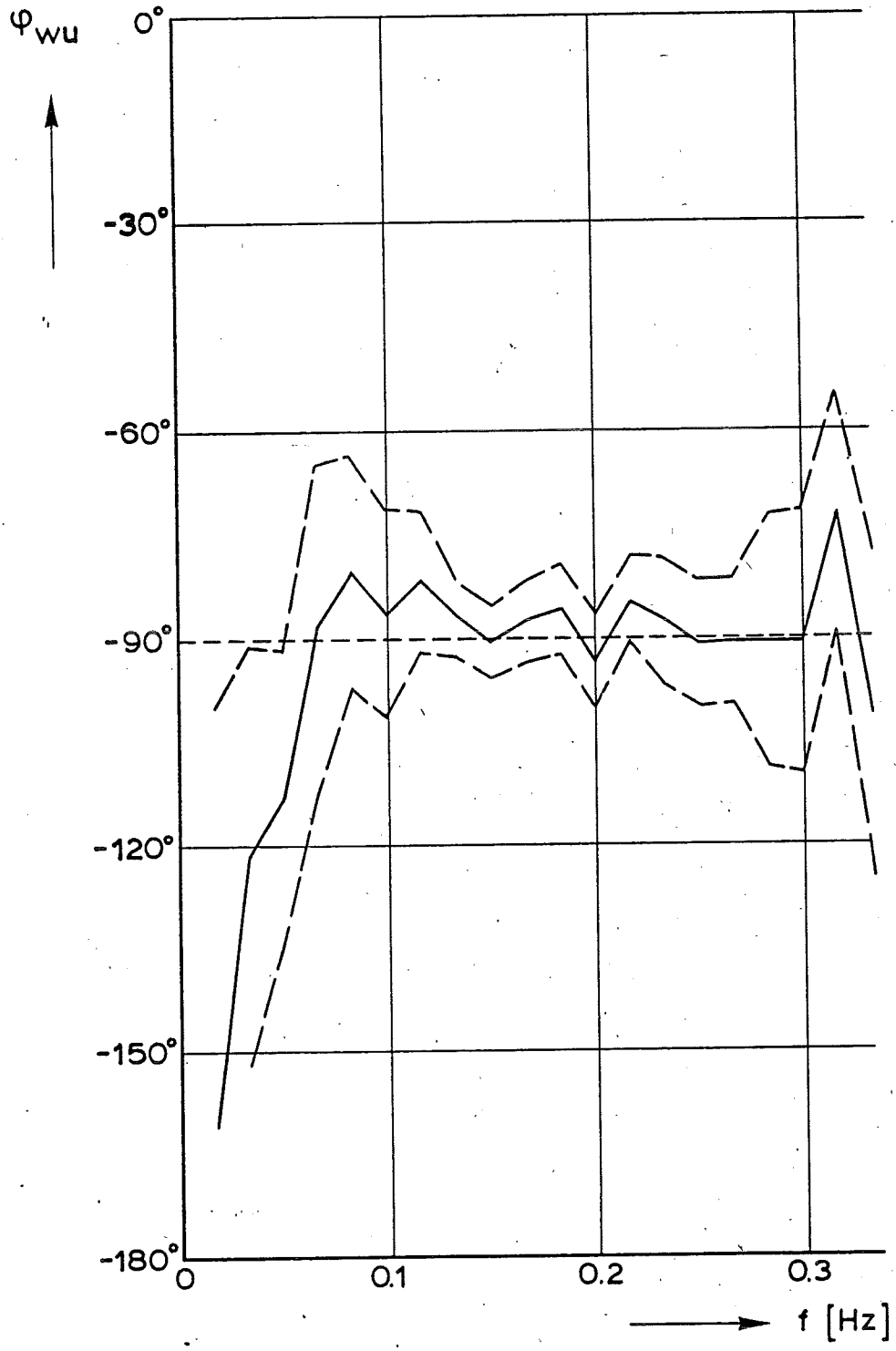

ijkswaterstaat irectie waterhuishouding en waterbeweging istrict kust en zee	get.		appendix 7. fig. 8
	gec.		projectcode L7709B00
IEASURED PHASEFUNCTION φ_{wu} (———) WITH 0% CONFIDENCE INTERVALS (— —) AND HEORETICAL PHASEFUNCTION (– – – –). 2501	gez.		nota WWKZ-83G.007
	akk.		A4 nr. 83 K.076

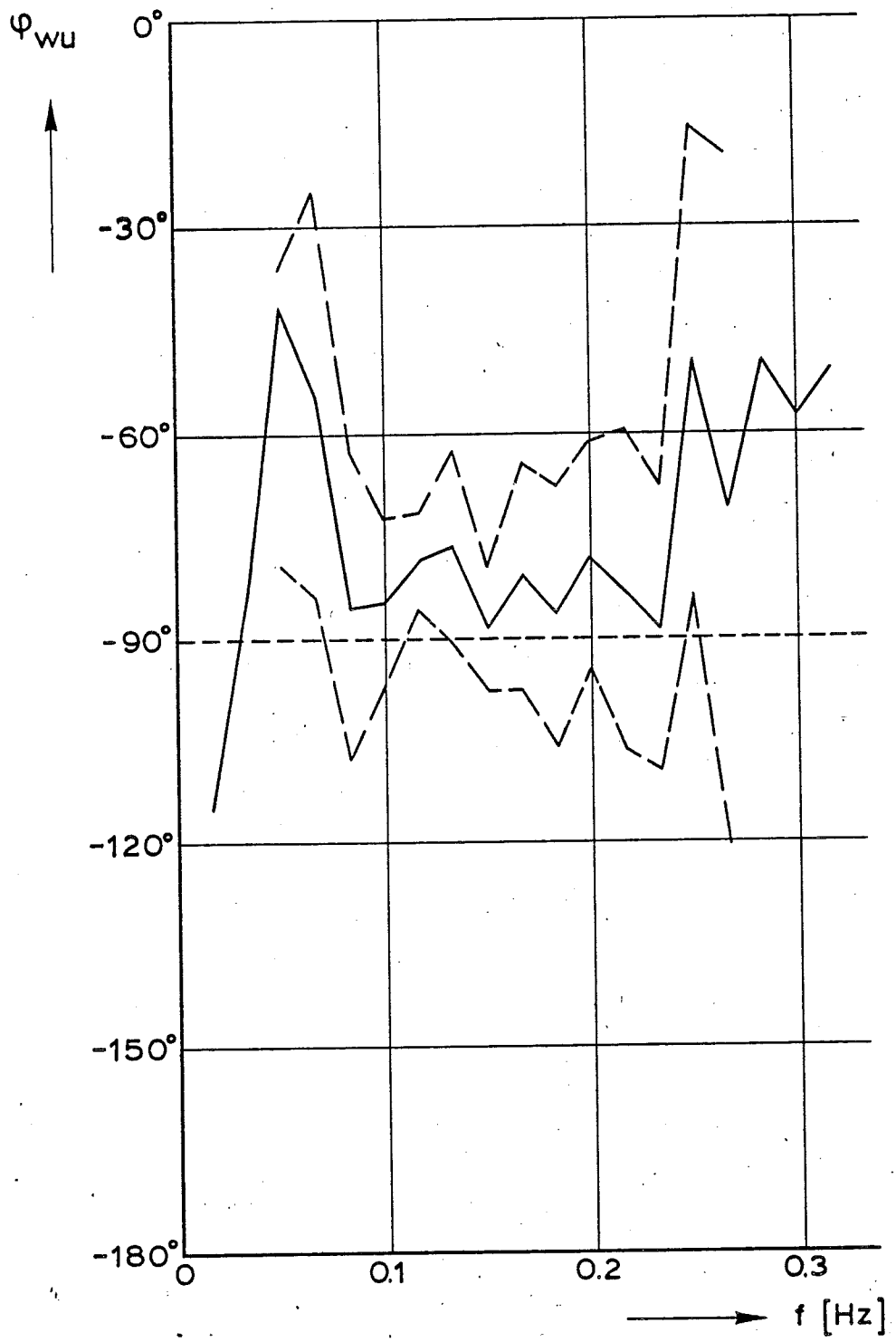

ijkswaterstaat irectie waterhuishouding en waterbeweging istrict kust en zee	get.	appendix 7. fig. 9
	gec.	projectcode L7709B00
MEASURED PHASEFUNCTION φ_{wu} (———) WITH 90% CONFIDENCE INTERVALS (— —) AND THEORETICAL PHASEFUNCTION (– – – –) . 2601	gez.	nota WWKZ-83G.007
	akk	A 4 | nr. 83 K.077

APPENDIX 8.

GAIN FUNCTIONS OF SURFACE ELEVATION AND HORIZONTAL VELOCITY COMPONENT.

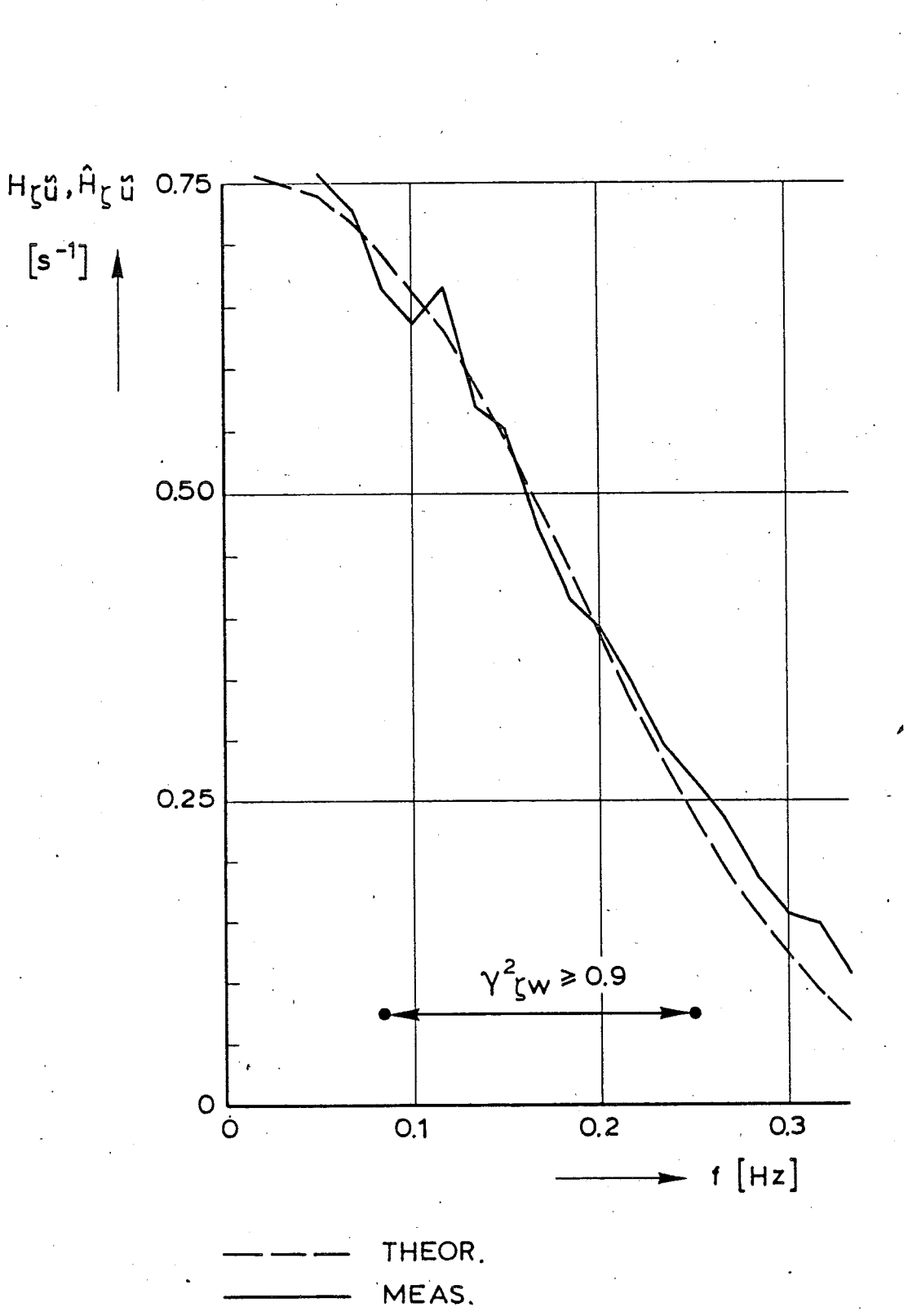

ijkswaterstaat irectie waterhuishouding en waterbeweging istrict kust en zee	get.		appendix 8. fig. 1
	gec.		projectcode L7709B00
MEASURED AND THEORETICAL GAINFUNCTION.	gez.		nota WWKZ-83G.007
APE 1501	akk.		A 4 nr. 83 K.078

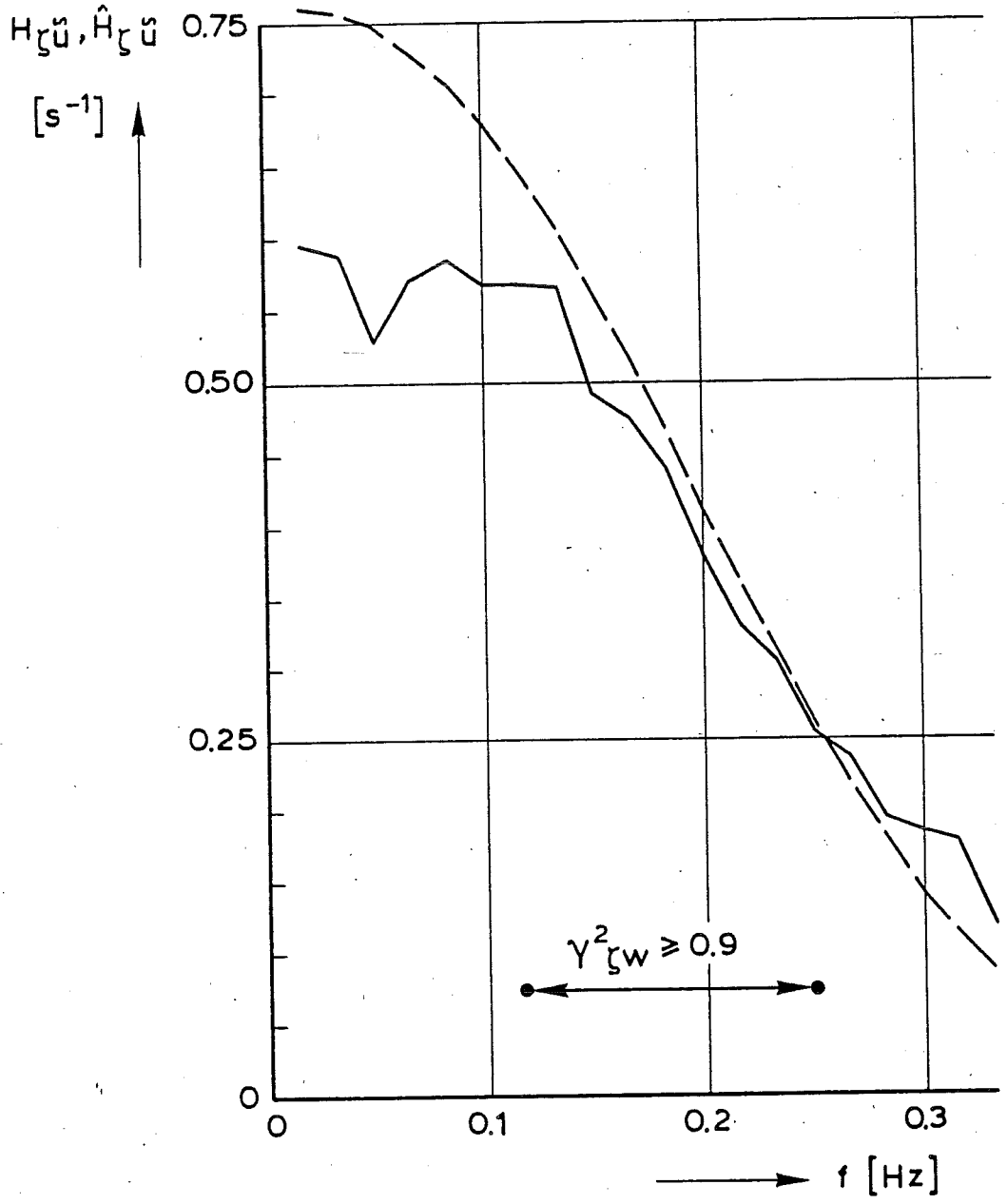

——— THEOR.

——— MEAS.

ijkswaterstaat irectie waterhuishouding en waterbeweging istrict kust en zee	get.		appendix 8. fig. 2
	gec.		projectcode L7709B00
MEASURED AND THEORETICAL GAINFUNCTION.	gez.		nota WWKZ-83G.007
APE 1601	akk.		A 4 nr. 83 K.079

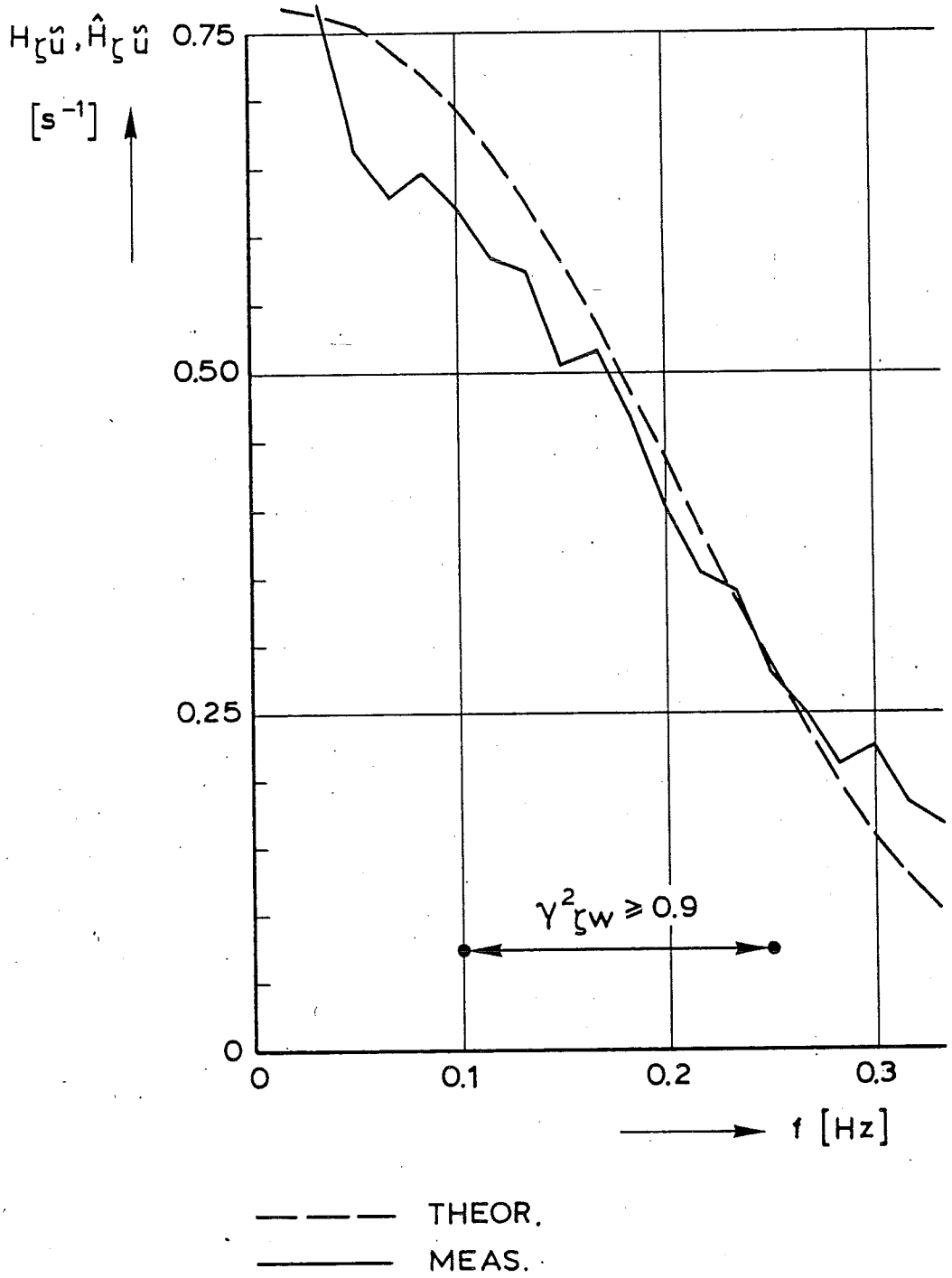

jkswaterstaat rectie waterhuishouding en waterbeweging istrict kust en zee	get.		appendix 8. fig. 3	
	gec.		projectcode L7709B00	
EASURED AND THEORETICAL GAINFUNCTION.	gez.		nota WWKZ-83G.007	
APE 1704	akk.		A 4	nr. 83K.080

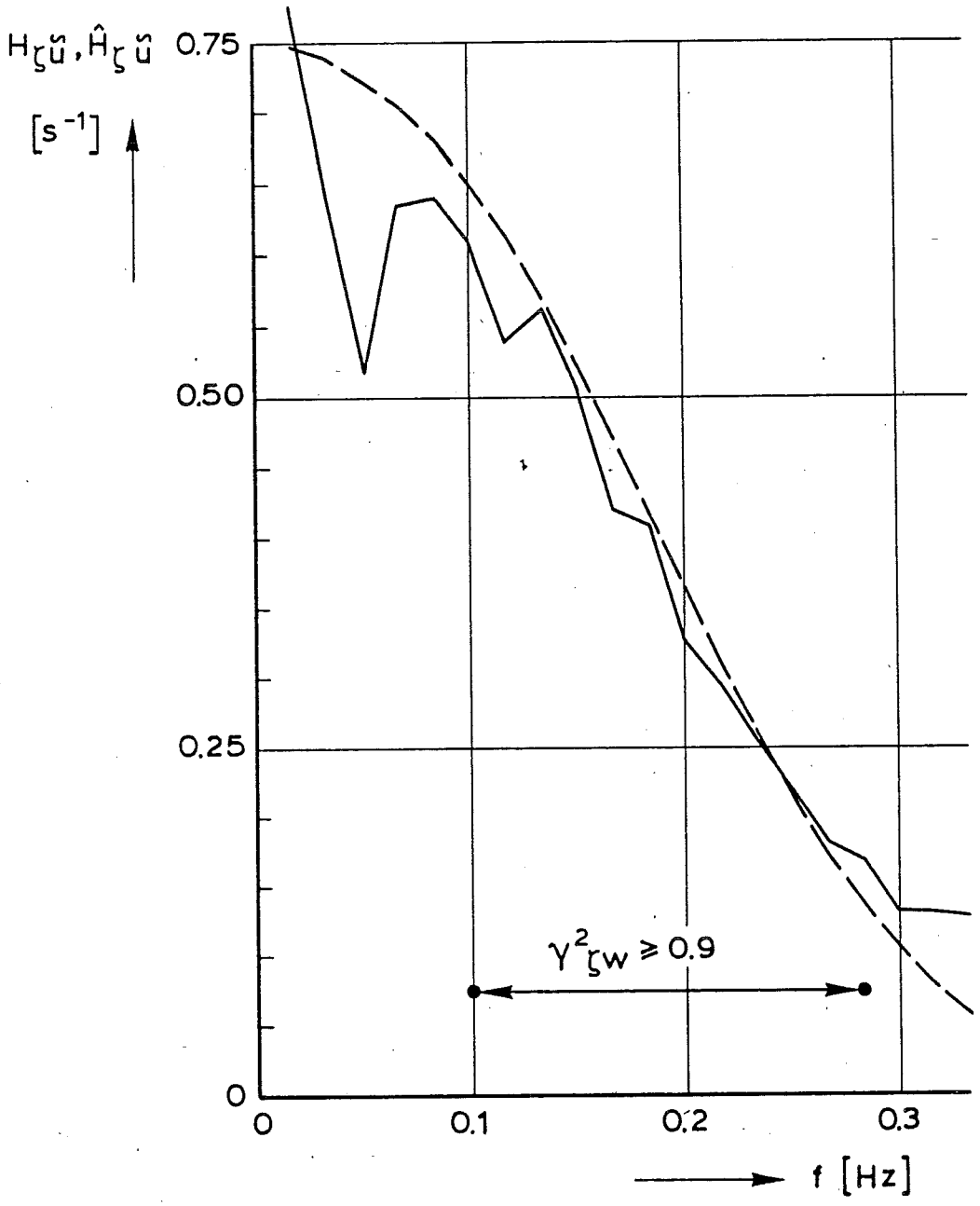

jkswaterstaat rectie waterhuishouding en waterbeweging strict kust en zee	get.		appendix 8. fig. 4	
	gec.		projectcode L7709B00	
EASURED AND THEORETICAL GAINFUNCTION: APE 1802	gez.		nota WWKZ-83G.007	
	akk.		A 4	nr. 83 K.081

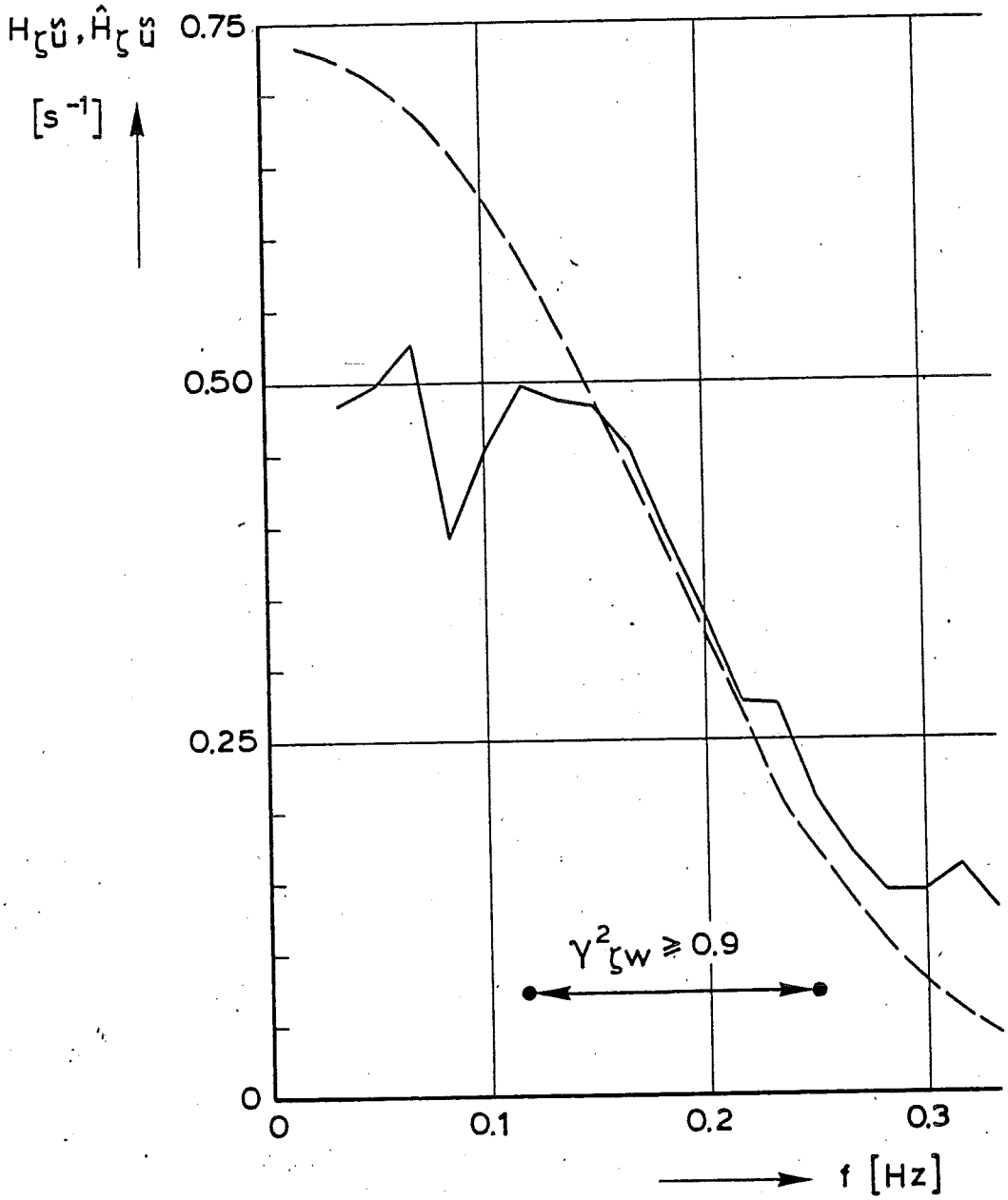

ijkswaterstaat irectie waterhuishouding en waterbeweging istrict kust en zee	get.		appendix 8. fig. 5	
	gec.		projectcode L7709B00	
IEASURED AND THEORETICAL GAINFUNCTION.	gez.		nota WWKZ-83G.007	
APE 2201	akk.		A 4	nr. 83K.082

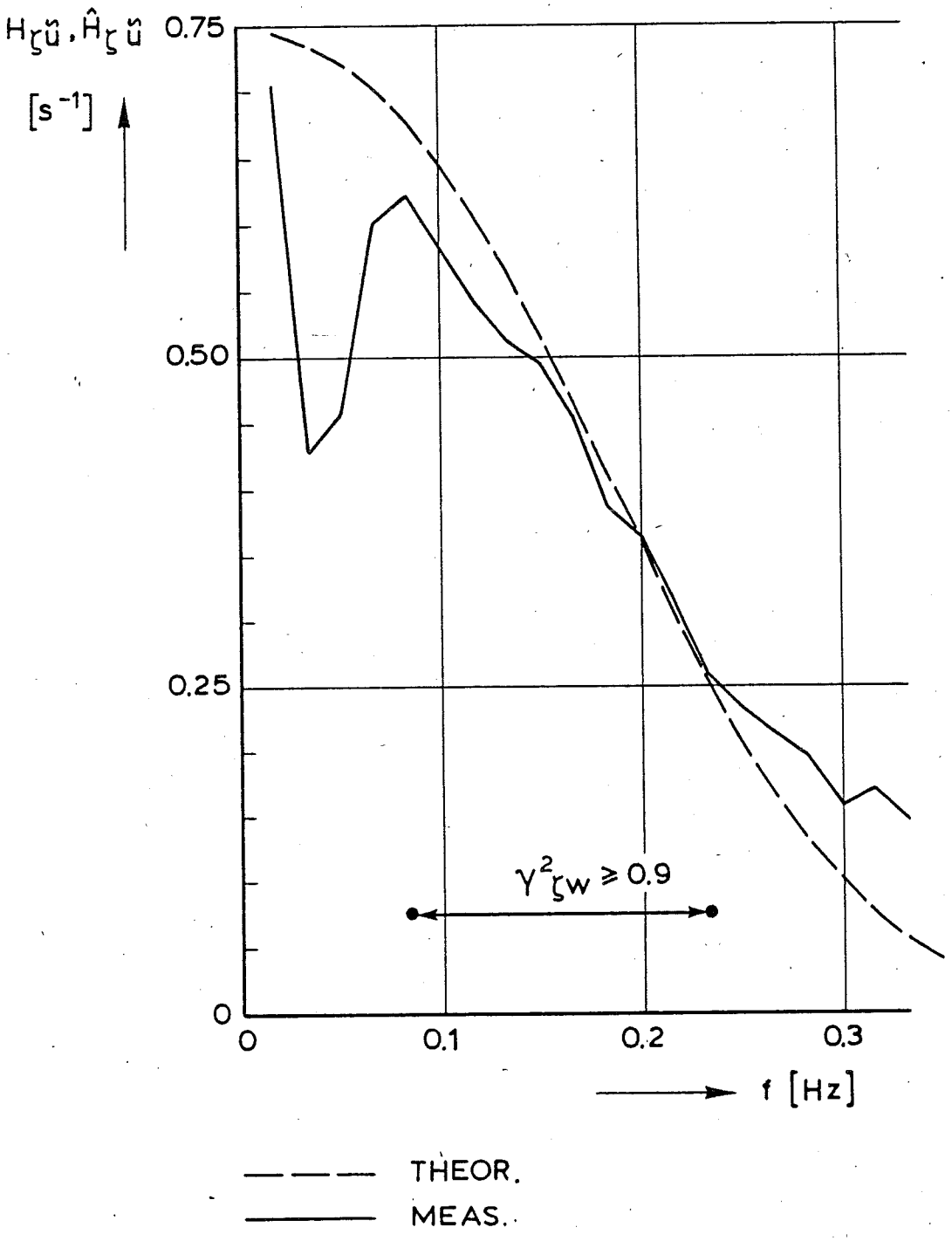

ijkswaterstaat irectie waterhuishouding en waterbeweging istrict kust en zee	get.		appendix 8. fig. 6	
	gec.		projectcode L7709B00	
IEASURED AND THEORETICAL GAINFUNCTION.	gez.		nota WWKZ-83G.007	
APE 2301	akk.		A 4	nr. 83 K.083

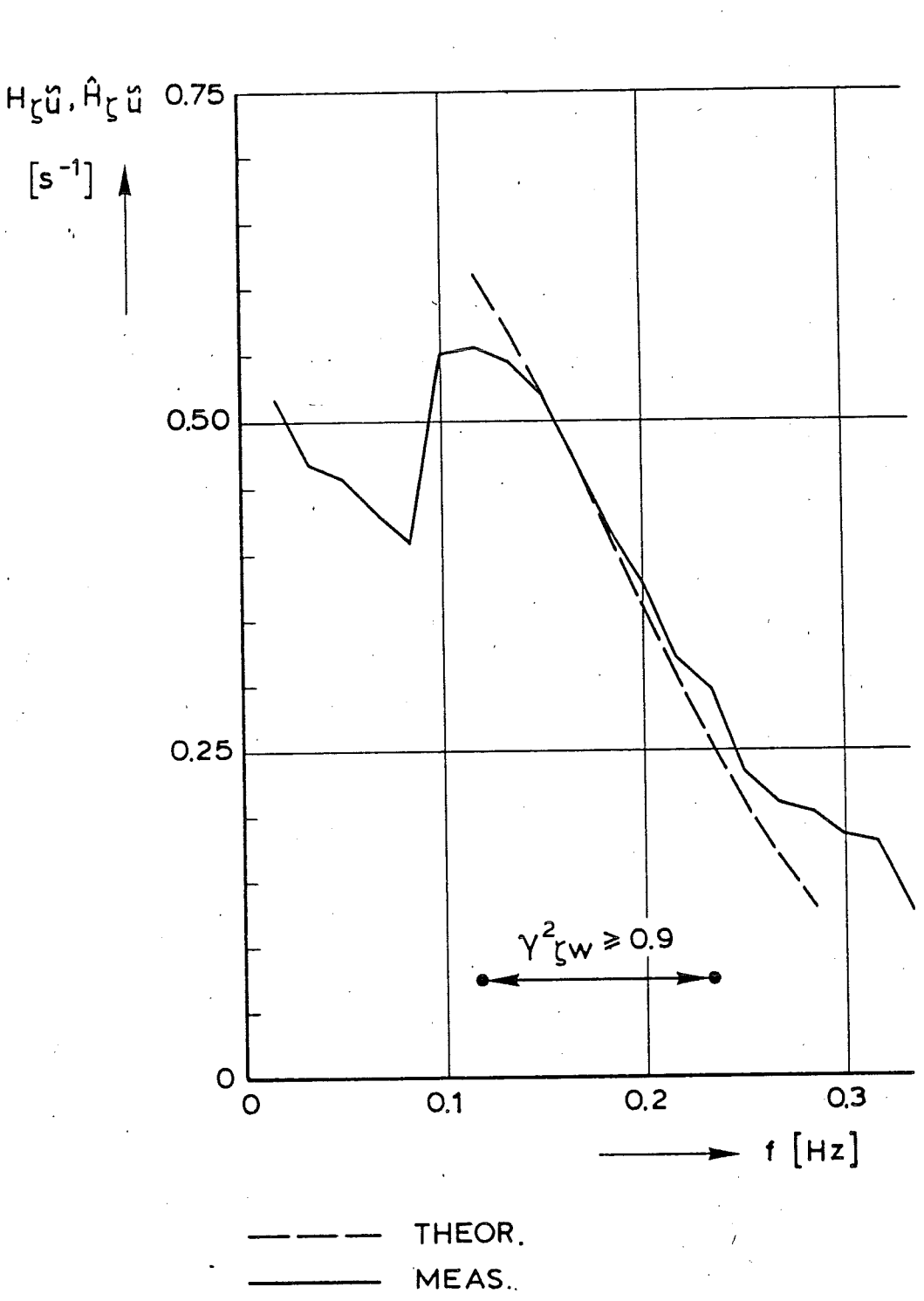

ijkswaterstaat irectie waterhuishouding en waterbeweging istrict kust en zee	get.		appendix 8. fig. 7	
	gec.		projectcode L7709B00	
MEASURED AND THEORETICAL GAINFUNCTION.	gez.		nota WWKZ-83G.007	
APE 2420	akk.		A 4	nr. 83K.084

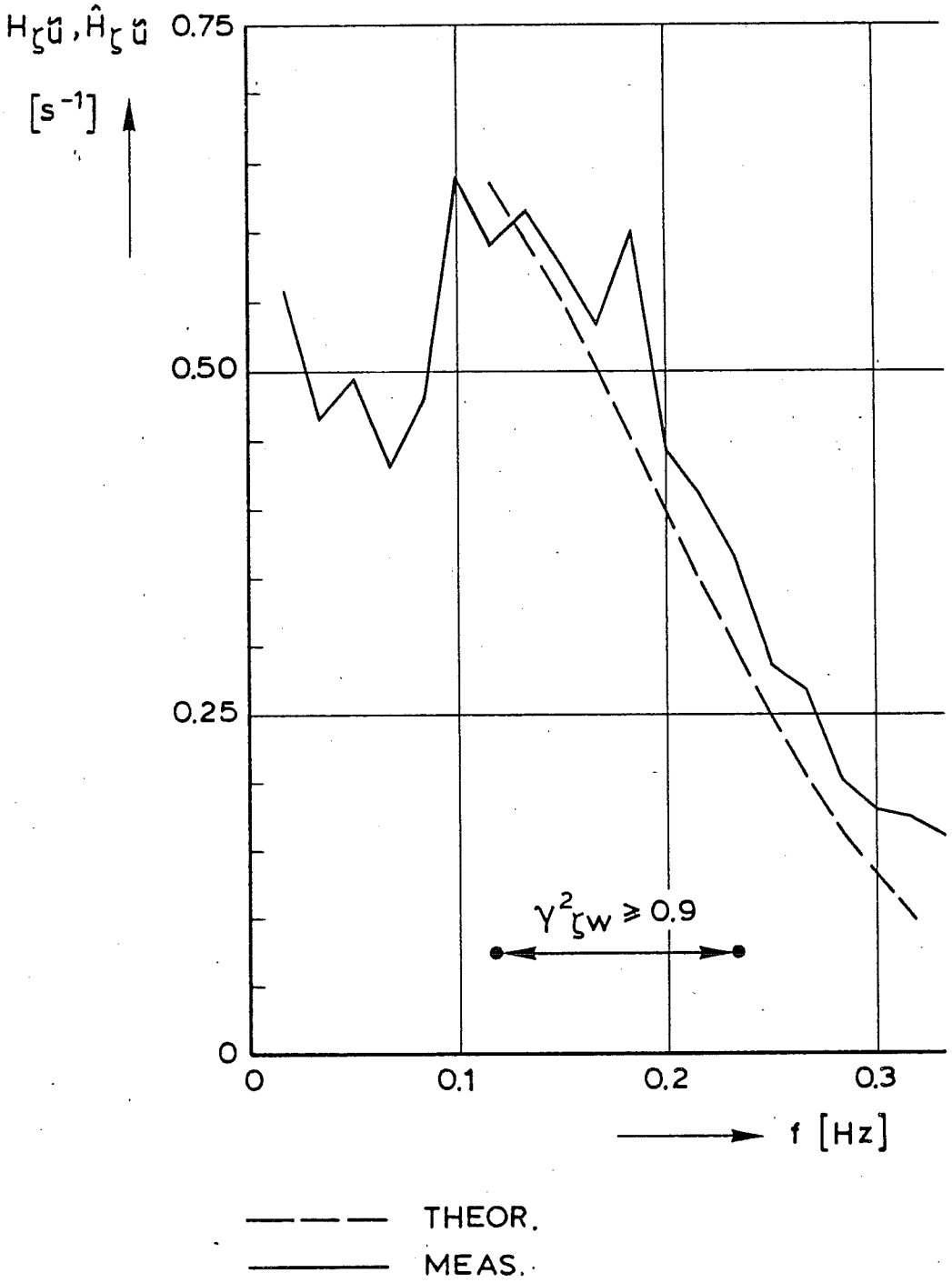

ijkswaterstaat irectie waterhuishouding en waterbeweging istrict kust en zee	get.		appendix 8. fig. 8	
	gec.		projectcode L7709B00	
IEASURED AND THEORETICAL GAINFUNCTION.	gez.		nota WWKZ-83G.007	
APE 2501	akk.		A 4	nr. 83 K.085

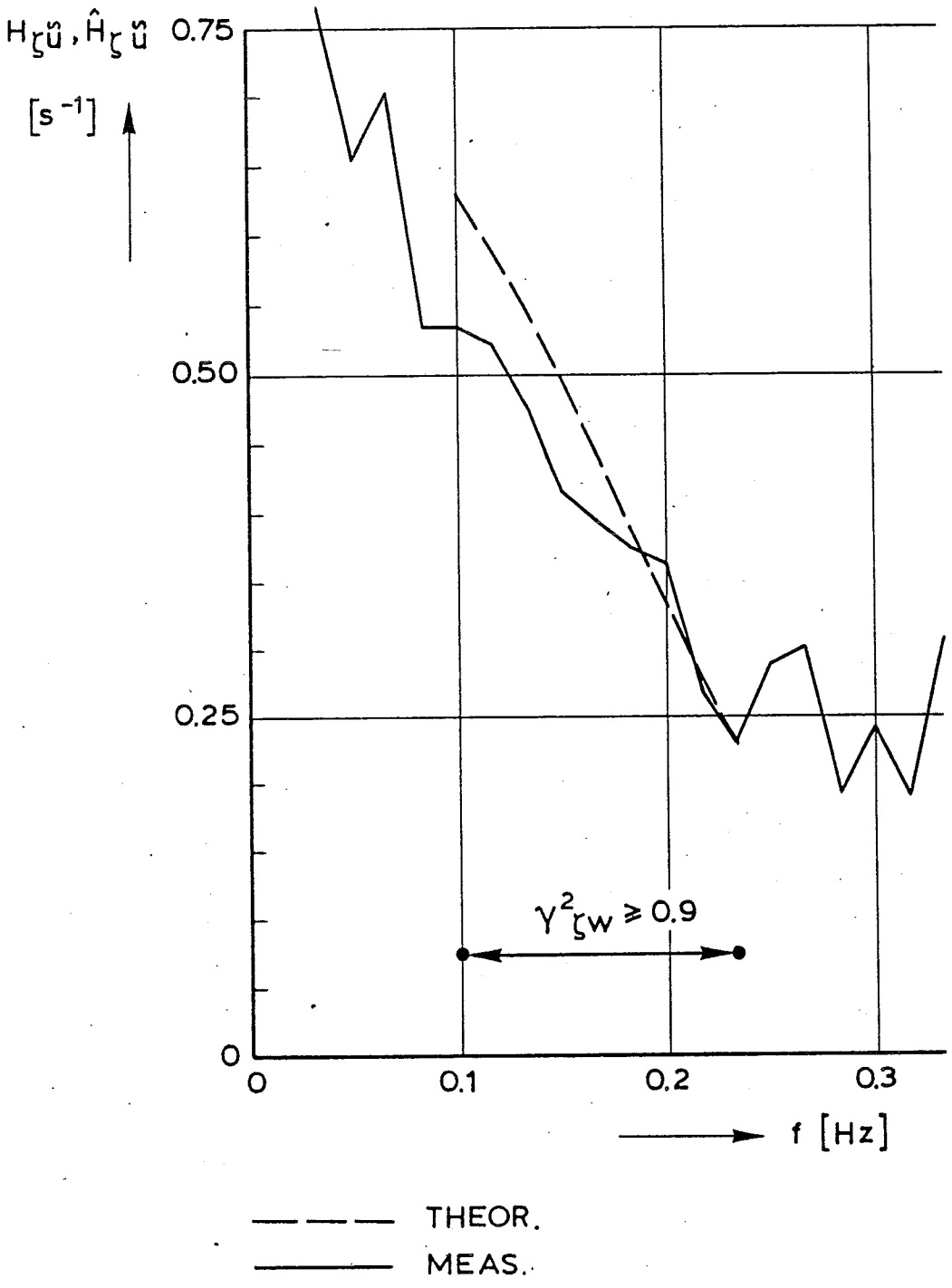

ijkswaterstaat irectie waterhuishouding en waterbeweging istrict kust en zee	get.		appendix 8. fig. 9	
	gec.		projectcode L7709B00	
MEASURED AND THEORETICAL GAINFUNCTION.	gez.		nota WWKZ-83G.007	
APE 2601	akk.		A 4	nr. 83K.086

APPENDIX 9.

COMPARISON MEASURED GAIN FUNCTIONS OF SURFACE ELEVATION AND HORIZONTALVELOCITY COMPONENT.

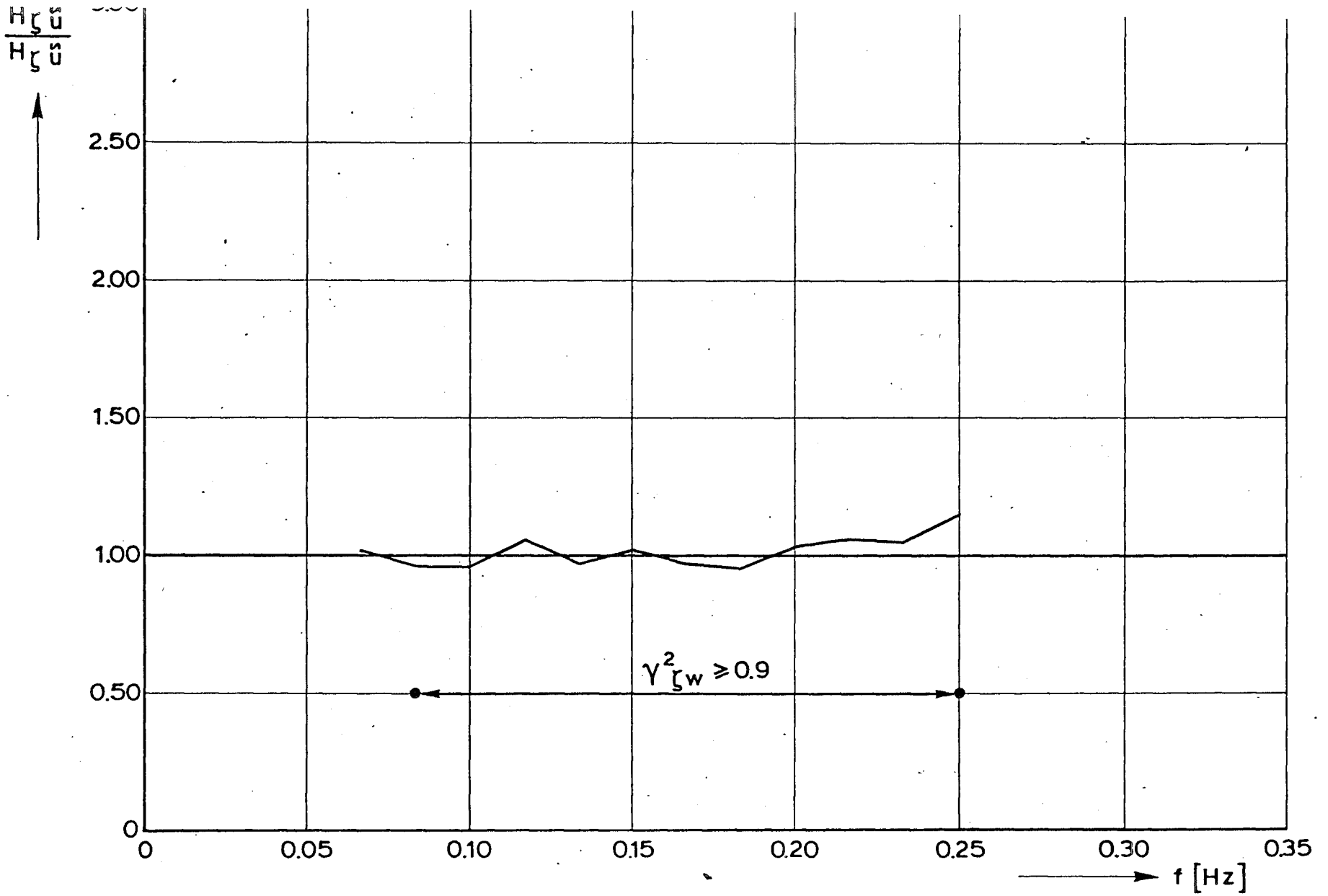

rijkswaterstaat directie waterhuishouding en waterbeweging district kust en zee	get.		appendix 9. fig. 1
	gec.		projectcode L7709B00
COMPARISON MEASURED GAINFUNCTION OF ζ AND $\tilde{u}$ WITH LINEAR THEORY (1501)	gez.		nota WWKZ-83G.007
	akk.		A4 nr. 83K.087

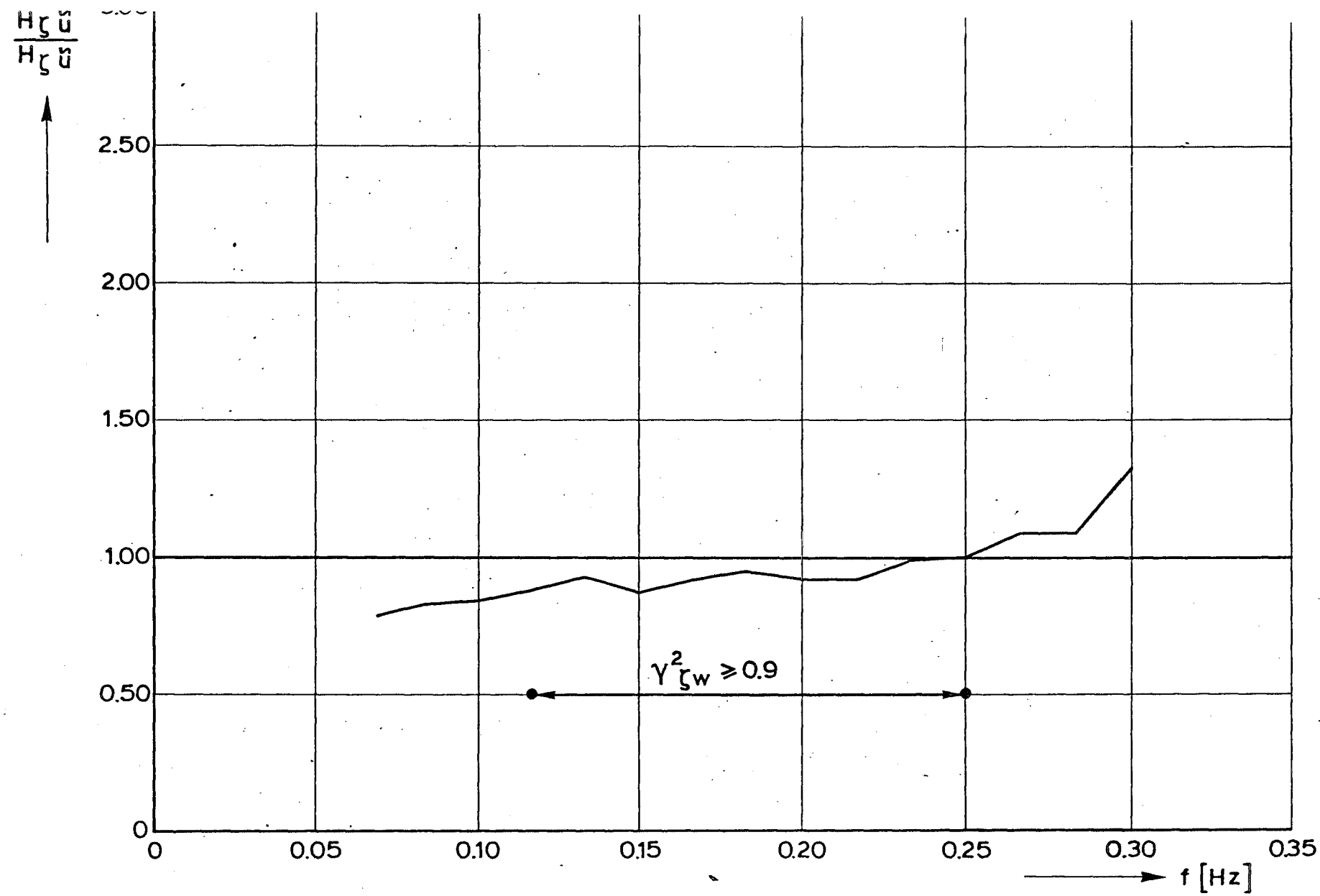

rijkswaterstaat directie waterhuishouding en waterbeweging district kust en zee	get.		appendix 9. fig. 2
	gec.		projectcode L7709B00
COMPARISON MEASURED GAINFUNCTION	gez.		nota WWKZ-83G.007
OF ζ AND $\ddot{u}$ WITH LINEAR THEORY (1601)	akk.		A4 nr. 83K.088

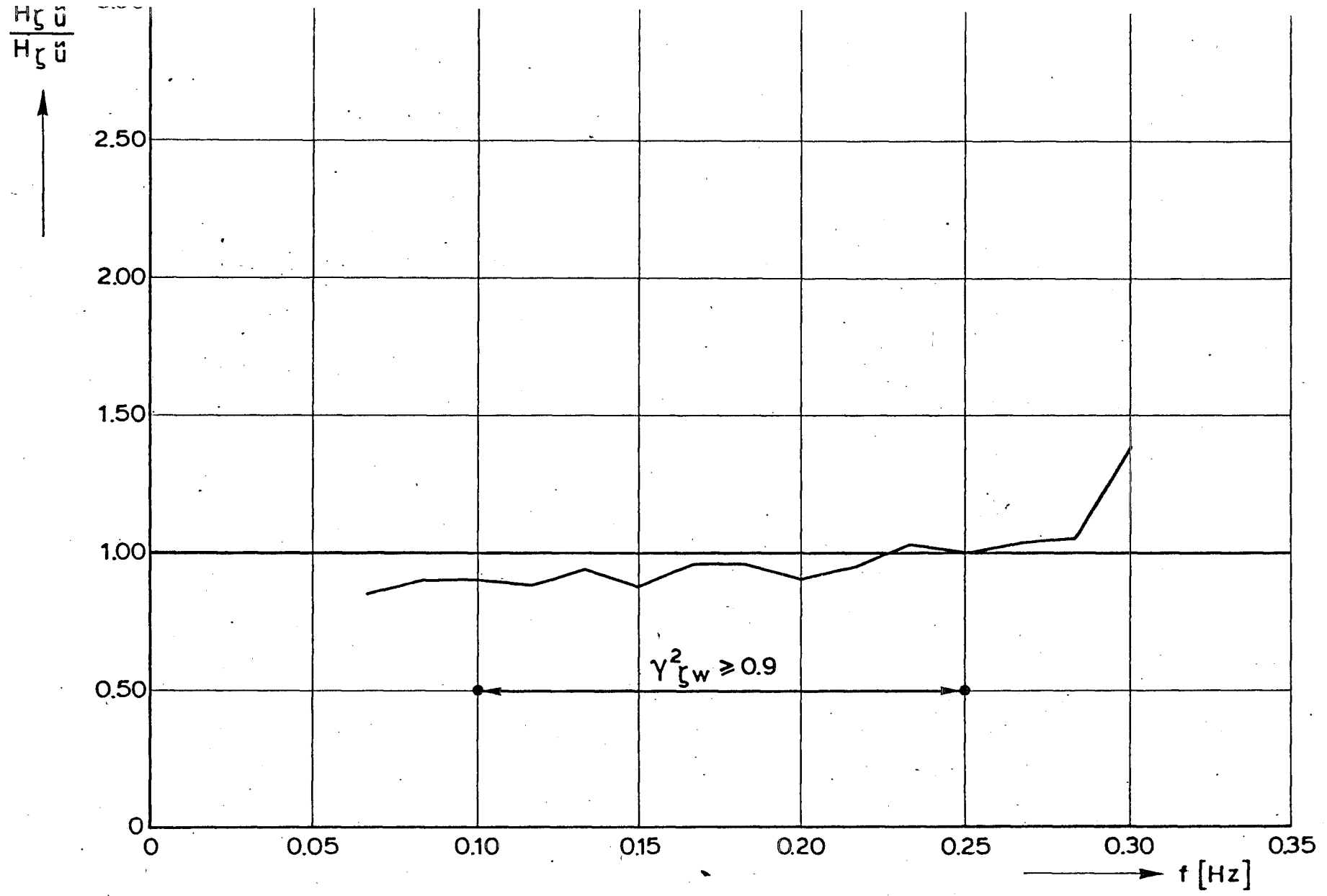

rijkswaterstaat directie waterhuishouding en waterbeweging district kust en zee	get.		appendix 9. fig. 3	
	gec.		projectcode L7709B00	
COMPARISON MEASURED GAINFUNCTION	gez.		nota WWKZ-83G.007	
OF ζ AND $\ddot{u}$ WITH LINEAR THEORY (1704)	akk.		A4	nr. 83K.089

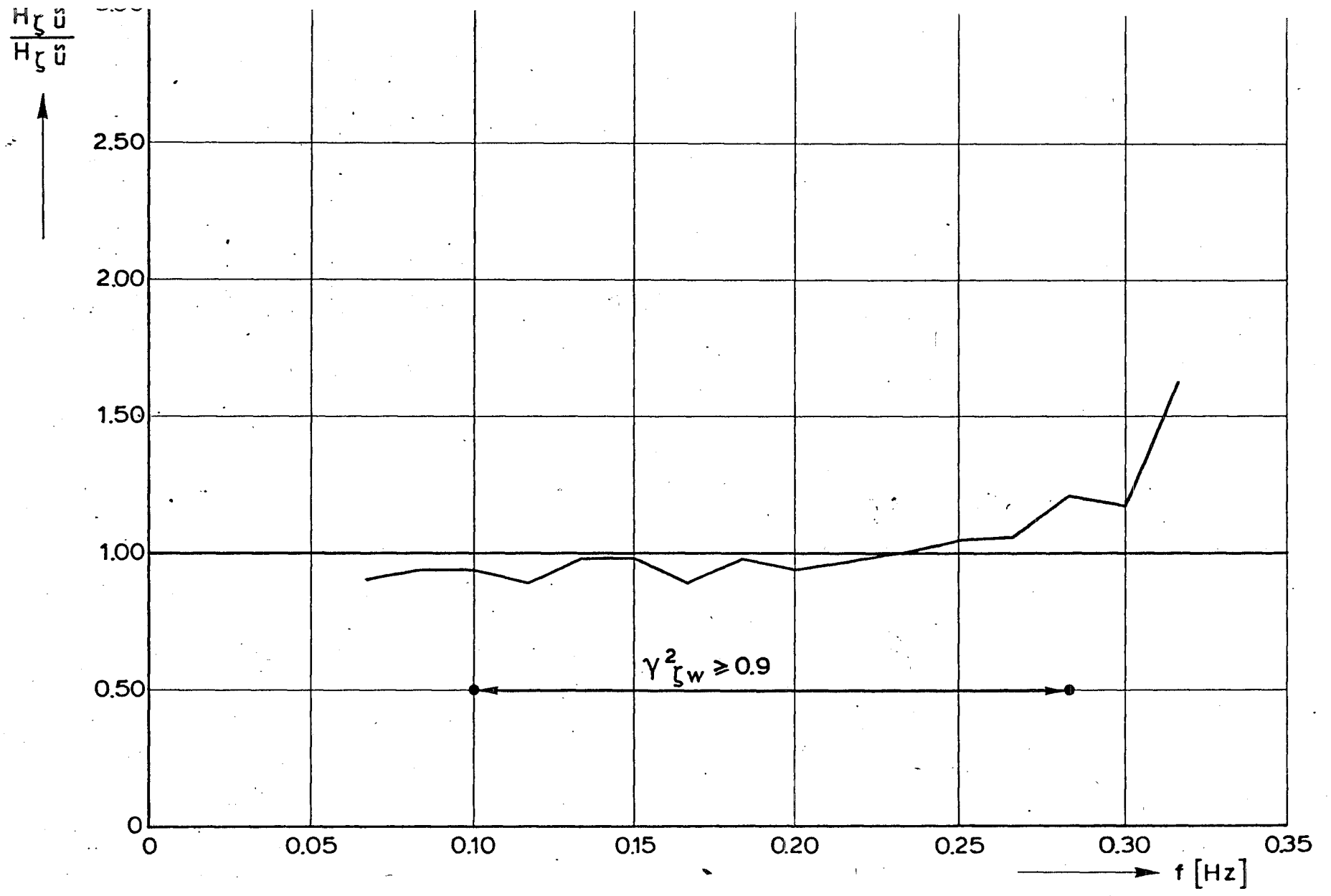

rijkswaterstaat directie waterhuishouding en waterbeweging district kust en zee	get.		appendix 9. fig. 4
	gec.		projectcode L7709B00
COMPARISON MEASURED GAINFUNCTION	gez.		nota WWKZ-83G.007
OF ζ AND $\hat{u}$ WITH LINEAR THEORY (1802)	akk.		A 4 nr. 83K.090

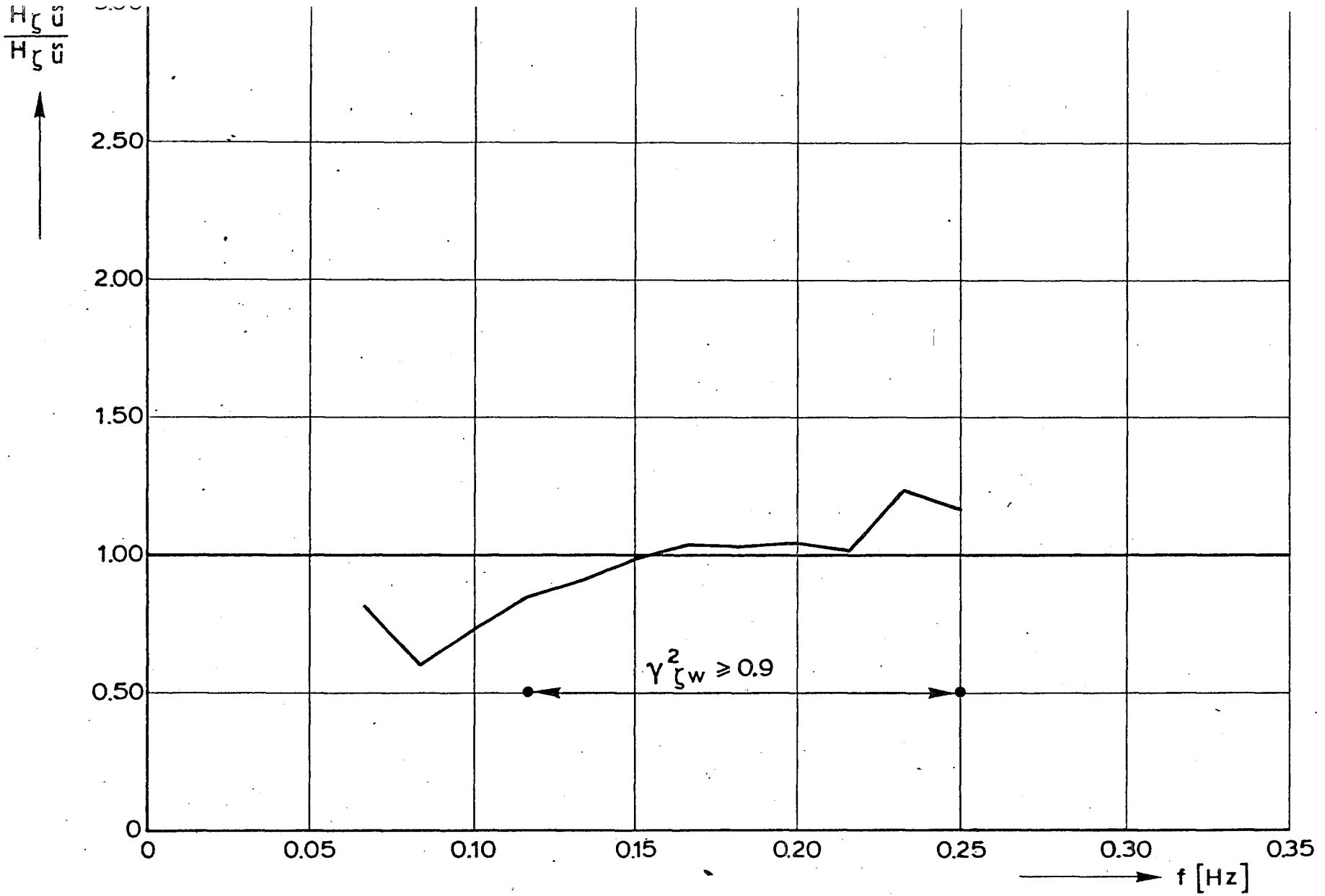

rijkswaterstaat directie waterhuishouding en waterbeweging district kust en zee	get.		appendix 9. fig. 5
	gec.		projectcode L7709B00
COMPARISON MEASURED GAINFUNCTION	gez.		nota WWKZ-83G.007
OF ζ AND $\hat{u}$ WITH LINEAR THEORY (2201)	akk.		A4 nr. 83K.091

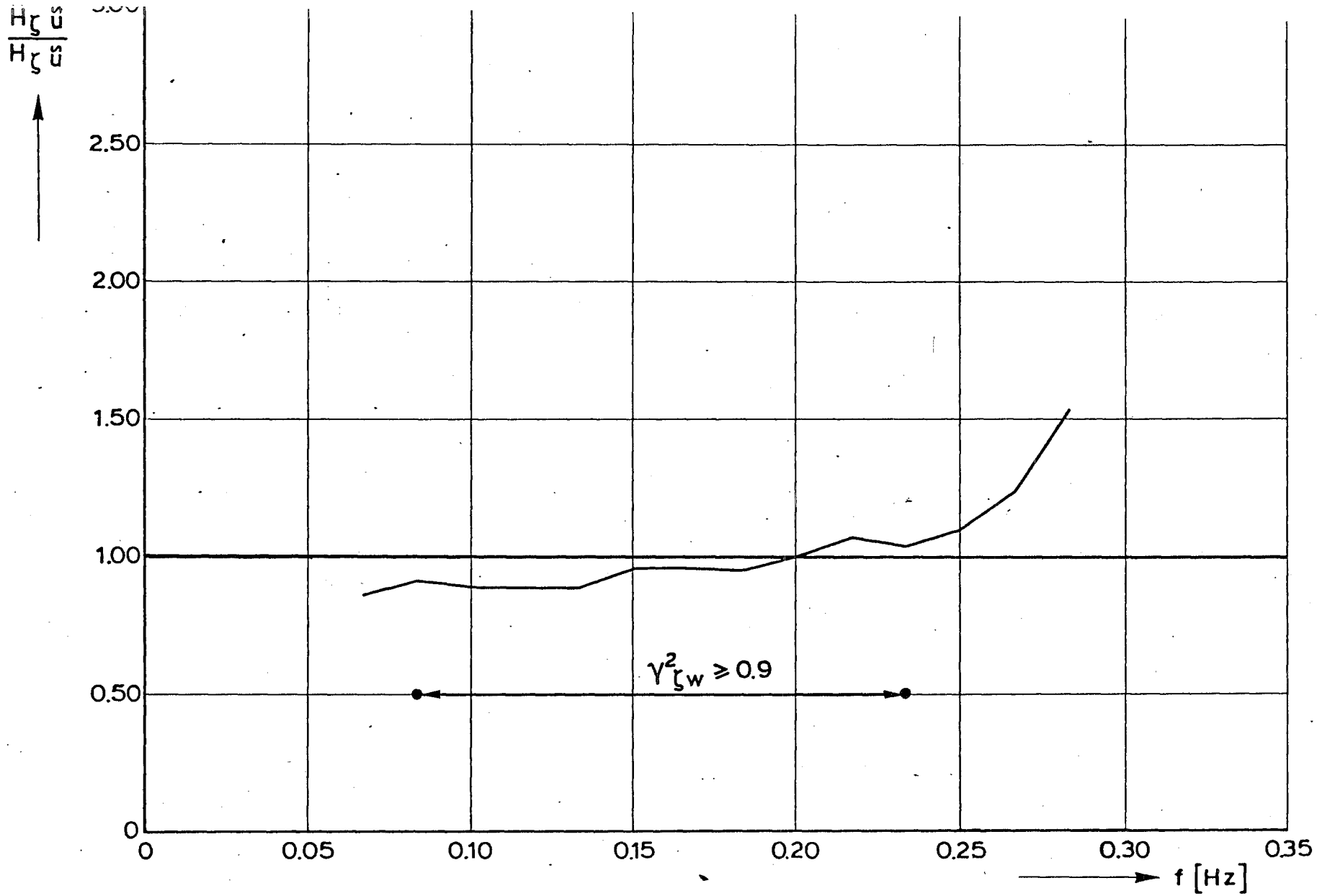

rijkswaterstaat directie waterhuishouding en waterbeweging district kust en zee	get.		appendix 9. fig. 6
	gec.		projectcode L7709B00
COMPARISON MEASURED GAINFUNCTION	gez.		nota WWKZ-83G.007
OF ζ AND $\hat{u}$ WITH LINEAR THEORY (2301)	akk.		A4 nr. 83K.092

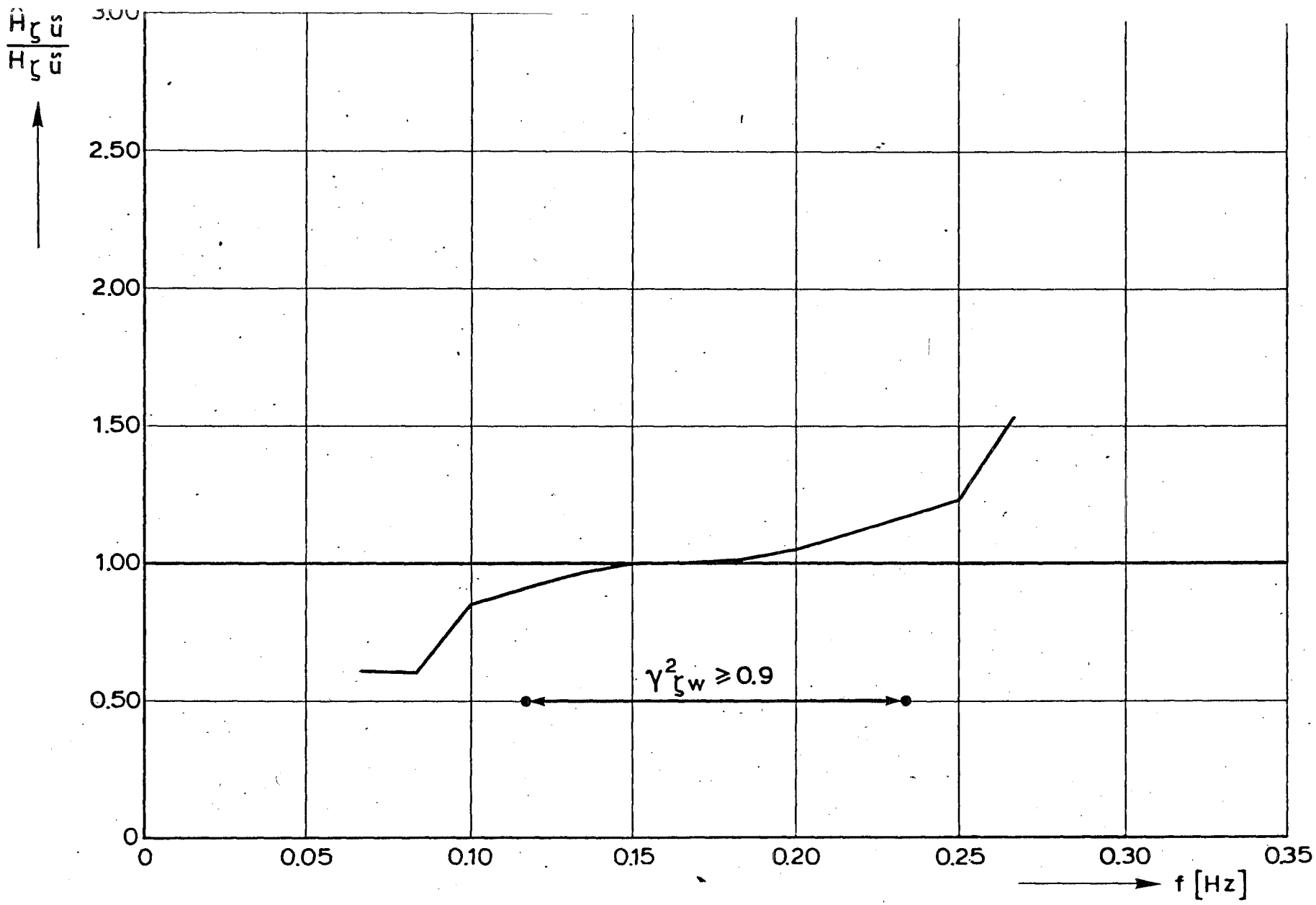

rijkswaterstaat directie waterhuishouding en waterbeweging district kust en zee	get.		appendix 9. fig. 7	
	gec.		projectcode L7709B00	
COMPARISON MEASURED GAINFUNCTION	gez.		nota WWKZ-83G.007	
OF ζ AND $\hat{u}$ WITH LINEAR THEORY (2420)	akk.		A4	nr. 83K.093

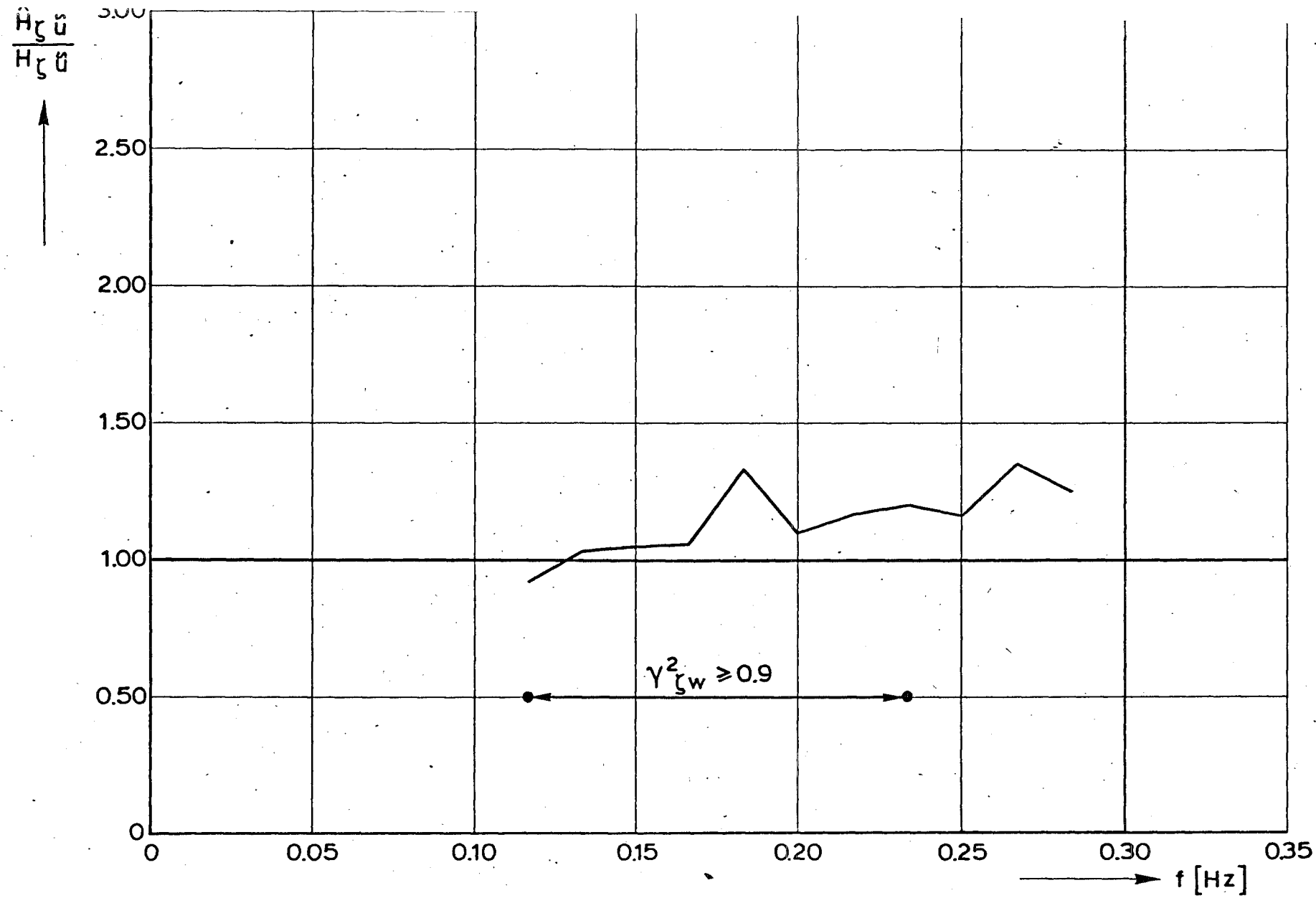

rijkswaterstaat directie waterhuishouding en waterbeweging district kust en zee	get.		appendix 9. fig. 8	
	gec.		projectcode L7709B00	
COMPARISON MEASURED GAINFUNCTION OF ζ AND $\ddot{u}$ WITH LINEAR THEORY (2501)	gez.		nota WWKZ-83G.007	
	akk.		A4	nr. 83K.094

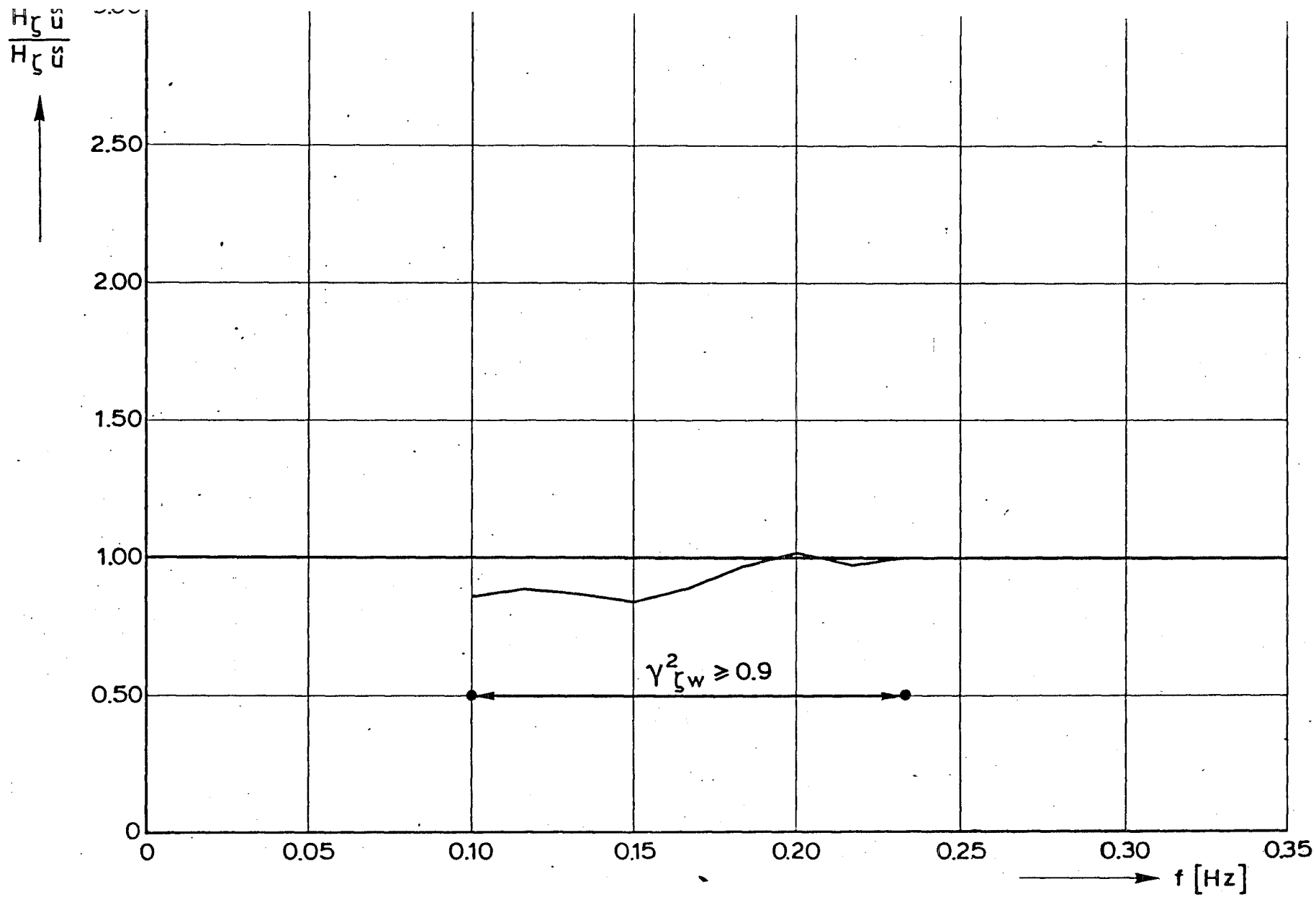

rijkswaterstaat directie waterhuishouding en waterbeweging district kust en zee	get.		appendix 9. fig. 9
	gec.		projectcode L7709B00
COMPARISON MEASURED GAINFUNCTION	gez.		nota WWKZ-83G.007
OF ζ AND $\ddot{u}$ WITH LINEAR THEORY (2601)	akk.		A4 nr. 83K.095

APPENDIX 10.

COMPARISON OF MEASURED AND CALCULATED SPECTRA OF HORIZONTAL VELOCITY COMPONENT.

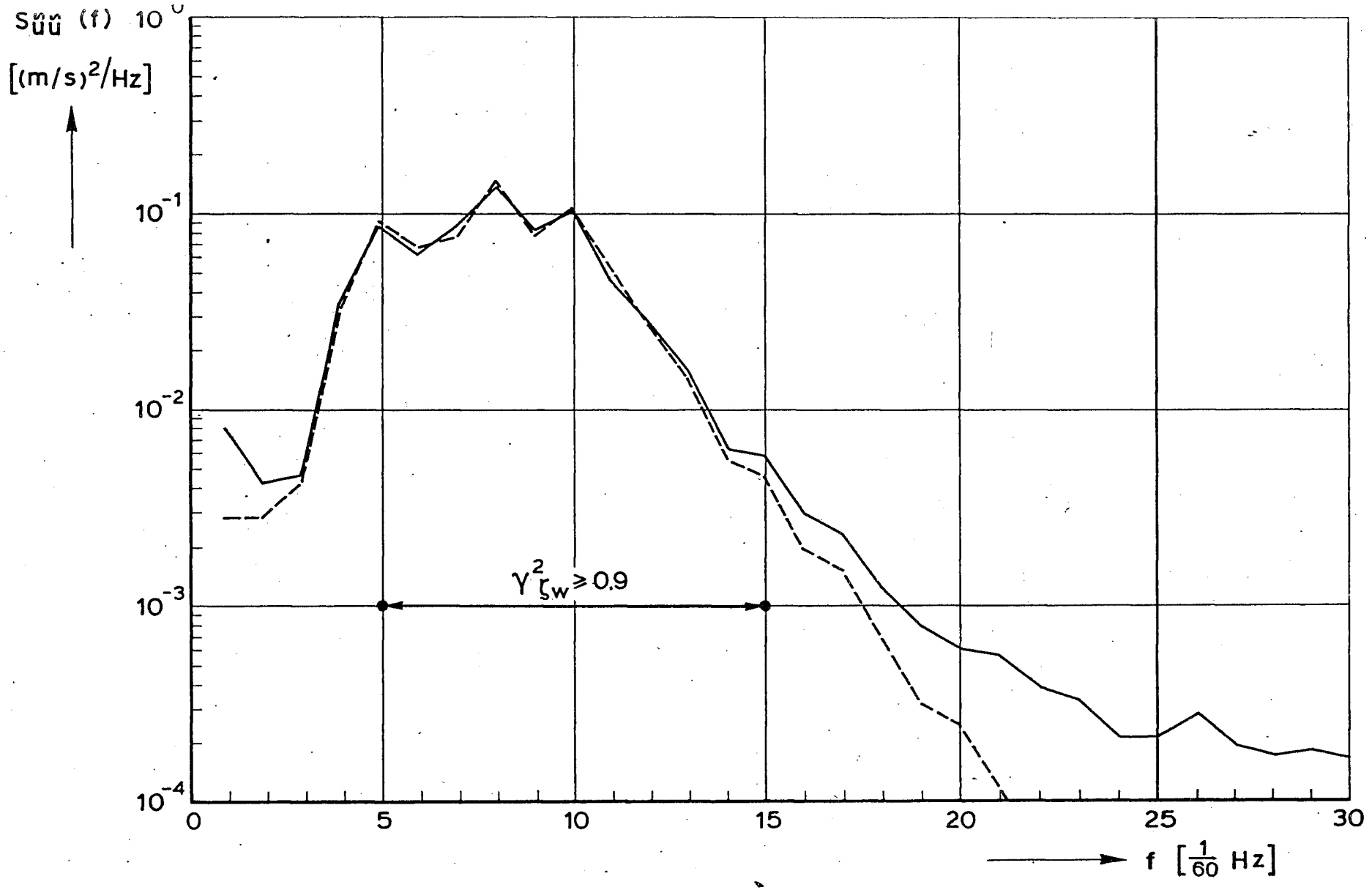

rijkswaterstaat directie waterhuishouding en waterbeweging district kust en zee	get.		appendix 10. fig. 1	
	gec.		projectcode L7709B00	
COMPARISON OF MEASURED AND CALCULATED SPECTRUM OF $\tilde{u}$ USING THE LINEAR THEORY (1501)	gez.		nota WWKZ-83G.007	
	akk.		A 4	nr. 83K.096

——— $S_{\tilde{u}\tilde{u}}$ (f)

— — — $H^2_{\zeta\tilde{u}}$ theor. (f) x $S_{\zeta\zeta}$ (f)

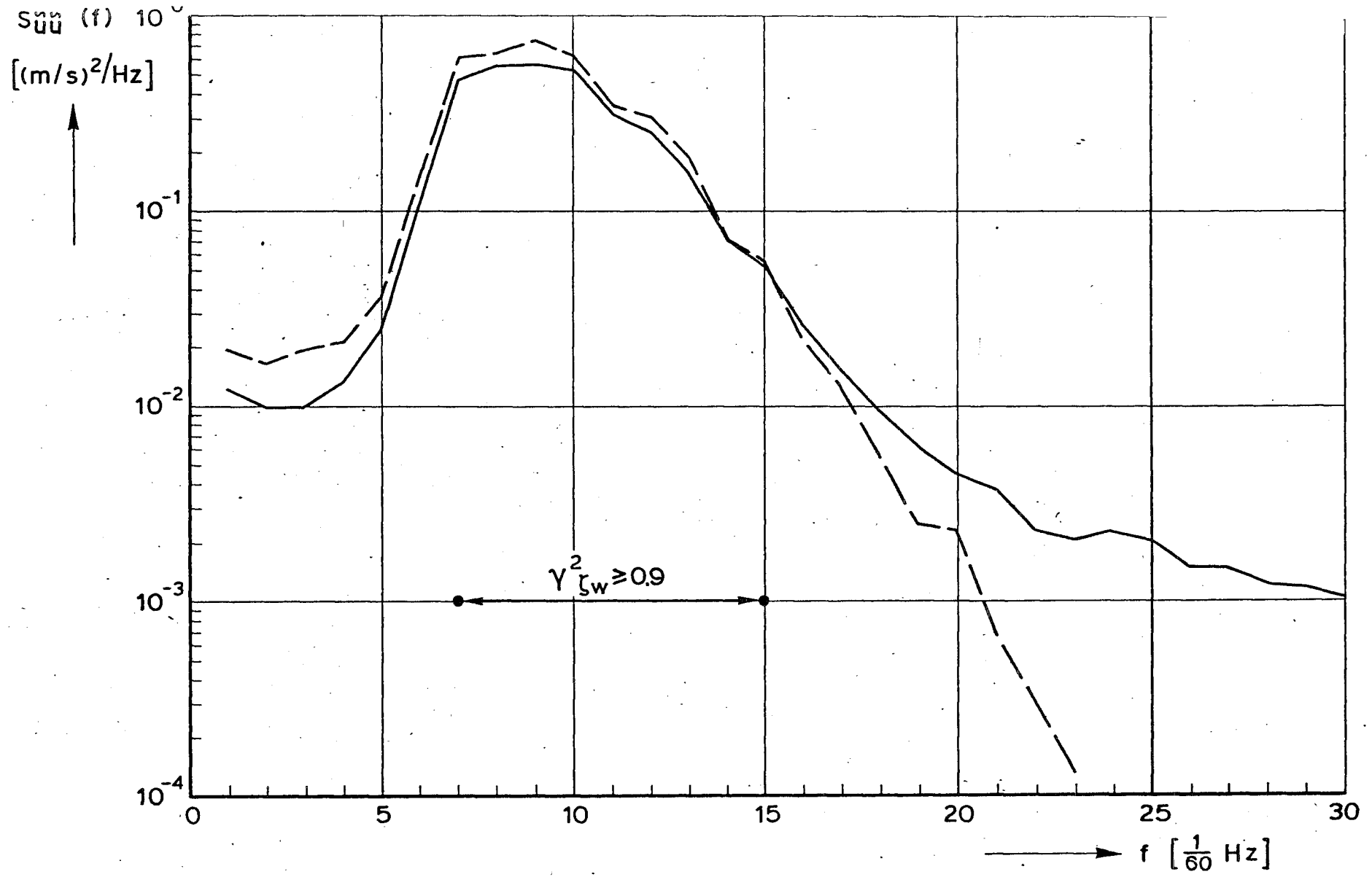

rijkswaterstaat directie waterhuishouding en waterbeweging district kust en zee	get.	appendix 10. fig. 2	
	gec.	projectcode L7709B00	
COMPARISON OF MEASURED AND CALCULATED SPECTRUM OF $\ddot{u}$ USING THE LINEAR THEORY (1601)	gez.	nota WWKZ-83G.007	
	akk.	A 4	nr. 83K.097

——— $S_{\ddot{u}\ddot{u}}$ (f)

— — — $H^2_{\zeta\,\ddot{u}}$ theor. (f) x $S_{\zeta\zeta}$(f)

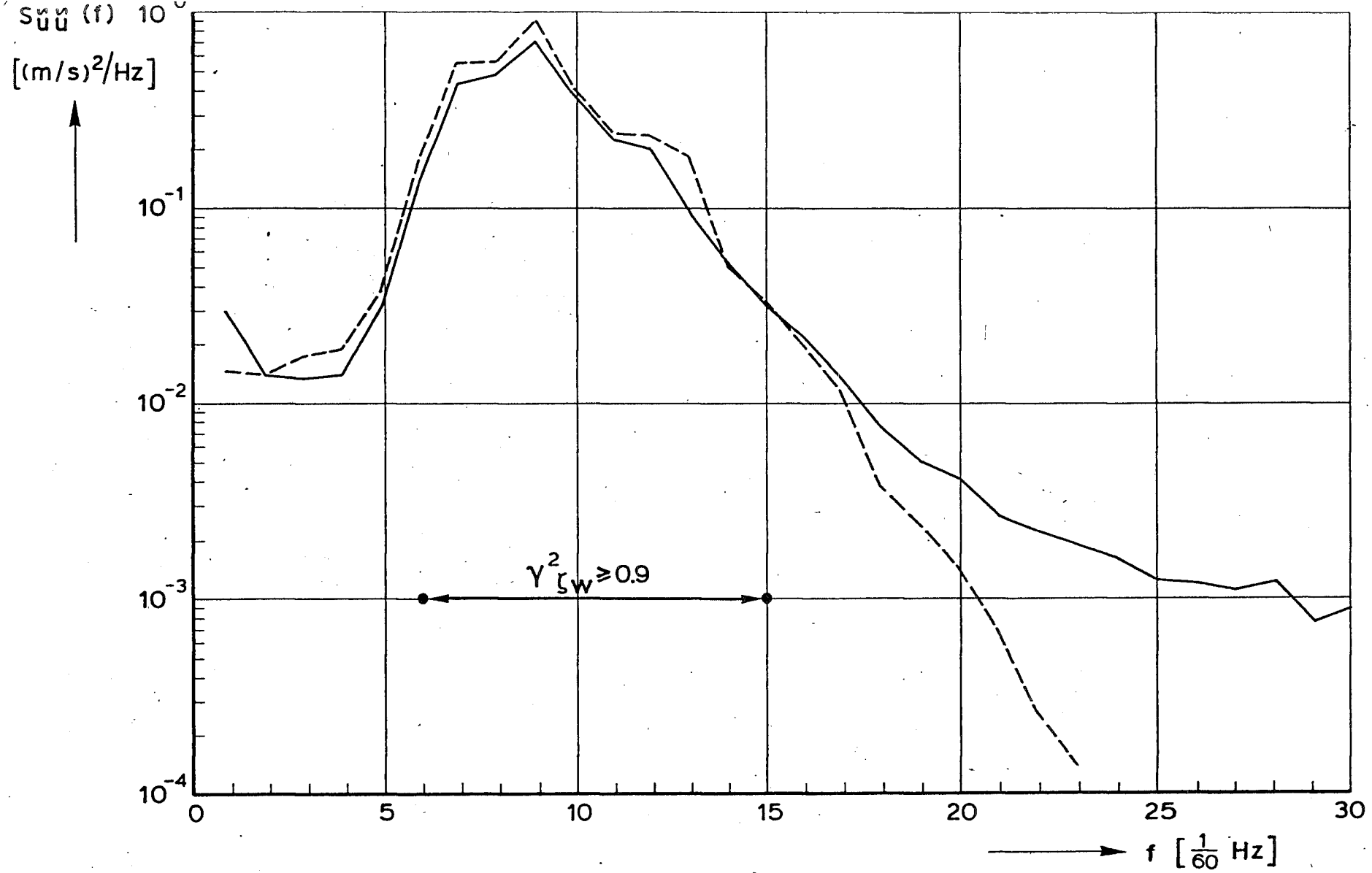

rijkswaterstaat directie waterhuishouding en waterbeweging district kust en zee	get.		appendix 10. fig.3	
	gec.		projectcode L7709B00	
COMPARISON OF MEASURED AND CALCULATED SPECTRUM OF $\tilde{u}$ USING THE LINEAR THEORY (1704)	gez.		nota WWKZ-83G.007	
	akk.		A 4	nr. 83K.098

——— $S_{\tilde{u}\tilde{u}}(f)$

— — — $H^2_{\zeta\tilde{u}}$ theor. $(f) \times S_{\zeta\zeta}(f)$

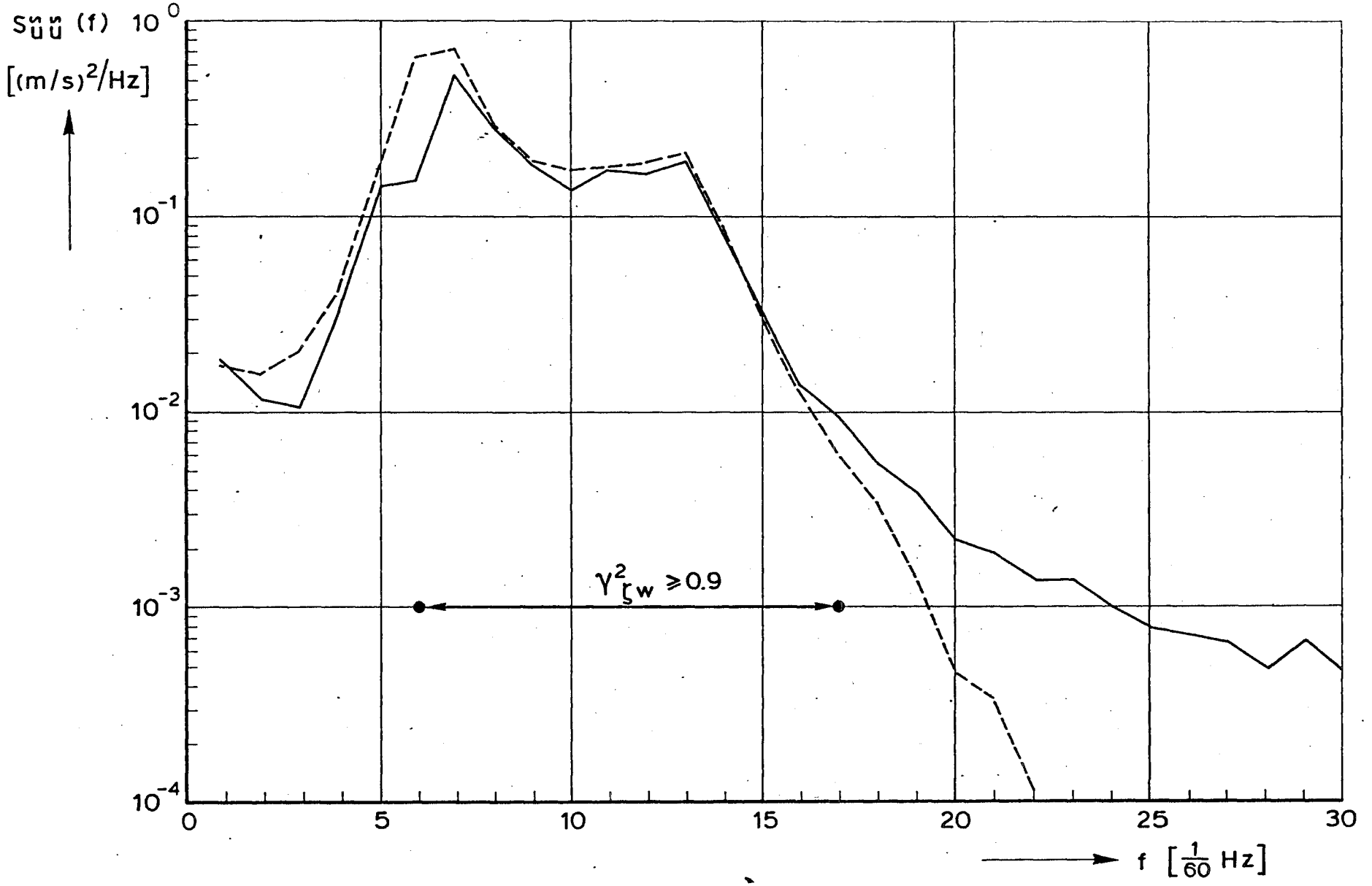

rijkswaterstaat directie waterhuishouding en waterbeweging district kust en zee	get.		appendix 10. fig. 4	
	gec.		projectcode L7709B00	
COMPARISON OF MEASURED AND CALCULATED SPECTRUM OF $\tilde{u}$ USING THE LINEAR THEORY (1802)	gez.		nota WWKZ-83G.007	
	akk.		A 4	nr. 83K.099

——— $S_{\tilde{u}\tilde{u}}$ (f)

— — — $H^2_{\zeta}\,\tilde{u}$ theor. (f) x $S_{\zeta\zeta}$(f)

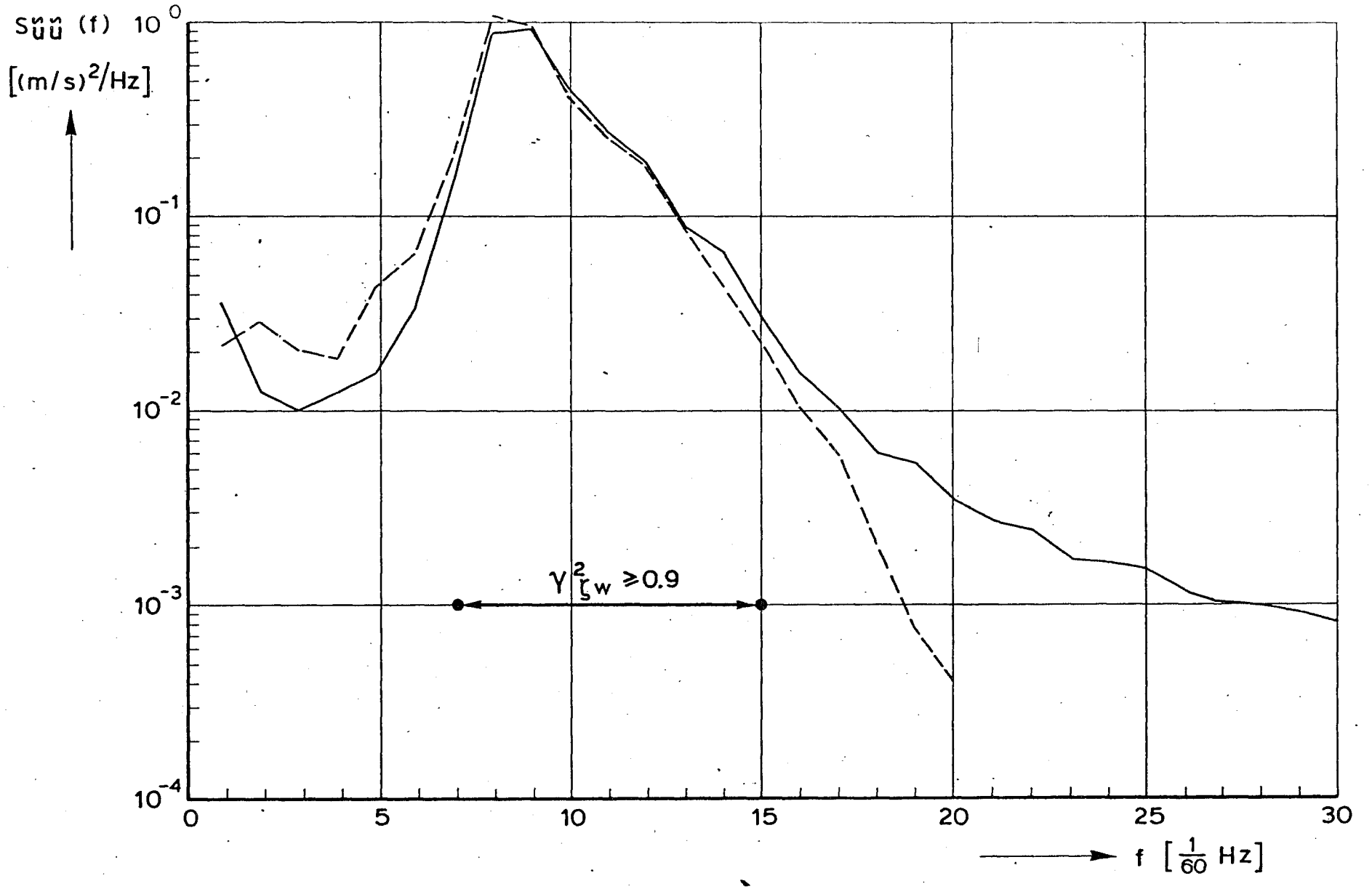

rijkswaterstaat directie waterhuishouding en waterbeweging district kust en zee	get.		appendix 10. fig. 5	
	gec.		projectcode L7709B00	
COMPARISON OF MEASURED AND CALCULATED SPECTRUM OF $\ddot{u}$ USING THE LINEAR THEORY (2201)	gez.		nota WWKZ-83G.007	
	akk.		A 4	nr. 83K.100

——— $S_{\ddot{u}\ddot{u}}$ (f)

— — — $H^2_{\zeta\ddot{u}}$ theor. (f) x $S_{\zeta\zeta}$(f)

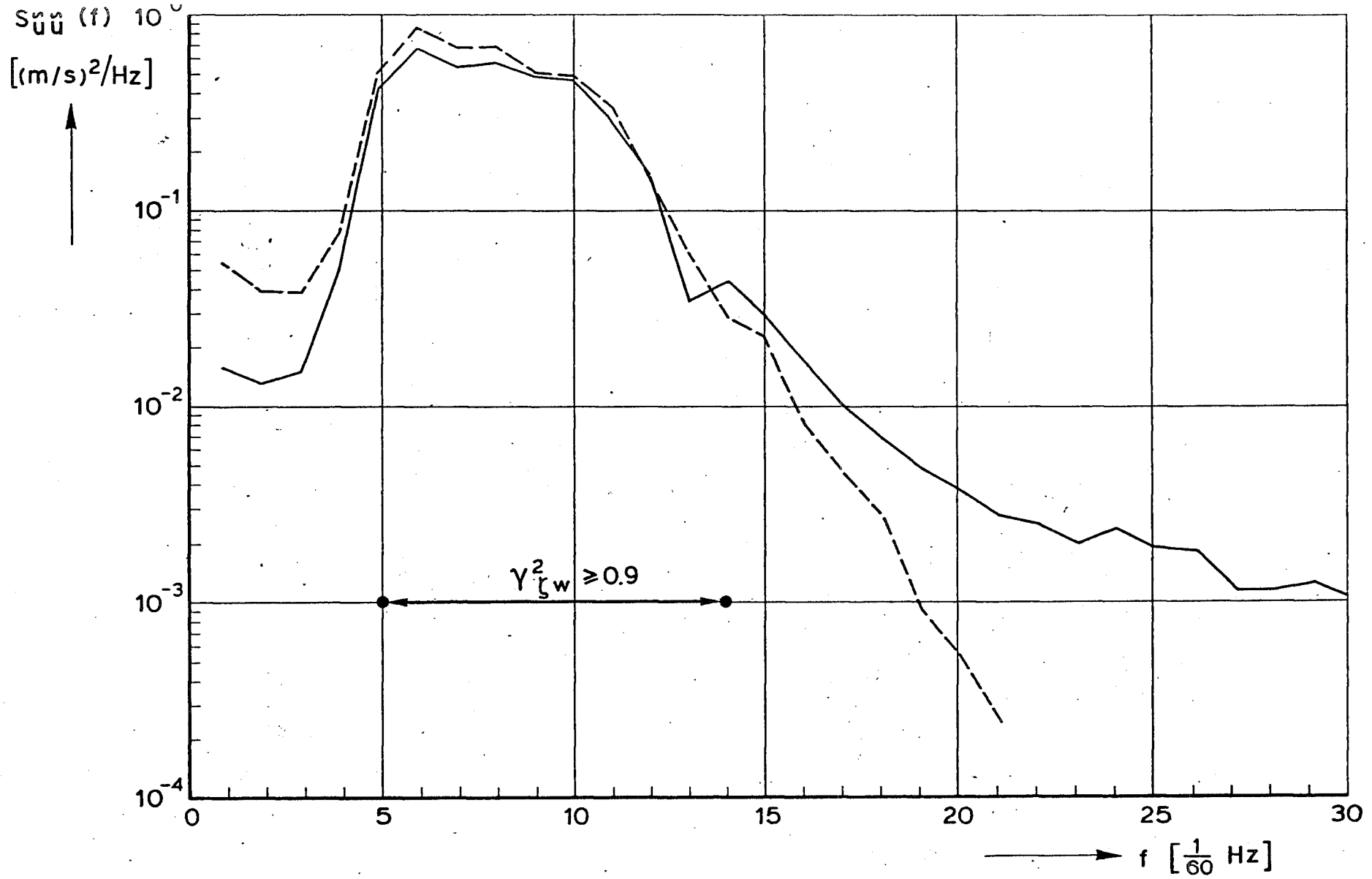

rijkswaterstaat directie waterhuishouding en waterbeweging district kust en zee	get.		appendix 10. fig. 6	
	gec.		projectcode L7709B00	
COMPARISON OF MEASURED AND CALCULATED SPECTRUM OF $\tilde{u}$ USING THE LINEAR THEORY (230.1)	gez.		nota WWKZ-83G.007	
	akk.		A 4	nr. 83K.101

——— $S_{\tilde{u}\tilde{u}}$ (f)

— — — $H^2_{\zeta\tilde{u}}$ theor. (f) x $S_{\zeta\zeta}$(f)

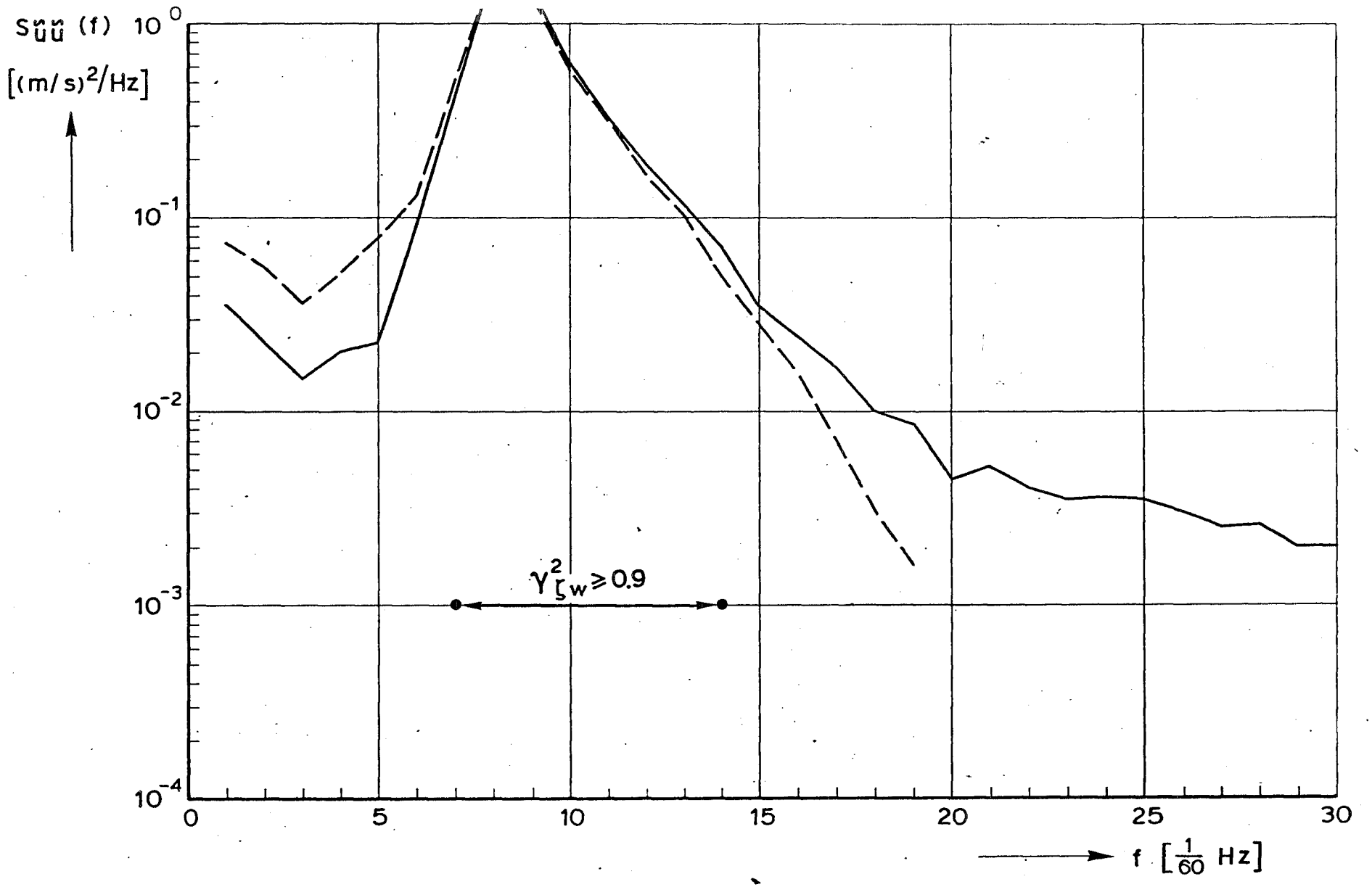

rijkswaterstaat directie waterhuishouding en waterbeweging district kust en zee	get.	appendix 10. fig. 7	
	gec.	projectcode L7709B00	
COMPARISON OF MEASURED AND CALCULATED SPECTRUM OF $\hat{u}$ USING THE LINEAR THEORY (2420)	gez.	nota WWKZ-83G.007	
	akk.	A 4	nr. 83K.102

——— $S_{\hat{u}\hat{u}}$ (f)

— — — $H^2_{\zeta\hat{u}}$ theor. (f) x $S_{\zeta\zeta}$(f)

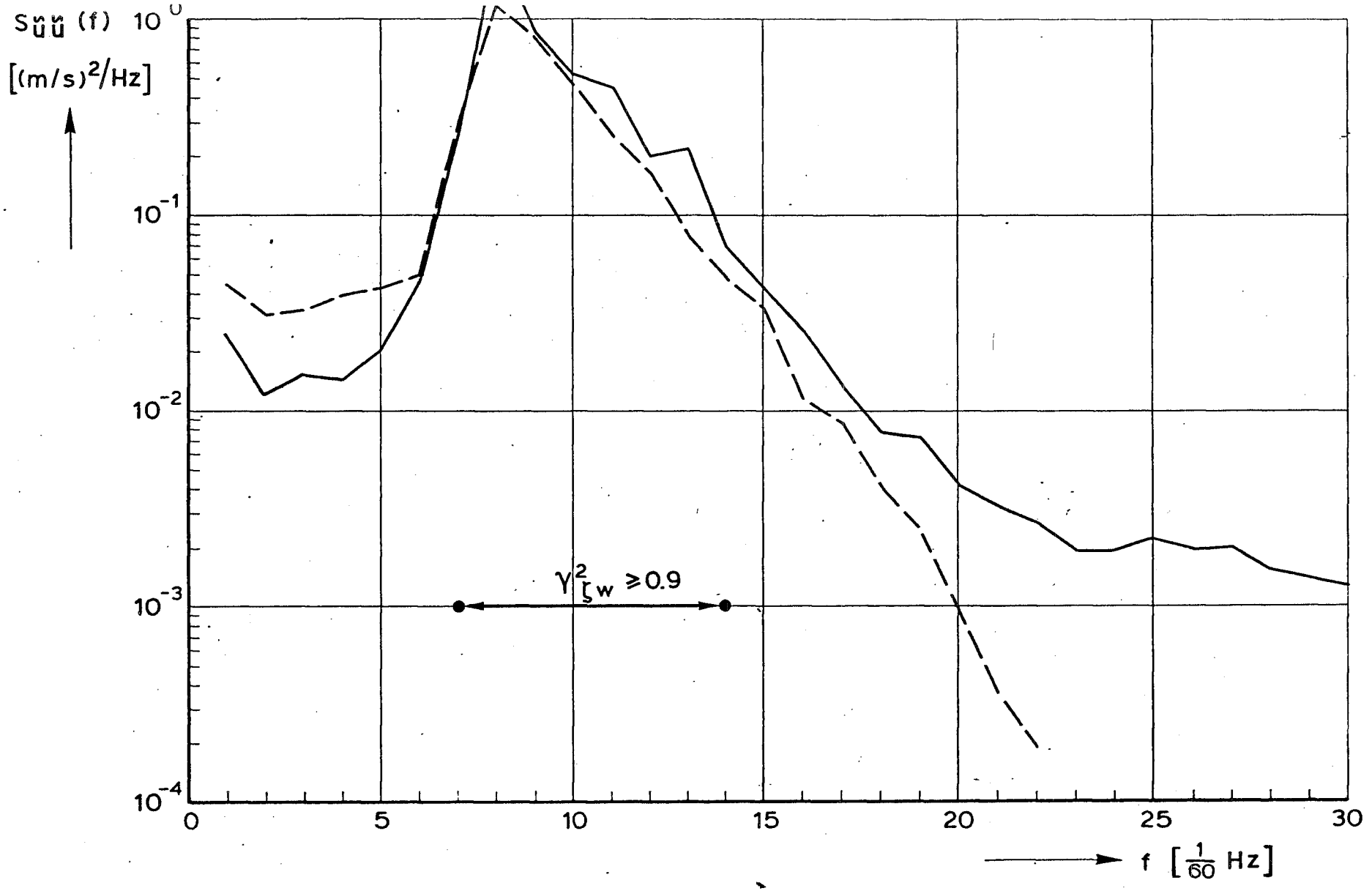

rijkswaterstaat directie waterhuishouding en waterbeweging district kust en zee	get.	appendix 10. fig. 8	
	gec.	projectcode L7709800	
COMPARISON OF MEASURED AND CALCULATED SPECTRUM OF $\tilde{u}$ USING THE LINEAR THEORY (2501)	gez.	nota WWKZ-83G.007	
	akk.	A 4	nr. 83K.103

——— $S_{\tilde{u}\tilde{u}}$ (f)

— — — $H^2_{\zeta\tilde{u}}$ theor (f) x $S_{\zeta\zeta}$(f)

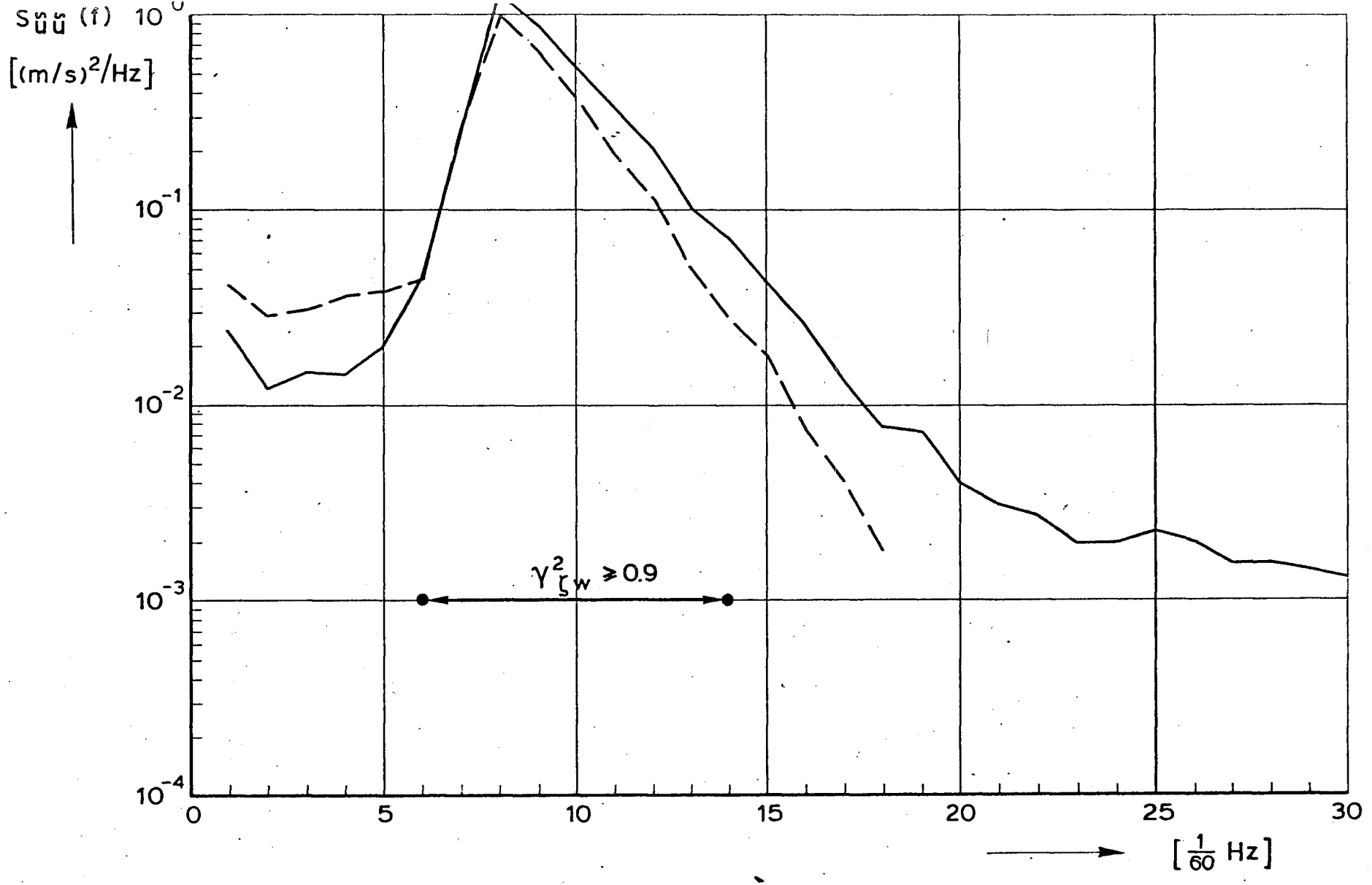

rijkswaterstaat directie waterhuishouding en waterbeweging district kust en zee	get.		appendix 10. fig. 9	
	gec.		projectcode L7709B00	
COMPARISON OF MEASURED AND CALCULATED SPECTRUM OF $\hat{u}$ USING THE LINEAR THEORY (2601)	gez.		nota WWKZ-83G.007	
	akk.		A 4	nr. 83K.104

——— $S_{\hat{u}\hat{u}}$ (f)

— — — $H^2_{\zeta\hat{u}}$ theor. (f) x $S_{\zeta\zeta}$(f)

APPENDIX 11.

RATIOS MEASURED GAIN FUNCTION TO THEORETICAL ONE

Appendix 11 - ratios measured gain function to theoretical one

series	Record number	$\hat{H}_{\zeta\tilde{u}}(f_m) / H_{\zeta\tilde{u}}(f_m)$	$\hat{H}_{\zeta w}(f_m) / H_{\zeta w}(f_m)$	$\hat{H}_{w\tilde{u}}(f_m) / H_{w\tilde{u}}(f_m)$
4	401	-	-	0.90
	402	-	-	0.96
	404	-	-	0.89
	405	-	-	0.90
5	501	-	-	0.98
	502	-	-	1.00
	503	-	-	0.98
	504	-	-	0.96
6	601	-	-	0.92
	602	-	-	0.90
	603	-	-	0.96
7	701	-	-	1.00
	702	-	-	0.95
	704	-	-	1.00
8	801	-	-	0.91
	802	-	-	1.00
	803	-	-	1.00
	804	-	-	1.00
9	901	-	-	1.04
	902	-	-	1.04
	903	-	-	1.01
	904	-	-	1.00
	905	-	-	0.88
15	1501	0.95	0.96	1.00
	1502	0.97	1.03	0.95
	1503	0.97	0.98	1.00
	1504	1.02	1.04	1.00
	1505	0.99	1.01	1.00
16	1601	0.92	0.97	0.96
	1602	0.91	0.94	0.98
	1603	0.88	0.98	0.91
	1605	0.97	0.98	1.01

series	Record number	$\hat{H}_{\zeta\tilde{u}}(fm) / H_{\zeta\tilde{u}}(fm)$	$\hat{H}_{\zeta w}(fm) / H_{\zeta w}(fm)$	$\hat{H}_{w\tilde{u}}(fm) / H_{w\tilde{u}}(fm)$
17	1702	0.90	0.99	0.91
	1704	0.87	0.94	0.93
18	1802	0.95	0.96	0.90
	1803	0.94	0.96	0.99
	1804	0.94	0.98	0.96
	1805	0.91	0.96	0.96
	1806	1.04	0.98	1.03
	1807	0.93	0.98	0.96
22	2201	0.99	1.00	1.00
	2202	0.92	0.96	0.97
	2203	1.00	0.95	1.05
	2204	0.91	0.87	1.04
23	2301	0.98	0.96	1.02
	2302	1.00	0.95	1.00
	2303	0.97	0.97	1.01
	2304	0.90	0.84	0.98
24	2406	0.92	1.12	0.83
	2411	1.01	1.11	0.92
	2416	1.08	1.18	0.91
	2420	0.96	1.07	0.90
25	2501	1.03	1.22	0.86
	2503	0.98	1.11	0.89
	2504	1.02	1.17	0.88
26	2601	0.89	0.97	0.92
	2602	0.87	1.01	0.87
	2603	0.92	0.99	0.93
	2604	0.90	0.97	0.94
	2605	0.96	0.94	1.00

APPENDIX 12.

STATISTICAL DISTRIBUTIONS OF SURFACE ELEVATION AND VELOCITY COMPONENTS

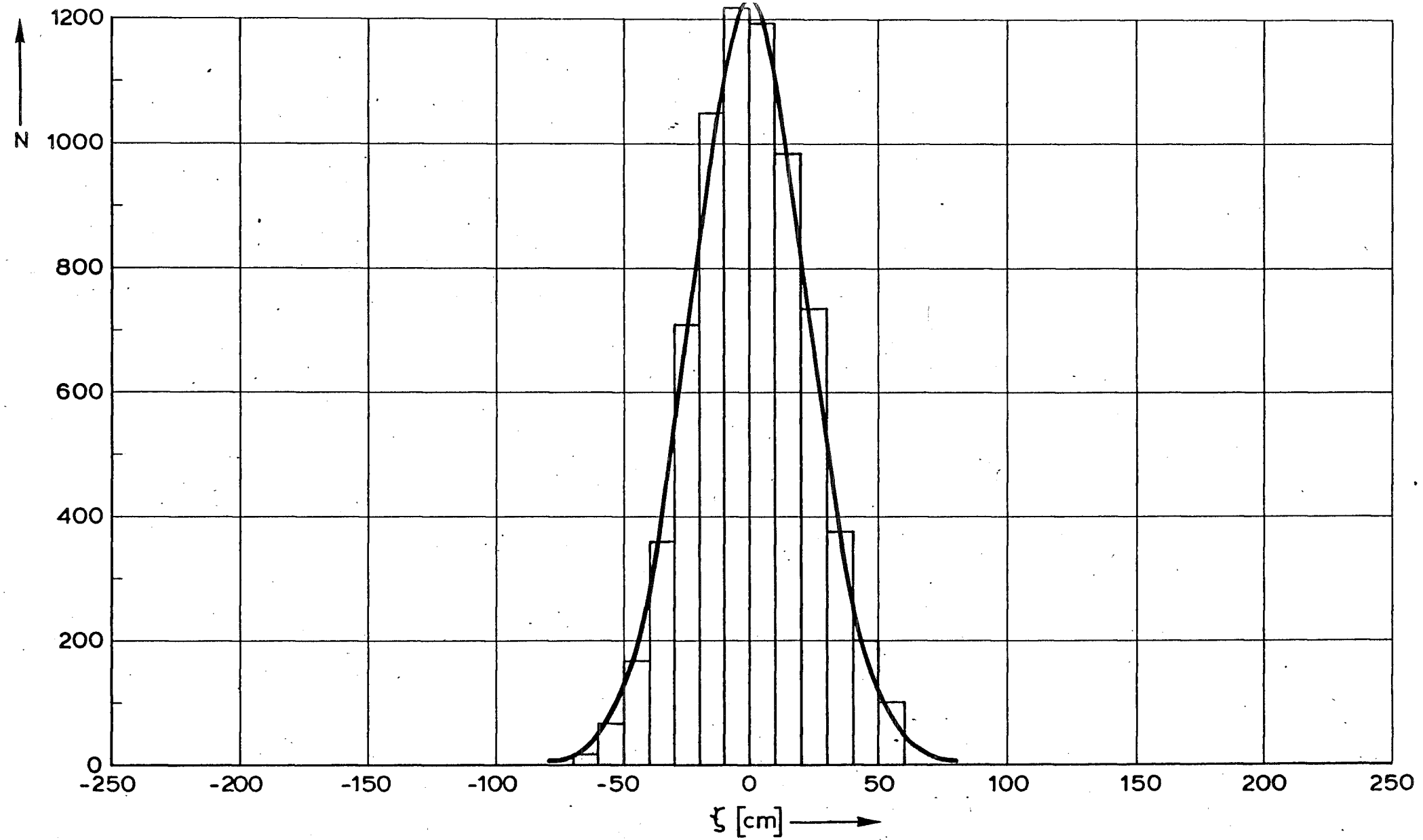

rijkswaterstaat
directie waterhuishouding en waterbeweging
district kust en zee

STATISTICAL DISTRIBUTION OF ζ (1501)
TOTAL NUMER OF DATA: 7200

get.		appendix 12. fig. 1
gec.		projectcode L7709 B 00
gez.		nota WWKZ-83G.007
akk.		A 4 nr. 83 K. 105

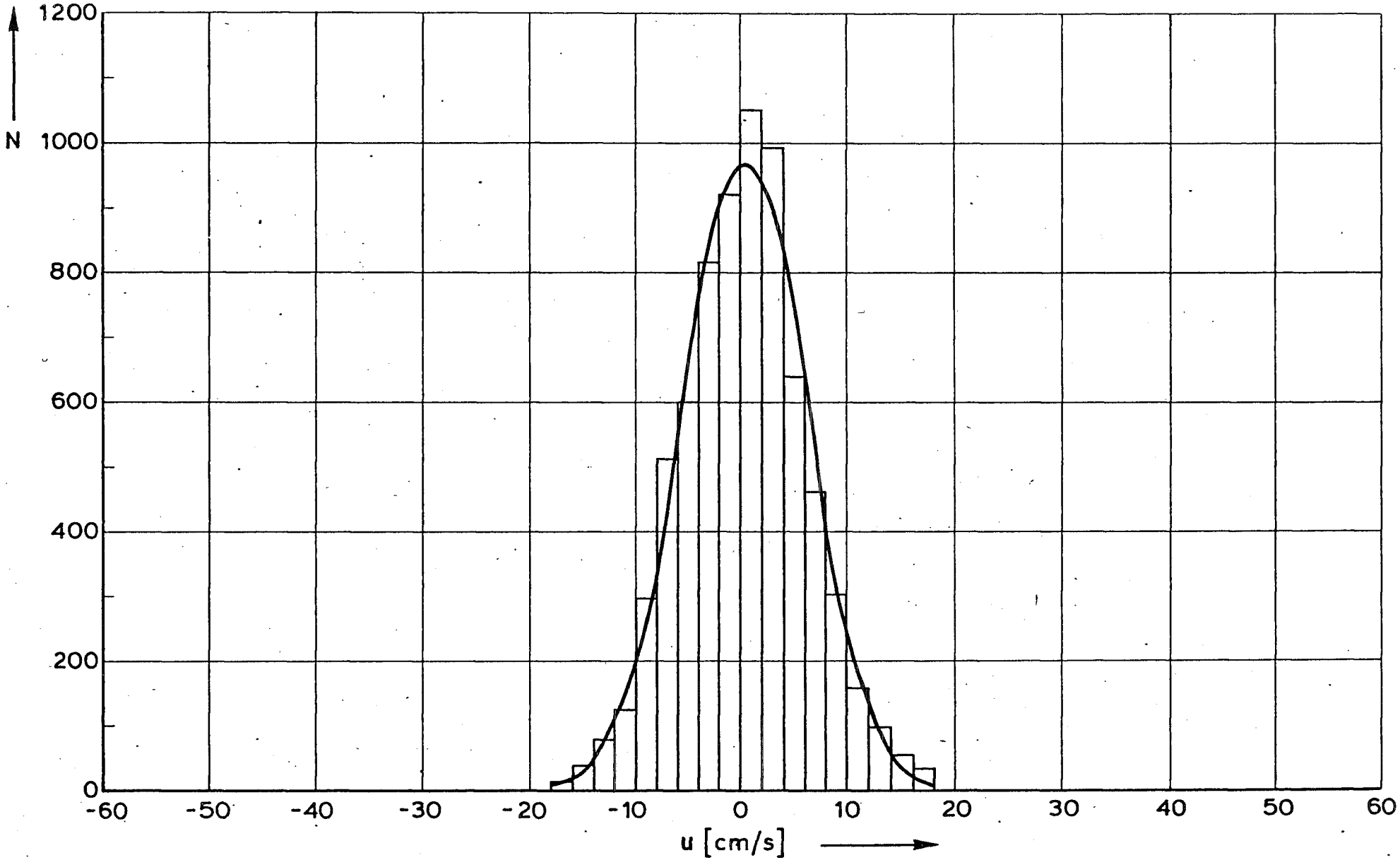

rijkswaterstaat directie waterhuishouding en waterbeweging district kust en zee	get.	appendix 12. fig. 2
	gec.	projectcode L7709B00
STATISTICAL DISTRIBUTION OF u (1501). TOTAL NUMER OF DATA : 7200	gez.	nota WWKZ-83G.007
	akk.	A 4 nr. 83K.106

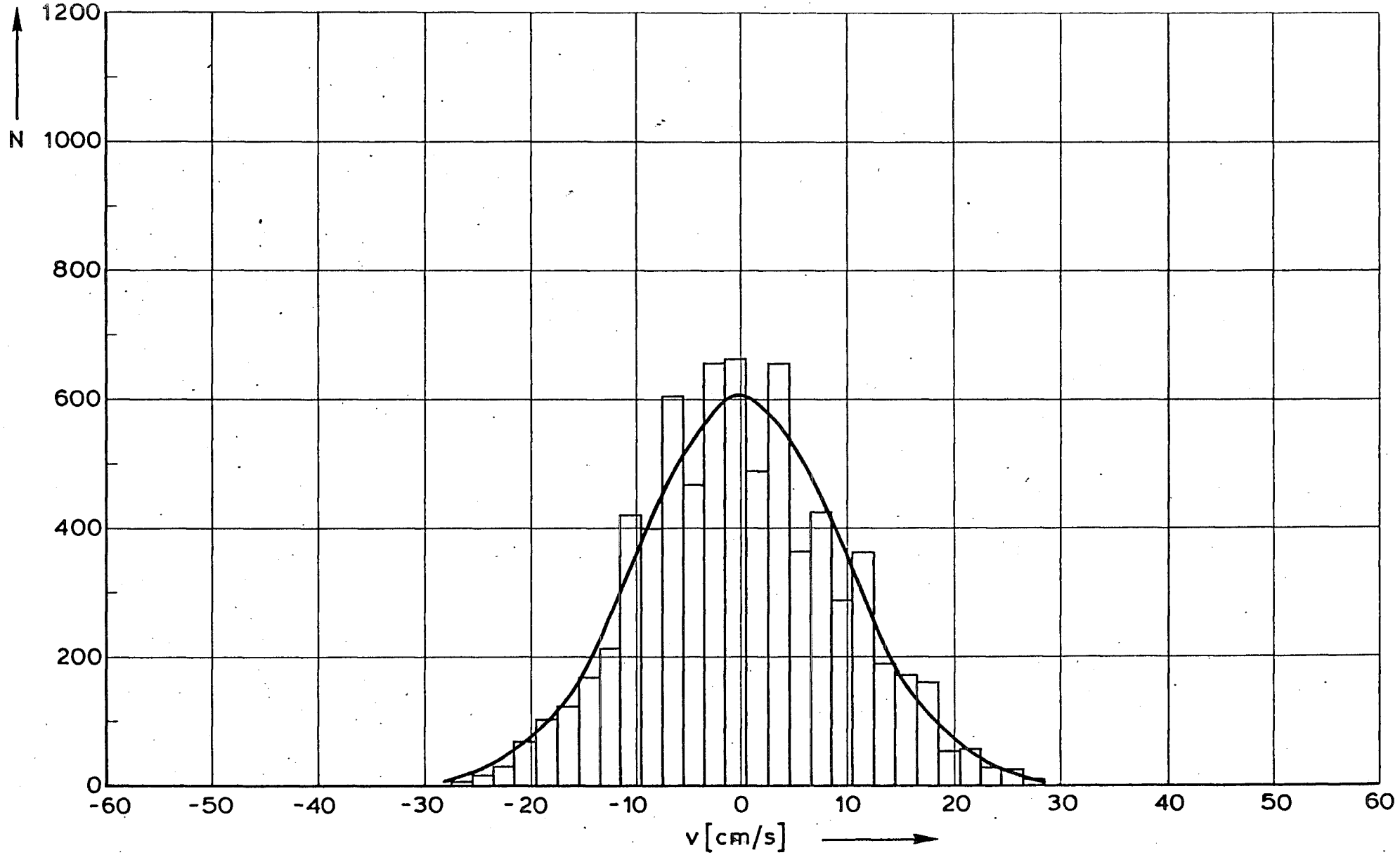

rijkswaterstaat directie waterhuishouding en waterbeweging district kust en zee	get.	appendix 12. fig. 3
	gec.	projectcode L7709B00
STATISTICAL DISTRIBUTION OF v (1501). TOTAL NUMER OF DATA : 7200	gez.	nota WWKZ-83G.007
	akk.	A 4 nr. 83K.107

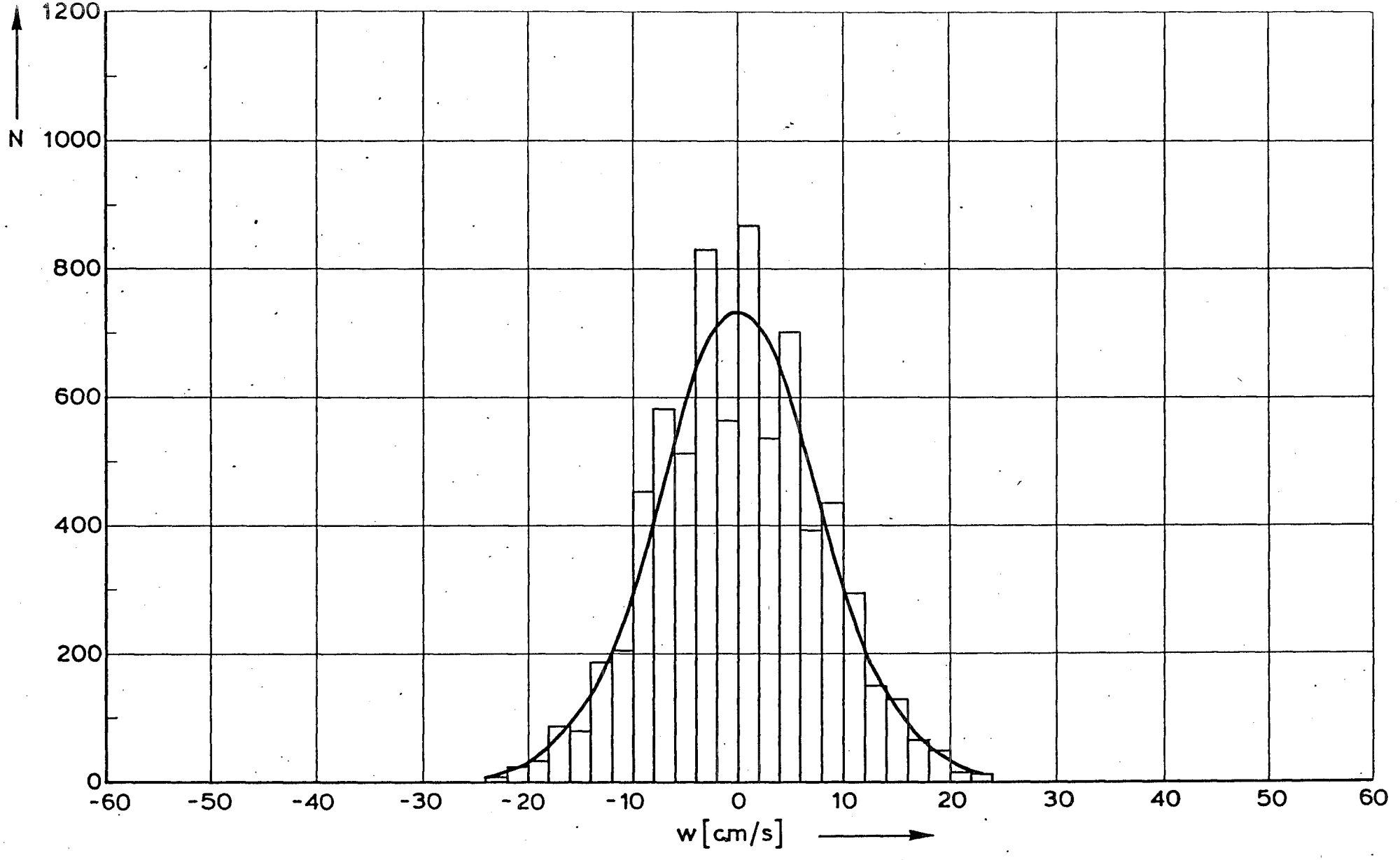

rijkswaterstaat directie waterhuishouding en waterbeweging district kust en zee	get.		appendix 12. fig. 4
	gec.		projectcode L7709B00
STATISTICAL DISTRIBUTION OF w (1501). TOTAL NUMER OF DATA : 7200	gez.		nota WWKZ-83G.007
	akk.		A 4 nr. 83K.108

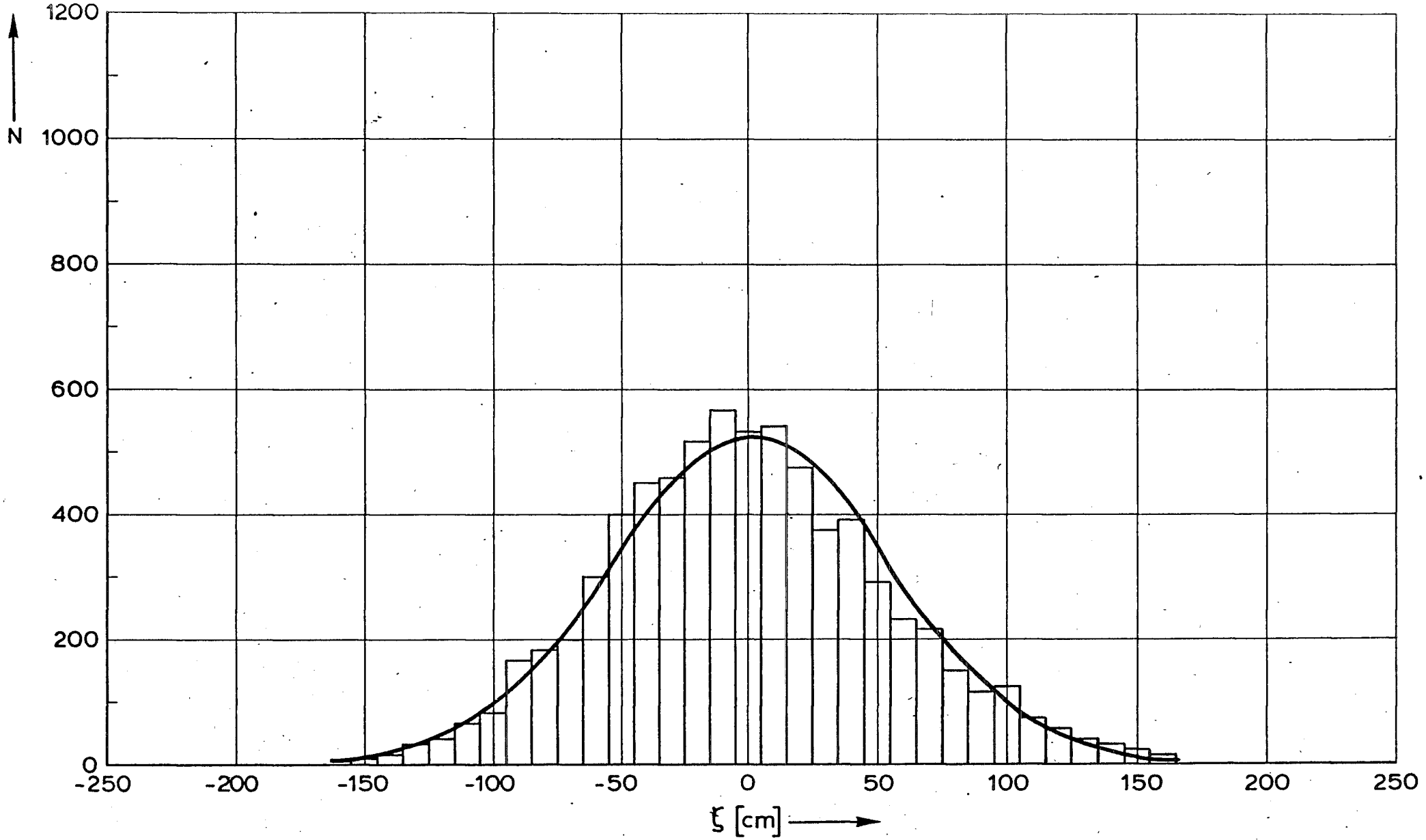

rijkswaterstaat directie waterhuishouding en waterbeweging district kust en zee	get.	appendix 12. fig. 5
	gec.	projectcode L7709 B00
STATISTICAL DISTRIBUTION OF ζ (1601) TOTAL NUMER OF DATA: 7200	gez.	nota WWKZ-83G.007
	akk.	A4 nr 83K.109

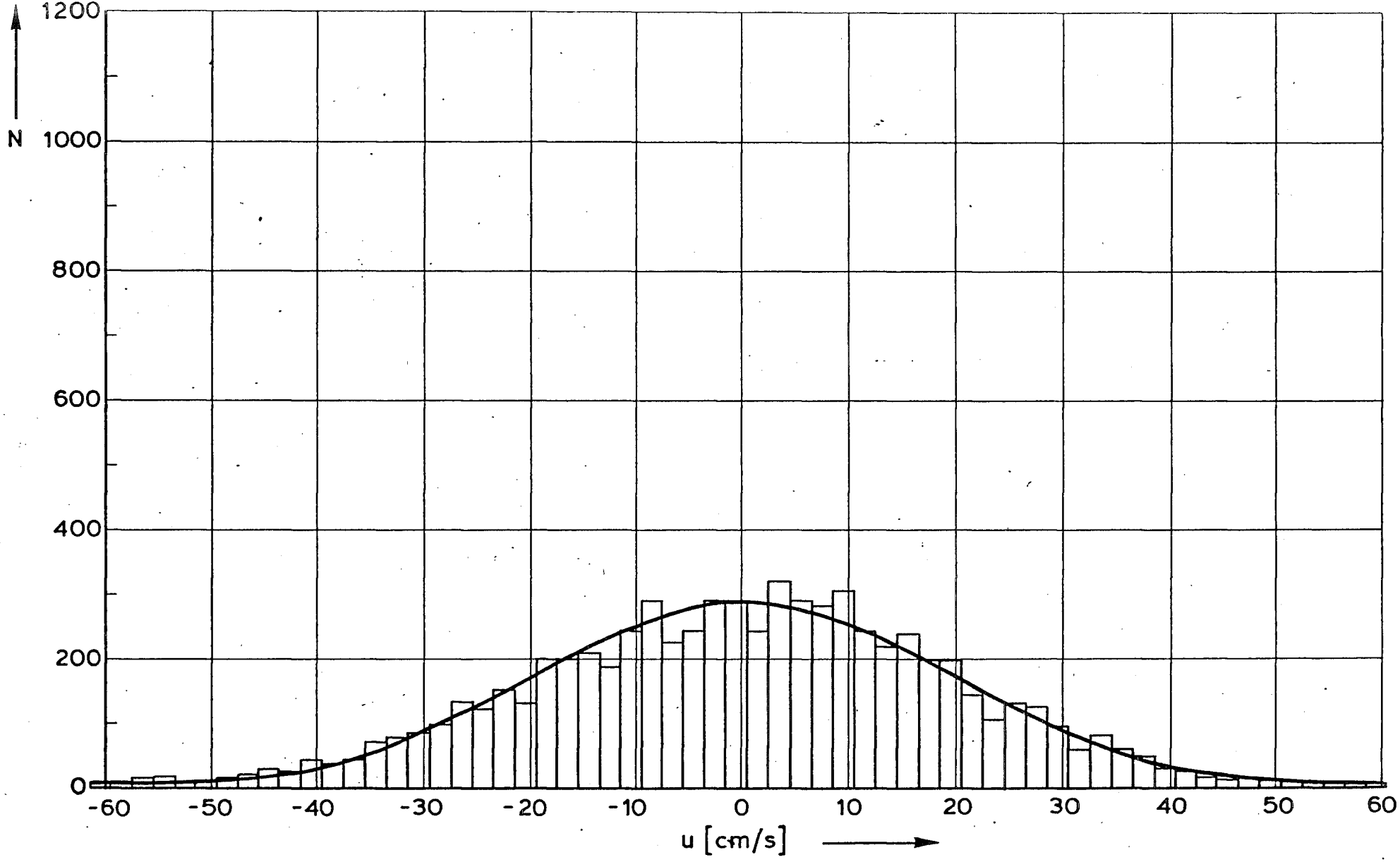

rijkswaterstaat directie waterhuishouding en waterbeweging district kust en zee	get.		appendix 12. fig. 6
	gec.		projectcode L7709B00
STATISTICAL DISTRIBUTION OF u (1601). TOTAL NUMER OF DATA : 7200	gez.		nota WWKZ-83G.007
	akk.		A 4 nr. 83K.110

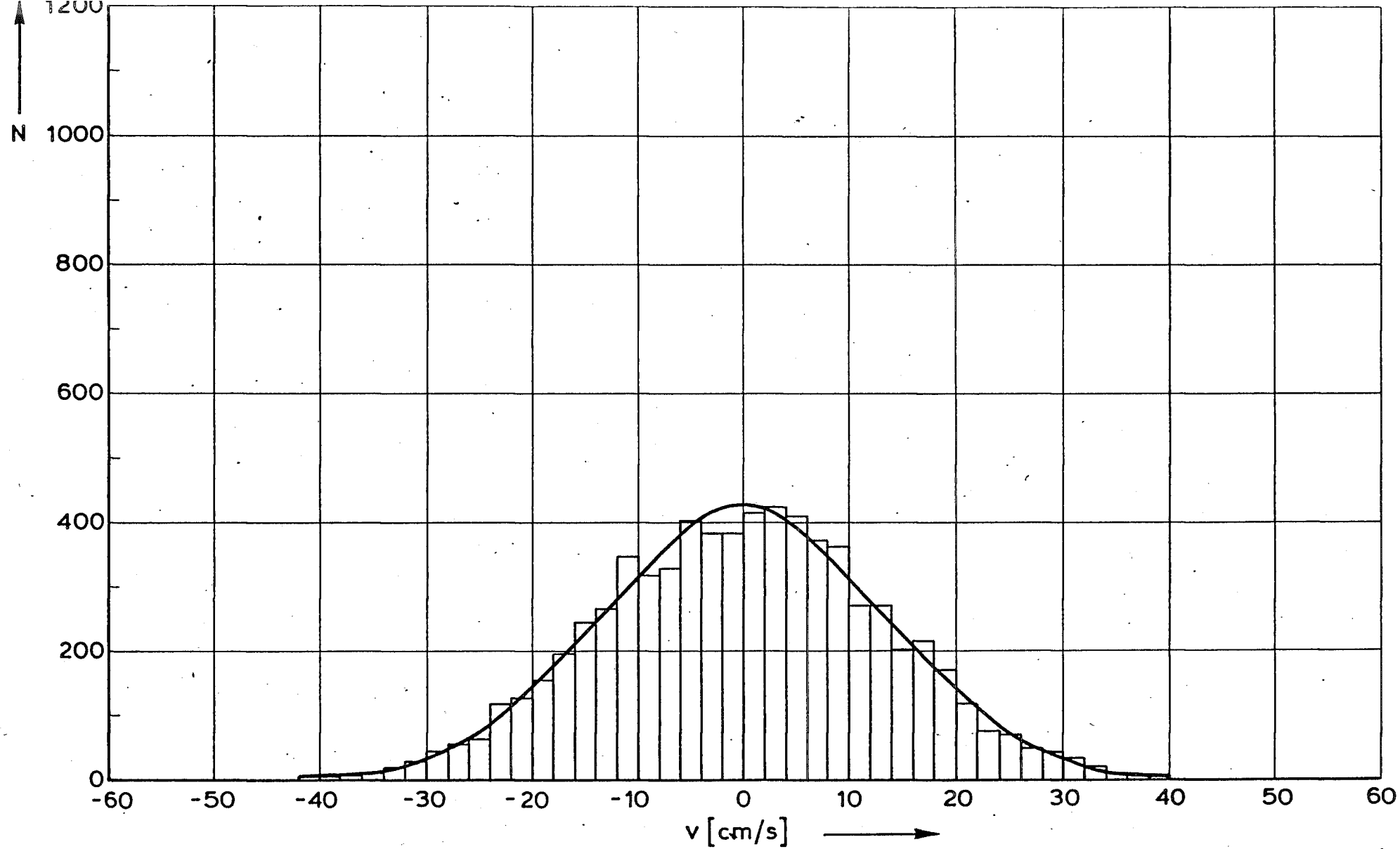

rijkswaterstaat
directie waterhuishouding en waterbeweging
district kust en zee

STATISTICAL DISTRIBUTION OF v (1601).
TOTAL NUMER OF DATA: 7200

get.		appendix 12. fig. 7	
gec.		projectcode L7709B00	
gez.		nota WWKZ-83G.007	
akk.		A 4	nr. 83K.111

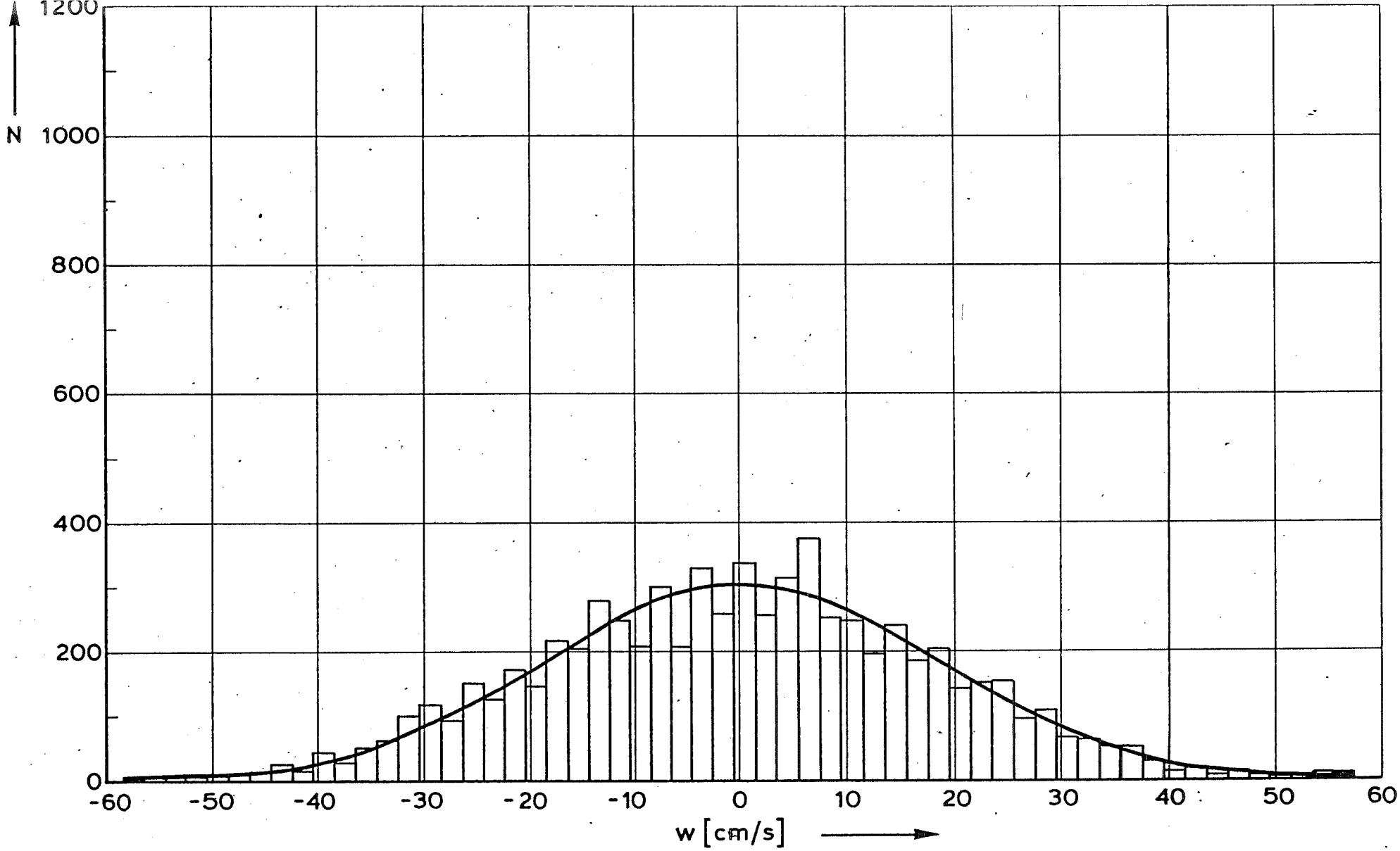

rijkswaterstaat directie waterhuishouding en waterbeweging district kust en zee	get.		appendix 1 . fig. 8
	gec.		projectcode L7709B00
STATISTICAL DISTRIBUTION OF w (1601). TOTAL NUMER OF DATA : 7200	gez.		nota WWKZ-83G.007
	akk.		A 4 nr. 83K.112